

## Optimization of small AC series commutator motors

**Citation for published version (APA):**

Dijken, R. H. (1971). *Optimization of small AC series commutator motors*. [Phd Thesis 1 (Research TU/e / Graduation TU/e), Electrical Engineering]. Technische Hogeschool Eindhoven. <https://doi.org/10.6100/IR111802>

**DOI:**

[10.6100/IR111802](https://doi.org/10.6100/IR111802)

**Document status and date:**

Published: 01/01/1971

**Document Version:**

Publisher's PDF, also known as Version of Record (includes final page, issue and volume numbers)

**Please check the document version of this publication:**

- A submitted manuscript is the version of the article upon submission and before peer-review. There can be important differences between the submitted version and the official published version of record. People interested in the research are advised to contact the author for the final version of the publication, or visit the DOI to the publisher's website.
- The final author version and the galley proof are versions of the publication after peer review.
- The final published version features the final layout of the paper including the volume, issue and page numbers.

[Link to publication](#)

**General rights**

Copyright and moral rights for the publications made accessible in the public portal are retained by the authors and/or other copyright owners and it is a condition of accessing publications that users recognise and abide by the legal requirements associated with these rights.

- Users may download and print one copy of any publication from the public portal for the purpose of private study or research.
- You may not further distribute the material or use it for any profit-making activity or commercial gain
- You may freely distribute the URL identifying the publication in the public portal.

If the publication is distributed under the terms of Article 25fa of the Dutch Copyright Act, indicated by the "Taverne" license above, please follow below link for the End User Agreement:

[www.tue.nl/taverne](http://www.tue.nl/taverne)

**Take down policy**

If you believe that this document breaches copyright please contact us at:

[openaccess@tue.nl](mailto:openaccess@tue.nl)

providing details and we will investigate your claim.

**OPTIMIZATION OF SMALL AC  
SERIES COMMUTATOR MOTORS**

**R. H. DIJKEN**

# OPTIMIZATION OF SMALL AC SERIES COMMUTATOR MOTORS

## PROEFSCHRIFT

TER VERKRIJGING VAN DE GRAAD VAN DOCTOR  
IN DE TECHNISCHE WETENSCHAPPEN AAN DE  
TECHNISCHE HOGESCHOOL TE EINDHOVEN,  
OP GEZAG VAN DE RECTOR MAGNIFICUS,  
PROF. DR. IR. A. A. TH. M. VAN TRIER, VOOR EEN  
COMMISSIE UIT DE SENAAT IN HET OPENBAAR  
TE VERDEDIGEN OP DINSDAG 19 OKTOBER 1971,  
DES NAMIDDAGS TE 4 UUR

DOOR

REINDER HENDRIK DIJKEN

GEBOREN TE NIEUWOLDA

DIT PROEFSCHRIFT WERD GOEDGEKEURD DOOR DE PROMOTOREN  
PROF. DR. IR. H. C. J. DE JONG EN PROF. DR. IR. J. G. NIESTEN



*aan Puck Vader Moeder  
Bert Durandus Cathrientje*

De onderzoekingen, beschreven in dit proefschrift, zijn grotendeels uitgevoerd in de laboratoria van de Hoofd Industrie Groep Huishoudelijke Apparaten der N.V. Philips' Gloeilampenfabrieken in Drachten en Leeuwarden.

De schrijver is de directie van deze Hoofd Industrie Groep zeer erkentelijk voor haar toestemming om de resultaten van deze onderzoekingen als proefschrift te mogen publiceren.

Ook is de schrijver veel dank verschuldigd aan allen die op enigerlei wijze hebben meegewerkt aan de totstandkoming van dit proefschrift. Dit zijn vooral de Heren: T. Blauw, ir. J. H. de Boer, A. Hoekstra, J. Jager, H. Klamer, J. Kwakernaak, L. B. Mulder, ir. W. Robberegt, ir. W. Terpstra, ir. J. Timmerman en A. de Vries.

## CONTENTS

INTRODUCTION . . . . .	1
1. THE SMALL SERIES MOTOR . . . . .	4
1.1. Characteristic features of small series motors . . . . .	4
1.2. The choice of the type of stator . . . . .	6
1.3. Some important parameters . . . . .	8
1.4. Formulas for the resistance of the rotor . . . . .	12
1.5. Formulas for the resistance of the stator . . . . .	15
1.6. A simplified description of the motor . . . . .	16
1.7. Imperfections of the simplified description . . . . .	18
1.8. Optimization . . . . .	20
1.9. Conclusions . . . . .	22
2. SATURATION IN SMALL SERIES MOTORS . . . . .	24
2.1. The normalized magnetization curve . . . . .	24
2.2. The normalized electrical differential equation . . . . .	28
2.3. Solution of the normalized electrical differential equation . . . . .	32
2.4. Conclusions . . . . .	35
3. IRON LOSS IN SMALL COMMUTATOR MACHINES . . . . .	37
3.1. The iron loss in the stator . . . . .	38
3.2. A method of measuring the iron loss in the rotor . . . . .	38
3.3. The types of steel sheet considered . . . . .	40
3.4. Measuring methods and results . . . . .	41
3.4.1. Magnetic measurements . . . . .	41
3.4.2. Iron-loss torques with DC excitation . . . . .	44
3.4.3. Thickness and resistivity of the various types of steel sheet . . . . .	45
3.4.4. Iron-loss torques with AC excitation . . . . .	48
3.4.5. Non-insulated steel sheet . . . . .	50
3.4.6. A solid steel stator . . . . .	51
3.4.7. Brass as shaft material . . . . .	51
3.4.8. A hollow steel shaft . . . . .	51
3.4.9. A 12-mm steel shaft . . . . .	52
3.5. Conclusions . . . . .	52
4. THE CARTER FACTOR OF SEMI-ENCLOSED ROTOR SLOTS OPPOSITE SMOOTH-FACED STATOR POLES . . . . .	53
4.1. Simulation of the air-gap field by means of a resistance network . . . . .	54
4.2. Determination of the carter factor with the aid of a two-dimensional resistance network . . . . .	57

4.3. Measuring method and results . . . . .	59
4.4. Graphical determination of the carter factor of semi-enclosed slots . . . . .	64
4.5. Conclusions . . . . .	66
<b>5. THE ACTIVE INDUCTANCE OF A ROTOR COIL OF SMALL COMMUTATOR MACHINES WITH RESPECT TO COMMUTATION . . . . .</b>	<b>67</b>
5.1. The relation between brush wear and the spark voltage between brush and segment . . . . .	68
5.2. The current in the commutating coil . . . . .	69
5.3. The method of measurement . . . . .	71
5.4. Description of the rotors and stators measured . . . . .	76
5.5. Measuring results . . . . .	79
5.6. Evaluation of the results of the measurements . . . . .	104
5.6.1. The active inductance . . . . .	104
5.6.2. The spark decay time with respect to the length of the sparks . . . . .	105
5.7. Conclusions . . . . .	105
<b>6. TEMPERATURE DISTRIBUTION AND HEAT TRANSPORT IN SMALL COMMUTATOR MACHINES . . . . .</b>	<b>106</b>
6.1. Losses in small commutator machines . . . . .	106
6.2. A thermal network . . . . .	107
6.3. Conclusions . . . . .	113
<b>7. DESCRIPTION, DIMENSIONING AND OPTIMIZATION . . . . .</b>	<b>114</b>
7.1. The concepts of description, design, dimensioning and optimization . . . . .	114
7.2. A method of optimizing electric machines . . . . .	114
7.3. Examples of descriptive formulas . . . . .	115
7.4. Examples of dimensioning formulas . . . . .	116
7.5. Examples of optimization formulas . . . . .	116
7.6. Rotor and stator resistances as parameters in dimensioning and optimization formulas . . . . .	117
7.7. Use of air-gap induction, current density and specific load as parameters in the development of similarity relations . . . . .	118
7.8. Current density and specific load as parameters in dimensioning and optimization formulas . . . . .	120
7.9. Magnetic induction in the iron and air-gap induction as parameters in dimensioning and optimization formulas . . . . .	121

7.10. Analysis of the rotor-dimensioning formula . . . . .	121
7.10.1. The optimum value of the relative rotor length . . . . .	126
7.10.2. The optimum value of the relative flux-conducting rotor width . . . . .	128
7.11. The optimum value of the relative flux-conducting rotor width at constant current density . . . . .	129
7.12. Conclusions . . . . .	134
8. THE OPTIMIZATION METHOD . . . . .	135
8.1. Formulas for the volume, weight and cost of the steel sheet re- quired . . . . .	135
8.2. Formulas for the volume, weight and cost of the winding wire of rotor and stator . . . . .	136
8.3. The motor to be optimized and the starting points for the op- timization calculation . . . . .	139
8.4. Survey of parameters used . . . . .	140
8.5. The computer programme . . . . .	143
8.6. Specimen calculation . . . . .	149
8.7. Results of the specimen calculation . . . . .	152
8.8. Evaluation of the results . . . . .	158
8.9. Comparison with the results of measurement . . . . .	159
8.10 Conclusions . . . . .	162
List of symbols . . . . .	163
References . . . . .	176
Summary . . . . .	177
Curriculum vitae . . . . .	178

## INTRODUCTION

Hundreds of millions of small electric motors are manufactured every year throughout the world. At least one hundred million of them are small bi-polar AC series commutator motors, without compensation coils or commutating poles. These small series motors are suitable for an AC or DC input voltage of about 100 to 240 V. They generally have 8 to 16 rotor slots and supply an output power of 20 to 500 W at 2 000 to 20 000 revolutions per minute. The useful life required of such a motor does not generally exceed 1 500 hours. From now on, the term "small series motor" will be used here to describe a motor of this type.

The small series motor is generally used in vacuum cleaners, hand tools, mixers, coffee grinders, shoe polishers, floor polishers, fruit presses, etc. So far, the dimensions and other parameters of the small series motor have generally been determined empirically. Considerable savings in manufacturing costs could be obtained if there were a reliable method of optimizing this motor. Such an optimization method is described in chapter 8 of this thesis. The first seven chapters deal with various considerations and investigations needed to establish the optimization method.

The total value of all the small motors manufactured throughout the world every year may well exceed that of large electric motors; yet much less has been published on small electric motors than on large ones. Some reasons for this are:

- (1) Almost anyone can make a small electric motor: the required life is short, and factors such as rotor field, demagnetization of permanent magnets and irregularities in rotational fields can be neglected. A crudely made motor will still run, though its efficiency may be low and it may vibrate or be noisy, etc.
- (2) There are few universities where much attention is paid to the study of small motors. One of the few is the Technische Hochschule in Stuttgart, which has produced many theses and other publications during the past two decades.

We will mention now a number of publications on small commutator machines, some of them dealing with mechanical aspects, some with electrical aspects:

SUBJECT	AUTHOR	REFERENCE
Cooling	Kiefer	1
Noise generated	Mühleisen	25
Statical and dynamical behaviour of brush springs	Hauschild	2
Influence of rotation on commutators	Woerner	3

SUBJECT	AUTHOR	REFERENCE
Commutating ability of brushes	F. Schröter	5
Commutator sparking	Binder	20
	Padmanabhan and	
	Srinivasan	7
Brush wear	Gruber	6
Commutation	Mohr	17
Commutation losses	Held	4
Flux variation due to rotation of the rotor	Pöllot	27
Permeance of the magnetic circuit	W. Schröter	28
	Kuhnle	11
Iron losses	Pustola	8

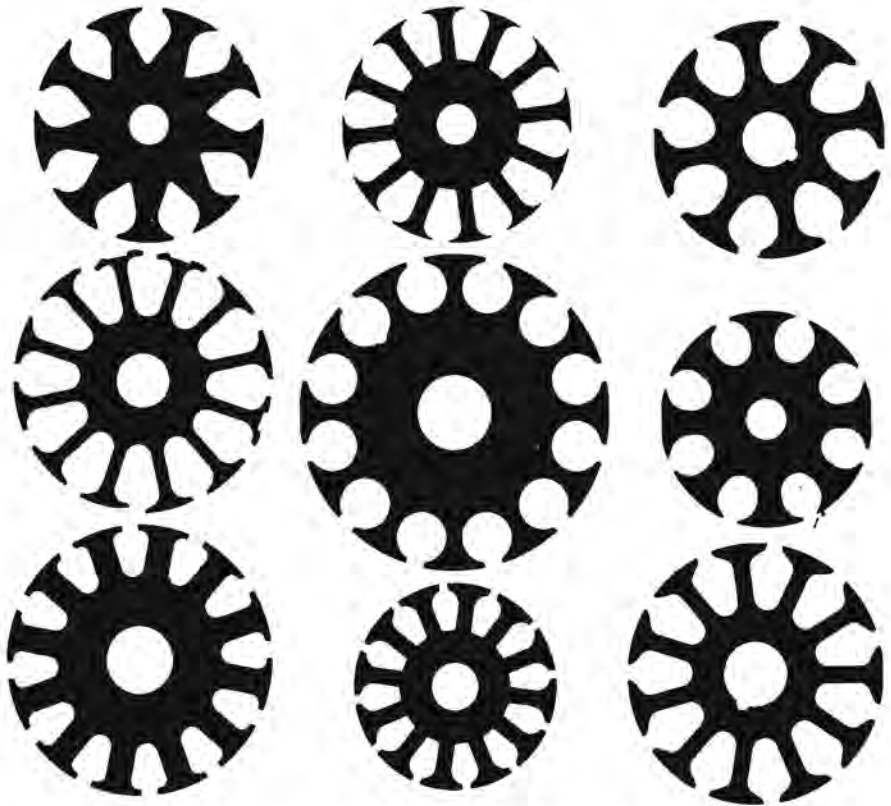


Fig. 1. Various shapes of rotor laminations as found in small commutator machines.



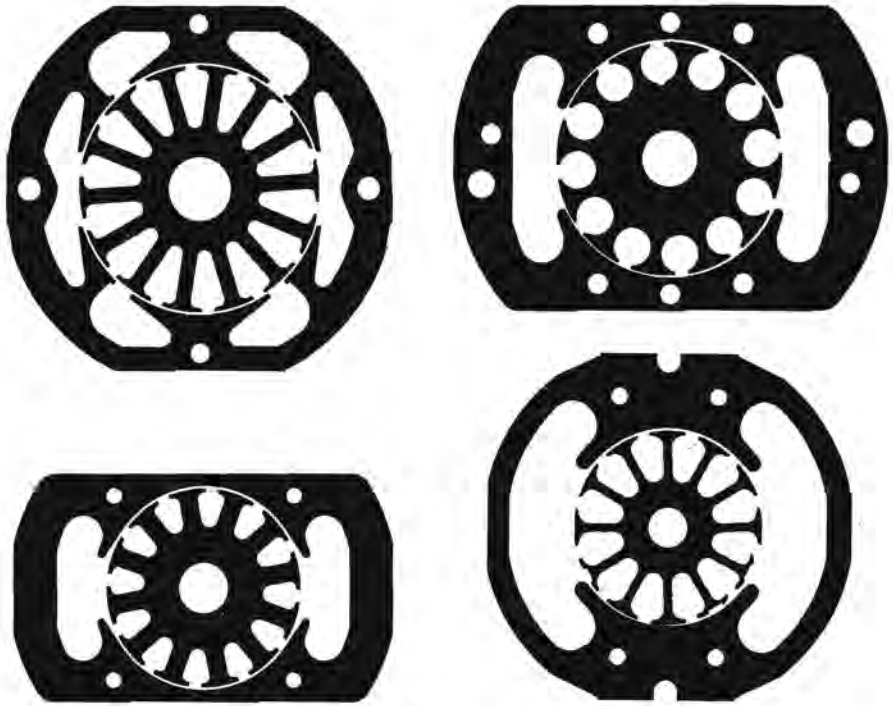


Fig. 2. Various shapes of stator laminations as found in small commutator machines.

Esson's formula is generally used as a starting point for the dimensioning of commutator machines (see e.g. Feldmann<sup>10</sup>), Still and Siskind<sup>18</sup>), and Postnikow<sup>16</sup>), including small commutator motors (see e.g. Grant, and Roszyk<sup>12</sup>), Gladun<sup>13,14</sup>), Stolov<sup>15</sup>), and Puchstein<sup>30</sup>).

Dimensioning is a highly important aspect of the design of commutator machines. Correct dimensioning gives a relatively small, cheap machine. As will be indicated in chapter 7, however, we consider Esson's formula to have serious disadvantages as a starting point for the dimensioning of small commutator motors. The study described in this thesis was started to develop a more efficient optimization method.

The importance of having a good optimization method may be indicated by the photographs in figs 1 and 2, which show widely divergent shapes of rotor and stator laminations as found in small series motors.

## 1. THE SMALL SERIES MOTOR

To optimize a small series motor, we must know the characteristic features of this type of motor. These are described in sec. 1.1. In sec. 1.2 we discuss the exact shape of the stator, which must be chosen before the optimization is started. The dimensions of the rotor and stator must now be expressed in terms of suitable parameters. These parameters are introduced in sec. 1.3 and applied to formulas for the resistance of the rotor and stator in secs 1.4 and 1.5.

The agreement between the physical model of the motor and the real motor is studied in secs 1.6 and 1.7.

Finally, the definition of an "optimum small series motor" is given in sec. 1.8.

### 1.1. Characteristic features of small series motors

Most of the characteristic features of small series motors mentioned below are well known. Many of these features are shared with other small motors.

#### *Operating life*

The operating life required of a small series motor varies from about 20 operating hours for a coffee grinder up to about 1500 operating hours for a vacuum cleaner. Because this life is relatively short, the wear of brushes and commutator may be relatively great, so that sparkless commutation is not required. Commutation sparks are influenced by the active inductance of the rotor coils at the end of commutation. This active inductance is studied in chapter 5.

#### *Cooling*

The heat generated in a motor flows to the outside surfaces or to the surfaces of cooling channels, where it is removed by the air, by a gas, by a liquid or by radiation. There are two problems involved in this cooling process:

- (a) how to transport the heat generated from the inside of the motor to the surface;
- (b) how to get rid of the heat at the surface.

Heat transport in small series motors is studied in chapter 6. It is found there that the temperature difference between the inside and the surface in small series motors is very small; so we are only left with the problem of how to remove the heat from the surface.

#### *Fixing of the laminations*

The laminations of the rotor are fixed on the shaft without the aid of a key. There is thus no key-way to interrupt the flux path through the rotor. The shaft can be used to conduct the stator flux.

### *Number and shape of rotor slots*

The number of rotor slots is small; generally 8 to 16. The rotor coils consist of many turns of thin wire that can fill up almost any shape of rotor slot; this gives freedom in choice of the shape of teeth and slots, when optimizing the motor.

### *Similarity relations*

It can be shown that the output power of a commutator motor is roughly proportional to  $d_r^4$ , if all the dimensions of the rotor are proportional to the rotor diameter  $d_r$ ; see e.g. Schuisky<sup>29</sup>). Schuisky remarks that this relation is not valid below about 4 kW. This problem is studied in sec. 7.7 for small commutator motors; it is found there that  $d_r^4$  should be replaced by  $d_r^5$  or  $d_r^{>5}$  in the low-power range in question.

### *Rotor field*

The small series motor does not require compensation coils or more than two stator poles, because the influence of the rotor field is limited. This can be shown as follows. If all the dimensions of the rotor are proportional to the rotor diameter  $d_r$ , and if we imagine the current density to be constant, the number of ampere turns of the rotor is  $U_{m r} \propto d_r^2$ .

If the width of the air gap is proportional to  $d_r$  and the magnetic induction in the rotor is constant, the number of ampere turns required for the stator will be  $U_{m s} \propto d_r$ . So

$$\frac{U_{m r}}{U_{m s}} \propto \frac{d_r^2}{d_r} = d_r.$$

If the air gap  $\delta$  is kept constant, we even have

$$\frac{U_{m r}}{U_{m s}} \propto d_r^{>1}.$$

### *Slot flux*

Because of the current through the wires in a rotor slot, lines of force enter or leave the sides of the teeth. The corresponding flux is relatively small, because the number of ampere wires in a slot is roughly proportional to  $d_r^2$ . Because the slots are semi-enclosed, the air-gap flux will almost completely pass through the teeth and not through the slots, so the slot flux is relatively small. Moreover, the rotor has only few, relatively wide teeth. That is why the magnetic flux through a tooth will have almost the same value in every cross-section.

### *Energy costs*

The cost of the total electrical energy required during the life of the small

series motor varies from about 15 Dutch cents (about 2 new pence, or 5 US \$ cents) for a coffee grinder up to about 40 Dutch guilders (about £5 or US \$ 12) for a vacuum cleaner. This is so little that it is not necessary to design small series motors with a high efficiency.

### *Skin effect*

Because the winding wire used for rotor and stator is generally much less than 0.5 mm in diameter, the influence of the skin effect of the current through the windings of rotor and stator can be neglected in practice. That is why e.g. slot pulsation losses under no-load conditions can also be neglected.

### **1.2. The choice of the type of stator**

In all cases considered in this section the rotor and the pole faces are identical.

Figures 1.1, 1.2 and 1.3 show three types of stator, referred to as types I, II and III from now on. In type I, the path for the lines of force passing the

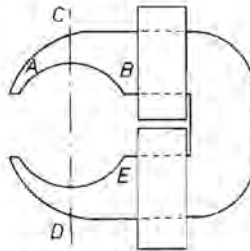


Fig. 1.1. Stator type I.

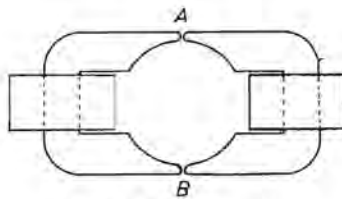


Fig. 1.2. Stator type II.

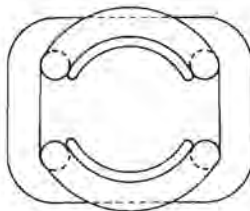


Fig. 1.3. Stator type III.

air gap at A is longer than for those passing at B, so the line CD will not be a line of magnetic symmetry. Especially if the circuit is saturated, the air-gap induction is concentrated at B and E. The level of asymmetry increases with the level of saturation. The angle between the neutral zones under both stator poles is not  $180^\circ$ , and moreover varies with the level of saturation. This causes commutation problems. Type I is however a good proposition if we want to use stator coils pre-wound on formers.

Type II is seldom used. The coils can only be fixed if the stator consists of two separate halves (preferably separated at A and B). The length of the stator turns is much less than in type III, but each coil requires as many ampere turns as both coils of type III together.

Type III is most widely used. It can be made with pre-wound coils, or the coils may be directly wound on the stator. It has a low stator leakage flux compared with types I and II.

Type III was chosen for this optimization calculation. However, the optimization method can easily be modified to make it suitable for type I or II.

Figures 1.4, 1.5, 1.6 and 1.7 show 4 variants of type III, which will be called types IV, V, VI and VII respectively.

Type IV requires a minimum of iron: if the stator stack were made lower, the right-hand and left-hand halves of the stator would be separated. This type

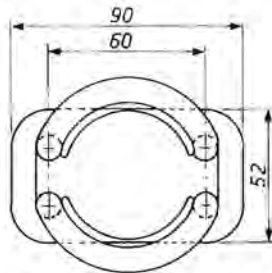


Fig. 1.4. Stator type IV.

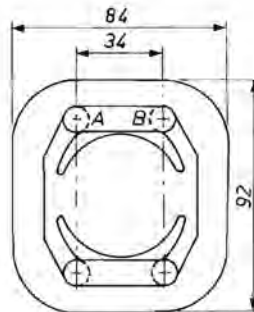


Fig. 1.5. Stator type V.

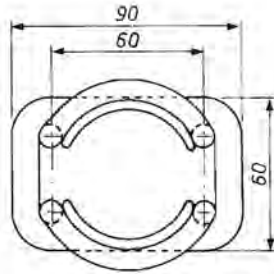


Fig. 1.6. Stator type VI.

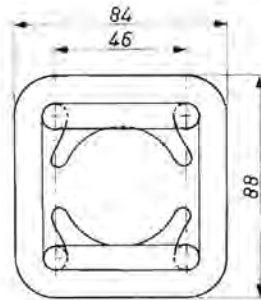


Fig. 1.7. Stator type VII.

requires a relatively large amount of copper. Type V requires a minimum of copper but a relatively large amount of iron. The cross-section AB is so wide that the stator flux can pass easily.

Type VI is a variant of type IV requiring more iron, and not much less copper. The total costs of copper and iron for type IV are in fact smaller than for type VI.

Type VII is a variant of type V requiring more copper, and not much less iron. The total costs of copper and iron for type V are less than for type VII. So if we imagine type IV to be progressively deformed to give type V, the costs of the stator will first increase and then decrease. The cheapest solution will be type IV or V but not one of the intermediate variants (like VI or VII).

Type V is only slightly narrower than type IV, but it is much higher. Type V has more stator leakage flux and this requires a wider cross-section locally. The coils of type V must be wound directly on the stator.

We have chosen type IV for the purposes of our optimization calculation, but as mentioned above the optimization method can also be modified to make it suitable for the other types.

### 1.3. Some important parameters

All the parameters used in the optimization calculation are listed in sec. 8.4.

In this section we shall introduce and briefly discuss the most important of these parameters.

Design calculations for a small commutator motor show that the rotor has the greatest influence on the behaviour and cost of the motor as a whole. It would therefore seem to be reasonable to start our description of the motor at the rotor. First of all we shall describe the shape of one rotor lamination.

As indicated in sec. 1.1 (slot flux), it can be assumed that the flux through a rotor tooth has about the same value at all heights. It has been established that optimum use is made of the materials of the rotor in this case if the rotor teeth have straight parallel sides. An optimized small commutator motor must thus have rotor teeth with straight parallel sides. All further considerations are based on this condition.

*The copper space factor  $k_{Cu r}$  and the fictive rotor diameter  $d$*

One of the parameters of the rotor is the space factor  $k_{Cu r}$  of the copper in the rotor slots. These slots cannot be filled with wire right up to the top, partly for mechanical reasons and partly in the interest of electrical safety. The slots are therefore generally filled up to a distance  $b_{23}$  from the periphery of the rotor (see fig. 1.8), this distance being more or less independent of the value of the rotor diameter  $d_r$  and the shape and dimensions of the slots.

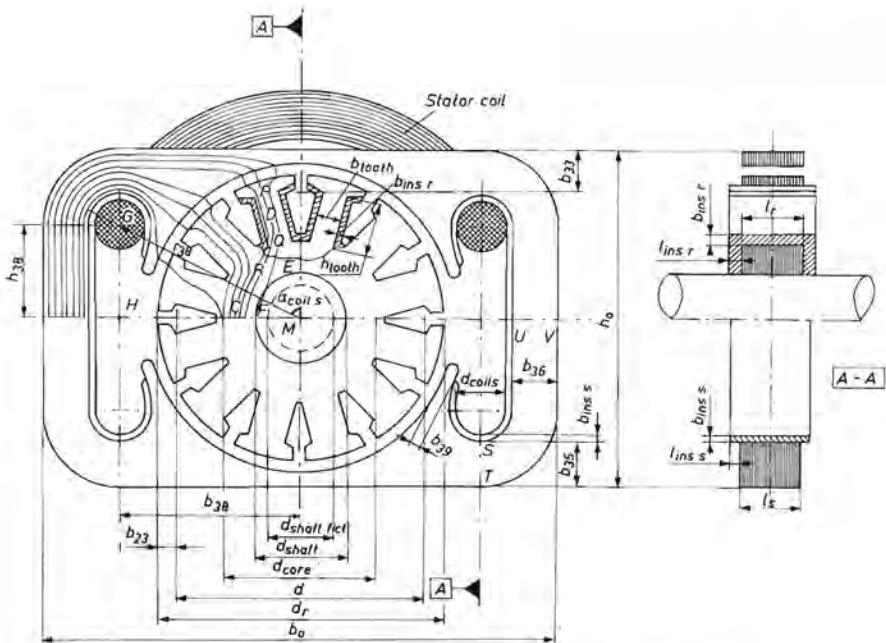


Fig. 1.8. A number of dimensions of a small series motor.



In an optimization calculation, we must take the width of the rotor tooth  $b_{\text{tooth}}$  as one of our variables. The cross-sectional area of the slots will then vary too; but the outside part of the slots, where there are no wires, will not behave in the same way. For a constant value of the rotor diameter  $d_r$ ,  $k_{\text{Cu } r}$  will thus depend on  $b_{\text{tooth}}$ .

In order to make  $k_{\text{Cu } r}$  an independent parameter, we define the fictive rotor diameter  $d$  as the diameter of the circle just fitting around the outermost wires in the slot:

$$d = d_r - 2 b_{2,3}. \quad (1.1)$$

Now  $k_{\text{Cu } r}$  can be defined for the net surface of the rotor slots within the fictive rotor diameter  $d$ ;  $k_{\text{Cu } r}$  can thus be considered as a practically independent parameter.

*The maximum magnetic induction  $B_{\text{max}}$  in the rotor*

The magnetic induction does not have the same value at every point of a rotor lamination. Figure 1.8 shows a number of lines of force. The highest induction in the teeth  $B_{\text{max tooth}}$  occurs near the centres of the pole faces, e.g. at point D. The highest induction in the core occurs at C. Moreover, in an AC motor the induction varies as a function of time. The peak values of  $B_{\text{max tooth}}$  and  $B_{\text{max core}}$  are denoted by  $B_{\text{peak tooth}}$  and  $B_{\text{peak core}}$ .

The stator does not fully surround the rotor. The reciprocal relative pole arc  $k_{\text{pole}}$  is introduced to take this into account:

$$k_{\text{pole}} = \frac{\pi}{\text{arc subtended by the stator pole, in radians}}. \quad (1.2)$$

$b_{\text{Fe teeth}}$  is the total width of the zone where the stator flux passes through the teeth. If  $z$  and  $b_{\text{tooth}}$  are the number of teeth and the width of a tooth respectively, then

$$b_{\text{Fe teeth}} = \frac{z b_{\text{tooth}}}{2 k_{\text{pole}}}. \quad (1.3)$$

$d_{\text{core}}$  is the diameter of the rotor core and  $d_{\text{shaft}}$  is the diameter of the shaft. If there is a good magnetic connection between shaft and laminations, part of the flux will pass through the shaft. The fictive shaft diameter  $d_{\text{shaft fct}}$  can now be defined on the basis of the following argument. Let us imagine that the flux in the shaft passes through an annular zone at the outside of the shaft so that the induction throughout this zone (F in fig. 1.8) will be equal to that at C, the induction in the rest of the shaft (of diameter  $d_{\text{shaft fct}}$ ) being zero. If  $b_{\text{Fe core}}$  is the width of the zone where the stator flux passes through the core, then

$$b_{\text{Fe core}} = d_{\text{core}} - d_{\text{shaft rict}} \quad (1.4)$$

With a rotating rotor, one would theoretically expect the flux to be partially forced out of the shaft by eddy currents. This problem is studied in sec. 3.4, where it is found that in rotor stacks comparable with the ones considered here, the flux through the rotor does not decrease as a result of rotation, with a shaft up to 10 mm in diameter and speeds up to 20 000 r.p.m. For the purposes of our problem we can thus conclude that the value of  $d_{\text{shaft rict}}$  is not influenced by rotation of the rotor in practice.

To determine the correct relation between  $B_{\text{max core}}$  and  $B_{\text{max tooth}}$  we must bear the following three points in mind.

- (a) As soon as the rotor becomes saturated, the number of ampere turns required per unit length of the lines of force in the rotor core increases extremely sharply with the magnetic induction.
- (b) The distance PQ (fig. 1.8) over which  $B_{\text{max tooth}}$  is found is roughly equal to the distance RC over which  $B_{\text{max core}}$  is found.
- (c) If  $b_{\text{Fe core}}$  is increased by e.g. 1% while the cross-sectional area of the slots is kept constant,  $b_{\text{Fe teeth}}$  must decrease by about 1%.

If conditions (b) and (c) are fully realized, optimum use will be made of the materials of the motor if  $B_{\text{max core}}$  and  $B_{\text{max tooth}}$  are equal. All our further considerations are therefore based on the conditions that

$$B_{\text{max core}} = B_{\text{max tooth}} = B_{\text{max}} \quad (1.5)$$

An incidental advantage is that the formulas used to describe the rotor are simplified by this equality.

*The relative flux-conducting rotor width  $\beta$  and the relative stack length  $\lambda$*

Now  $b_{\text{Fe r}}$  and  $\beta$  are defined by the following relation:

$$b_{\text{Fe teeth}} = b_{\text{Fe core}} = b_{\text{Fe r}} = \beta d \quad (1.6)$$

$\beta$  may be called the relative flux-conducting rotor width.

$l_r$  is the length of the rotor stack (excluding the insulation discs at both ends of the stack). We may define the relative stack length  $\lambda$  by

$$l_r = \lambda d \quad (1.7)$$

Note: in eqs (1.6) and (1.7), the fictive rotor diameter  $d$  is used instead of the real rotor diameter  $d_r$ .

*The magnetic flux  $\phi^{(1)}$  in terms of the other parameters*

The magnetic flux occurring in the formulas for torque and for rotational e.m.f. is called  $\phi^{(1)}$ ; this is the average flux enclosed by the turns of a rotor coil in the neutral position. Flux measurements described in sec. 3.4 show that

the flux passing through the slots beside the rotor core (in the region HC of fig. 1.8) can be almost neglected in practice compared with the flux passing through the core and the shaft. We may thus write:

$$\phi^{(1)} = l_r b_{Fe r} B_{max}. \quad (1.8)$$

With the aid of eqs (1.6), (1.7) and (1.8),  $\phi^{(1)}$  can now be written as

$$\phi^{(1)} = \beta \lambda d^2 B_{max}. \quad (1.9)$$

Note:  $B_{max}$  is defined for the cross-section of a stack, including the insulating layers between the laminations; the real magnetic induction in the iron is thus a little higher than  $B_{max}$ .

#### 1.4. Formulas for the resistance of the rotor

The rotational e.m.f. of a bi-polar commutator machine is given by the well-known formula

$$e = 2 n w_r \phi^{(1)}, \quad (1.10)$$

where  $n$  is the machine speed in revolutions per second and  $w_r$  is the number of rotor turns;  $\phi^{(1)}$  was defined at the end of sec. 1.3.

In commutator machines,  $e$  is partially short-circuited by the brushes. In machines having a commutator with many segments, the short-circuited part of  $e$  is almost negligible compared with  $e$ ; but in small machines with about 12 segments, it must be taken into account as is done here by means of the factor  $k_E$ :

$$e = 2 k_E n w_r \phi^{(1)}. \quad (1.11)$$

In large commutator machines  $k_E$  is about 1, but in small machines  $k_E$  is generally between 0.9 and 1. For a given machine,  $k_E$  can be considered as a constant.

Eliminating  $\phi^{(1)}$  from eq. (1.11) with eq. (1.8) gives

$$e = 2 k_E n w_r b_{Fe r} l_r B_{max}. \quad (1.12)$$

In an AC motor,  $B_{max}$  and  $e$  are not constant, but eqs (1.10), (1.11) and (1.12) hold for the instantaneous values of  $B_{max}$  and  $e$  too.

$R_r$ , the resistance of the rotor as seen between the brushes, is also partially short-circuited by the brushes. The factor  $k_R$  is introduced to take this into account:

$$R_r = \frac{\rho_{Cu r} k_R w_r s_{w r}}{4 a_{Cu r}}, \quad (1.13)$$

where  $s_{w r}$  is the average length of a rotor turn and  $a_{Cu r}$  is the cross-sectional area of the copper core of a rotor wire. The factor 4 appears in the denominator

of eq. (1.13) because the windings of the rotor are connected as two circuits in parallel. In large commutator machines,  $k_R$  (like  $k_E$ ) is about unity. In small commutator machines,  $k_R$  is about 0.8 to 1. For a given machine,  $k_R$  can be considered as a constant.

$A_{\text{slots } r}$  is the total cross-sectional area of all rotor slots within the fictive rotor diameter  $d$ . The slots are covered inside with an insulating layer of thickness  $b_{\text{ins } r}$ . The cross-sectional area of the coils  $A_{\text{coils } r}$  equals  $A_{\text{slots } r}$  less the cross-sectional area of the insulating layers. Now

$$k_{\text{Cu } r} A_{\text{coils } r} = 2 w_r a_{\text{Cu } r}. \quad (1.14)$$

Equation (1.14) also serves to define  $k_{\text{Cu } r}$ . As may be seen,  $k_{\text{Cu } r}$  refers to the copper cores of the winding wire, and not to the whole wire including its insulating layer.

Eliminating  $a_{\text{Cu } r}$  from eq. (1.13) with eq. (1.14) and eliminating  $w_r$  with eq. (1.12) we find

$$R_r = \frac{l}{8} \frac{\rho_{\text{Cu } r}}{k_{\text{Cu } r}} \frac{k_R}{B_{\text{max}}^2 k_E^2} \frac{s_{w r}}{A_{\text{coils } r} (b_{\text{Fe } r})^2 l_r^2 n^2} e^2. \quad (1.15)$$

As may be seen from fig. 1.8, each rotor turn consists of two straight parts of length  $l_r + 2 l_{\text{ins } r}$  and two end windings, the length of which can be called  $s_{\text{head } r}$ ;  $s_{\text{head } r}$  is about 0.6  $d$  for a rotor with 3 slots and about  $d$  for a small rotor with about 10 slots or more. We may thus write:

$$s_{w r} = 2 (l_r + 2 l_{\text{ins } r} + s_{\text{head } r}). \quad (1.16)$$

$k_{\text{ins head } r}$  and  $k_{\text{head } r}$  are defined by

$$l_{\text{ins } r} = k_{\text{ins head } r} d, \quad (1.17)$$

$$s_{\text{head } r} = k_{\text{head } r} d. \quad (1.18)$$

So

$$s_{w r} = 2 d (\lambda + 2 k_{\text{ins head } r} + k_{\text{head } r}). \quad (1.19)$$

Now the rotor function  $f_{(r)}$  is defined by

$$A_{\text{coils } r} = \frac{\pi}{4} d^2 f_{(r)}. \quad (1.20)$$

It follows from fig. 1.8 and from eqs (1.4) and (1.6) that

$$\begin{aligned} 2 h_{\text{tooth}} &= d - d_{\text{core}} = d - b_{\text{Fe } r} - d_{\text{shaft fict}} = \\ &= d - \beta d - d_{\text{shaft fict}}. \end{aligned} \quad (1.21)$$

$k_{\text{shaft}}$  and  $k_{\text{ins slots } r}$  are defined by

$$d_{\text{shaft fict}} = k_{\text{shaft}} d, \quad (1.22)$$

$$b_{\text{ins } r} = k_{\text{ins slots } r} d. \quad (1.23)$$

Now we may write  $A_{\text{colls } r}$  with the aid of eqs (1.3), (1.4), (1.6), (1.20), (1.21), (1.22) and (1.23) as

$$\begin{aligned} A_{\text{colls } r} &= \frac{\pi}{4} d^2 - \frac{\pi}{4} d_{\text{core}}^2 - z b_{\text{tooth}} h_{\text{tooth}} + \\ &\quad - (\pi d_{\text{core}} - z b_{\text{tooth}}) b_{\text{ins } r} - 2 z h_{\text{tooth}} b_{\text{ins } r} = \\ &= \frac{\pi}{4} d^2 \left[ (1 - \beta - k_{\text{shaft}}) \left( 1 + \beta + k_{\text{shaft}} - \frac{4}{\pi} \beta k_{\text{pole}} \right) + \right. \\ &\quad - 4 \left( \beta + k_{\text{shaft}} - \frac{2}{\pi} \beta k_{\text{pole}} \right) k_{\text{ins slots } r} + \\ &\quad \left. - \frac{4}{\pi} (1 - \beta - k_{\text{shaft}}) z k_{\text{ins slots } r} \right] = \\ &= \frac{\pi}{4} d^2 f_{(r)}. \end{aligned} \quad (1.24)$$

With the aid of eqs (1.6), (1.7), (1.19) and (1.20), we can rewrite eq. (1.15) as

$$R_r = \frac{1}{\pi} \frac{\rho_{\text{Cu } r}}{k_{\text{Cu } r} B_{\text{max}}^2 k_E^2} \frac{k_R k_{\text{head } r} + \lambda + 2 k_{\text{ins head } r}}{\lambda^2} \frac{1}{\beta^2 f_{(r)}} \frac{e^2}{n^2 d^5}, \quad (1.25)$$

where  $f_{(r)}$  satisfies eq. (1.24).

Equation (1.25) can also be written in the form

$$d^5 = \frac{1}{\pi} \frac{\rho_{\text{Cu } r}}{k_{\text{Cu } r} B_{\text{max}}^2 k_E^2} \frac{k_R k_{\text{head } r} + \lambda + 2 k_{\text{ins head } r}}{\lambda^2} \frac{1}{\beta^2 f_{(r)}} \frac{e^2}{R_r n^2}. \quad (1.26)$$

In the above, all the dimensions of the rotor were expressed in terms of the fictive rotor diameter  $d$ , with the aid of the parameters  $\lambda$ ,  $\beta$ ,  $k_{\text{head } r}$ ,  $k_{\text{ins head } r}$ ,  $k_{\text{ins slots } r}$ ,  $k_{\text{shaft}}$  and  $k_{\text{pole}}$ . In this way, the resistance of the rotor  $R_r$  can be expressed in terms of independent or almost independent parameters (eq. (1.25)). The influence of each of these independent parameters can now be studied separately; this is done in sec. 7.10. The use of the parameters  $\beta$  (the relative flux-conducting rotor width; see eq. (1.6)) and  $f_{(r)}$  (the rotor function; see eq. (1.20)) allow the influence of the copper and the iron on the resistance of the rotor to be separated; in the term  $1/\beta^2 f_{(r)}$  of eq. (1.25),  $\beta^2$  represents the contribution of the iron and  $f_{(r)}$  that of the copper.

### 1.5. Formulas for the resistance of the stator

The type of stator chosen for the optimization calculation was described in sec. 1.2, while fig. 1.8 shows a small series motor with such a stator. The flux through a pole horn falls when a slot opening passes the horn, and is maximum when no slot opening is opposite the horn face. The value of the magnetic induction in the horn should preferably not exceed the maximum rotor induction  $B_{\max}$ .

To meet this requirement, the horn width  $b_{39}$  (see fig. 1.8) should satisfy the inequality

$$b_{39} \geq 0.5 \beta d k_{\text{car}} \left( 1 - \frac{2 \alpha_{\text{coll } s} k_{\text{pole}}}{\pi} \right), \quad (1.27)$$

where  $k_{\text{car}}$  is the carter factor (studied in chapter 4) and  $\alpha_{\text{coll } s}$  is shown in fig. 1.8. If the pole horns are too narrow, the stator laminations cannot be stamped properly. The minimum horn width required for this purpose is denoted  $b_{39 \text{ min}}$ . In practice  $b_{39 \text{ min}}$  is about 2 mm if the thickness of the laminations is 0.5 mm. In small series motors,  $b_{39}$  calculated from eq. (1.27) is mostly smaller than  $b_{39 \text{ min}}$ ; we therefore give  $b_{39}$  a fixed value of 2 mm in the specimen optimization calculation of sec. 8.6.

$b_{35}$  and  $b_{36}$  are the widths of the cross-sections ST and UV respectively in fig. 1.8.  $b_{35}$  and  $b_{36}$  should be chosen so that the magnetic induction in the cross-sections ST and UV does not exceed  $B_{\max}$ . The factors  $k_{35}$  and  $k_{36}$  are defined by

$$b_{35} = 0.5 \beta d k_{35}, \quad (1.28)$$

$$b_{36} = 0.5 \beta d k_{36}. \quad (1.29)$$

Figure 1.9 shows that in a stator like that of fig. 1.8,  $k_{35}$  and  $k_{36}$  should both be about 1.1.

The two coils have together  $w_s$  turns, each coil having 0.5  $w_s$  turns. The cross-section of the coil in the slots is approximately a circle, of diameter  $d_{\text{coll } s}$ .

An average turn consists of two straight sections of length  $l_s + 2 l_{\text{ins } s}$  each, and approximately two arcs of a circle of radius  $r_{38}$  subtending an angle  $2 \alpha_{\text{coll } s}$  radians;  $r_{38}$  equals the distance GM. It may be deduced from fig. 1.8 that

$$h_{38} = 0.5 d + b_{33} - b_{35} - b_{\text{ins } s} - 0.5 d_{\text{coll } s}, \quad (1.30)$$

$$r_{38} = 0.5 d + b_{23} + \delta + b_{39} + b_{\text{ins } s} + 0.5 d_{\text{coll } s}, \quad (1.31)$$

$$\alpha_{\text{coll } s} = \cos^{-1} \frac{h_{38}}{r_{38}}. \quad (1.32)$$

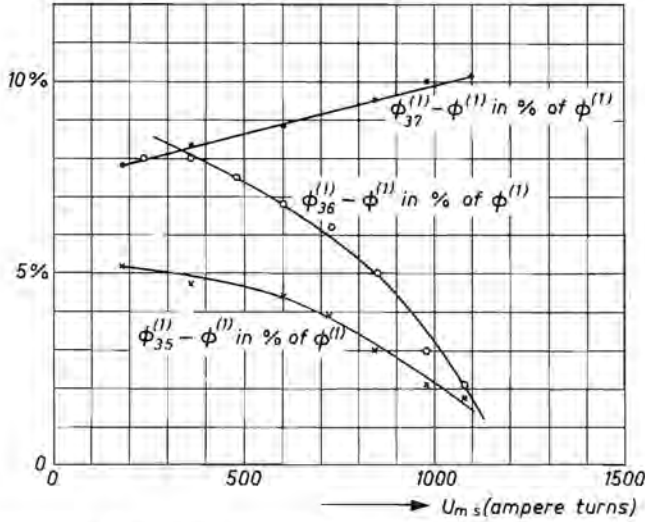


Fig. 1.9. The magnetic fluxes  $\phi_{37}^{(1)}$  (generated by the stator) and  $\phi_{35}^{(1)}$  and  $\phi_{36}^{(1)}$  (passing through the zones  $b_{35}$  and  $b_{36}$  in fig. 1.8), expressed as percentages of  $\phi^{(1)}$  for a motor with a stator like that of fig. 1.8 or fig. 1.4, as functions of the ampere turns of the stator.

The average length of a stator turn is

$$s_{w s} = 2 l_s + 4 l_{ins s} + 4 r_{38} \alpha_{coil s}. \quad (1.33)$$

The space factor of the stator coils is  $k_{Cu s}$ ; this refers to the copper core of the conductors, just like  $k_{Cu r}$ . The cross-sectional areas of a stator coil and of the core of one conductor are  $A_{coil s}$  and  $a_{Cu s}$  respectively:

$$a_{Cu s} = \frac{2 k_{Cu s} A_{coil s}}{w_s} = \frac{\pi k_{Cu s} (d_{coil s})^2}{2 w_s}. \quad (1.34)$$

The resistance of both coils together is

$$R_s = \frac{\rho_{Cu s} s_{w s} w_s}{a_{Cu s}} = \frac{2 \rho_{Cu s} s_{w s} w_s^2}{\pi k_{Cu s} (d_{coil s})^2}. \quad (1.35)$$

### 1.6. A simplified description of the motor

According to Kirchoff's second law, an idealized small series motor without saturation in the magnetic circuit satisfies

$$u - i(R_r + R_s) - L \frac{di}{dt} - e = 0, \quad (1.36)$$

where  $u$  is the instantaneous value of the terminal voltage,  $e$  is the instantaneous value of the rotational e.m.f. and  $L$  is the total inductance of the motor. The



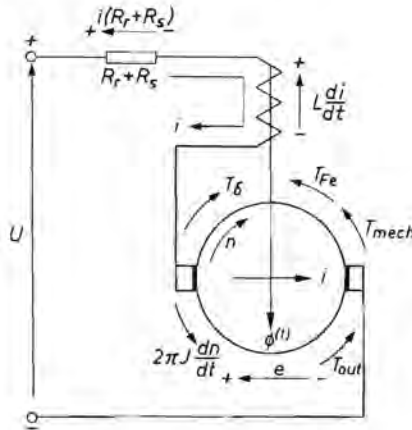


Fig. 1.10. Directions of current, speed, voltages and torques in the small series motor.

directions of all voltages, torques, the current and the speed are shown in fig. 1.10, where  $e$  satisfies

$$e = 2 n w_r \phi^{(1)}. \quad (1.37)$$

The balance of the torques gives:

$$T_\delta - T_{out} - T_{Fe} - T_{mech} - 2 \pi J \frac{dn}{dt} = 0, \quad (1.38)$$

where  $T_\delta$ ,  $T_{out}$ ,  $T_{Fe}$  and  $T_{mech}$  are the instantaneous values of the air-gap torque, output torque, iron-loss torque and mechanical-loss torque respectively;  $J$  is the moment of inertia of the rotor and other coupled masses. Multiplying eq. (1.36) and (1.38) by  $i$  and  $2 \pi n$  respectively, we find for the balance of electrical and mechanical power respectively

$$u i - i^2 (R_r + R_s) - L i \frac{di}{dt} - e i = 0, \quad (1.39)$$

$$p_\delta - p_{out} - p_{Fe} - p_{mech} - 4 \pi^2 J n \frac{dn}{dt} = 0. \quad (1.40)$$

Equations (1.39) and (1.40) are coupled by the terms  $e i$  and  $p_\delta$ , both of which equal the internal power or air-gap power.

According to eqs (1.37), (1.39) and (1.40)

$$e i = 2 n w_r \phi^{(1)} i = p_\delta = 2 \pi n T_\delta, \quad (1.41)$$

or

$$T_\delta = \frac{w_r \phi^{(1)} i}{\pi}. \quad (1.42)$$

The imperfections of the simplified description just described are summed up in sec. 1.7.

### 1.7. Imperfections of the simplified description

The simplified description of sec. 1.6 can be used to give a rough impression of the properties and behaviour of a small series motor, but it is not good enough to serve as basis for the optimization of such a motor.

The most important imperfections of the simplified model are discussed below. A more refined treatment of the first 5 points is given separately in chapters 2 to 6.

Nowadays, the DC version of the small series motor is hardly worth discussion. Moreover, all details of this case can be derived from the description of the small AC series motor. We can thus limit our considerations to the small AC series motor, as is done below.

#### *Saturation*

The magnetic induction in a small series motor is so high that the magnetic circuit will be saturated. The inductance  $L$  will thus be variable, so that the simplified equations (1.36) and (1.39) are no longer strictly applicable. Moreover, hysteresis is neglected. The magnetic flux and the current through the motor do not vary sinusoidally with time, but are distorted. Under these conditions, it is difficult to calculate the torque and the copper losses.

The effects of saturation are investigated in chapter 2. It is found to be possible to express the influence of the saturation level on the torque and copper losses by means of the torque distortion factor  $c_{mech}$  and the current distortion factor  $c_e$  respectively, which can be calculated from the motor parameters.

#### *Commutation*

The basic equation (1.36) tells us nothing about the quality of the commutation; this must be described separately. In a given motor, all the voltages and resistances influencing the current in the commutating coil can be calculated, at least approximately; but the active inductance of the commutating coil cannot be measured or calculated without a very careful study. The active inductance is discussed in chapter 5.

#### *Carter factor*

The influence of the slot apertures on the permeance of the air gap is represented by the carter factor  $k_{car}$ . The value of  $k_{car}$  can easily be calculated for rectangular rotor slots, but the rotor of a small commutator machine generally has semi-enclosed slots. For such machines,  $k_{car}$  is studied in chapter 4.

#### *Temperature rise*

The formulas of sec. 1.6 do not give any information about the temperature rise in the motor. However, it is important to limit the temperature rise, in order to ensure long life of the motor parts, safety and good commutation.

An optimization calculation must include determination of the temperature rise as a function of the parameters of the motor.

In chapter 6 this problem will be studied for small commutator machines.

### *Iron losses*

The formulas of sec. 1.6 do not give any information about the iron losses in the motor. However, an optimization calculation must also include the calculation of the iron losses as a function of the parameters of the motor. This question is studied in chapter 3.

### *The influence of short-circuiting of rotor coils by the brushes*

At any given moment, some of the rotor coils of a commutator machine will be short-circuited by the brushes. The real rotor resistance will thus be smaller than the theoretical value. Moreover, the rotational e.m.f. in the short-circuited rotor coils is generally non-zero. The real rotational e.m.f. generated will thus be smaller than the theoretical value. In small commutator machines these phenomena cannot be neglected, because the number of rotor coils is so small. In sec. 1.4 these two phenomena were taken into account by the factors  $k_R$  and  $k_E$ .

### *Rotor field*

In a real motor, neither the rotor field nor the corresponding inductance can be neglected. Moreover, these two variables depend on the position of the brushes and the instantaneous position of the rotor.

### *Magnetic coupling of inductances*

There is a magnetic coupling between the inductances of the rotor and stator coils, because in general the brushes are not situated in their neutral position.

### *Flux pulsation due to rotor slotting*

The slot apertures of the rotor influence the reluctance of the air gap, so that this reluctance and hence the flux through the rotor and stator coils varies with the position of the rotor. This flux variation is only small, but its frequency is high ( $nz$  if  $z$  is even and  $2nz$  if  $z$  is odd, where  $n$  is the rotor speed and  $z$  is the number of rotor slots); the voltage induced by it cannot thus be neglected. During commutation, the coupling of a rotor coil with this flux pulsation is maximum, so this voltage has maximum influence in this position too. Such a transformer e.m.f. due to rotation is known to have a very bad effect on commutation. This phenomenon was studied e.g. by Schröter<sup>28)</sup> and Pöllot<sup>27)</sup>. Schröter describes a method of calculating the flux variation with and without saturation. Pöllot gives three ways of attacking the problem in practice. If  $z$  is

odd, the e.m.f. is found to be smaller than if  $z$  is even. The flux variation is completely suppressed if the rotor stack is skewed by exactly one tooth pitch. A cheap but adequate solution is to widen the air gap at the end of the pole horns by an appropriate amount and to make the pole horns so wide that they are not saturated. In this way the flux variation can be made negligible at any level of saturation in the motor.

#### *Dynamic eccentricity of the rotor*

The circumference of the rotor is not exactly circular and its centre does not lie exactly on the line joining the centres of the holes in which the bearings are fixed. This too causes a variation in the reluctance of the air gaps and hence generation of a voltage. This influence is generally negligible, particularly because the frequency of the flux variation is low ( $2n$ , where  $n$  is the motor speed).

#### *Static eccentricity of the rotor*

If the rotor is not situated symmetrically in the bore of the stator, a radial magnetic force exists between rotor and stator. This causes radial forces in the bearings and also extra wear and power losses. In a small series motor with rotor length  $l_r = 25$  mm, rotor diameter  $d_r = 40$  mm and air-gap induction  $B_g = 0.6$  Wb/m<sup>2</sup>, this force may be up to 200 N in practice.

#### *Brush losses*

The resistance between the brushes and the commutator is known to be variable. Moreover, the corresponding current is divided between two or more paths by the brushes. It is thus not easy to describe the losses in the brushes and in the contact resistances. These losses are not taken into account in eqs (1.36) and (1.39). If desired, they can be approximated to by introducing a fixed brush resistance  $R_{\text{brush}}$ .

### **1.8. Optimization**

There are many different ways of defining an optimum motor. However, in the consumer-products industry, there is one very important optimum: the cheapest motor that satisfies all the specifications.

Table 1-I shows a rough breakdown of the costs of a small bi-polar AC series commutator motor without compensation coils or commutating poles. The output power is about 300 W at 18 000 r.p.m. The costs are shown as percentages of the total cost, which might be about Hfl. 10,— (10 Dutch guilders).

The first two columns are for a motor that has been rather arbitrarily designed without the aid of an optimization calculation. The costs of winding wire in rotor and stator are denoted by  $C_{\text{Cu r}}$  and  $C_{\text{Cu s}}$ . The costs of the steel

TABLE 1-I

Comparison of the costs of an optimized and a non-optimized small series motor with an output power of about 300 W at 18 000 r.p.m.

rough prices as percentages of the total cost of the non-optimized motor						
	non-optimized		optimized		sav-ings in $C_o$	saving in other costs
	$C_a = C_{Cu r} + C_{Cu s} + C_{Fe} + C_{stamp}$		$C_o = C_{Cu r} + C_{Cu s} + C_{Fe} + C_{stamp}$			
materials and parts						
steel sheet	5.5	5.5	3.5	3.5	2	
rotor winding wire	4	4	2.5	2.5	1.5	
stator winding wire	3.5	3.5	2	2	1.5	
shaft	2		1.8			0.2
bearings	18		18			
commutator	10		10			
brushes	3.5		3.5			
brush holders	5		5			
housing	8		7			1
impregnation lacquer	1		0.8			0.2
insulating parts	1		0.8			0.2
interference suppressors	8		8			
various small parts	6		6			
	75.5	13	68.9	8	5	1.6
manufacturing costs						
stamping the laminations	3.5	3.5	2	2	1.5	
winding the rotor	1		0.9			0.1
winding and fixing the stator coils	1.5		1.3			0.2
miscellaneous	18.5		18.5			
	24.5	3.5	22.7	2	1.5	0.3
total costs	100	16.5	91.6	10	6.5	1.9

sheet required and the costs of stamping it are  $C_{Fe}$  and  $C_{stamp}$ . The “over-all variable costs”  $C_o$  are now defined as

$$C_o = C_{Cu r} + C_{Cu s} + C_{Fe} + C_{stamp}. \quad (1.43)$$

For this non-optimized motor,  $C_o$  is about 16.5% of the total cost of the motor. Nowadays, the cost of winding the rotor and the stator is hardly influenced by the required number of turns. The winding costs are therefore not considered as part of  $C_o$  but of the other costs.

In the optimized version,  $C_o$  decreases by about 40%, from 16.5 to 10%, but the total cost of the motor decreases only by about 8.4% — from 100 to 91.6%.

In chapter 8, a method is developed for calculation of the lowest possible value of the over-all variable costs  $C_o$ . It is very difficult to calculate the variation of the other costs of table 1-I when the motor parameters are varied. However, we may state that if  $C_o$  is minimum, the dimensions of rotor and stator will be roughly minimum too, and so will the other costs. We therefore define an optimal motor as: a motor that satisfies all the specifications with the lowest possible value of the over-all variable costs  $C_o$ .

Note: In some cases the costs not included in  $C_o$  may also be strongly influenced by the dimensioning. For example:

- (1) because of incorrect dimensioning, commutation may be so bad that more rotor coils and a commutator with more segments are required;
- (2) because of incorrect dimensioning, the radio interference caused by the motor may be so high that more interference suppression is needed.

## 1.9. Conclusions

The most important parameters of a small AC series motor are the fictive rotor diameter  $d$ , the relative flux-conducting rotor width  $\beta$  and the relative stack length  $\lambda$ . The fictive rotor diameter  $d$  is defined in such a way that the space factor  $k_{Cu r}$  of the copper in the rotor slots is more or less independent of the dimensions of the slots and can generally be considered as a constant. An optimum motor satisfies the following two conditions:

- (a) The rotor teeth have straight parallel sides.
- (b) The maximum induction in the rotor teeth  $B_{max\ tooth}$  is approximately equal to the maximum induction in the rotor core,  $B_{max\ core}$ .

The shape of a rotor lamination is almost entirely determined by these two conditions. Similarly, the copper-iron ratio of the rotor is almost entirely determined by  $\beta$ , the relative flux-conducting rotor width (see sec. 1.3).

In secs 1.4 and 1.5, the rotor resistance  $R_r$  and the stator resistance  $R_s$  are expressed in terms of the motor parameters. Equation (1.26) derived from the expression for  $R_r$  is a very important rotor-dimensioning formula. It is analyzed in sec. 7.10. Finally, an optimum motor is defined in sec. 1.8 as:

A motor satisfying all the specifications with the lowest possible over-all variable costs  $C_o = C_{Cu\ r} + C_{Cu\ s} + C_{Fe} + C_{stamp}$ , where  $C_{Cu\ r}$  and  $C_{Cu\ s}$  are the costs of the winding wire in the rotor and stator,  $C_{Fe}$  is the cost of the steel sheet required and  $C_{stamp}$  is the cost of stamping this steel sheet.



## 2. SATURATION IN SMALL SERIES MOTORS

The magnetic circuit of small AC series motors may be saturated; the current, flux, rotational e.m.f. and transformer e.m.f. may thus be non-sinusoidal. To be able to calculate the internal power and the power losses in the rotor resistance  $R_r$  and the stator resistance  $R_s$ , we must know the exact forms of the flux  $\phi^{(1)}$  and the current  $i$ .

First, the relation between  $\phi^{(1)}$  and  $i$  must be known. This relation is substituted into the electrical differential equation of the small series motor, which can then be solved to give  $i$  and  $\phi^{(1)}$  as functions of time. Finally, the influence of  $i$  and  $\phi^{(1)}$  on the power losses in  $R_r$  and  $R_s$  and on the internal power must be described in such a way that it can be mathematically incorporated in the optimization calculation.

### 2.1. The normalized magnetization curve

For low values of the magnetic induction, the reluctance of both air gaps together is large compared with the reluctance of the rest of the magnetic circuit of a small series motor. The beginning of the magnetization curve is therefore almost linear. As the current  $i$  increases, the slope of the curve decreases until finally the curve is almost linear again.

If the two linear portions of the curve are extrapolated, they will intersect somewhere above the knee. If the coordinate system is now transformed so that the coordinates of the point of intersection become (1;1), we obtain the normalized magnetization curve of the small series motor.

The abscissa of the normalized magnetization curve, the normalized m.m.f., is denoted by  $j$ ; the ordinate is  $f_{(j;m)}$ , the normalized flux.

The normalized magnetization curves of all small series motors show a high degree of similarity. The knee begins at about  $j = 0.65$ ;  $f_{(j;m)}$  is about 0.85 at  $j = 1$ , and the knee ends at about  $j = 1.85$ . The tangent of the angle which the right-hand linear portion of the curve makes with the horizontal axis is denoted by  $m$ . This quantity ranges from about 0.08 to about 0.16 for small series motors, the average value being about 0.12. The value of  $m$  increases with the length of the air gap.

$f_{(j;m)}$  must be described mathematically if it is to be introduced into a computer programme. It is possible to describe  $f_{(j;m)}$  as a polynomial as has been done e.g. by Lawrenz <sup>26</sup>). It is then easy to calculate  $f_{(j;m)}$  for a given value of  $j$ , but not to calculate  $j$  for a given value of  $f_{(j;m)}$ , as must be done in the optimization calculation. We therefore decided to use the following linear approximation for  $f_{(j;m)}$ :

$$\begin{aligned}
 j < -1.85: & f_{(j;m)} = -1 + m(j + 1), \\
 -1.85 \leq j < -1.35: & f_{(j;m)} = -1 + 1.7m(j + 1.35), \\
 -1.35 \leq j < -1: & f_{(j;m)} = -0.86 + 0.4(j + 1), \\
 -1 \leq j < -0.65: & f_{(j;m)} = -0.65 + 0.6(j + 0.65), \\
 -0.65 \leq j < 0.65: & f_{(j;m)} = j, \\
 0.65 \leq j < 1: & f_{(j;m)} = 0.65 + 0.6(j - 0.65), \\
 1 \leq j < 1.35: & f_{(j;m)} = 0.86 + 0.4(j - 1), \\
 1.35 \leq j < 1.85: & f_{(j;m)} = 1 + 1.7m(j - 1.35), \\
 1.85 \leq j & : f_{(j;m)} = 1 + m(j - 1).
 \end{aligned} \tag{2.1}$$

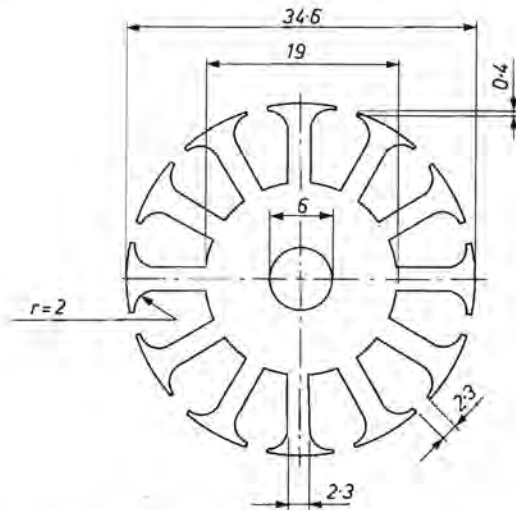


Fig. 2.1. Shape and dimensions of the rotor laminations of a small series motor, considered in fig. 2.3.

Figure 2.3 shows the experimental curve for  $f_{(j;m)}$  and the approximation of eq. (2.1) for an arbitrarily chosen small series motor, of which are sketched the rotor and stator laminations in figs 2.1 and 2.2.

$f_{(j;m)}$  was also measured for 5 other small series motors with quite different shapes, some with various air-gap lengths. For none of the measured motors and for no value of  $j$  up to 2.5 did  $f_{(j;m)}$  differ by more than 0.04 from the approximation given by eq. (2.1). The accuracy of this approximation is thus quite sufficient for an optimization calculation.

Equation (2.1) also deals with negative values of  $j$  and  $f_{(j;m)}$ ; it is thus suitable for use with DC motors as well as AC motors.

Equation (2.1) has only one parameter:  $m$ . The value of  $m$  for a motor in the design state can be estimated, but the exact value of  $m$  can only be measured on a real motor. One way out of this problem is to choose  $m = 0.12$  initially for all optimization calculations. When a prototype model of the motor

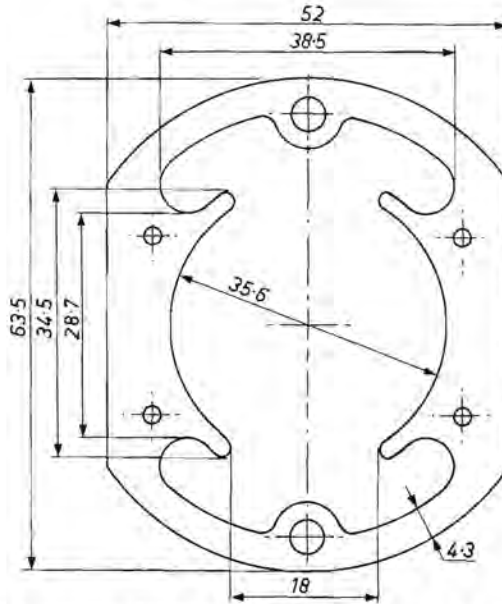


Fig. 2.2. Shape and dimensions of the stator laminations of a small series motor, considered in fig. 2.3.

is made, the real value of  $m$  can be measured. If the measured value of  $m$  differs too much from the estimated value, the optimization calculation must be repeated. In practice, this will hardly ever be necessary. The optimum value of the peak magnetic induction  $B_{\text{peak}}$  is generally so low that the influence of  $m$

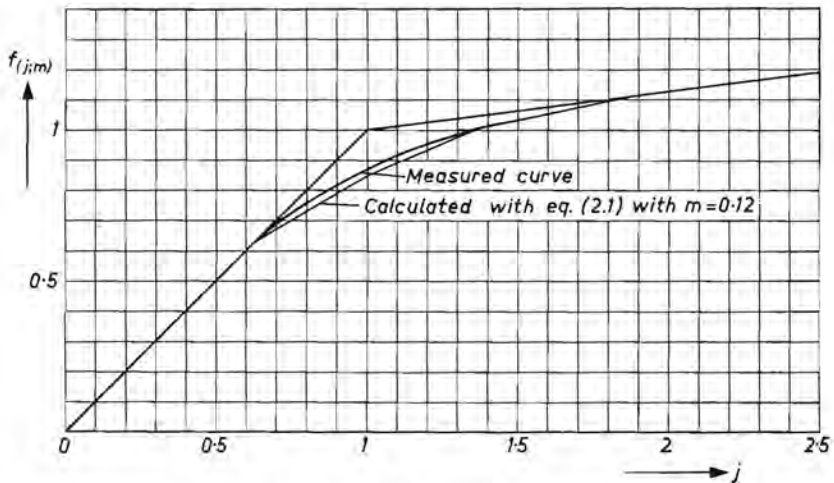


Fig. 2.3. Measured and calculated normalized magnetization curves of a small series motor with rotor and stator laminations as in figs 2.1 and 2.2, respectively.

is small. In the specimen calculation of sec. 8.6, it is found that the results do not change noticeably when  $m$  is varied from 0.10 to 0.14.

Finally the over-all m.m.f.  $u_{m\ o}$  and the flux  $\phi^{(1)}$  must be expressed in terms of  $j$  and  $f_{(j;m)}$  respectively.

The total reluctance of the two air gaps is

$$R_{m\ 2\delta} = \frac{4\ \delta\ k_{\text{pole}}\ k_{\text{car}}}{\pi\ \mu_o\ l_r\ d_r} \quad (2.2)$$

The length of the flux path of the magnetic circuit where the induction is  $B_{\text{max}}$  is about  $3\ d$ . The reluctance calculated along this path is

$$R_{m\ Fe} = \frac{3\ d}{\mu_r\ \mu_o\ \beta\ d\ l_r} = \frac{3}{\mu_r\ \mu_o\ \beta\ l_r} \quad (2.3)$$

The permeance of the complete circuit is

$$A_{m\ o} = \frac{1}{R_{m\ 2\delta} + R_{m\ Fe}} = \frac{R_{m\ 2\delta}}{R_{m\ 2\delta} + R_{m\ Fe}} A_{m\ 2\delta} = c_{41} A_{m\ 2\delta} \quad (2.4)$$

Equation (2.4) also serves to define the correction factor  $c_{41}$ . It follows from eqs (2.2), (2.3) and (2.4) that

$$c_{41} = \frac{4\ \delta\ k_{\text{pole}}\ k_{\text{car}}\ \beta\ \mu_r}{4\ \delta\ k_{\text{pole}}\ k_{\text{car}}\ \beta\ \mu_r + 3\ \pi\ d_r} \quad (2.5)$$

In practice,  $c_{41}$  is found to be about 0.9, as long as no saturation occurs. If we denote the angle through which the brushes are turned against the direction of rotation of the rotor by  $\alpha_{\text{brush}}$ , then the longitudinal component of the number of ampere turns of the rotor is  $i\ w_r\ \alpha_{\text{brush}}/\pi$ . The net number of ampere turns generating  $\phi^{(1)}$  is thus

$$u_{m\ o} = i \left( w_s - \frac{w_r\ \alpha_{\text{brush}}}{\pi} \right) \quad (2.6)$$

$B_{\text{prop}}$  is the value of  $B_{\text{max}}$  above which  $\phi^{(1)}$  is no longer proportional to  $u_{m\ o}$ .

In the normalized magnetization curve, this corresponds to  $j = f_{(j;m)} = 0.65$ . Now eq. (1.8) can be written:

$$\phi^{(1)}_{\text{prop}} = l_r\ b_{Fe\ r}\ B_{\text{prop}} = \beta\ d\ l_r\ B_{\text{prop}} \quad (2.7)$$

For  $j < 0.65$  and writing  $1/0.65 = 1.5$  we find:

$$\phi^{(1)} = 1.5\ \beta\ d\ l_r\ B_{\text{prop}}\ j \quad (2.8)$$

If values of  $j > 0.65$  and  $j < -0.65$  must also be considered,  $j$  must be replaced by  $f_{(j;m)}$ . In general, therefore,

$$\phi^{(1)} = 1.5\ \beta\ d\ l_r\ B_{\text{prop}}\ f_{(j;m)} \quad (2.9)$$

This is the desired expression for  $\phi^{(1)}$  in terms of  $f_{(j,m)}$ .

If  $B_{\max} = B_{\text{prop}}$ ,  $u_{m\ o} = u_{m\ \text{prop}}$ ; it follows that

$$u_{m\ \text{prop}} = \frac{\phi^{(1)}_{\text{prop}}}{\Lambda_{m\ o}} = \frac{\beta d l_r B_{\text{prop}}}{\Lambda_{m\ o}}. \quad (2.10)$$

For every value of  $j$ ,  $u_{m\ o}$  is proportional to  $j$ . If  $j = 0.65$ ,  $B_{\max} = B_{\text{prop}}$ , so

$$u_{m\ o} = \frac{\beta d l_r B_{\text{prop}}}{\Lambda_{m\ o}} \frac{j}{0.65} = \frac{1.5 \beta d l_r B_{\text{prop}}}{\Lambda_{m\ o}} j. \quad (2.11)$$

This is the desired expression for  $u_{m\ o}$  in terms of  $j$ .

Equations (2.6) and (2.11) can be combined to give

$$i = \frac{1.5 \beta d l_r B_{\text{prop}}}{\Lambda_{m\ o} (w_s - w_r \alpha_{\text{brush}}/\pi)} j. \quad (2.12)$$

In eqs (2.11) and (2.12),  $\Lambda_{m\ o}$  satisfies eq. (2.4).

## 2.2. The normalized electrical differential equation

Equation (1.36) is the general electrical differential equation of a non-saturated small series motor. If the magnetic circuit is saturated,  $L di/dt$  must be replaced by  $d\phi/dt$ :

$$u - i(R_r + R_s) - \frac{d\phi}{dt} - e = 0, \quad (2.13)$$

where  $e$  is the rotational e.m.f. and  $d\phi/dt$  is the total of other e.m.f.s, including the transformer e.m.f. We shall now normalize this equation with the aid of the parameters of the normalized magnetization curve.

The magnetic fields in the motor are generated by the currents through the rotor and stator coils. The stator coils have a total of  $w_s$  turns, through each of which a current  $i$  flows. The rotor coils have a total of  $w_r$  turns, connected in parallel in two circuits each with  $w_r/2$  turns. A current  $i/2$  flows through

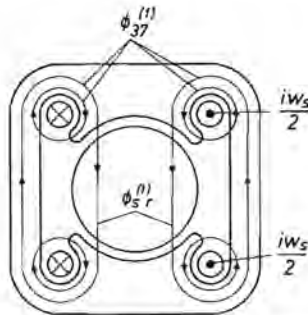


Fig. 2.4. Magnetic lines of force generated by  $u_{m\ s}$ .

each circuit. The rotor turns can thus be considered as one circuit with  $w_r/2$  turns, through which a current  $i$  flows.

The number of ampere turns of the stator is

$$u_{m\ s} = i w_s; \tag{2.14}$$

$u_{m\ s}$  generates a flux  $\phi^{(1)}_{37}$ , of which a part  $\phi^{(1)}_{s\ r}$  passes through the rotor in a direction parallel to the polar axis (see fig. 2.4).  $\phi^{(1)}_{37}$  can be expressed as

$$\phi^{(1)}_{37} = c_{37} \phi^{(1)}_{s\ r}. \tag{2.15}$$

As may be seen from fig. 1.9,  $c_{37}$  is about 1.1 for a stator like that of fig. 1.8 or fig. 1.4. The brushes are turned against the direction of rotation of the rotor through an angle  $\alpha_{brush}$ . The flux generated by the rotor can thus be resolved into a component  $\phi^{(1)}_{r\ s}$ , parallel to the polar axis, and a component  $\phi^{(1)}_{r\ perp}$  perpendicular to the polar axis.  $\phi^{(1)}_{r\ s}$  is always in anti-phase with  $\phi^{(1)}_{s\ r}$  (see figs 2.4 and 2.5). The number of ampere turns generating  $\phi^{(1)}_{r\ s}$  is written  $u_{m\ r\ par}$ .

$$u_{m\ r\ par} = \frac{w_r}{2} \frac{2 \alpha_{brush}}{\pi} i = \frac{\alpha_{brush}}{\pi} i w_r. \tag{2.16}$$

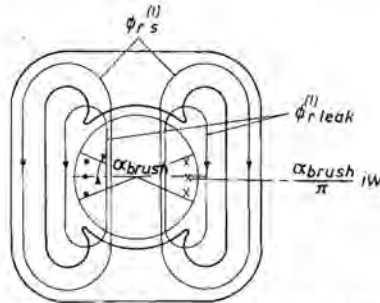


Fig. 2.5. Magnetic lines of force generated by  $u_{m\ r\ par}$ .

The leakage flux  $\phi^{(1)}_{r\ leak}$  due to  $u_{m\ r\ par}$  is neglected in the calculations, because in practice  $\phi^{(1)}_{r\ leak} \ll \phi^{(1)}_{r\ s} \ll \phi^{(1)}_{s\ r}$ . The number of ampere turns generating  $\phi^{(1)}_{r\ perp}$  is written  $u_{m\ r\ perp}$  (see fig. 2.6):

$$u_{m\ r\ perp} = \frac{w_r}{2} \left( 1 - \frac{2 \alpha_{brush}}{\pi} \right) i = \left( \frac{1}{2} - \frac{\alpha_{brush}}{\pi} \right) i w_r. \tag{2.17}$$

Note: the sum of  $u_{m\ r\ par}$  and  $u_{m\ r\ perp}$  equals  $i w_r/2$ ;

$w_s$  surrounds  $\phi^{(1)}_{37}$  and  $\phi^{(1)}_{r\ s}$ ;  $w_{r\ par}$  surrounds  $\phi^{(1)}_{s\ r}$  and  $\phi^{(1)}_{r\ s}$ ;

$w_{r\ perp}$  partially surrounds  $\phi^{(1)}_{r\ perp}$ ;

so  $w_s$  and  $w_{r\ par}$  are magnetically coupled by  $\phi^{(1)}_{r\ s}$  and  $\phi^{(1)}_{r\ par}$ , but

$w_{r\ perp}$  is not coupled with  $w_s$ , nor with  $w_{r\ par}$ .

In the absence of saturation,

$$\phi_{s r}^{(1)} = A_{m o} u_{m s} = c_{41} A_{m 2 \delta} i w_s, \quad (2.18)$$

where  $c_{41}$  is as defined in eq. (2.4);

$$\phi_{37}^{(1)} = c_{37} \phi_{s r}^{(1)} = c_{37} c_{41} A_{m 2 \delta} i w_s; \quad (2.19)$$

$$\phi_{r s}^{(1)} = A_{m o} u_{m r \text{ par}} = c_{41} A_{m 2 \delta} \frac{\alpha_{\text{brush}}}{\pi} i w_r. \quad (2.20)$$

Since the direction of  $\phi_{r s}^{(1)}$  is opposite to that of  $\phi_{s r}^{(1)}$ , the total flux parallel to the polar axis will be

$$\begin{aligned} \phi_{\text{par}} &= w_s (\phi_{37}^{(1)} - \phi_{r s}^{(1)}) - \frac{\alpha_{\text{brush}}}{\pi} w_r (\phi_{s r}^{(1)} - \phi_{r s}^{(1)}) = \\ &= c_{41} A_{m 2 \delta} i \left( c_{37} w_s^2 - \frac{2 \alpha_{\text{brush}}}{\pi} w_r w_s + \frac{(\alpha_{\text{brush}})^2}{\pi^2} w_r^2 \right). \end{aligned} \quad (2.21)$$

The total flux perpendicular to the polar axis can be calculated by consideration of the magnetic energy  $W_{\text{perp}}$  generated by  $u_{m r \text{ perp}}$ . Since

$$W_{\text{perp}} = \frac{1}{2} L_{\text{perp}} i^2 = \frac{1}{2} i (L_{\text{perp}} i) = \frac{1}{2} i \phi_{\text{perp}}, \quad (2.22)$$

it follows that

$$\phi_{\text{perp}} = \frac{2 W_{\text{perp}}}{i}. \quad (2.23)$$

In the absence of saturation,  $W_{\text{perp}}$  is equal in practice to the air-gap energy  $W_{\delta}$ , generated by  $u_{m r \text{ perp}}$ . The value of  $W_{\delta}$  is found by integrating  $B_{\delta}^2/2 \mu_0$  over the volume of both air gaps, where  $B_{\delta}$  is the air-gap induction.

The rotor slots carry  $2 w_r$  wires, through each of which a current  $i/2$  flows. Let us imagine that these ampere wires are evenly distributed around the circumference of the rotor; the number of ampere wires per radian will thus be  $i w_r/2\pi$ .

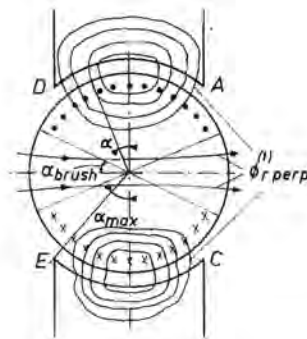


Fig. 2.6. Magnetic lines of force generated by  $u_{m r \text{ perp}}$ .

Figure 2.6 shows some lines of force generated by  $u_{m r \text{ perp}}$ . A line of force crossing the air gap (shown in fig. 2.6) at an angle  $\alpha$  surrounds  $(i w_r / 2\pi) 2\alpha = i w_r \alpha / \pi$  ampere wires.

If the reluctance of the iron of rotor and stator through which these lines of force pass is neglected, we may write:

$$2 \delta B_x = \frac{\mu_o i w_r \alpha}{\pi} \quad (2.24)$$

or

$$B_x = \frac{\mu_o i w_r \alpha}{2 \pi \delta}; \quad (2.25)$$

$B_x$  is the air-gap induction at angle  $\alpha$  and  $\delta$  is the air-gap length. The flux leaving the rotor between A and C and entering between D and E in fig. 2.6 is neglected compared with the flux crossing the air gap.

If the carter factor  $k_{car}$  is also taken into consideration,  $W_{perp}$  is approximately equal to

$$\begin{aligned} W_{perp} &= \frac{4}{k_{car}} \int_0^{\alpha_{max}} \frac{B_x^2}{2 \mu_o} \delta l_r \frac{d_r}{2} d\alpha = \\ &= \frac{\mu_o i^2 w_r^2 l_r d_r}{12 \pi^2 \delta k_{car}} \alpha^3 \Big|_0^{\alpha_{max}} \end{aligned} \quad (2.26)$$

$$\text{Since } 2 \alpha_{max} = \frac{\pi}{k_{pole}}$$

$$\alpha_{max} = \frac{\pi}{2 k_{pole}}, \quad (2.27)$$

$$W_{perp} = \frac{\pi \mu_o i^2 w_r^2 l_r d_r}{96 k_{car} k_{pole}^3 \delta} \quad (2.28)$$

According to eq. (2.2)

$$A_{m 2\delta} = \frac{\pi \mu_o l_r d_r}{4 k_{car} k_{pole} \delta} \quad (2.29)$$

So

$$W_{perp} = \frac{A_{m 2\delta} i^2 w_r^2}{24 k_{pole}^2} \quad (2.30)$$

If eq. (2.30) is substituted into eq. (2.23) we find:

$$\phi_{perp} = \frac{2 W_{perp}}{i} = \frac{A_{m 2\delta} i w_r^2}{12 k_{pole}^2} \quad (2.31)$$

As the current  $i$  increases, the magnetic circuits of  $\phi_{par}$  and  $\phi_{perp}$  will both



become saturated, but not from exactly the same value of  $i$ ; moreover, the normalized magnetization curve will not have precisely the same form in the two cases.  $\phi_{\text{par}}$  and  $\phi_{\text{perp}}$  pass partially through the same rotor teeth; it follows that, when one of these fluxes starts to reach saturation, the other will also do so.

Moreover,  $\phi_{\text{perp}} \ll \phi_{\text{par}}$ . We therefore assume that both  $\phi_{\text{perp}}$  and  $\phi_{\text{par}}$  have the same normalized magnetization curve. If now  $i$  is eliminated from eqs (2.21) and (2.31) with the aid of eq. (2.12), and  $j$  is replaced by  $f_{(j;m)}$ , the formulas for  $\phi_{\text{par}}$  and  $\phi_{\text{perp}}$  are also valid when the system is saturated.

According to eqs (1.11) and (2.9),

$$e = 2 k_E n w_r \phi^{(1)} = 3 k_E n w_r \beta d l_r B_{\text{prop}} f_{(j;m)}, \quad (2.32)$$

$u$  in eq. (2.13) can be written

$$u = U_{\text{peak}} \sin \omega t. \quad (2.33)$$

If now eqs (2.33), (2.32), (2.31) and (2.21) are substituted into eq. (2.13) and all terms are divided by  $3 k_E n w_r \beta d l_r B_{\text{prop}}$ , eq. (2.13) can finally be written:

$$U_{\text{norm}} \sin \omega t - j R_{\text{norm}} - L_{\text{norm}} \frac{d}{dt} f_{(j;m)} - f_{(j;m)} = 0, \quad (2.34)$$

where

$$U_{\text{norm}} = \frac{U_{\text{peak}}}{3 k_E n w_r \beta d l_r B_{\text{prop}}}, \quad (2.35)$$

$$R_{\text{norm}} = \frac{R_r + R_s}{2 c_{41} k_E n w_r A_m 2\delta (w_s - w_r \alpha_{\text{brush}}/\pi)}, \quad (2.36)$$

$$L_{\text{norm}} = \frac{1}{2 k_E n w_r (w_s - \alpha_{\text{brush}} w_r/\pi)} \left[ \frac{w_r^2}{12 c_{41} k_{\text{pole}}^2} + c_{37} w_s^2 - \frac{2 \alpha_{\text{brush}}}{\pi} w_r w_s + \frac{(\alpha_{\text{brush}})^2 w_r^2}{\pi^2} \right]. \quad (2.37)$$

Equation (2.34) is called the normalized electrical differential equation of the small series motor. Apart from the time  $t$ , this equation only contains four parameters:  $U_{\text{norm}}$ ,  $R_{\text{norm}}$ ,  $L_{\text{norm}}$  and  $m$ . The values of  $U_{\text{norm}}$ ,  $R_{\text{norm}}$  and  $L_{\text{norm}}$  can be calculated from the parameters of the motor in the design stage. Though the exact value of  $m$  can only be measured on an existing motor, it can be taken as 0.12 to a good approximation for the initial optimization calculation.

### 2.3. Solution of the normalized electrical differential equation

As we have just seen, the coefficients  $U_{\text{norm}}$ ,  $R_{\text{norm}}$  and  $L_{\text{norm}}$  of the normalized electrical differential equation (2.34) can be expressed in terms of the motor parameters. If  $j$  and  $f_{(j;m)}$  can be determined as functions of time by

solving eq. (2.34),  $i$  and  $\phi^{(1)}$  are also known as functions of time. The copper losses and the internal power can then be calculated by integrating  $i^2$  and  $i\phi^{(1)}$ .

The results of the solution of eq. (2.34) can be introduced into an optimization calculation in two ways:

- (1) Equation (2.34) is solved each time it is needed in the optimization calculation of chapter 8. This method requires more memory capacity in the digital computer and more calculating time than the following.
- (2) Separate from the optimization calculation, eq. (2.34) is solved once and for all, for all combinations of  $U_{\text{norm}}$ ,  $R_{\text{norm}}$ ,  $L_{\text{norm}}$  and  $m$  that can be expected to occur in practice.

The second method was chosen; it was executed as follows:

As long as  $j_{\text{peak}}$  is smaller than 0.65, saturation does not occur. The value of  $U_{\text{norm}}$  corresponding to  $j_{\text{peak}} = 0.65$  will be called  $U_{\text{norm prop}}$ . This quantity is given by

$$(U_{\text{norm prop}})^2 = (0.65 R_{\text{norm}} + 0.65)^2 + (0.65 \omega L_{\text{norm}})^2. \quad (2.38)$$

We now may introduce the factor  $c_u$ :

$$c_u = \frac{U_{\text{norm}}}{U_{\text{norm prop}}}. \quad (2.39)$$

The distortion levels of the current and the internal torque may be expressed in the current distortion factor  $c_e$  and the torque distortion factor  $c_{\text{mech}}$  respectively:

$$c_e = \frac{j_{\text{eff}}}{j_{\text{peak}}} = \frac{I_{\text{eff}}}{I_{\text{peak}}}, \quad (2.40)$$

$$c_{\text{mech}} = \frac{[j f(j; m)]_{\text{average}}}{j_{\text{peak}} f(j; m)_{\text{peak}}} = \frac{[i \phi^{(1)}]_{\text{average}}}{I_{\text{peak}} \phi^{(1)}_{\text{peak}}}. \quad (2.41)$$

We then have:

$$P_{\text{Cu r}} = c_e^2 I_{\text{peak}}^2 R_r, \quad (2.42)$$

$$P_{\text{Cu s}} = c_e^2 I_{\text{peak}}^2 R_s, \quad (2.43)$$

and according to eqs (1.11), (1.41) and (2.41) the internal power is given by

$$P_\delta = 2 k_E c_{\text{mech}} n \omega_r \phi^{(1)}_{\text{peak}} I_{\text{peak}}. \quad (2.44)$$

Introduction of  $c_e$  and  $c_{\text{mech}}$  allows the optimization calculation for an AC series motor to be changed into a calculation for a DC motor with current  $I_{\text{peak}}$  and flux  $\phi^{(1)}_{\text{peak}}$ .

The normalized differential equation (2.34) is solved numerically with the

aid of a digital computer for all combinations of the following values of the parameters:

$$\begin{aligned} R_{\text{norm}} &= 0, \quad 0.15, \quad 0.3; \\ \omega L_{\text{norm}} &= 0.3, \quad 0.6, \quad 0.9; \\ m &= 0.08, \quad 0.16, \quad 0.24; \\ U_{\text{norm}} &= \text{various values between } U_{\text{norm prop}} \text{ and } 2.1. \end{aligned}$$

If  $i$  and  $\phi^{(1)}$  are sinusoidal,  $c_e = 0.5 \sqrt{2}$ ,  $c_{\text{mech}} = 0.5$  and  $c_e = c_{\text{mech}} \sqrt{2}$ . The results of the calculations show that the ratio of  $c_e$  and  $c_{\text{mech}}$  never differs by more than 3% from  $\sqrt{2}$ . The following approximate relation could therefore be used for the optimization calculation:

$$c_e = c_{\text{mech}} \sqrt{2}. \quad (2.45)$$

For the optimization calculation, we need a formula expressing  $c_{\text{mech}}$  in terms of  $R_{\text{norm}}$ ,  $\omega L_{\text{norm}}$ ,  $m$  and  $j_{\text{peak}}$ . The results of the calculation gave the following approximate expressions for  $c_{\text{mech}}$  for the various ranges of  $j_{\text{peak}}$ :

$$\begin{aligned} j_{\text{peak}} \leq 0.65: \quad c_{\text{mech}} &= 0.5; \\ 0.65 < j_{\text{peak}} \leq 1.35: \quad c_{\text{mech}} &= 0.5 - (0.086 - 0.143 R_{\text{norm}}) (j_{\text{peak}} - 0.65); \\ 1.35 < j_{\text{peak}}: \quad c_{\text{mech}} &= 0.44 + 0.1 R_{\text{norm}} - \left( 0.1 + 0.1 R_{\text{norm}} + \right. \\ &\quad \left. - 0.375 m - 0.1 (1 - 2.5 m) \frac{R_{\text{norm}}}{\omega L_{\text{norm}}} \right) (j_{\text{peak}} - 1.35). \end{aligned} \quad (2.46)$$

Similarly,  $c_u$  was given by the approximate expressions

$$\begin{aligned} j_{\text{peak}} \leq 0.65: \quad c_u &= \frac{j_{\text{peak}}}{0.65}; \\ 0.65 < j_{\text{peak}} \leq 1.35: \quad c_u &= 1 + (0.743 + 0.43 R_{\text{norm}}) (j_{\text{peak}} - 0.65); \\ 1.35 < j_{\text{peak}}: \quad c_u &= 1.52 + 0.3 R_{\text{norm}} + \left( 0.18 + 2 (m - 0.08) + \right. \\ &\quad \left. + \frac{0.29 R_{\text{norm}}}{\omega L_{\text{norm}}} \right) (j_{\text{peak}} - 1.35). \end{aligned} \quad (2.47)$$

Equations (2.46) and (2.47) were found by trial and error. However, the values of  $c_{\text{mech}}$  and  $c_u$  calculated in this way differed by only a few per cent from the calculated values.

The calculations show that  $f_{(j;m)}$  is sinusoidal for any level of saturation as long as  $R_{\text{norm}} = 0$ , but that  $j$  is distorted. Figure 2.7 shows the curves obtained in such a case. If  $R_{\text{norm}} > 0$ , both  $j$  and  $f_{(j;m)}$  are distorted. The distortion level of  $j$  and  $f_{(j;m)}$  increases as  $U_{\text{norm}}$  increases and  $m$  decreases. Figure 2.8 illustrates such a case.

An average small series motor will have roughly  $R_{\text{norm}} = 0.1$ ;  $\omega L_{\text{norm}} = 0.5$ ;  $m = 0.12$  and  $j_{\text{peak}} = 1.5$ . Equation (2.46) now gives  $c_{\text{mech}} = 0.443$  while eq.

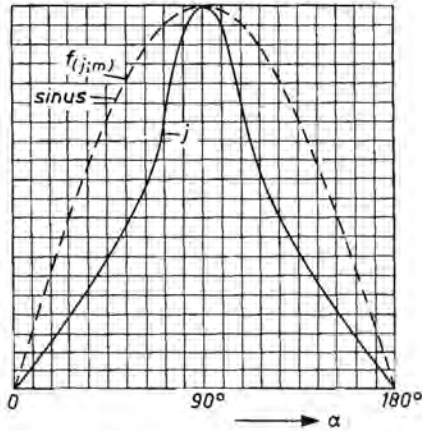


Fig. 2.7.  $f_{(j;m)}$  and  $j$  as functions of time compared with the shape of a sine function for the case  $m = 0.08$ ,  $R_{norm} = 0$  and  $\omega L_{norm} = 0.6$ ;  $U_{norm} = 1.30$ ,  $c_u = 1.71$ ,  $c_e = 0.517$ ,  $c_{mech} = 0.353$ ,  $j_{top} = 2.53$ ,  $f_{(j;m) peak} = 1.12$ .

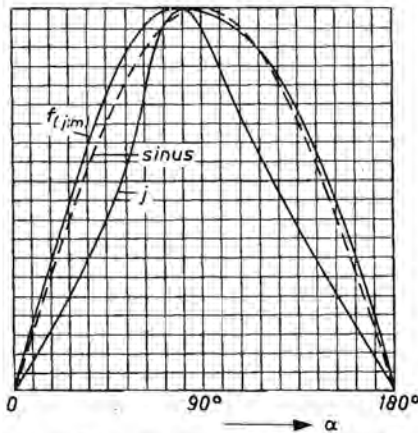


Fig. 2.8.  $f_{(j;m)}$  and  $j$  as functions of time compared with the shape of a sine function for the case  $m = 0.08$ ,  $R_{norm} = 0.3$  and  $\omega L_{norm} = 0.6$ ;  $U_{norm} = 1.75$ ,  $c_u = 1.88$ ,  $c_e = 0.568$ ,  $c_{mech} = 0.409$ ,  $j_{top} = 2.09$ ,  $f_{(j;m) peak} = 1.09$ .

(2.47) gives  $c_u = 1.60$ . Equation (2.38) leads to  $U_{norm prop} = 0.787$  and eq. (2.39) gives  $U_{norm} = 1.26$ . Finally, eq. (2.45) shows that  $c_e$  is about 0.62.

### 2.4. Conclusions

The magnetization curves of all small series motors resemble one another so much that it appears possible to introduce a normalized magnetization curve with only one parameter  $m$ , expressing the level of saturation (see sec. 2.1). In practice, it is found that  $m$  never differs much from 0.12.

Substitution of the normalized magnetic flux  $f_{(j;m)}$  (the ordinate of the

normalized magnetization curve) in the basic electrical differential equation (1.36) gives the normalized differential equation (2.34).

The influence of distortion of the magnetic flux and of the current on the internal power and on the power losses in  $R_r$  and  $R_s$  is described with the aid of the torque distortion factor  $c_{mech}$  and the current distortion factor  $c_e$  respectively, which can be calculated from eq. (2.34) as functions of the motor parameters, and then introduced into the optimization calculation. This allows the optimization of a small AC series motor to be simplified into the optimization of a small DC motor in which the AC influence is expressed by means of  $c_e$  and  $c_{mech}$ .

### 3. IRON LOSS IN SMALL COMMUTATOR MACHINES

In general, the quality of the steel sheet used in electric machines and transformers is characterized by loss figures such as the well-known  $V_{10}$  and  $V_{15}$ , defined in the German standard DIN 46.400.  $V_{10}$  ( $V_{15}$ ) is the total iron loss in  $\text{W kg}^{-1}$  of steel sheet, for a unidirectional sinusoidal magnetic field with a maximum value of  $1 \text{ Wb m}^{-2}$  ( $1.5 \text{ Wb m}^{-2}$ ) at a frequency of 50 Hz. For other values of the magnetic induction, the iron loss can be estimated by interpolation or extrapolation with the aid of  $V_{10}$  and  $V_{15}$ .  $V_{10}$  and  $V_{15}$  give a good idea of the iron loss in transformers and machines, if a sinusoidal unidirectional magnetic field of 50 Hz is involved.

However,  $V_{10}$  and  $V_{15}$  are not really applicable to small commutator machines, for the following four reasons.

(1) Mechanical deformation

If steel sheet about 0.5 mm thick is stamped, a zone up to 2 mm wide at the edges of the stamping is deformed mechanically, which makes the hysteresis losses increase considerably in this zone. The rotor teeth are so narrow that the deformed zones often account for half the width of the teeth or more.

(2) Non-unidirectional field

In the rotor teeth and in the stator, the magnetic field is unidirectional; but in the rotor core, the shaft and the pole faces, its change is partly rotational.

(3) Non-sinusoidal field

In a DC commutator machine, the magnetic induction in a rotor tooth is determined by the position of the tooth. This induction is thus alternating, but not sinusoidal. In an AC commutator machine the situation is complicated by the variation of the input voltage with time.

(4) Alternation frequency of field

The speed of a small commutator machine is generally much more than 50 revolutions per second, and may be up to 400 r.p.s. The frequency  $\nu$  of the field alternations in the rotor is thus much higher than 50 Hz.

In principle, the contribution of eddy-current losses and hysteresis losses to the total iron loss can be separated, but only for low frequencies, e.g. 50 or 60 Hz. At high frequencies (e.g. 400 Hz), these two losses are no longer exactly proportional to  $\nu^2$  and  $\nu$  respectively, so the iron losses at higher frequencies cannot be calculated with the aid of  $V_{10}$  and  $V_{15}$ .

A method of determining the iron losses in the rotor of small commutator machines is described in this chapter. Different types of steel sheet in combination with different types of shaft are measured and their applicability is compared. First of all, however, we will show that the iron losses in the stator can be neglected in the optimization calculation.

### 3.1. The iron loss in the stator

It may be seen from fig. 1.8 that the magnetic induction in the field poles of the stator is much smaller than in the yoke.

Moreover, the volume of the field poles is small compared with that of the yoke. The iron loss in the field poles is thus almost negligible compared with that in the yoke. The length of the flux path through the yoke is about twice the rotor diameter  $d_r$ . If the length of the stator stack is  $l_s$ , the width of each half of the yoke is  $b_{36}$  and the density of the steel sheet is  $g_{Fe}$ , then the weight of steel sheet in which most of the iron loss in the stator is generated is about

$$G_{yoke} = 4 d_r l_s b_{36} g_{Fe}. \quad (3.1)$$

For a motor with the parameters mentioned in sec. 6.2,  $G_{yoke}$  is about 0.3 kg. Even if the induction were so high and the quality of the steel sheet so poor that the iron loss per kg were 20 W, the total iron loss in the stator would be only  $20 \times 0.3 = 6$  W.

Since this quantity is small compared with the other losses in the motor, while the cooling of the stator is good and the thermal contact with the stator coils is poor, these losses can be neglected in an optimization calculation.

The extra iron loss in the field poles, caused by variation of the magnetic induction when the apertures of the rotor slots pass the field poles, has not been mentioned so far. Because of the high frequency, this consists mainly of eddy-current losses. It is supplied by the moving rotor and can be measured as an extra loss torque of the rotor, as described in the next section.

### 3.2. A method of measuring the iron loss in the rotor

Because the iron loss in the rotor of a small commutator machine cannot be calculated with the aid of loss figures such as  $V_{10}$  and  $V_{15}$ , we need a method of measuring the loss of a given type of steel sheet under conditions similar to those encountered in a rotor.

The iron loss in the rotor is a combination of the two types of loss described below.

#### (1) Transformation loss

This iron loss is caused by the alternating magnetic field in a fixed rotor excited by an AC current in the stator coils. The transformation loss is supplied by the current through the stator coils as electrical energy.

The values of the magnetic induction in rotor and stator yoke are about equal, and so are the widths of the flux paths in rotor and stator yoke. However, the lengths of the flux paths in rotor and stator yoke are more or less in the ratio 1 : 2. The transformation iron loss in the rotor is thus

only about half the iron loss in the stator, and can thus be neglected in practice compared with the total iron loss in the rotor.

(2) Rotation loss

The iron loss in a rotating rotor excited with a DC current in the stator coils is supplied by the rotor itself and causes a loss torque in the rotor. The iron loss in the rotating rotor of a DC commutator machine is all rotation loss. The iron loss generated in the rotor of an AC commutator motor is a combination of transformation and rotation losses, though not their sum.

The contribution of the transformation loss is so small in practice that it can be neglected compared with the rotation loss. If the iron loss in the rotor of a small commutator machine is to be determined, it is therefore sufficient to measure the loss torque alone with DC excitation for a DC machine and AC excitation for an AC machine.

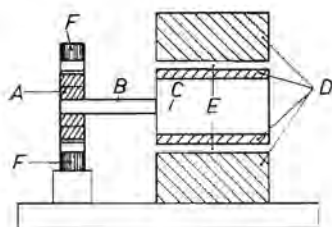


Fig. 3.1. Principle of a device for measuring iron loss in the rotor of a small commutator machine.

This measurement can be made with the device sketched in fig. 3.1. A rotor stack A without windings is fixed on the shaft B. The properties and dimensions of shaft B are the same as in a real motor. Shaft B is connected to the shaft of the drive motor C. A fixed stator F surrounds the rotor and sends a direct or an alternating magnetic field through it. The torque required to drive the rotor is the sum of the iron-loss torque  $T_{Fe}$  and the loss torque  $T_{air}$  due to air friction. Drive motor C is built inside an aerodynamic bearing D with air gap E.

When drive motor C drives the rotor stack, the reaction torque on the drive motor is exactly equal to  $T_{Fe} + T_{air}$ . Since the friction of the aerodynamic bearing is completely negligible, the reaction torque on the motor ( $T_{Fe} + T_{air}$ ) can be measured exactly.

Figure 3.2 shows a photograph of the measuring device.  $T_{air}$  can be measured when the stator is not excited. For rotors with dimensions of the order of those discussed below,  $T_{air}$  increases roughly quadratically with speed up to about  $2.10^{-3}$  Nm at 18 000 r.p.m.



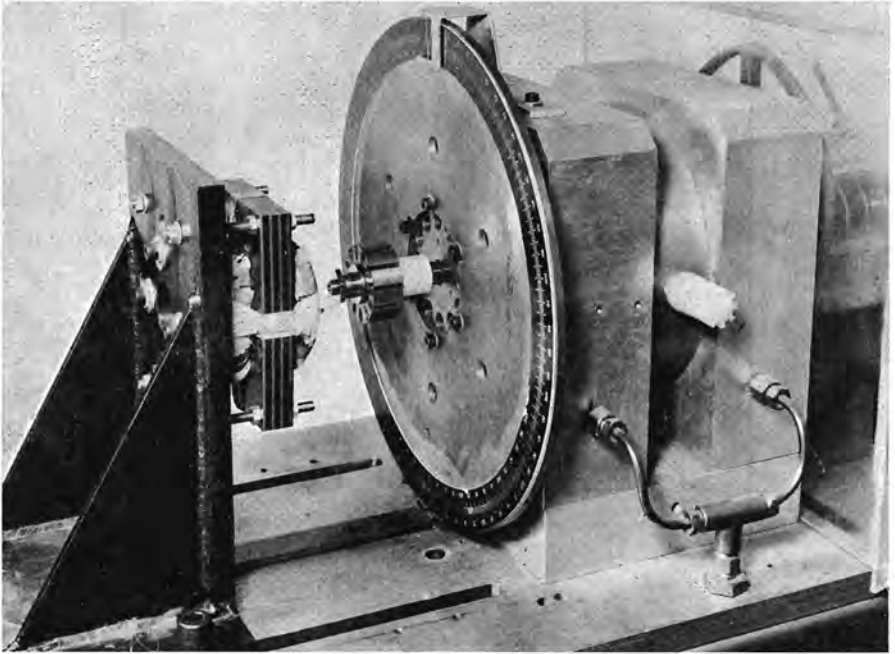


Fig. 3.2. Photograph of the device for measuring iron loss in the rotor of a small commutator machine.

### 3.3. The types of steel sheet considered

Figures 3.3 and 3.4 show the shape of the laminations of rotor and stator. The shape of the rotor laminations is almost optimal in accordance with the conclusions of chapter 8. The air gap is 0.4 mm. The pole faces of the stator are shaped as in a real motor. The flux path through the stator is so wide that

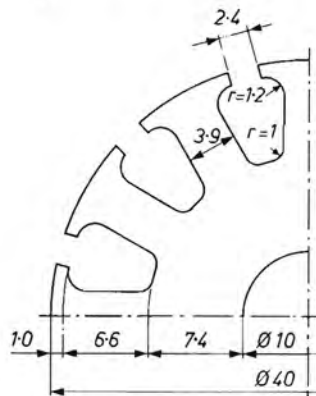


Fig. 3.3. The rotor laminations for the iron-loss measurements.

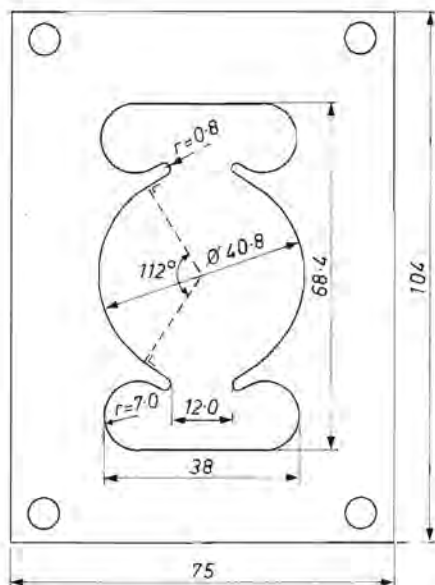


Fig. 3.4. The stator laminations for the iron-loss measurements.

saturation never occurs in it. In this way the number of ampere turns required is limited, and the need for artificial cooling of the stator coils is reduced. The thickness of the stator laminations is 0.5 mm, and their resistivity is about  $0.35 \Omega \text{ mm}^2 \text{ m}^{-1}$ . All stator laminations are insulated from one another so that no eddy currents can flow from one lamination to another in the field poles.

Table 3-1 is a survey of the 11 types of steel sheet considered here. Losil and Bochum B.D.K. are brand names. N290 is a Dutch standards code for steel sheet with no special magnetic properties.

### 3.4. Measuring methods and results

Measurements were carried out to study not only the quality of all types of steel sheet, but also the influence of some rotor parameters, the shaft materials, and the insulation between the rotor laminations and a solid steel stator. Details of these measurements and of the results obtained are given in the following subsections.

#### 3.4.1. Magnetic measurements

These measurements concern the relation between the stator ampere turns and the magnetic fluxes and inductions in different zones of the rotor.

The measured fluxes  $\phi^{(1)}$  and  $\phi_1^{(1)}$  are plotted in fig. 3.5a and fig. 3.5b. Figure 3.6 indicates the width of the zones in the rotor through which  $\phi^{(1)}$  and  $\phi_1^{(1)}$  pass.  $\phi_1^{(1)}$  is almost equal to the air-gap flux, while  $\phi^{(1)}$  is the flux occur-

TABLE 3-1

Survey of the eleven types of steel sheet for which the iron loss has been measured when used in the rotor of a small commutator machine

serial no. of rotor	type of steel sheet	$V_{10}$ (W/kg)	$l_{lam}$ (mm)	length of stack, $l_r$ (mm)	%Si	$\rho_{Fe}$ ( $\Omega \text{ mm}^2/\text{m}$ )	$\frac{l_{lam}^2}{\rho_{Fe}}$ ( $\Omega^{-1} \text{ m}$ )
1	Losil 19	2	0.52	$29 \times 0.52 = 15.1$	1.7	0.39	0.69
2	Losil 19	1.5	0.40	$38 \times 0.40 = 15.2$	1.7	0.39	0.41
3	Losil 19	2.5	0.64	$24 \times 0.65 = 15.6$	1.7	0.39	1.05
4	N 290	6	0.33	$48 \times 0.33 = 15.8$	0	0.12	0.90
5	N 290	7	0.55	$28 \times 0.55 = 15.4$	0	0.12	2.50
6	N 290	8	0.605	$25 \times 0.605 = 15.1$	0	0.12	3.00
7	Bochum BDK	3.6	0.52	$29 \times 0.51 = 14.8$	0.7	0.27	1.00
8	Bochum BDK	2.3	0.53	$29 \times 0.52 = 15.1$	2.3	0.35	0.80
9	Bochum BDK	3	0.55	$29 \times 0.52 = 15.1$	1	0.28	1.08
10	Bochum BDK	2.6	0.52	$30 \times 0.52 = 15.6$	1.7	0.36	0.75
11	Bochum BDK	2.6	0.49	$31 \times 0.50 = 15.5$	1.2	0.35	0.69

ring in the formulas for internal torque and rotational e.m.f.;  $\phi^{(1)}$  is smaller than  $\phi_1^{(1)}$ . The air-gap flux is poorly utilized if the ratio  $\phi^{(1)}/\phi_1^{(1)}$  is low.

$U_{ms}$  is the number of ampere turns of the stator. Figure 3.5a shows the relation between  $\phi^{(1)}$ ,  $\phi_1^{(1)}$  and  $U_{ms}$  for the steel shaft and for a brass shaft of the same dimensions. As was to be expected, the magnetization curves of all eleven types of steel sheet hardly differ. It is thus sufficient to show only one of them.

As soon as the rotor core is saturated, the flux in the rotor with the brass shaft is lower than that in the rotor with the steel shaft; this indicates that when the core is saturated, part of  $\phi^{(1)}$  passes through the steel shaft. Figure 3.5b shows that the ratio  $\phi_1^{(1)}/\phi^{(1)}$  increases with the saturation level. In the rotor with the brass shaft,  $\phi_1^{(1)}/\phi^{(1)}$  increases more than in the rotor with the steel shaft.

To see how deep  $\phi^{(1)}$  penetrates into the steel shaft, this shaft was replaced in some measurements by one of the same external diameter but with a circular hole of diameter 7 mm through it (this hollow steel shaft is thus in fact

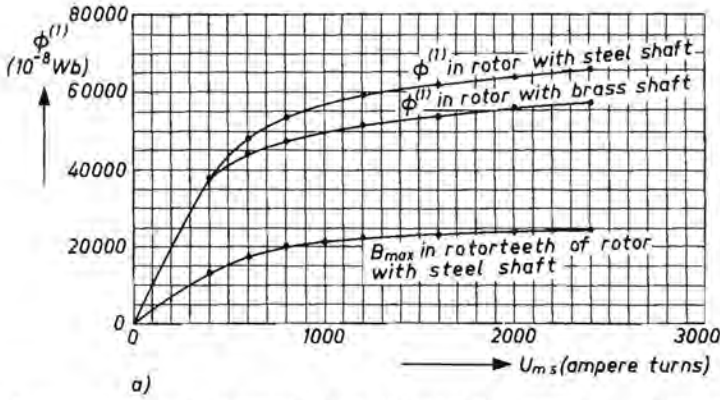


Fig. 3.5a. Measured values of the magnetic flux  $\phi^{(1)}$  and the induction  $B_{max}$  as functions of the number of stator ampere turns  $U_{m_s}$ . For the dimensions of the rotors and stators on which these measurements were carried out, see figs 3.3 and 3.4.

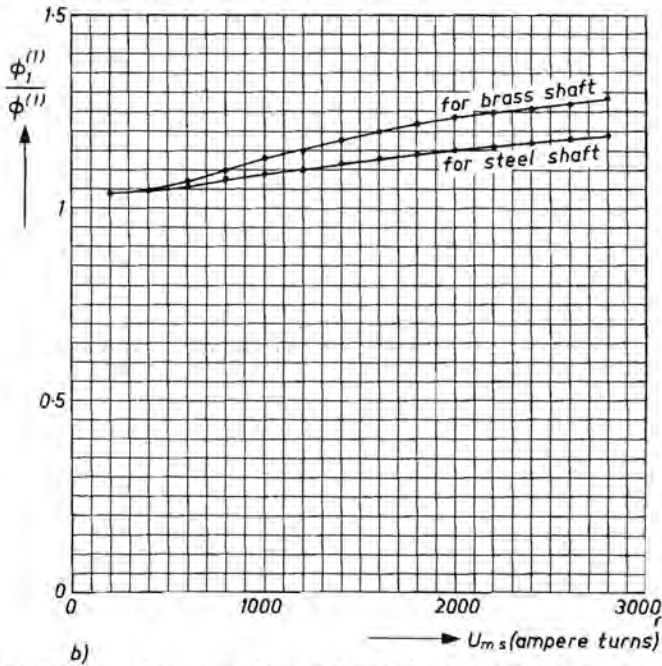


Fig. 3.5b.  $\phi_1^{(1)}/\phi^{(1)}$  as a function of  $U_{m_s}$  for identical rotors with a steel and a brass shaft.

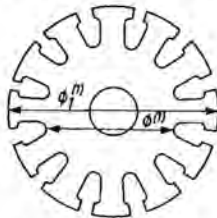


Fig. 3.6. Width of the zones in the rotor through which the fluxes  $\phi^{(1)}$  and  $\phi_1^{(1)}$  pass.

a steel tube of wall thickness 1.5 mm). At the same values of  $U_{\text{rot}}$ , the values of  $\phi^{(1)}$  and  $\phi_1^{(1)}$  for the solid steel shaft and the hollow one did not differ to a measurable degree. This means that in rotors with dimensions like those considered here,  $\phi^{(1)}$  does not penetrate more than 1.5 mm into the steel shaft.

As the rotors rotate,  $\phi^{(1)}$  and  $\phi_1^{(1)}$  might be expected to decrease under the influence of the eddy currents generated in the laminations and the shaft. However, measurements on the eleven rotors with the solid steel shaft, the hollow steel shaft and the brass shaft showed that  $\phi^{(1)}$  and  $\phi_1^{(1)}$  did not decrease measurably at speeds of up to 18 000 r.p.m. and excitations of up to 3000 ampere turns.

### 3.4.2. Iron-loss torques with DC excitation

Table 3-II shows the iron-loss torque  $T_{Fe}$  of the 11 rotors for various speeds and various values of  $\phi^{(1)}$ . All the results given here are for the solid steel shaft. The loss torque due to air friction  $T_{\text{air}}$  has already been subtracted. In a unidirectional sinusoidal magnetic field, the hysteresis losses  $P_{\text{hyst}}$  should be proportional to the frequency  $\nu$ , and the eddy-current losses  $P_{\text{eddy}}$  to  $\nu^2$ . For these measurements,  $\nu$  may be replaced by  $n$ . We may then write:

$$P_{Fe} = P_{\text{hyst}} + P_{\text{eddy}} = c_{\text{hyst}} n + c_{\text{eddy}} n^2 \quad (3.2)$$

and

$$T_{Fe} = T_{\text{hyst}} + T_{\text{eddy}} = \frac{c_{\text{hyst}}}{2\pi} + \frac{c_{\text{eddy}} n}{2\pi} \quad (3.3)$$

Equation (3.3) predicts a linear relation between the iron-loss torque and the rotor speed. The experimentally determined form of this relation for rotor No. 2 is indicated in fig. 3.7, which shows  $T_{Fe}$  as a function of the rotor speed  $n$  for various values of the flux  $\phi^{(1)}$ . Above about 5000 r.p.m., the losses are mainly eddy-current losses. The linearity of the curves is poor; the increase in  $T_{Fe}$  is less than proportional to  $n$ . This non-linearity is discussed in sec. 3.4.3.

In a unidirectional sinusoidal magnetic field,  $P_{\text{eddy}}$  should be proportional

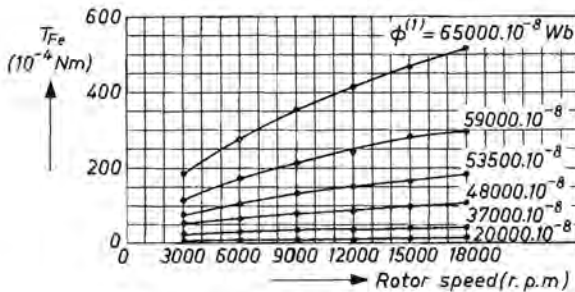


Fig. 3.7. Iron-loss torque as a function of flux  $\phi^{(1)}$  and rotor speed  $n$  for rotor No. 2.

to  $B_{\max}^2$  and  $P_{\text{hyst}}$  to something like  $B_{\max}^{1.6}$ , i.e. approximately to  $B_{\max}^2$  as well.

We may thus expect a quadratic relation between the iron-loss torque  $T_{\text{Fe}}$  and the maximum induction  $B_{\max}$ . For rotor number 6, fig. 3.8 shows  $T_{\text{Fe}}$  as a function of  $\phi^{(1)}$  for various rotor speeds. As soon as the rotor core is saturated i.e. from about  $35\,000 \cdot 10^{-8}$  Wb,  $T_{\text{Fe}}$  is found to increase much more than proportionately to the square of  $B_{\max}$ . This must be because under these conditions  $\phi^{(1)}$  penetrates the shaft and generates eddy-current losses there.

### 3.4.3. Thickness and resistivity of the various types of steel sheet

At high rotor speeds, the eddy-current losses  $P_{\text{eddy}}$  are much larger than the hysteresis losses  $P_{\text{hyst}}$ , as may be confirmed by inspection of fig. 3.7. We shall therefore only consider  $P_{\text{eddy}}$  in our investigation of the reason for the non-linearity of the curves of fig. 3.7. If the eddy currents generated are relatively small, then for a unidirectional sinusoidal magnetic field in laminated steel,  $P_{\text{eddy}}$  is proportional to  $l_{\text{lam}}^2/\rho_{\text{Fe}}$ , where  $l_{\text{lam}}$  is the thickness of the steel sheet in question and  $\rho_{\text{Fe}}$  is its resistivity (see e.g. Pustola<sup>8</sup>), p. 237).

As is well known, the value of  $P_{\text{eddy}}$  will be less than proportional to  $l_{\text{lam}}^2/\rho_{\text{Fe}}$  as soon as a field displacement due to eddy currents occurs in the laminations. Figure 3.9 shows  $T_{\text{eddy}}$  as a function of  $l_{\text{lam}}^2/\rho_{\text{Fe}}$  for all eleven rotors at 18 000 r.p.m. and  $\phi^{(1)} = 48\,000 \cdot 10^{-8}$  Wb m<sup>-2</sup> or  $\phi^{(1)} = 65\,000 \cdot 10^{-8}$  Wb m<sup>-2</sup>. When  $l_{\text{lam}}^2/\rho_{\text{Fe}} = 0$ , the contribution of the laminations to  $T_{\text{eddy}}$  is zero, but  $T_{\text{eddy shaft}}$ , the contribution of the shaft, and  $T_{\text{pole}}$ , the torque required because of the extra iron loss in the pole faces, will be non-zero. The value of  $T_{\text{eddy shaft}} + T_{\text{pole}}$  can be estimated by extrapolation of the curves of fig. 3.9 to  $l_{\text{lam}}^2/\rho_{\text{Fe}} = 0$ . No matter what value is found for  $T_{\text{eddy shaft}} + T_{\text{pole}}$ , we would expect  $T_{\text{eddy}}$  to increase proportionately to  $l_{\text{lam}}^2/\rho_{\text{Fe}}$ . However, just as in fig.

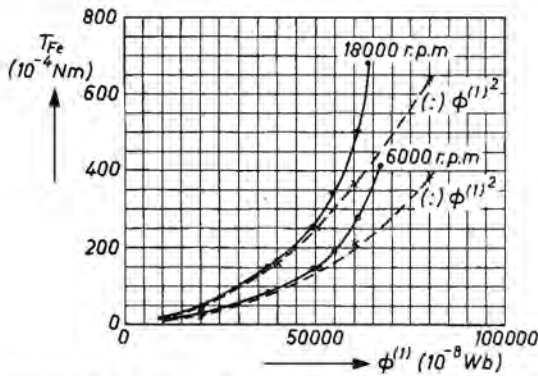


Fig. 3.8. Iron-loss torques as a function of the flux  $\phi^{(1)}$  for rotor No. 6, at 6000 and 18 000 r.p.m. (drawn lines). The dashed lines are proportional to  $\phi^{(1)2}$ , and are included for the sake of comparison.

TABLE 3-II

Iron-loss torque as a function of flux  $\phi^{(1)}$  and rotor speed  $n$  for the eleven rotors, with DC excitation

$U_m$ s →	200	400	600	800	1200	1600	2000	2400	200	400	600	800	1200	1600	2000	2400
flux $\phi^{(1)}$ rotor speed $n$ (r.p.m.)	20000	37500	48000	53400	59000	62000	64000	65500	20000	37000	48000	53500	59000	62000	63500	65000
	rotor 1								rotor 2							
3000	8	26	57	81	128	156	174	197	7	24	54	77	115	144	163	189
6000	9	35	75	121	185	224	258	294	9	30	67	109	173	208	243	278
9000	10	41	93	148	229	281	327	369	9	35	80	132	213	263	306	354
12000	12	46	105	169	271	331	393	461	9	37	94	151	246	309	376	419
15000	16	51	117	189	298	377	441	506	11	41	100	167	281	339	406	469
18000	20	55	126	205	330	412	482	563	16	48	110	183	295	382	453	520
flux $\phi^{(1)}$ rotor speed $n$ (r.p.m.)	20000	36000	46000	52000	58000	60500	62500	64000	19500	37000	48000	53500	59500	62500	64500	66500
	rotor 3								rotor 4							
3000	10	33	59	88	130	157	178	204	15	48	85	114	167	195	216	238
6000	11	40	83	127	195	235	274	307	18	56	102	149	222	270	310	351
9000	12	47	99	160	242	296	346	396	18	65	121	182	279	342	395	441
12000	16	57	120	187	284	353	412	471	22	65	136	206	318	406	476	533
15000	20	62	132	204	319	399	463	526	29	79	147	225	356	453	531	596
18000	24	73	153	223	354	445	522	594	31	87	161	242	392	492	578	654
flux $\phi^{(1)}$ rotor speed $n$ (r.p.m.)	20000	37500	48500	54500	60500	63000	65000	67000	19500	37500	49000	54500	61000	63500	66000	67000
	rotor 5								rotor 6							

3000	18	62	102	138	187	220	244	268	20	60	102	139	189	214	237	266	
6000	20	70	131	174	254	305	343	391	29	77	142	197	275	326	375	415	
9000	29	87	155	218	318	389	441	494	30	98	172	243	354	427	482	518	
12000	34	97	187	260	391	479	551	611	31	116	204	285	413	496	555	623	
15000	37	109	197	286	433	531	604	678	37	129	224	312	461	546	624	692	
18000	39	124	216	313	471	585	673	745	44	150	250	350	500	606	680	764	
$\frac{\text{flux } \phi^{(1)}}{\text{rotor speed } n \text{ (r.p.m.)}}$	20000	38000	48000	54000	60000	63000	65000	66000	20000	37000	48000	54000	60000	63000	65000	66500	
	rotor 7								rotor 8								
3000	7	26	56	82	128	155	179	204	7	22	50	78	118	147	172	194	
6000	9	30	70	119	196	235	276	312	8	30	69	113	181	224	262	297	
9000	12	41	97	155	244	394	349	404	11	34	84	140	227	282	331	384	
12000	13	50	109	179	284	355	415	472	11	42	99	166	269	338	400	457	
15000	19	56	123	194	315	396	467	530	20	48	108	184	298	374	446	506	
18000	21	61	136	215	347	440	516	590	20	54	120	200	325	410	484	564	
$\frac{\text{flux } \phi^{(1)}}{\text{rotor speed } n \text{ (r.p.m.)}}$	20000	37000	47500	53500	59000	62000	64000	66000	20500	38000	49000	54500	60500	63000	65000	67000	
	rotor 9								rotor 10								
3000	8	25	56	85	133	160	185	205	7	22	45	72	120	147	172	197	
6000	10	35	74	119	185	220	264	312	7	24	67	108	174	217	259	295	
9000	12	41	95	149	137	294	345	392	10	37	82	138	222	279	327	366	
12000	15	50	107	175	280	351	431	475	13	43	99	159	260	322	381	448	
15000	20	57	121	194	312	400	469	546	18	51	111	184	288	366	431	496	
18000	20	65	132	212	344	435	515	586	20	56	123	197	320	406	477	552	
$\frac{\text{flux } \phi^{(1)}}{\text{rotor speed } n \text{ (r.p.m.)}}$	20000	37500	48500	54000	60000	62000	64000	66000									
	rotor 11																
3000	5	20	45	74	113	144	170	193									
6000	9	33	74	114	180	223	260	295									
9000	12	39	88	142	223	277	328	375									
12000	15	44	101	161	274	316	383	440									
15000	18	51	113	175	290	364	431	488									
18000	20	57	122	190	314	401	471	540									



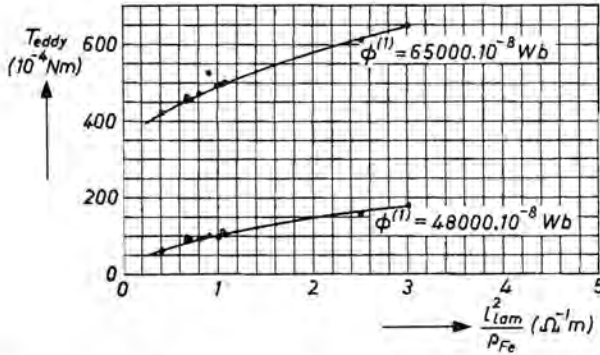


Fig. 3.9. Iron-loss torques due to eddy-current loss  $T_{eddy}$ , as a function of  $l_{lam}^2/\rho_{Fe}$  for the eleven rotors at 18 000 r.p.m., with  $\phi^{(1)} = 65\,000 \cdot 10^{-8}$  Wb and  $\phi^{(1)} = 48\,000 \cdot 10^{-8}$  Wb.  $l_{lam}$  is the thickness of the rotor laminations, and  $\rho_{Fe}$  their resistivity.

3.7 this increase is found to be less than proportionate to  $l_{lam}^2/\rho_{Fe}$  and to  $n$ . We may conclude that the value of the eddy-current losses in rotors of small commutator machines with speeds and dimensions comparable with those considered here is extremely limited by field displacement caused by the eddy currents themselves.

The influence of field displacement on the eddy-current losses has been studied e.g. by Agarwal <sup>9</sup>).

### 3.4.4. Iron-loss torques with AC excitation

In sec. 3.4.2 we considered the measured iron-loss torque  $T_{Fe}$  as a function of flux and rotor speed with DC excitation. However, we are really more interested in AC excitation, because most small commutator machines are AC series motors.

If the rotor speed is very high, for instance 18 000 r.p.m.,  $\phi^{(1)}$  will not vary much during one rotation of the rotor. In that case, the iron-loss torque with AC excitation can probably be written approximately as

$$T_{Fe \sim calc} = n \int_0^{1/n} T_{Fe=} dt, \tag{3.4}$$

where  $T_{Fe=}$  is the loss torque for a constant flux equal to the instantaneous value of the AC flux. The measured loss torque  $T_{Fe \sim}$  is compared with  $T_{Fe \sim calc}$  in fig. 3.10 for rotor No. 5 with  $\phi^{(1)}_{peak} = 58\,000 \cdot 10^{-8}$  Wb. Especially at high speeds,  $T_{Fe \sim}$  and  $T_{Fe \sim calc}$  do not differ much;  $T_{Fe \sim}$  is then about  $\frac{1}{2} T_{Fe=}$ .

The results of fig. 3.10 and other measurements indicate that in the neighbourhood of 3000 r.p.m. (50 r.p.s.) the measured value  $T_{Fe \sim}$  is beginning to fall off compared with the calculated value. The reason is that at exactly 50 r.p.s. we can no longer really speak of AC magnetization, but only of a varying DC magnetization.

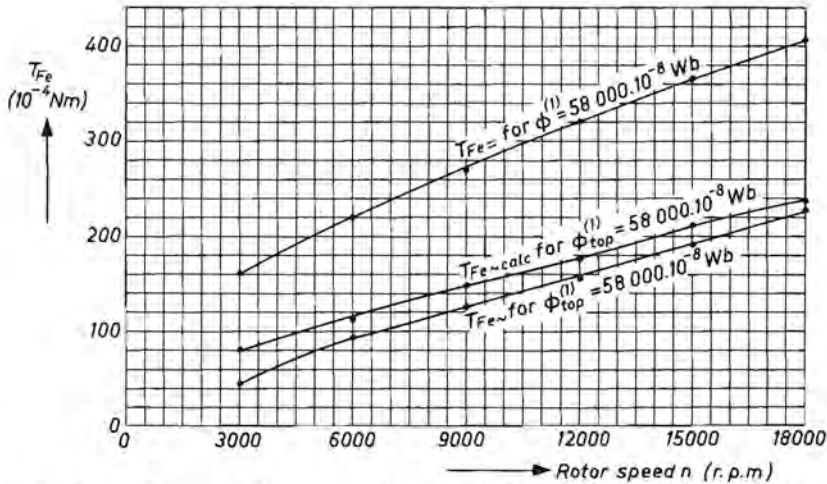


Fig. 3.10.  $T_{Fe} =$ ,  $T_{Fe} \sim$  and  $T_{Fe} \sim_{calc}$  as functions of the rotor speed  $n$  for rotor No. 5, with  $\phi_{peak}^{(1)} = 58\,000 \cdot 10^{-8}$  Wb.

TABLE 3-III

Iron-loss torque  $T_{Fe}$  ( $10^{-4}$  Nm) for rotors made of insulated and non-insulated steel sheet

rotor speed (r.p.m.)	serial no. of rotor	ins. or non-ins.	$\phi^{(1)}$ ( $10^{-8}$ Wb)						
			37 000	48 000	54 000	60 000	63 000	65 000	66 500
3000	8	ins.	22	50	78	118	147	172	194
	8	non-ins.	33	68	100	150	182	210	236
	5	ins.	62	102	138	187	220	244	268
	5	non-ins.	65	110	148	204	240	272	298
6000	8	ins.	30	69	113	181	224	262	297
	8	non-ins.	46	99	152	232	286	326	364
	5	ins.	70	131	174	254	305	343	391
	5	non-ins.	84	148	212	300	357	412	460
9000	8	ins.	34	84	140	227	282	331	384
	8	non-ins.	61	132	198	300	365	425	485
	5	ins.	87	155	218	318	389	441	494
	5	non-ins.	103	186	266	388	470	546	615
12 000	8	ins.	42	99	166	269	338	400	457
	8	non-ins.	72	152	232	353	446	517	585
	5	ins.	97	187	260	391	479	551	611
	5	non-ins.	120	215	308	457	556	628	698
15 000	8	ins.	48	108	184	298	374	446	506
	8	non-ins.	85	175	275	420	513	590	666
	5	ins.	109	197	286	433	531	604	678
	5	non-ins.	135	242	344	515	625	712	790
18 000	8	ins.	54	120	200	325	410	484	564
	8	non-ins.	98	202	305	472	582	663	743
	5	ins.	124	216	313	471	585	673	745
	5	non-ins.	152	270	392	580	694	785	868

### 3.4.5. Non-insulated steel sheet

Non-insulated steel sheet is often used in small motors, because it is cheaper. We tested the effect of the insulation on rotor No. 5, made of poor-quality steel sheet (N290), and on rotor No. 8 made of very-good-quality sheet (Bochum 2.3).

A rotor stack without insulation was made from both types of sheet, the non-insulated lamination being pressed together as firmly as might be expected in a real motor.

The measured iron-loss torques for the four rotors are compared in table 3-III. It will be seen that at high rotor speeds the stack made of insulated N290 is nearly as good as the stack made of non-insulated Bochum 2.3. The cost of Bochum 2.3 per kg, the cost of N290 per kg and the cost of insulating one kg of steel sheet are roughly in the ratio 100 : 60 : 5. The cost of insulation is so low, and the effect of the insulation layer on  $T_{Fe}$  so high, that insulated steel sheet should always be used for the rotor if iron loss in the latter gives rise to problems concerning efficiency or temperature rise.

TABLE 3-IV

Iron-loss torques  $T_{Fe}$  ( $10^{-4}$  Nm) for rotor No. 8 with a laminated or a solid steel stator, as a function of flux  $\phi^{(1)}$  and rotor speed  $n$

rotor speed (r.p.m.)		$\phi^{(1)}$ ( $10^{-8}$ Wb)			
		37 000	54 000	60 000	63 000
3000	lam.	33	100	150	182
3000	solid	38	132	232	308
6000	lam.	46	152	232	286
6000	solid	53	188	345	482
9000	lam.	61	198	300	365
9000	solid	65	242	452	620
12 000	lam.	72	232	353	446
12 000	solid	81	285	526	724
15 000	lam.	85	275	420	513
15 000	solid	93	330	600	815
18 000	lam.	98	305	472	582
18 000	solid	110	368	657	890

### 3.4.6. A solid steel stator

Beside the laminated stator made of insulated steel sheet 0.5 mm thick, a solid steel stator was also tested. The resistivity of the solid steel used is about  $0.12 \Omega \text{ mm}^2 \text{ m}^{-1}$ . The solid stator has the same shape and dimensions as the laminated one.

The measured values of the iron-loss torque  $T_{Fe}$  for rotor No. 8 with the two stators are compared in table 3-IV. Especially at high fluxes and rotor speeds, the extra eddy-current losses in the pole faces of the stator have an extremely large influence on  $T_{Fe}$ .

The results show that a solid stator should be avoided in commutator machines with speeds and dimensions in the ranges considered here.

### 3.4.7. Brass as shaft material

For rotor No. 6,  $T_{Fe}$  was also measured with a brass shaft having the same dimensions as the steel one. Figure 3.11 shows  $T_{Fe}$  as a function of  $\phi^{(1)}$  at 12000 r.p.m. for the solid steel shaft and the brass shaft. Measurements on other rotors and at other speeds gave comparable results. At low values of  $\phi^{(1)}$ , the rotor with the steel shaft gives more losses, but at high values of  $\phi^{(1)}$  the losses of the rotor with the brass shaft were higher.

This may be explained as follows. Even if the rotor core is not saturated,  $\phi^{(1)}$  passes partially through the steel shaft and causes extra eddy-current losses. If the rotor core is not saturated, hardly any flux will pass through the brass shaft on the other hand; but when the core is saturated, part of  $\phi^{(1)}$  will be forced through the latter. This is responsible for the extra eddy-current losses, since the resistivity of brass is low.

### 3.4.8. A hollow steel shaft

The iron-loss torque  $T_{Fe}$  was also measured with the hollow steel shaft with a wall thickness of 1.5 mm mentioned in sec. 3.4.1. The loss torques of the

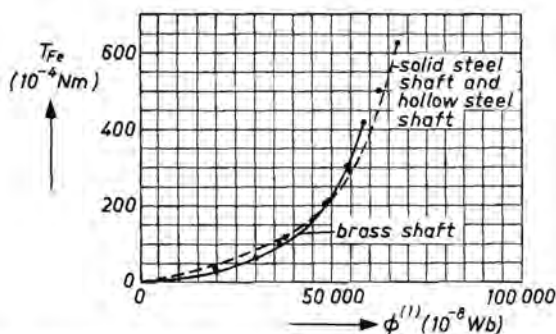


Fig. 3.11. Iron-loss torques of rotor No. 6 measured as a function of  $\phi^{(1)}$  at 12 000 r.p.m. Comparison between a solid steel shaft, a hollow steel shaft and a brass shaft.

rotors with the solid steel shaft and the hollow steel shaft did not differ, as may be seen from fig. 3.11.

It would thus appear that  $T_{Fe}$ , like the flux  $\phi^{(1)}$  (see sec. 3.4.1), is not influenced by the presence of the 7-mm hole in the steel shaft.

### 3.4.9. A 12-mm steel shaft

To get more information on the division of the iron loss between rotor stack and shaft, the 10-mm steel shaft was replaced by a 12-mm steel shaft in some measurements. The magnetization curve was found not to be influenced by the diameter of the shaft, rotating as well as non-rotating. This means that in the case of the 12-mm shaft a larger part of  $\phi^{(1)}$  must pass through the shaft. We may thus expect  $T_{Fe}$  to be larger with the 12-mm shaft, and this was found to be the case. For example,  $T_{Fe}$  for rotor No. 7 with  $\phi^{(1)} = 65\,500 \cdot 10^{-8}$  Wb and  $n = 18\,000$  r.p.m. increased from  $590 \cdot 10^{-4}$  Nm to  $850 \cdot 10^{-4}$  Nm. This increase is mainly due to the extra eddy-current losses in the shaft.

## 3.5. Conclusions

As shown in sec. 3.1, the iron losses in the stator of a small AC series motor can be neglected in an optimization calculation. The iron losses in the rotor and the extra eddy-current losses in the field poles can be determined by measuring the torque by the method described in sec. 3.2. At rotor speeds above about 5000 r.p.m., the iron losses in the rotor are mainly due to eddy-current losses, which might be expected to increase roughly proportionately to  $n^2 B_{max}^2$ . However, measurements show that the iron losses in the rotor increase less than proportionately to  $n^2$  because of field displacement inside the laminations, caused by the eddy currents themselves (see secs 3.4.2 and 3.4.3).

The flux passes partially through the shaft. As  $B_{max}$  increases, the flux through the shaft increases relatively more, causing more eddy-current losses than might be expected. This means that the iron losses are more than proportional to  $B_{max}^2$ , especially when the rotor core is saturated.

Because of the influence of the field displacement, low-resistivity steel sheet gives better results than expected (see sec. 3.4.3).

Non-insulated steel sheet should not be used in the rotor, especially at high speeds (see sec. 3.4.5). A non-magnetic (brass) shaft is not a good means of avoiding eddy-current losses in the shaft (see sec. 3.4.7).

In the optimization calculation of chapter 8, the iron losses in the rotor at one speed are written as follows:

$$P_{Fe r} = p_{Fe} \beta d^2 l_r B_{peak}^2. \quad (3.5)$$

We call  $p_{Fe}$  the specific iron loss.

The results presented in this chapter indicate that  $P_{Fe r}$  is not exactly proportional to  $B_{peak}^2$  and perhaps not exactly to  $\beta$  either. However, it is shown in sec. 8.7 that the assumptions underlying eq. (3.5) are acceptable in the optimization calculation.

#### 4. THE CARTER FACTOR OF SEMI-ENCLOSED ROTOR SLOTS OPPOSITE SMOOTH-FACED STATOR POLES

Except at the ends of the pole horns, the faces of the field poles in small commutator machines are generally circular and provide an air gap of constant width  $\delta$ . There are no stator slots. The rotor, on the other hand, is generally slotted, and these slots influence the reluctance of the air gap. If the width of the slots,  $b_{\text{slot}}$ , is kept constant and the number of slots,  $z$ , increases, or if  $z$  is kept constant and the width of the slots increases, the reluctance of the air gap increases.

The reluctance and permeance of the air gap per tooth pitch will be denoted by  $R_{m \text{ pitch}}$  and  $A_{m \text{ pitch}}$  respectively. The corresponding values extrapolated to slot width zero will be denoted by  $R_{m \text{ pitch fict}}$  and  $A_{m \text{ pitch fict}}$ . The carter factor  $k_{\text{car}}$  is now defined as

$$k_{\text{car}} = \frac{R_{m \text{ pitch}}}{R_{m \text{ pitch fict}}} = \frac{A_{m \text{ pitch fict}}}{A_{m \text{ pitch}}}. \quad (4.1)$$

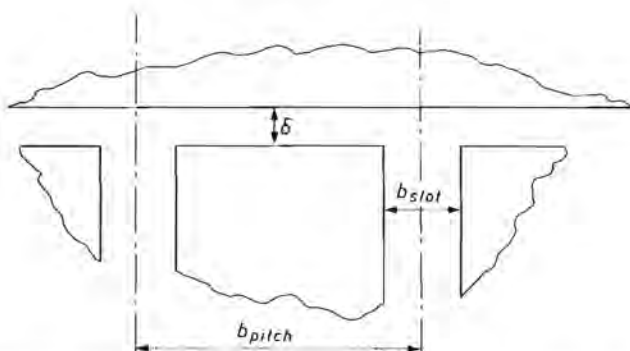


Fig. 4.1. Model of the slotted rotor used for the determination of the carter factor  $k_{\text{car}}$ .

For rotors of infinite diameter with rectangular slots (see fig. 4.1),  $k_{\text{car}}$  can be calculated with the aid of a conformal mapping (see Richter<sup>31</sup>), which gives the final result

$$k_{\text{car}} = \frac{b_{\text{pitch}}}{b_{\text{pitch}} - \gamma \delta}, \quad (4.2)$$

where

$$\gamma = \frac{4}{\pi} \left\{ \frac{b_{\text{slot}}}{2\delta} \tan^{-1} \frac{b_{\text{slot}}}{2\delta} - \ln \left[ 1 + \left( \frac{b_{\text{slot}}}{2\delta} \right)^2 \right]^{1/2} \right\}; \quad (4.3)$$

The significance of  $b_{\text{pitch}}$ ,  $b_{\text{slot}}$  and  $\delta$  is illustrated in fig. 4.1;  $\gamma$  can be simplified to

$$\gamma = \frac{(b_{\text{slot}}/\delta)^2}{5 + b_{\text{slot}}/\delta}. \quad (4.4)$$

If  $2 < b_{\text{slot}}/\delta < 12$ , the above expression can be simplified further to

$$\gamma = 0.75 b_{\text{slot}}/\delta - 1. \quad (4.5)$$

Equations (4.2)–(4.5) are correct as long as the distance between neighbouring slots is so large that the field pattern around one slot is not distorted by the presence of other slots, and as long as no saturation occurs in the iron.

The above method can also be applied to a rotor of finite diameter and with slots of finite depth without noticeable error. However, the rotors of e.g. small commutator machines have semi-enclosed slots; the influence on  $k_{\text{car}}$  of the widening of the slots below their top apertures cannot be neglected in this case.  $k_{\text{car}}$  can thus no longer be calculated from eqs (4.2) and (4.3).

However, the magnetic field in the air gap and the slots can be simulated by means of a resistance network, and  $k_{\text{car}}$  can be estimated by this analog method.

Further details of the simulation procedure and its application are given in this chapter.

#### 4.1. Simulation of the air-gap field by means of a resistance network

Though formal mathematical calculation of  $k_{\text{car}}$  is not possible, the value of this factor can be estimated by numerical analysis or by an analog method involving measurements on resistance paper or a resistance network. The last-mentioned method was chosen here, because a suitable network was available. Figure 4.2 shows the principle of the resistance network. A number of terminals are placed in a regular (generally square) pattern and identical resistors of e.g.  $1000 \Omega$  are connected between these terminals. This “medium” is of course neither homogeneous nor isotropic; but it has been found to behave almost like a homogeneous, isotropic medium, if the part of the network representing the air gap is bridged by a sufficient number of resistors in series. The permeability of air is represented by the conductivity of the network as a whole.

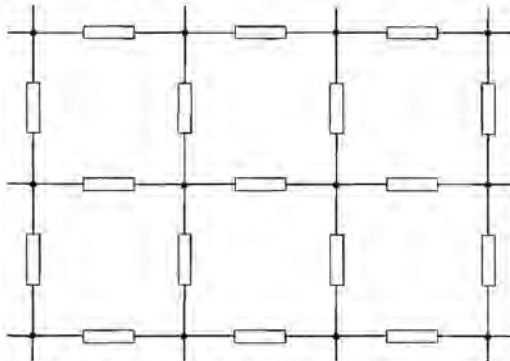


Fig. 4.2. Principle of part of the resistance network.



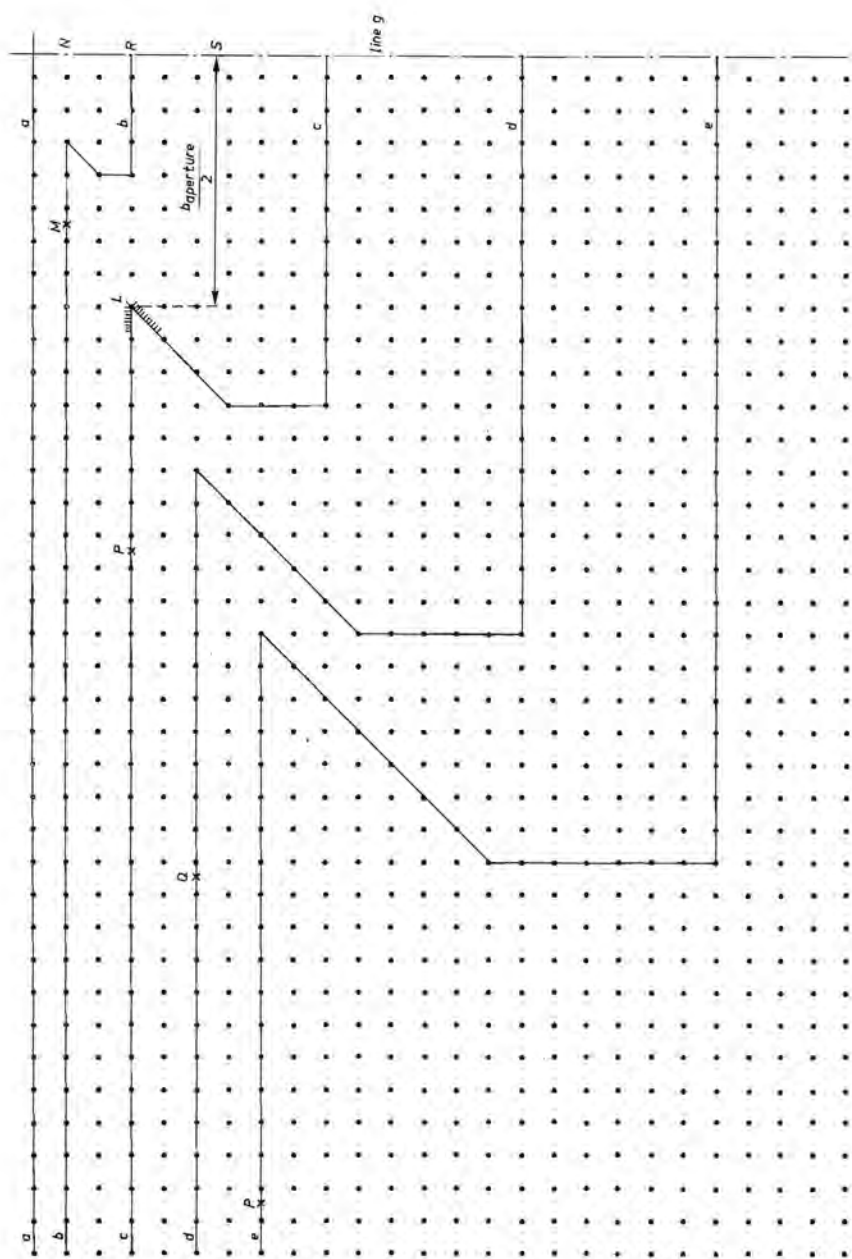


Fig. 4.3. Simulation of half a rotor slot with the aid of the resistance network (line g represents the line of symmetry of the slot).



If the permeability of the field poles and the top of the rotor teeth is thought to be infinite, their shape can be represented by short-circuiting the appropriate terminals.

Since the slots are symmetrical, we only need to map half a slot in this way; see fig. 4.3, where the line of symmetry of a slot corresponds with line g in the network (the distance from line g to the neighbouring terminals equals half the distance between successive terminals).

In fig. 4.3, the short-circuited terminals of line a represent the pole face. The short-circuited terminals of lines b, c, d and e all represent the same slot and air gap, the difference being that the air gap is bridged by 1, 3, 5 and 7 resistors in series respectively. The points M, P, Q and R thus all represent the same point on the face of the rotor tooth.

If a voltage  $U$  is connected between line a and e.g. line d, the current  $I$  delivered by the voltage source can be measured. Now to the left of Q there are 12 vertical rows of 5 resistors in series between line a and line d.

The current  $I_1$  flowing through them from line a to line d may be written:

$$I_1 = \frac{12 U}{5 \times 1000} = 0.0024 U. \quad (4.6)$$

To the right of Q, a current  $I_2$  runs from line a to line d:

$$I_2 = I - I_1. \quad (4.7)$$

Now the resistance between line a and line d of the portion to the right of Q can be calculated as

$$R = \frac{U}{I_2} = \frac{U}{I - I_1} = \frac{U}{I - 0.0024 U}. \quad (4.8)$$

The measured values of  $R$  for the various cases are tabulated in table 4-I. As the number of resistors bridging the air gap tends to infinity,  $R$  may be expected to tend to about 269  $\Omega$ .

TABLE 4-I

Influence of the number of resistors bridging the air gap on the accuracy of the simulation

resistance measured between lines	number of resistors in series	$R$ ( $\Omega$ )	increase in $R$ (%)
a and b	1	246.3	—
a and c	3	259.1	5.2
a and d	5	264.2	2.0
a and e	7	266.7	0.95

The measurements described below were carried out with 5 resistors in series. Seven resistors in series would have been still more accurate, but the network available was too small to allow this in all cases. In the example of table 4-1, five resistors in series give an error of about 1.8% in  $R$ . However, the error in  $k_{car}$  will be much smaller, for the following two reasons.

- (1) The resistance  $R$  only refers to a narrow zone, hardly wider than the air gap.
- (2) Most errors caused by simulation with such a network occur in regions representing sharp protrusions, such as tips of teeth. However, protrusions as sharp as those shown in fig. 4.3 do not occur in reality and are not investigated in this chapter.

Note: The measurements described in this chapter refer to slots shaped as shown in fig. 4.5. In practice, the tips of the teeth of such rotors and the field poles will never be saturated, neither by the stator field, nor by the rotor field.

#### 4.2. Determination of the carter factor with the aid of a two-dimensional resistance network

Figure 4.4 shows the resistance network used for these measurements. The resistors are not shown; only the terminals are represented as dots. There are 26 rows of 52 terminals in the actual network. However, not all 52 terminals in each row were used, so only 37 of them are drawn in each row.

The axis of symmetry of the slot is represented by line  $g$ , and the axis of symmetry of the tooth by line  $h$ ; the network thus represents half a tooth pitch. Five resistors in series bridge the air gap. If the air gap is e.g. 0.5 mm wide, the distance between two terminals corresponds to 0.1 mm. The tooth pitch simulated is thus  $b_{pitch} = 2 \times 26 \times 0.1 = 5.2$  mm. The lines drawn in the figure represent conductors joining the terminals. Line  $a$  at the top represents the pole face. Line  $ABCD$  represents the tooth face and the slot face. If a voltage is applied between the lines  $a$  and  $ABCD$ , the network offers a certain total resistance to the passage of current, which we shall denote by  $R_{pitch}$ . If all the terminals between  $B$  and  $E$  are connected with the terminals between  $A$  and  $B$ , an air gap without slots is simulated. The resistance between the lines  $a$  and  $ABE$  is called  $R_{pitch\ fict}$ . The ratio  $R_{pitch}/R_{pitch\ fict}$  corresponds to the ratio  $R_{m\ pitch}/R_{m\ pitch\ fict}$  mentioned in the introduction to this chapter. The carter factor of the air gap simulated by the network is thus approximately equal to

$$k_{car} = \frac{R_{pitch}}{R_{pitch\ fict}}. \quad (4.9)$$

The value of  $\gamma$  for the simulated air gap can be calculated with the aid of eqs (4.2) and (4.9) as

$$\gamma = \frac{b_{pitch}}{\delta} \frac{k_{car} - 1}{k_{car}} = \frac{b_{pitch}}{\delta} \left( 1 - \frac{R_{pitch\ fict}}{R_{pitch}} \right). \quad (4.10)$$

In sec. 4.3, measured values of  $\gamma$  are shown in diagrams. Such a value of  $\gamma$

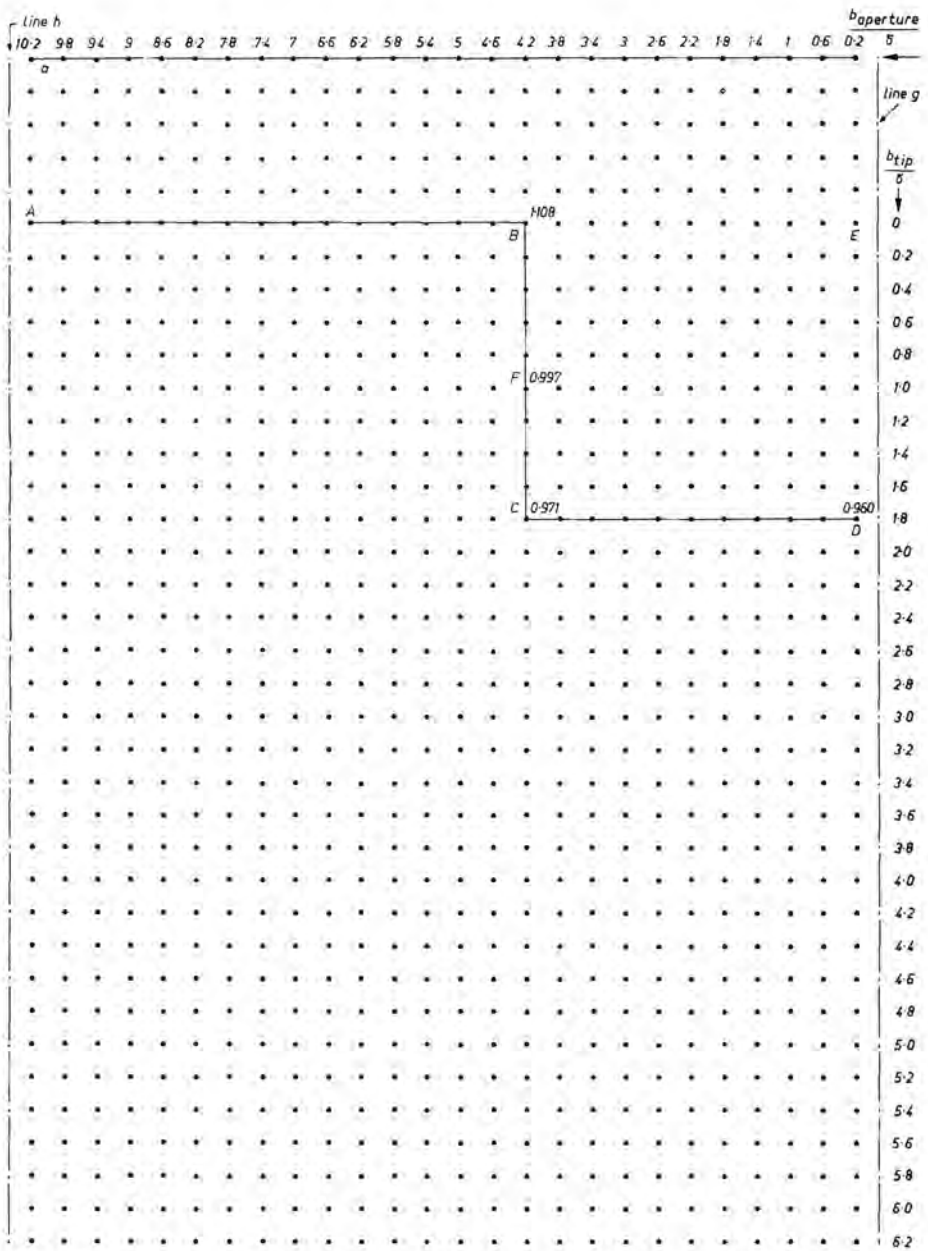


Fig. 4.4. Resistance network used to simulate rotor slots, with some measured values of the parameter  $\gamma$  (see eq. (4.2)).

refers to the tooth face represented by the portion of the line above the indicated value of  $\gamma$ . For instance, in fig. 4.7 the number 1.840 to the right of terminal D is the value of  $\gamma$  for the tooth face represented by the line ABCD. Similarly, the value of  $\gamma$  for the tooth face ABCDE is 1.828. It will be clear that for the lines ABCD and ABCDE the tooth face is not completed.

### 4.3. Measuring method and results

Figure 4.5 shows a rotor slot of a shape which is often used in small commutator machines and asynchronous motors. The shape shown in fig. 4.6 is also used sometimes; however, we shall consider fig. 4.5 first.

Section KLMN corresponds to the upper part of a rectangular slot of infinite depth. This is simulated in fig. 4.7 for two forms of the tooth tip, both with a large value of  $b_{\text{aperture}}/\delta$ . It might be expected that the flux leaving or entering the bottom of the tooth tip was relatively large. If this were the case, the measured value of  $\gamma$  at E would be much smaller than at D. However, this is found not to be the case. It follows that instead of simulating the face ABCDE it is sufficient in practice to simulate the face ABCD. If  $b_{\text{aperture}}/\delta$  is smaller, the error is still less.

In fig. 4.8 the tips of the teeth are shown rounded off near the air gap. The corresponding increase in  $\gamma$  (and in  $k_{\text{car}}$ ) is not negligible.

Figure 4.9 shows a resistance network simulating sharp tooth tips. The values of  $\gamma$  (and  $k_{\text{car}}$ ) for the faces DAB and DAC are almost equal, while the value for DAE is much higher than for DAB. Figure 4.10 shows  $\gamma$  as a function of  $b_{\text{aperture}}/\delta$  and  $b_{\text{tip}}/\delta$  at many points on the resistance network. Even if  $b_{\text{aperture}}/\delta$

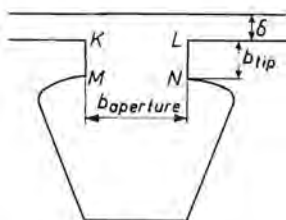


Fig. 4.5. A commonly used shape of rotor slot.

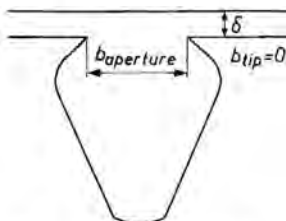


Fig. 4.6. A possible shape of rotor slot with  $b_{\text{tip}} = 0$ ; see also fig. 4.5.

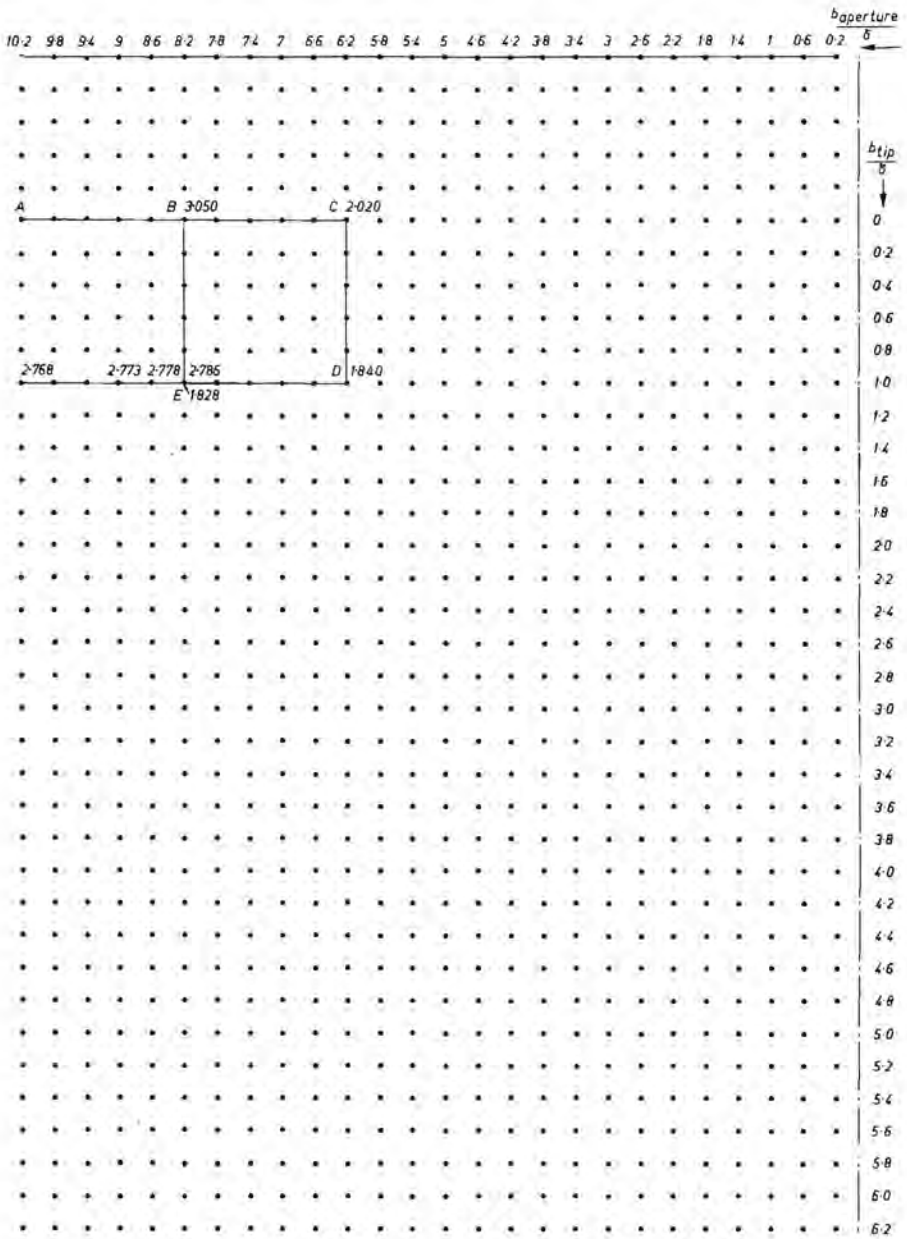


Fig. 4.7. Resistance network simulating the upper part of a rotor slot as in fig. 4.5 for two forms of the tooth tip. The values given against the curves represent measured values of the parameter  $\gamma$  of eq. (4.2).

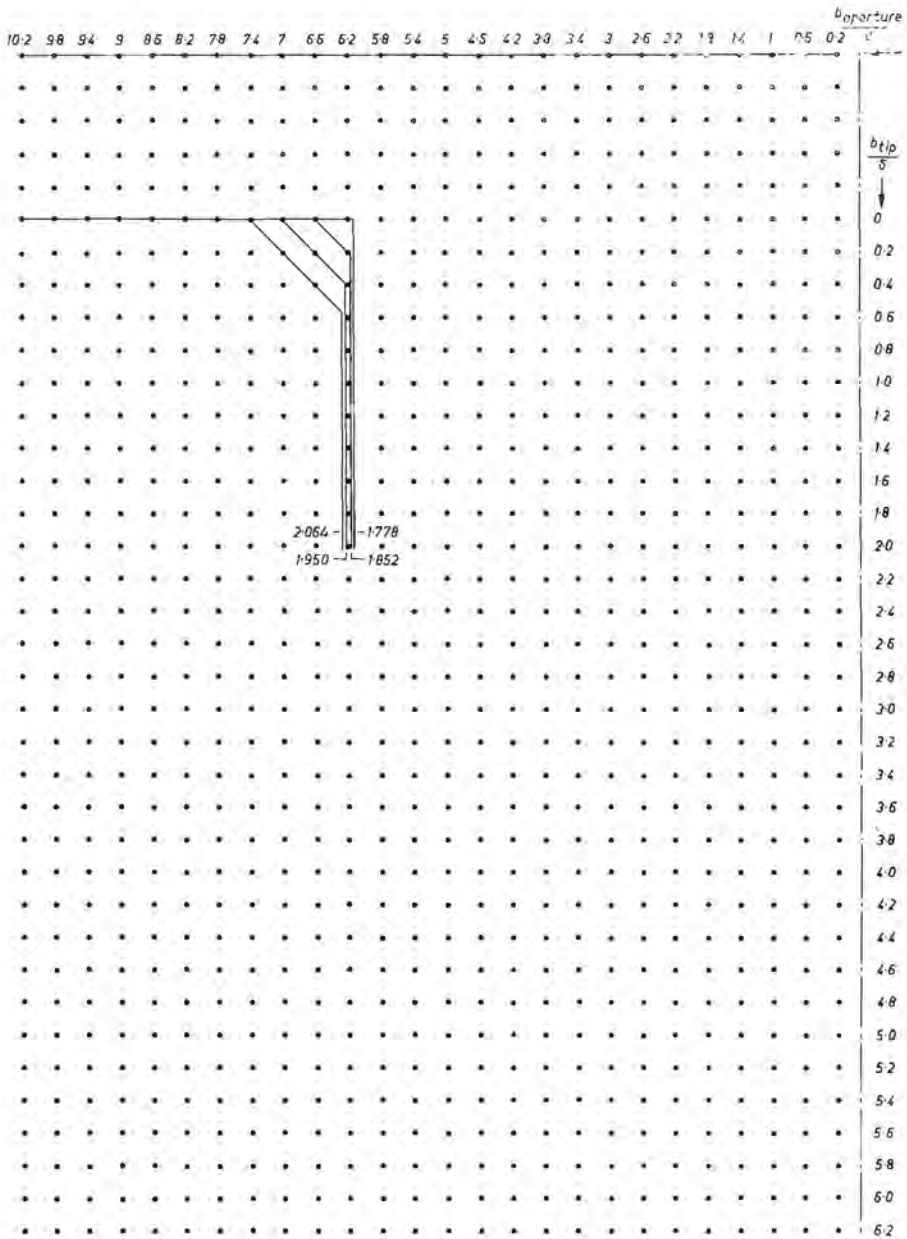


Fig. 4.8. Resistance network simulating the upper part of a rotor slot with tooth tips rounded off. The values given against the curves represent measured values of the parameter  $\gamma$  of eq. (4.2).

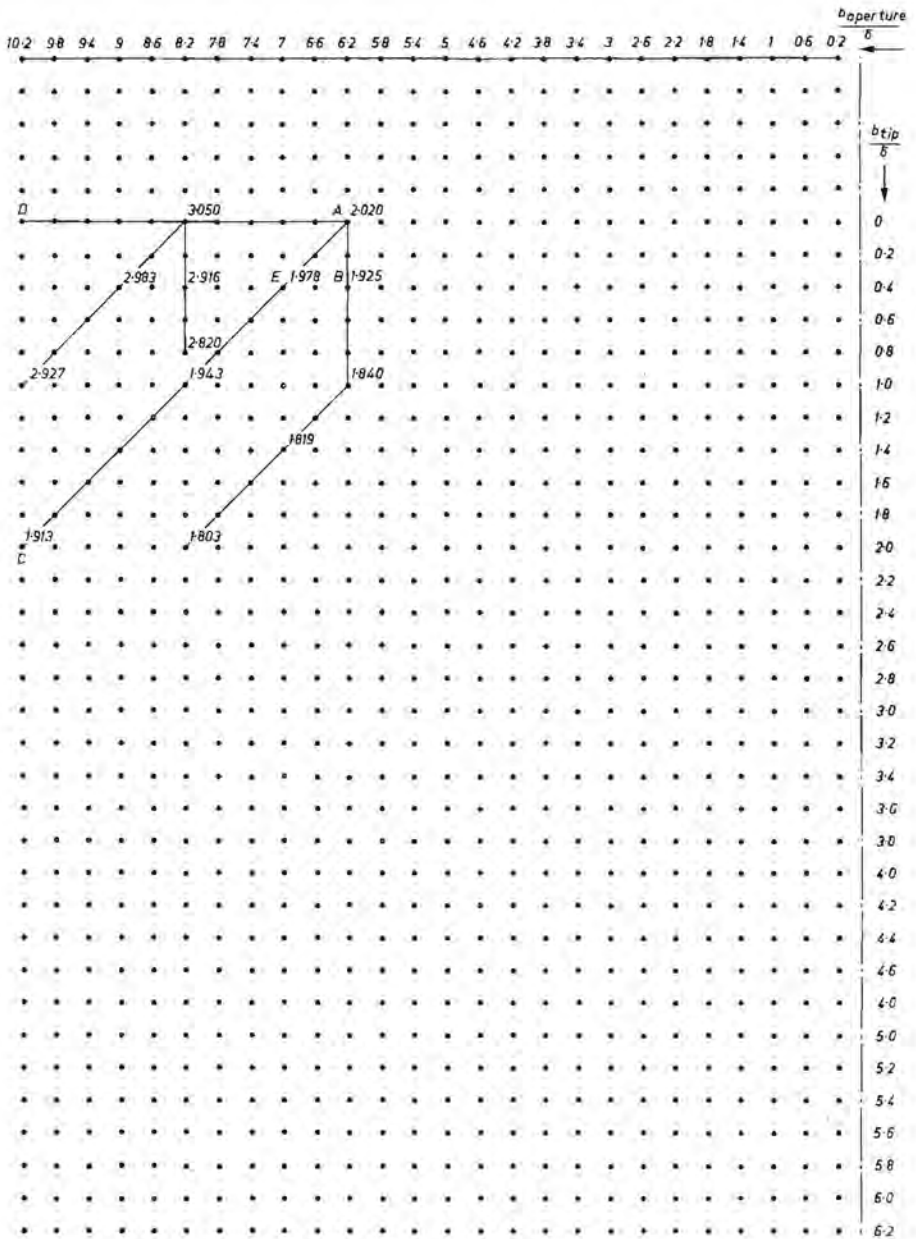


Fig. 4.9. Resistance network simulating the upper part of a rotor slot with sharp tooth tips. The values given against the curves represent measured values of the parameter  $\gamma$  of eq. (4.2).

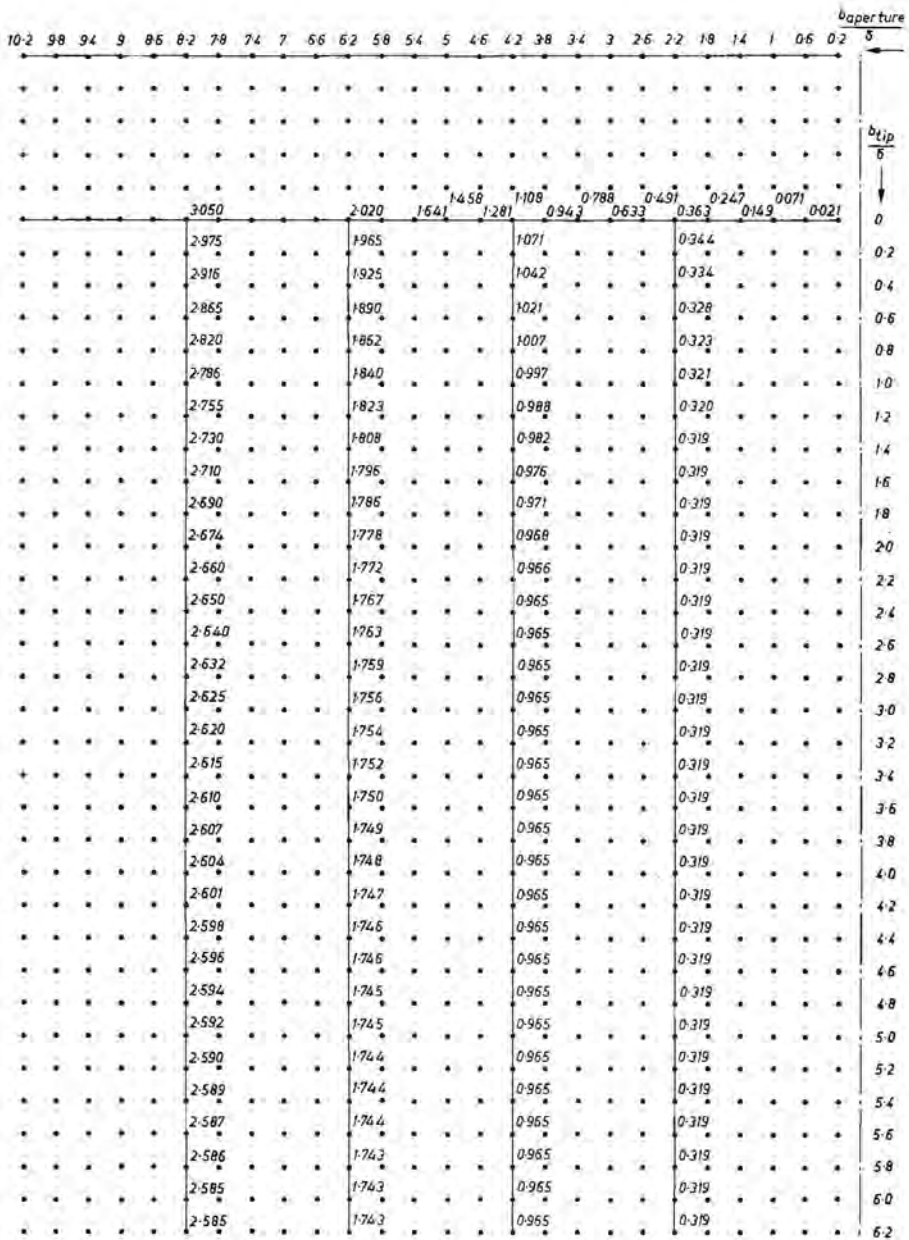


Fig. 4.10. Resistance network simulating rotor slots with various values of  $b_{aperture}/\delta$  and  $b_{tip}/\delta$ . The values given against the curves represent measured values of the parameter  $\gamma$  of eq. (4.2).



is very large (for instance 8.2), an increase in  $b_{tip}/\delta$  beyond about 3 has hardly any influence on  $\gamma$ . In practice, therefore,  $k_{car}$  is determined by the slot aperture and the shape of the tip of the tooth and not by the shape and dimensions of the rest of the slot. In fig. 4.10 the connections between the terminals representing the bottom of the slots are omitted. The values of  $\gamma$  at C and D in fig. 4.4 indicate that this procedure is acceptable.

#### 4.4. Graphical determination of the carter factor of semi-enclosed slots

The results of fig. 4.10 are presented graphically in fig. 4.11. It will be seen that the influence of  $b_{aperture}/\delta$  is of more importance than that of  $b_{tip}/\delta$ . The lowest possible value of  $b_{aperture}$  depends on the winding method used and on the thickness of the winding wire. In general,  $b_{aperture}$  is about 2.5 to 3 mm.

The width of the air gap  $\delta$  is seldom less than 0.4 mm, so  $b_{aperture}/\delta$  is generally less than about 8.

Figure 4.11 shows that the influence of  $b_{tip}/\delta$  increases as  $b_{aperture}/\delta$  increases. But even if  $b_{aperture}/\delta = 8$ ,  $b_{tip}/\delta$  need not be more than 3 in practice to give the minimum carter factor. If  $\delta = 0.5$  mm and  $b_{tip}/\delta = 3$ ,  $b_{tip} = 3 \times 0.5 = 1.5$  mm. In fact,  $b_{tip}$  is generally about 1.5 mm, in connection with the life

TABLE 4-II

Some values of the carter factor  $k_{car}$ , calculated with the aid of fig. 4.11 and eq. (4.2)

air-gap width $\delta$ (mm)	aperture width of slot $b_{aperture}$ (mm)	slot tip width $b_{tip}$ (mm)	$b_{aperture}$	$b_{tip}$	parameter $\gamma$ of eq. (4.2) read off from fig. 4.11	$\gamma \delta$ (mm)	carter factor $k_{car}$
			$\delta$	$\delta$			
0.4	2.4	0	6	0	3.85	1.440	1.168
0.4	2.4	1.2	6	3	3.33	1.332	1.154
0.4	2.4	2.4	6	6	3.33	1.332	1.154
0.4	3.2	0	8	0	5.90	2.360	1.309
0.4	3.2	1.2	8	3	5.07	2.028	1.254
0.4	3.2	2.4	8	6	5.00	2.000	1.250
0.8	2.4	0	3	0	1.26	1.008	1.112
0.8	2.4	1.2	3	1.5	1.10	0.880	1.096
0.8	2.4	2.4	3	3	1.10	0.880	1.096
0.8	3.2	0	4	0	2.04	1.632	1.195
0.8	3.2	1.2	4	1.5	1.78	1.424	1.166
0.8	3.2	2.4	4	3	1.78	1.424	1.166

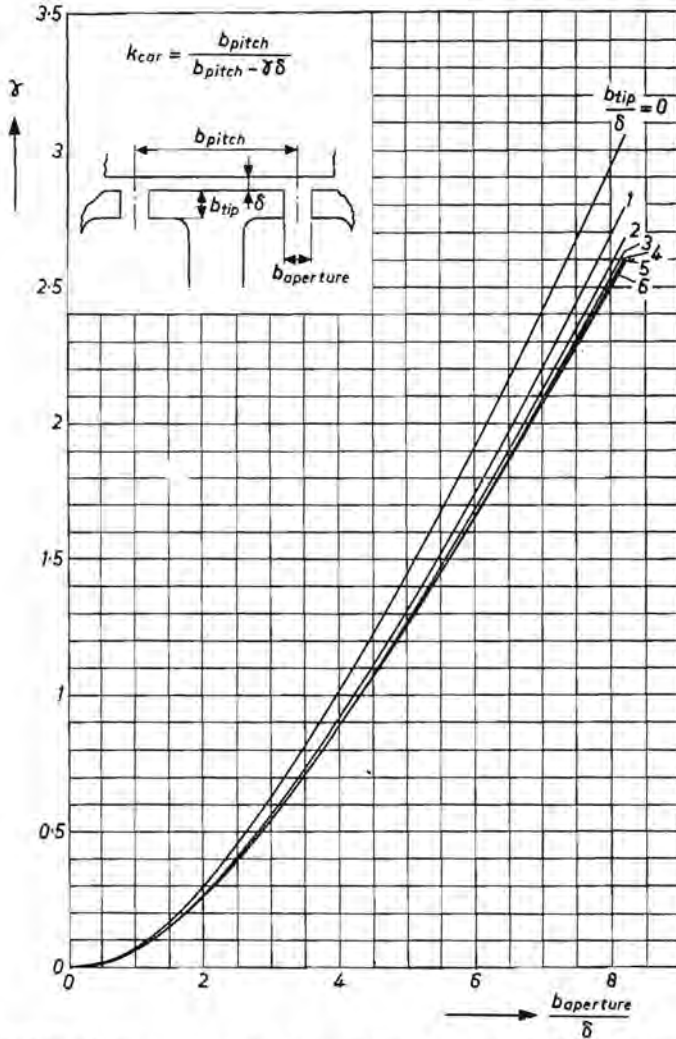


Fig. 4.11. Values of the parameter  $\gamma$  (see eq. (4.2)), measured on the resistance network of fig. 4.10, as a function of  $b_{aperture}/\delta$  and  $b_{tip}/\delta$  (see insert).

required for the die for stamping the laminations. Table 4-II shows some values of  $k_{car}$  calculated with the aid of the graph in fig. 4.11.

In all cases, the rotor was imagined to have 12 slots and  $d_r = 38.22$  mm. It follows that  $b_{pitch} = 10$  mm.  $k_{car}$  is calculated to 4 significant figures; of course the absolute accuracy is not as high as this, but the differences between the various values of  $k_{car}$  are indicated quite accurately.

Of course, the determination of  $\gamma$  with the resistance network is only an approximation. To indicate the level of accuracy obtained, values of  $\gamma$  determined in four different ways are compared in table 4-III.

TABLE 4-III

Values of  $\gamma$  (see eq. (4.2)) determined by four different methods

method		$b_{\text{aperture}}/\delta$			
		2	4	6	8
1	read off from fig. 4.11 for $b_{\text{tip}}/\delta = 6$	0.540	1.780	3.320	5.000
2	calculated from eq. (4.3)	0.558	1.794	3.306	4.950
3	calculated from eq. (4.4)	0.572	1.778	3.272	4.922
4	calculated from eq. (4.5)	0.500	2.000	3.500	5.000

The agreement between the results of methods 1 and 2 is striking. As shown in sec. 4.1, the measured value of  $R$  is a little too low; the values of  $\gamma$  in fig. 4.11 will thus all be a little too low as well.

Figure 4.11 shows that for low values of  $b_{\text{aperture}}/\delta$  the influence of  $b_{\text{tip}}$  is low; but at higher values of  $b_{\text{aperture}}/\delta$ , the value of  $\gamma$  for  $b_{\text{tip}}/\delta = 6$  is higher than for  $b_{\text{tip}}/\delta = \infty$ . These two factors mean that for low values of  $b_{\text{aperture}}/\delta$ , the values of  $\gamma$  determined by method 1 will be a little smaller than those determined by method 2, while for large values of  $b_{\text{aperture}}/\delta$  they will be a little larger.

Note: The specimen optimization calculation in sec. 8.6 was carried out before this study of the carter factor. The carter factor was therefore given a fixed value  $k_{\text{car}} = 1.1$  there.

#### 4.5. Conclusions

The carter factor  $k_{\text{car}}$  of rotors of small commutator machines having semi-enclosed slots cannot be calculated directly from the well-known formulas (4.2) and (4.3). However, it is possible to simulate the air-gap field with the aid of a resistance network and to estimate  $k_{\text{car}}$  from the values of the parameter  $\gamma$  measured on this network, as described in secs 4.1 and 4.2.

In practice, the slots of small commutator motors are generally shaped as shown in fig. 4.5 (with the faces KM and LN shown in that figure, parallel). The carter factor  $k_{\text{car}}$  of such a slot can be calculated in practice as if we were dealing with a rectangular slot of infinite depth, as long as KM is more than about 3 times the air-gap width  $\delta$  (see sec. 4.3). In this case eqs (4.2) and (4.3) can be used in practice to calculate  $k_{\text{car}}$ . In other cases the carter factor can be calculated with the aid of values of  $\gamma$  read off from fig. 4.11.

Tooth tips shaped as shown in fig. 4.6 or 4.8 should be avoided, as they give unfavourable values of the carter factor (see sec. 4.3).

## 5. THE ACTIVE INDUCTANCE OF A ROTOR COIL OF SMALL COMMUTATOR MACHINES WITH RESPECT TO COMMUTATION

In this chapter, the term “brush wear” will be used to cover wear of both commutator and brushes, while “brush life” will refer to the life of this combination.

Brush wear is the biggest problem encountered in the development of small commutator machines; a great deal of work is generally required to achieve the desired brush life. As is well known, brush wear is caused by the following factors.

- (1) Mechanical friction and the passage of current. In small commutator machines, the wear due to both these effects is generally much less than 1 micron per hour. Since, as we have mentioned, the brush life required seldom exceeds 1500 hours while the useful length of the brushes is generally more than 10 mm, it will be clear that this factor can be neglected in practice.
- (2) Sparking between the brushes and the commutator caused by jumping of the brushes. Jumping is caused by mechanical imperfections, such as unroundness of the commutator, vibrating brush holders; etc.
- (3) Sparking between the brushes and the commutator due to breaking of contact at the end of commutation. These commutation sparks are studied in this chapter.

Item (2) is often the main cause of brush wear; good mechanical construction thus forms the basis for the design of any small commutator machine.

In large electric machines, sparkless commutation is provided, generally with the aid of commutating poles and by using a relative large number of rotor coils. These means are too expensive to be used in small machines. Besides, they are not usually really necessary because the required life of the small machine is generally so short that sparking and rather serious brush wear are permissible; it just has to be limited.

There are many publications about various aspects of brush wear in small commutator machines. For instance:

- (1) the quality of commutators has been studied by Woerner <sup>3)</sup>;
- (2) the dynamic behaviour of brush springs has been studied by Hauschild <sup>2)</sup>;
- (3) the influence of brush material on commutation has been studied by Schröter <sup>5)</sup>;
- (4) commutation sparks have been studied by Padmanabhan and Srinivasan <sup>7)</sup>;
- (5) conditions for sparkless commutation in small commutator machines have been studied by Mohr <sup>17)</sup>.

The inductance of the commutating coil is an important factor, not only during commutation but also at the end of this process (during the spark). The commutating coil is magnetically coupled with the other rotor and stator coils and with eddy-current paths. This explains the frequency influence in the

coil inductance shown in fig. 5.1. Moreover, this commutating coil forms part of the electrical circuit of the machine.

It is therefore not clear what value of the inductance should be taken into account during commutation. The active inductance  $L_{comm}$  (the value of the inductance which must be reckoned with at the end of commutation during sparking) is studied in this chapter.

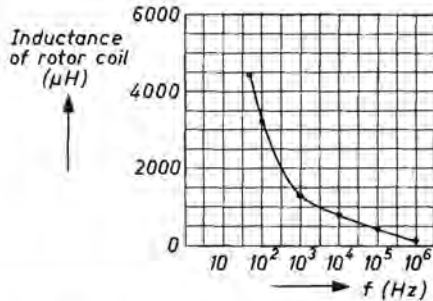


Fig. 5.1. Inductance of a rotor coil of 40 turns, measured with the aid of an AC bridge, of a motor with complete stator, detailed in fig. 5.13, relative stack length  $\lambda$  being 0.5.

### 5.1. The relation between brush wear and the spark voltage between brush and segment

In commutator machines, a spark is produced each time the contact between a brush and a segment ends, provided that the voltage drop between brush and segment is high enough. This voltage drop can be varied and brush wear can be measured with the device sketched in fig. 5.2. For this purpose, slip ring  $d$  is connected with segment  $a$ . The slip ring and both segments are fixed on a shaft, the speed of which is adjustable. A variable DC voltage  $U$  is applied between the brushes  $c$  and  $e$  in series with the variable resistor  $R$ . There is no inductance other than parasitic inductance in the circuit.

When segment  $a$  makes contact with brush  $c$ , a current  $i$  flows from the voltage source via  $c$ ,  $a$ ,  $d$ ,  $e$  and  $R$  back to the voltage source. When the contact

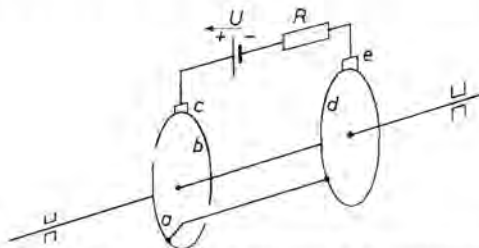


Fig. 5.2. Principle of a device for measuring the influence of the voltage between a segment and brush on commutation sparking and brush wear.

between a and c is broken, the current  $i$  falls from  $U/R$  to 0. During this period, the spark-voltage drop  $U - iR$  increases from about 0 to  $U$ . If we neglect parasitic induction voltages, the voltage drop between brush and segment never exceeds the value of  $U$ .

With a fixed rotor speed of e.g. 10 000 r.p.m., brush wear can be measured in microns per hour for various values of  $U$  and  $R$ . As long as  $U$  is smaller than about 12 V, brush wear is negligible ( $\ll 1$  micron per hour), and under normal atmospheric conditions independent of the value of  $R$  (and  $i$ ). At values of  $U$  above about 12 V, the brush wear increases sharply with voltage. These results confirm the findings of Padmanabhan and Srinivasan <sup>7)</sup>, who found a spark voltage of about 12 V, almost independent of the spark current  $i$ .

It follows that in the determination of the active inductance of a rotor coil during sparking, the spark can be simulated by a Zener diode with a Zener voltage of about 12 V.

### 5.2. The current in the commutating coil

Figure 5.3 shows three possible positions of the rotor of a commutator machine, with 6 rotor coils. Let us concentrate our attention on coil 4. In fig. 5.3a this coil is still in the left-hand circuit. In fig. 5.3b it is short-circuited by the lower brush and in fig. 5.3c it is in the right-hand circuit. The direction of the current through the coil changes correspondingly as it moves in this way.

Figure 5.4 shows the three possible ways in which the current can change during commutation. In fig. 5.4a the current changes too little; most probably a spark will be generated. In fig. 5.4c the current changes too much; in this case too, a spark will most probably be generated. Figure 5.4b shows ideal commutation. Even in this case, if the instantaneous value of the sum of all

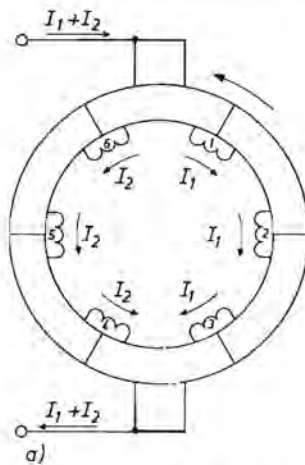


Fig. 5.3. Principle of the electric circuit of the rotor of a small commutator machine.

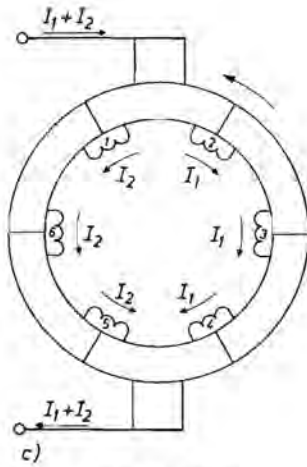
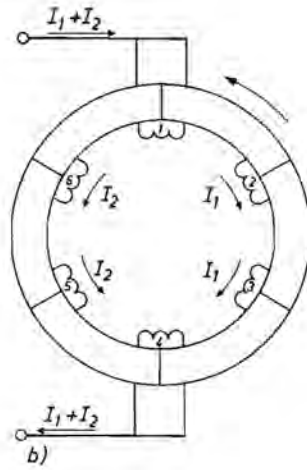


Fig. 5.3 b and c.

the voltages in the short-circuited coil is more than about 12 V at the end of commutation, it is still possible that a spark will be generated.

The current jump at the end of commutation may have various values, but it will generally be less than  $I_1$ . In order to make the measuring results reproducible, however, the current jump was always taken from 0 to  $I_1$  in the measurements described below.

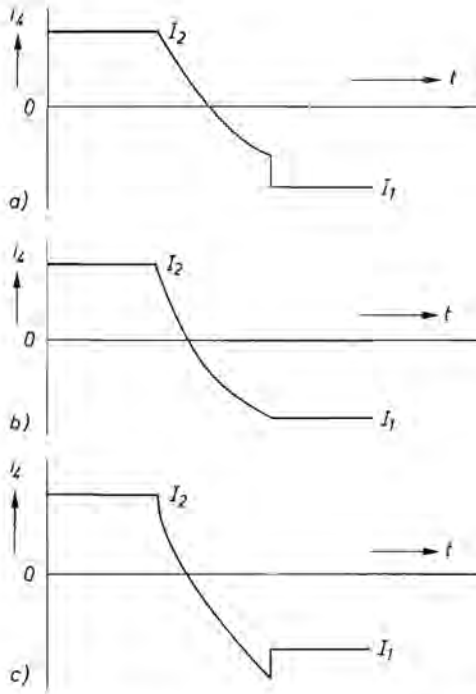


Fig. 5.4. Three possible forms for the current in a commutating coil of a small commutator motor.

### 5.3. The method of measurement

The inductance of the commutating coil is of importance because it influences the energy dissipated in the commutation spark, and this energy causes the brush wear. We shall now describe how this active inductance can be measured. The motor circuit used for the measurement is indicated in fig. 5.10a. A stator coil with  $w_s$  turns may be connected in series or in parallel with the rotor. Let us consider rotor coil 1. Figure 5.5 shows three possible positions of this coil occurring before, during and after the sparking period.  $d\phi/dt$  is the total voltage induced in coil 1;  $I_2$  is the current in the left-hand circuit of the rotor (rotor coils 7-12). The inductance of these six coils together tends to keep  $I_2$  constant. Similarly, the current  $I_1$  through coils 2-6 tends to be kept constant by the inductance of these five coils. During the spark,  $I_1$  and  $I_2$  are almost constant, but  $dI_1/dt$  and  $dI_2/dt$  cannot be neglected. Let the current in coil 1 be called  $i_1$ . In the position shown in fig. 5.5a, there is no relation between  $i_1$  and  $I_1$ . The current through the spark in the position of fig. 5.5b is denoted by  $i_{\text{spark}}$ . In this case:

$$i_{\text{spark}} = I_1 - i_1. \quad (5.1)$$



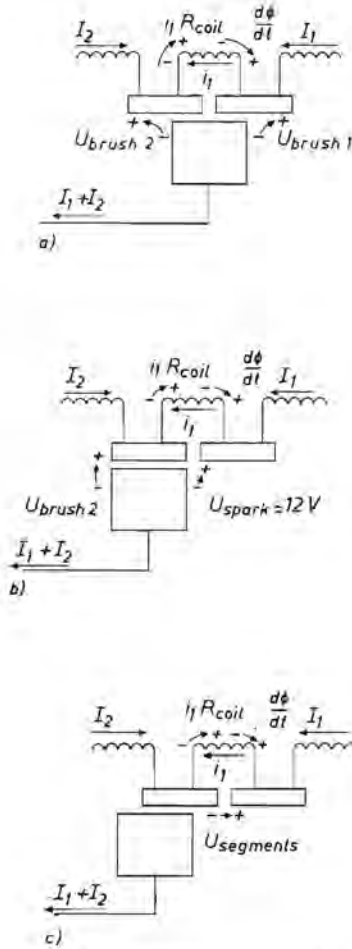


Fig. 5.5. The currents and voltages in a commutating coil of a small commutator motor; (a): during commutation, (b): during sparking, and (c): after sparking.

As we have seen above,  $I_1$  is roughly constant during the spark discharge. In the situation of fig. 5.5c we have

$$i_1 = I_1. \quad (5.2)$$

$U_{brush 1}$  and  $U_{brush 2}$  are the voltage drops between the brush and the right-hand and left-hand segments of coil 1 respectively.  $U_{spark}$  is the voltage drop in the spark. As we saw in sec. 5.1,  $U_{spark} \approx 12$  V. The voltage  $U_{segments}$  in fig. 5.5c does not have a fixed value. It is roughly equal to the voltage between the two brushes divided by half the number of segments.

During sparking,  $i_1$  varies from a certain initial value to  $I_1$ . Now  $i_1$  satisfies the equation

$$U_{\text{brush } 2} + i_1 R_{\text{coil}} + \frac{d\phi}{dt} - U_{\text{spark}} = 0. \quad (5.3)$$

$\phi$  is generated by the currents through all the rotor coils and the current  $i_s$  through the stator coils. These contributions to  $\phi$  also depend on the position  $\alpha$  of the rotor:

$$\phi = \phi_{1(\alpha; i_1)} + \phi_{2(\alpha; i_2)} + \dots + \phi_{3(\alpha; i_{12})} + \phi_{s(\alpha; i_s)}, \quad (5.4)$$

whence

$$\frac{d\phi}{dt} = \frac{\partial \phi_1}{\partial \alpha} \frac{\partial \alpha}{\partial t} + \frac{\partial \phi_1}{\partial i_1} \frac{\partial i_1}{\partial t} + \dots \quad (5.5)$$

In eq. (5.4), magnetic fluxes generated by eddy currents are neglected. In eqs (5.4) and (5.5),  $i_2$  to  $i_6$  and  $i_7$  to  $i_{12}$  are generally equal to  $I_1$  and  $I_2$  respectively;  $i_1$ ,  $I_1$  and  $I_2$  are interdependent. A variation in  $i_1$  induces voltages in the other coils; moreover, all the coils are galvanically connected in the electric circuit of the motor. These two effects cannot be neglected here.

The influence of rotation on  $d\phi/dt$  must be eliminated. We must ensure that the terms

$$\frac{\partial \phi_1}{\partial \alpha} \frac{\partial \alpha}{\partial t}, \quad \frac{\partial \phi_2}{\partial \alpha} \frac{\partial \alpha}{\partial t}, \quad \dots, \quad \frac{\partial \phi_s}{\partial \alpha} \frac{\partial \alpha}{\partial t} \quad \text{are zero;}$$

this can be done by keeping the rotor stationary; then  $d\alpha/dt = 0$ .

If the motor is supplied by an AC voltage,  $I_1$  and  $I_2$  vary roughly sinusoidally. This gives rise to an extra transformer e.m.f. in coil 1, which can be eliminated for the measurements by supplying the motor with a DC voltage.

Since the rotor does not rotate,  $U_{\text{brush } 2}$  can be eliminated by replacing the contact between segment and brush by a soldered connection.

If now the spark is simulated by a Zener diode of Zener voltage  $U_Z$ , eq. (5.3) becomes

$$i_1 R_{\text{coil}} + \frac{\partial \phi_1}{\partial i_1} \frac{\partial i_1}{\partial t} + \dots + \frac{\partial \phi_{12}}{\partial i_{12}} \frac{\partial i_{12}}{\partial t} + \frac{\partial \phi_s}{\partial i_s} \frac{\partial i_s}{\partial t} - U_Z = 0. \quad (5.6)$$

The difference between the situations of fig. 5.5a and b can be simulated by short-circuiting the Zener diode in fig. 5.5a, which makes  $U_Z = 0$  in eq. (5.6). In the situation of fig. 5.5a, the steady-state value of  $I_1$  equals the voltage between the two brushes divided by the resistance of five coils. When the Zener diode is no longer short-circuited,  $I_1$  flows through six rotor coils in the steady state. In practice,  $i_1 R_{\text{coil}} \ll U_Z$ . If the relation between  $\phi_1, \phi_2, \dots, \phi_{12}$  and  $\phi_s$  on the one hand and  $i_1, i_2, \dots, i_{12}$  and  $i_s$  respectively on the other hand is linear and if the relation between  $di_1/dt$  and the contribution

of  $di_1/dt$ ,  $di_2/dt$ ,  $di_3/dt$ , ...,  $di_{12}/dt$  and  $di_s/dt$  is also linear, then the terms

$$\frac{\partial \phi_1}{\partial i_1} \frac{\partial i_1}{\partial t} + \frac{\partial \phi_2}{\partial i_2} \frac{\partial i_2}{\partial t} + \dots + \frac{\partial \phi_{12}}{\partial i_{12}} \frac{\partial i_{12}}{\partial t} + \frac{\partial \phi_s}{\partial i_s} \frac{\partial i_s}{\partial t}$$

can be written simply:

$$L_{\text{comm}} \frac{di_1}{dt},$$

Equation (5.6) then becomes

$$i_1 R_{\text{coll}} + L_{\text{comm}} \frac{di_1}{dt} - U_Z = 0, \quad (5.7)$$

and if  $i_1 R_{\text{coll}}$  can be neglected:

$$L_{\text{comm}} \frac{di_1}{dt} - U_Z = 0. \quad (5.8)$$

Measurements show that  $i_1$  varies about linearly from a certain value (e.g.  $i_1 = 0$ ) to  $I_1$ , which means that the assumptions on which the use of  $L_{\text{comm}} di_1/dt$  is based are quite well justified. In our measurements,  $i_1$  always starts from  $i_1 = 0$ . The time interval during which  $i_1$  increases (nearly linearly) from 0 to  $I_1$  is denoted by  $t_Z$ ; we may call this the spark decay time. We thus have

$$\frac{di_1}{dt} \approx \frac{I_1}{t_Z}. \quad (5.9)$$

It follows from eqs (5.8) and (5.9) that

$$L_{\text{comm}} = \frac{U_Z t_Z}{I_1}. \quad (5.10)$$

During the time that  $i_1$  increases about linearly from 0 to  $I_1$ , the current through the Zener diode  $i_Z$  decreases roughly linearly from  $I_1$  to 0, since

$$i_Z = I_1 - i_1. \quad (5.11)$$

The energy dissipated in the Zener diode corresponding to the energy dissipated in the spark in a real motor is approximately

$$\begin{aligned} W_Z &= \int_0^{t_Z} i_Z U_Z dt = \int_0^{t_Z} (I_1 - i_1) U_Z dt = \\ &= I_1 U_Z t_Z - \frac{1}{2} I_1 U_Z t_Z = \frac{1}{2} I_1 U_Z t_Z. \end{aligned} \quad (5.12)$$

If  $U_Z t_Z / I_1$  in eq. (5.12) is replaced by  $L_{\text{comm}}$  in accordance with eq. (5.10), we obtain:

$$W_Z = \frac{1}{2} L_{\text{comm}} I_1^2; \quad (5.13)$$

$L_{\text{comm}}$  has the dimensions of an inductance, and together with  $I_1$  it determines the energy dissipated in the Zener diode.

We can now describe the measuring method, with reference to the circuit diagram of fig. 5.6. The coils 1–12 correspond to the rotor coils 1–12 in fig. 5.10a.

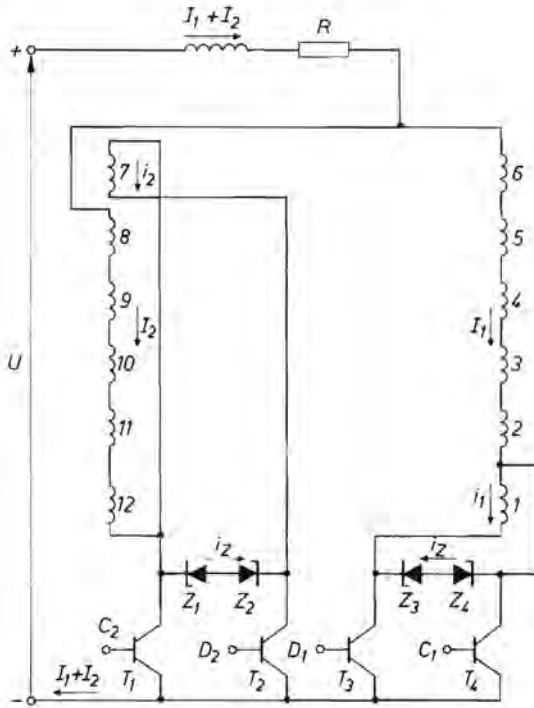


Fig. 5.6. Circuit for measurement of the active inductance of a commutating rotor coil  $L_{\text{comm}}$ .

Commutation is simulated in coils 1 and 7, with the aid of transistors  $T_1$ ,  $T_2$ ,  $T_3$  and  $T_4$ . If the mechanical position of coil 7 remains the same, it can be connected electrically below coil 12; this simplifies the switching of the four transistors. When  $T_4$  is conducting and  $T_3$  is cut off, coil 1 is short-circuited. When  $T_3$  is conducting and  $T_4$  is cut off,  $I_1$  passes through coil 1, and part of this current will temporarily pass through the Zener diode. If  $T_3$  and  $T_4$  are switched periodically by means of a square-wave voltage, then a display of  $U_Z$  and  $i_Z$  on the screen of an oscilloscope will give a stationary image. If the time base of the oscilloscope is calibrated, the time interval  $t_Z$  can be read off. Normally, the transistor  $T_2$  is conducting and  $T_1$  is cut off, so  $I_2$  passes through coil 7. If the base of  $T_1$  is connected to the base of  $T_4$  and the base of  $T_2$  to that of  $T_3$ , simultaneous commutation of coils 1 and 7 is simulated.

Figure 5.7 shows the image as displayed on the oscilloscope screen during this measurement, and indicates how  $t_z$  can be read off. If the Zener voltage  $U_z$  is known and  $I_1$  is determined from the supply voltage  $U$  and the coil resistances, the value of  $L_{\text{comm}}$  can now be calculated from eq. (5.10).

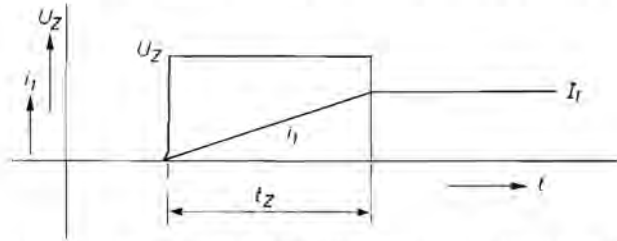


Fig. 5.7. Principle of the determination of the spark decay time  $t_z$  from the image on the oscilloscope screen.

#### 5.4. Description of the rotors and stators measured

Commutator machines can have different types of stators, which can be classified as follows.

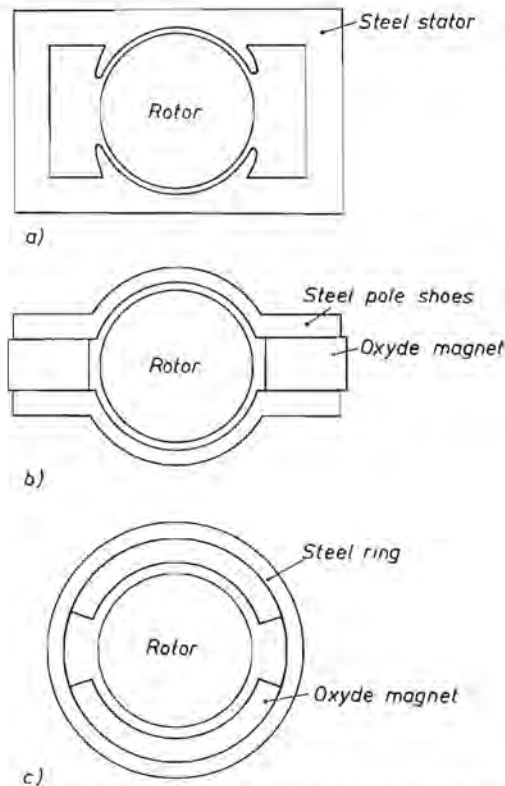


Fig. 5.8. Three possible types of stator for a small commutator motor.

*Stator type A.* A complete steel stator, excited by a current through the stator coils; see fig. 5.8a.

*Stator type B.* Block-shaped ceramic magnets, fixed beside the rotor. The flux is conducted through the rotor via laminated steel pole shoes; see fig. 5.8b. As far as the magnetic fields generated by the rotor are concerned, these magnets behave like air, and no eddy currents can be generated in them. The magnets thus have no influence on  $L_{\text{comm}}$ , unless they saturate the iron of the rotor. For the determination of  $L_{\text{comm}}$ , the pole shoes can be used without the ceramic magnets.

*Stator type C.* A ring or segments made of ceramic magnets or comparable materials; see fig. 5.8c. The magnets again behave like air as far as the magnetic fields generated by the rotor are concerned. A steel ring surrounds the ring or segments. This ring is so far away that it is found not to influence  $L_{\text{comm}}$  in practice. For such motors,  $L_{\text{comm}}$  can be measured with the stator removed.

Variants which hardly ever occur, such as type B with steel magnets, are not considered here.

The shape of the laminations of the rotor and the stator is shown as accurately as possible above the tabulated measuring results in sec. 5.5. The indication that the relative rotor length  $l_r = 0$  in these tables means that the rotor coils are wound on insulating discs shaped like a rotor lamination. The rotor thus consists entirely of end windings, shaped as in a real rotor.

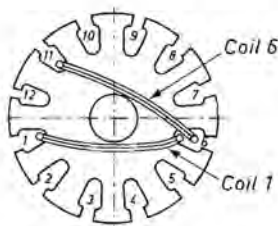


Fig. 5.9. A rotor lamination with numbered slots, with two coils (1 and 6) shown in position.

Figure 5.9 shows the shape of a rotor lamination with slots numbered 1–12. The measurements are carried out on rotors with 12 or 24 coils.

Table 5-I gives the arrangement of the rotor coils in the slots, and shows whether a given side of a rotor coil is situated underneath or on top in a rotor slot. The rotor and stator stacks are made of steel sheet 0.5 mm thick with a resistivity of about  $0.3 \Omega \text{ mm}^2 \text{ m}^{-1}$ . All the laminations of the rotors and stators are insulated from one another.

Different situations will be considered. Most of them are combinations of the following possibilities:

TABLE 5-1

Arrangement of the coils in the rotor slots

rotor with 12 coils			rotor with 24 coils		
coil No.	No. of the slot in which one side of the coil is situated	No. of the slot in which the other side of the coil is situated	coil No.	No. of the slot in which one side of the coil is situated	No. of the slot in which the other side of the coil is situated
1	1 below	6 below	1	1 below	6 below
2	2 below	7 below	2	1 below	6 below
3	3 below	8 below	3	2 below	7 below
4	4 below	9 below	4	2 below	7 below
5	5 below	10 below	5	3 below	8 below
6	6 on top	11 below	6	3 below	8 below
7	7 on top	12 below	7	4 below	9 below
8	8 on top	1 on top	8	4 below	9 below
9	9 on top	2 on top	9	5 below	10 below
10	10 on top	3 on top	10	5 below	10 below
11	11 on top	4 on top	11	6 on top	11 below
12	12 on top	5 on top	12	6 on top	11 below
			13	7 on top	12 below
			14	7 on top	12 below
			15	8 on top	1 on top
			16	8 on top	1 on top
			17	9 on top	2 on top
			18	9 on top	2 on top
			19	10 on top	3 on top
			20	10 on top	3 on top
			21	11 on top	4 on top
			22	11 on top	4 on top
			23	12 on top	5 on top
			24	12 on top	5 on top

- (1) the brushes are narrower than 1 commutator segment or they are wider than 1 but narrower than 2 segments;
- (2) commutation of a given coil ends before, at the same time as, or later than commutation of the opposite coil.

Combination of (1) and (2) gives a total of 6 possibilities, which are sketched in fig. 5.10. The value of  $L_{\text{comm}}$  measured for  $\lambda = 0.5$  and a wound stator (type A) in the cases of fig. 5.10 is indicated alongside each figure. Short-circuiting a neighbouring coil or an opposite coil has a striking effect on the value found for  $L_{\text{comm}}$ . A brush narrower than 1 segment should therefore never be used in practice. The situation shown in fig. 5.10d is called the "common case".

### 5.5. Measuring results

The results of the measurements are tabulated in tables 5-II to 5-XI. The corresponding experimental conditions are shown in figs 5.11–5.14 and figs 5.17–5.22. We shall now discuss various points emerging from the results.

#### *The influence of short-circuited rotor coils*

See figs 5.11, 5.12 and 5.13. Some values of  $L_{\text{comm}}$  found in these measurements are also plotted in fig. 5.10. The value of  $L_{\text{comm}}$  for a given rotor coil falls sharply when other rotor coils are short-circuited, especially in the case with the complete stator; this effect is least marked in the set-up "without stator or pole shoes". In the cases 4, 5 and 6, one rotor coil is short-circuited each time. The difference is that coil 6 (case 4) and coil 8 (case 6) each have one end in one of the slots in which coil 1 is situated. This decreases  $L_{\text{comm}}$  in the cases without stator or pole shoes. It is found to be unfavourable if commutation ends exactly at the same moment in opposite coils, especially in the cases with pole shoes and stator.

#### *The influence of tapped coils*

See fig. 5.14. In small commutator machines a rotor with 12 slots is often used together with a commutator having 24 segments. Under these conditions each coil is tapped half-way (see the right-hand column in table 5-I). Tapping the coils makes  $L_{\text{comm}}$  decrease extremely sharply, as may be seen from a comparison of fig. 5.14 with fig. 5.13. When commutation of the first half of a tapped coil ends, the second half of the coil, situated in the same slots, is short-circuited. When commutation of the second half ends, the first half of the next coil is short-circuited; but this half coil is situated with both ends in other slots. To see how striking this difference is, cases 3 and 5 in fig. 5.14 should be compared with cases 7 and 8. This explains why the state of the commutator segments in such motors is often alternately good and bad.



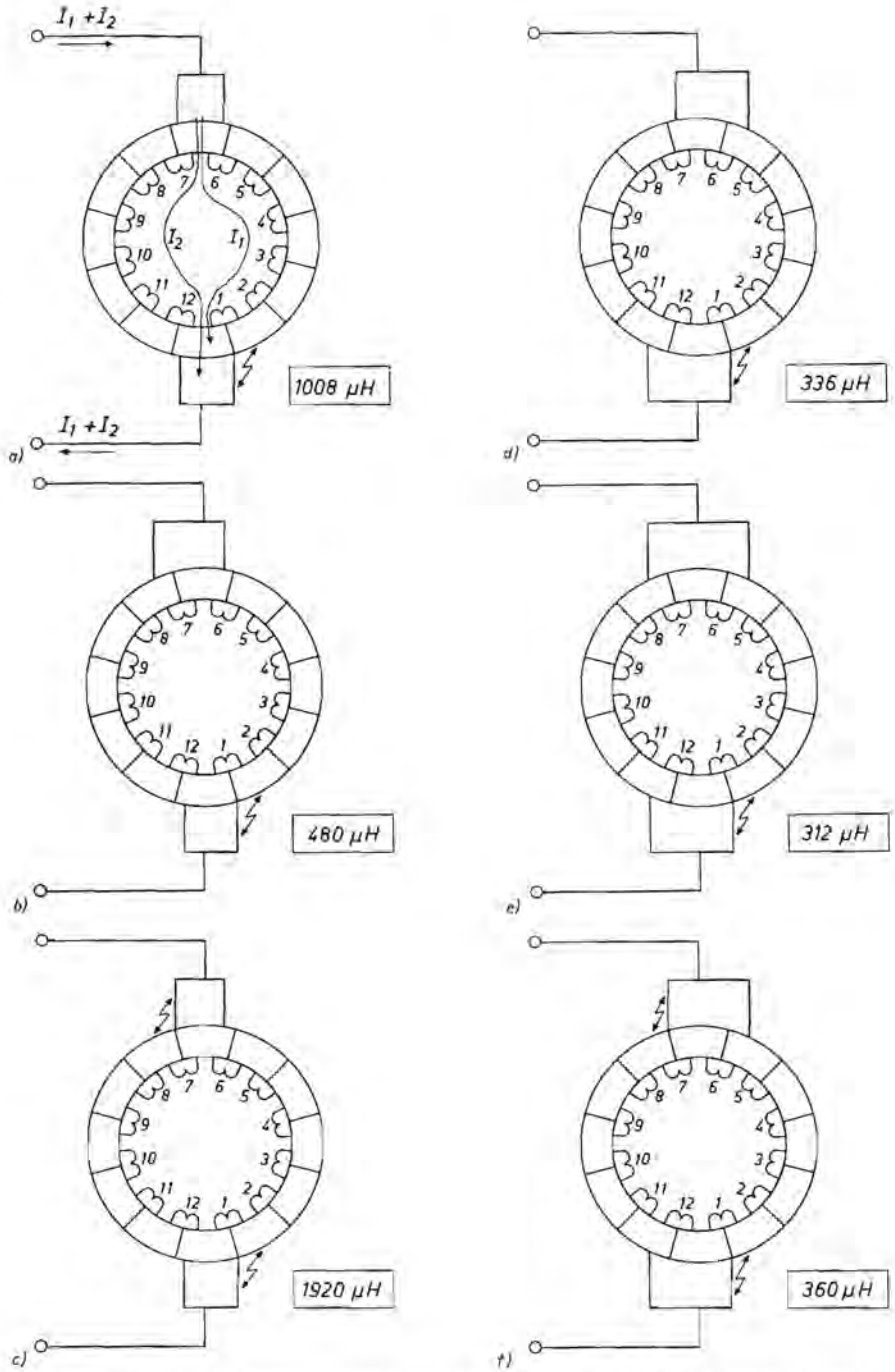


Fig. 5.10. Various possible ways of short-circuiting rotor coils as functions of the width and the position of the brushes.

*The influence of the values of  $I_1$ ,  $U_Z$  and  $w_{\text{coil } r}$*

In the definition of  $L_{\text{comm}}$  it was assumed that for a given motor the value of  $L_{\text{comm}}$  does not depend on the values of  $U_Z$  and  $I_1$ . If this is correct,  $L_{\text{comm}}$  can be expressed as

$$L_{\text{comm}} = (w_{\text{coil } r})^2 A, \quad (5.14)$$

where  $A$  is constant. If now  $w_{\text{coil } r}$  is varied,  $L_{\text{comm}}$  varies proportionately to  $w_{\text{coil } r}$ , but the ratio  $L_{\text{comm}}/(w_{\text{coil } r})^2$  is constant. If  $L_{\text{comm}}$  varies when  $U_Z$  or  $w_{\text{coil } r}$  is varied,  $L_{\text{comm}}$  must also depend on  $I_1$ , because in the formula for the magnetic energy of a rotor coil  $I_1$  and  $w_{\text{coil } r}$  appear as the product  $I_1 w_{\text{coil } r}$ . Figure 5.15 shows that  $L_{\text{comm}}/(w_{\text{coil } r})^2$  is not quite constant, but decreases for high values of  $U_Z$ . This quantity also decreases sharply when  $w_{\text{coil } r}$  falls below 40.

Figure 5.16 shows that  $L_{\text{comm}}$  also decreases for low values of  $I_1$ .

Conclusion:  $L_{\text{comm}}$  is lower for low values of the product  $I_1 w_{\text{coil } r}$ . It is also a little lower for high values of  $U_Z$ .

*The influence of the brush resistance in series with neighbouring short-circuited rotor coils*

In the measurements, one or more rotor coils were often fully short-circuited to simulate short-circuiting by a brush. However, brushes do not fully short-circuit a rotor coil, especially if they are jumping. To study the influence of the brush resistance, the terminals of coil 12 were connected to the resistor  $R_1$ ; see fig. 5.17. Even for values of  $R_1$  up to 100  $\Omega$ ,  $L_{\text{comm}}$  increases only slightly; 100  $\Omega$  is much more than the real brush resistance. However, if the brushes are jumping, the brush resistance or brush voltage may rise so far that  $L_{\text{comm}}$  increases more. This may be another reason for increased brush wear in motors with jumping brushes. See also item (2) on p. 67.

*The influence of short-circuited stator coils*

Short-circuiting the stator coils in commutator machines will influence  $L_{\text{comm}}$ . In a shunt motor, for example, the stator coils are short-circuited via the internal resistance of the voltage supply source. Figure 5.18 shows that fully short-circuiting the 400 turns of the stator coils reduces  $L_{\text{comm}}$ , even if some rotor coils were already short-circuited. The same improvement can be obtained by connecting a resistor of 100  $\Omega$  or a capacitor of 0.02  $\mu\text{F}$  parallel to the stator. In a real machine, the same result can be obtained by shunting a resistor or capacitor across the stator coils. The use of a resistor has the disadvantage that the power losses will be increased. The capacitor gives no power loss and even the current through it can be neglected, for 0.02  $\mu\text{F}$  corresponds to about 160 000  $\Omega$  at 50 Hz.

Figs. 5.11.—5.14. Conditions for the measurement of the active inductance of a rotor coil,  $L_{comm}$ . The results are shown in tables 5-II–5-V.

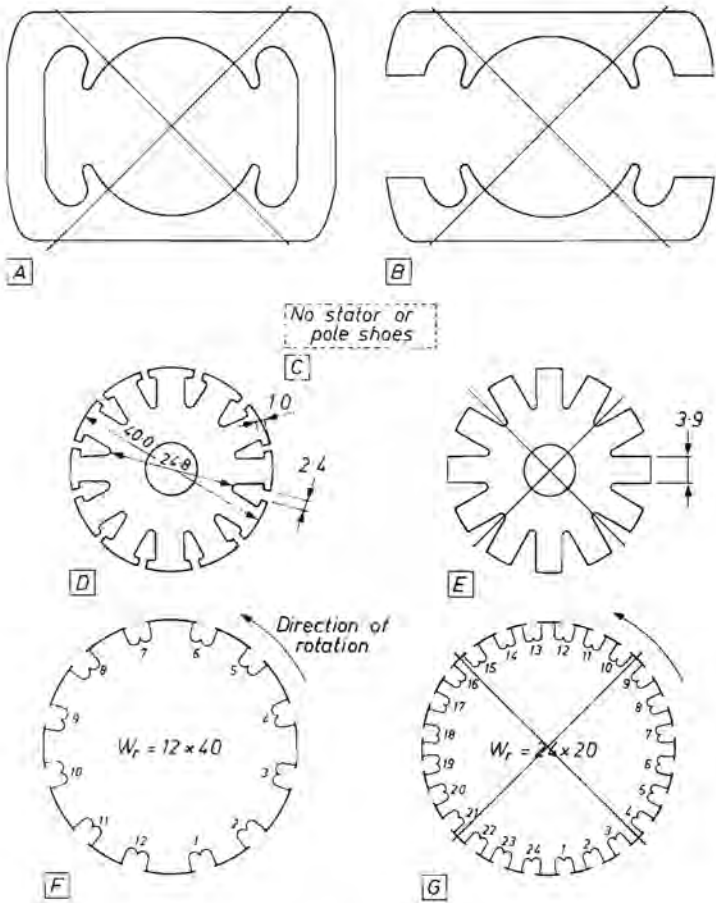


Fig. 5.11, see also table 5-II.

TABLE 5-II

measurement 1	short-circuited rotor coils; no stator or pole shoes													
case No.	rotor type	winding of the rotor	sta- tor type	$w_s$	$\lambda$	$\delta$ (mm)	$I_z$ ( $\mu$ S)	$I_1$ (A)	$U_z$ (V)	$L_{comm}$ ( $\mu$ H)	commu- tating coils	short- circuited coils	see fig.	remarks
1	D	F	C	—	0.5	—	13	0.5	12	312	1	—	5.10a	common case
2	D	F	C	—	0.5	—	10	0.5	12	240	1	2	—	
3	D	F	C	—	0.5	—	10	0.5	12	240	1	12	—	
4	D	F	C	—	0.5	—	10	0.5	12	240	1	6	—	
5	D	F	C	—	0.5	—	11	0.5	12	264	1	7	5.10b	
6	D	F	C	—	0.5	—	10	0.5	12	240	1	8	—	
7	D	F	C	—	0.5	—	8	0.5	12	192	1	6;8	—	
8	D	F	C	—	0.5	—	9	0.5	12	216	1	6;12	5.10d	
9	D	F	C	—	0.5	—	8	0.5	12	192	1	6;7;12	5.10e	
10														
11	D	F	C	—	0.5	—	14	0.5	12	336	1;7	—	5.10c	
12	D	F	C	—	0.5	—	11	0.5	12	264	1;7	12	—	
13	D	F	C	—	0.5	—	9	0.5	12	216	1;7	6;12	5.10f	
14														
15														
16														
17														
18														

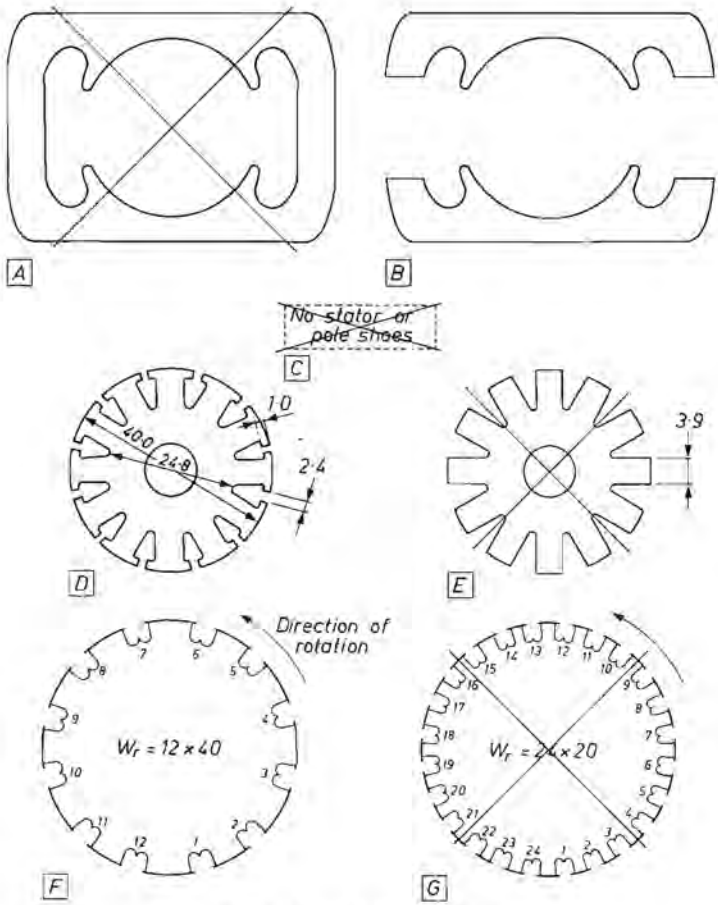


Fig. 5.12, see also table 5-III.

TABLE 5-III

measurement 2	short-circuited rotor coils; with pole shoes													
case No.	rotor type	winding of the rotor	sta- tor type	$w_s$	$\lambda$	$\delta$ (mm)	$t_z$ ( $\mu s$ )	$I_1$ (A)	$U_z$ (V)	$L_{comm}$ ( $\mu H$ )	commu- tating coils	short- cir- cued coils	see fig.	remarks
1	D	F	B	—	0.5	0.4	17	0.5	12	408	1	—	5.10a	common case
2	D	F	B	—	0.5	0.4	13	0.5	12	312	1	2	—	
3	D	F	B	—	0.5	0.4	13	0.5	12	312	1	12	—	
4	D	F	B	—	0.5	0.4	13	0.5	12	312	1	6	—	
5	D	F	B	—	0.5	0.4	13	0.5	12	312	1	7	5.10b	
6	D	F	B	—	0.5	0.4	13	0.5	12	312	1	8	—	
7	D	F	B	—	0.5	0.4	10	0.5	12	240	1	6;8	—	
8	D	F	B	—	0.5	0.4	10	0.5	12	240	1	6;12	5.10d	
9	D	F	B	—	0.5	0.4	9.5	0.5	12	228	1	6;7;12	5.10e	
10														
11	D	F	B	—	0.5	0.4	26	0.5	12	624	1;7	—	5.10c	
12	D	F	B	—	0.5	0.4	17	0.5	12	408	1;7	12	—	
13	D	F	B	—	0.5	0.4	11	0.5	12	264	1;7	6;12	5.10f	
14														
15														
16														
17														
18														

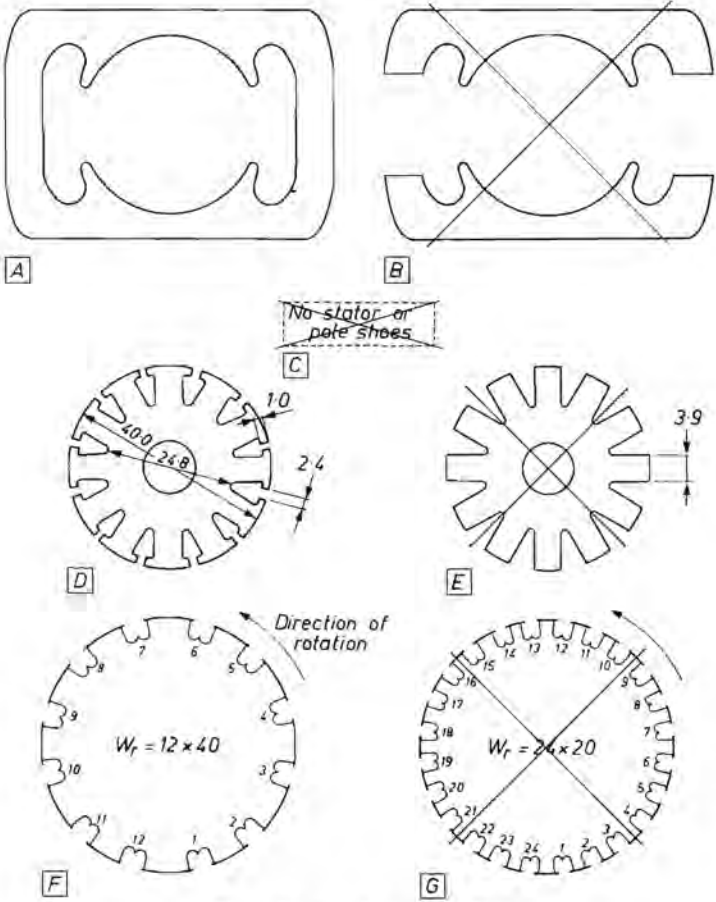


Fig. 5.13, see also table 5-IV

TABLE 5-IV

measurement 3	short-circuited rotor coils; with stator													
case No.	rotor type	winding of the rotor	stator type	$w_s$	$\lambda$	$\delta$ (mm)	$t_z$ ( $\mu s$ )	$I_1$ (A)	$U_z$ (V)	$L_{comm}$ ( $\mu H$ )	commu- tating coils	short- cir- cued coils	see fig.	remarks
1	D	F	A	—	0.5	0.4	42	0.5	12	1008	1	—	5.10a	common case
2	D	F	A	—	0.5	0.4	20	0.5	12	480	1	2	—	
3	D	F	A	—	0.5	0.4	20	0.5	12	480	1	12	—	
4	D	F	A	—	0.5	0.4	20	0.5	12	480	1	6	—	
5	D	F	A	—	0.5	0.4	20	0.5	12	480	1	7	5.10b	
6	D	F	A	—	0.5	0.4	20	0.5	12	480	1	8	—	
7	D	F	A	—	0.5	0.4	14	0.5	12	336	1	6;8	—	
8	D	F	A	—	0.5	0.4	14	0.5	12	336	1	6;12	5.10d	
9	D	F	A	—	0.5	0.4	13	0.5	12	312	1	6;7;12	5.10e	
10														
11	D	F	A	—	0.5	0.4	80	0.5	12	1920	1;7	—	5.10c	
12	D	F	A	—	0.5	0.4	30	0.5	12	720	1;7	12	—	
13	D	F	A	—	0.5	0.4	15	0.5	12	360	1;7	6;12	5.10f	
14														
15														
16														
17														
18														



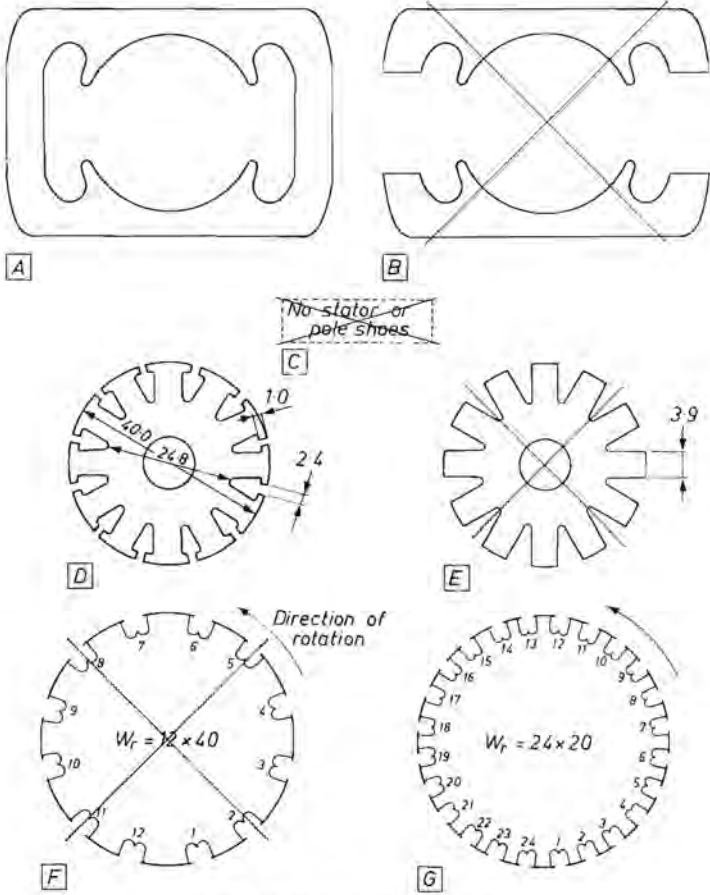


Fig. 5.14, see also table 5.V

TABLE 5-V

measurement 4	tapped coils													
case No.	rotor type	winding of the rotor	sta- tor type	$w_s$	$\lambda$	$\delta$ (mm)	$t_z$ ( $\mu s$ )	$I_1$ (A)	$U_z$ (V)	$L_{comm}$ ( $\mu H$ )	commu- tating coils	short- cir- cued coils	see fig.	remarks
1	D	G	A	—	0.5	0.4	4.2	0.5	12	101	1	—	5.10a	(with 24 coils)
2	D	G	A	—	0.5	0.4	3.6	0.5	12	86	1	12	5.10b	(with 24 coils)
3	D	G	A	—	0.5	0.4	3.6	0.5	12	86	1	24	—	
4	D	G	A	—	0.5	0.4	2.5	0.5	12	60	1	12;24	5.10d	(with 24 coils)
5														
6														
7	D	G	A	—	0.5	0.4	4.2	0.5	12	101	2	—	5.10a	(with 24 coils)
8	D	G	A	—	0.5	0.4	3.6	0.5	12	86	2	13	5.10b	(with 24 coils)
9	D	G	A	—	0.5	0.4	0.8	0.5	12	19	2	1		
10	D	G	A	—	0.5	0.4	0.8	0.5	12	19	2	1;13	5.10d	(with 24 coils)
11														
12														
13														
14														
15														
16														
17														
18														

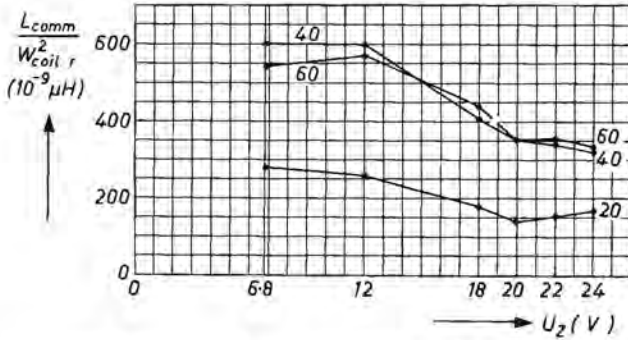


Fig. 5.15. Measured values of  $L_{comm}/(w_{coil r})^2$  as a function of the simulated spark voltage  $U_z$ , for various values of  $w_{coil r}$ ;  $L_{comm}$  is the active inductance of the rotor coil and  $w_{coil r}$  is the number of turns of the rotor coil.

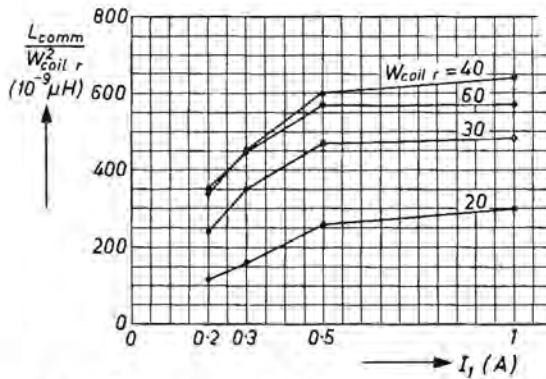


Fig. 5.16. Measured values of  $L_{comm}/(w_{coil r})^2$  as a function of the current  $I_1$  (see fig. 5.6) for various values of the number of turns of a rotor coil  $w_{coil r}$ ;  $L_{comm}$  is the active inductance of the coil.

### The influence of saturating the magnetic circuit

In order to saturate the magnetic circuit, a current must be passed through the stator coils; these will then be short-circuited by the source that delivers the current in question. If a lower value of  $L_{comm}$  is measured under these conditions, it will not be clear whether this is due to saturation or to the short-circuiting of the stator coils. If e.g. rotor coils 6 and 12 are short-circuited as in the "common case", it is found that short-circuiting the stator coils has relatively little influence on  $L_{comm}$ . These measurements were therefore carried out with the coils 6 and 12 short-circuited. Figure 5.19 shows that saturation does have some influence there; but if it is desired to use this effect to improve commutation, the stator must be given an extremely large number of ampere

turns, which is very expensive. A much cheaper and yet effective solution is to shunt e.g. a capacitor of 0.02  $\mu\text{F}$  across the stator coils, as in case 15 of table 5-VII.

#### *The influence of the rotor length*

Figure 5.20 shows the influence of the rotor length  $l_r$  on  $L_{\text{comm}}$ . It may be seen that  $L_{\text{comm}}$  is nearly proportional to  $l_r$ . The influence of the end windings on  $L_{\text{comm}}$  can thus be neglected in practice. If  $L_{\text{comm}}$  is proportional to  $l_r$ , we may perhaps also assume that  $L_{\text{comm}}$  is proportional to the rotor diameter  $d_r$ , if  $w_{\text{coil } r}$  is kept constant. This implies that  $L_{\text{comm}}$  will more or less satisfy

$$L_{\text{comm}} \propto (w_{\text{coil } r})^2 l_r d_r. \quad (5.15)$$

#### *The influence of the width of the air gap*

Figure 5.21 shows the influence of the width of the air gap  $\delta$  on  $L_{\text{comm}}$ . If  $L_{\text{comm}}$  were proportional to the permeance of the air gap,  $L_{\text{comm}}$  would be proportional to  $\delta^{-1}$ . This appears not to be so at all; a wider air gap has hardly any influence on  $L_{\text{comm}}$ . A wider air gap is thus not a means of improving commutation. Moreover, it would be expensive, for a wider air gap requires more ampere turns in the stator coils.

#### *The influence of the shape of the rotor teeth*

Figure 5.22 shows that when the measurements are made without a stator,  $L_{\text{comm}}$  hardly depends on the shape of the rotor teeth. With the stator, or with the pole shoes, the shape of the rotor teeth does have some influence on  $L_{\text{comm}}$ . This difference is mainly due to the difference in reluctance of the air gap. A rotor shape like that of type E should never be chosen to improve commutation, for the reasons mentioned in the previous item.

#### *The values of $L_{\text{comm}}$ for the first coil to be wound, and for the last coil*

The first coil to be wound has each end at the bottom of a slot, while the last coil wound has each end at the top of a slot (cf. coils 1 and 12 in table 5-I). When the set-up is provided with pole shoes or stator, the value of  $L_{\text{comm}}$  for coil 1 is 5–10% higher than for coil 12. This is why in small series motors the commutator segments of the coils which are wound first often look worse than those wound last.

#### *The influence of the position of the commutating coil on the value of $L_{\text{comm}}$*

All the measurements with pole shoes and stators were carried out with the commutating coil in the geometrically neutral position. If the position of the rotor is varied by up to 90 degrees, the value of  $L_{\text{comm}}$  decreases by only a

Figs. 5.17.–5.22. Conditions for the measurement of the active inductance of a rotor coil,  $L_{comm}$ . The results are shown in tables 5-VI–5-XI.

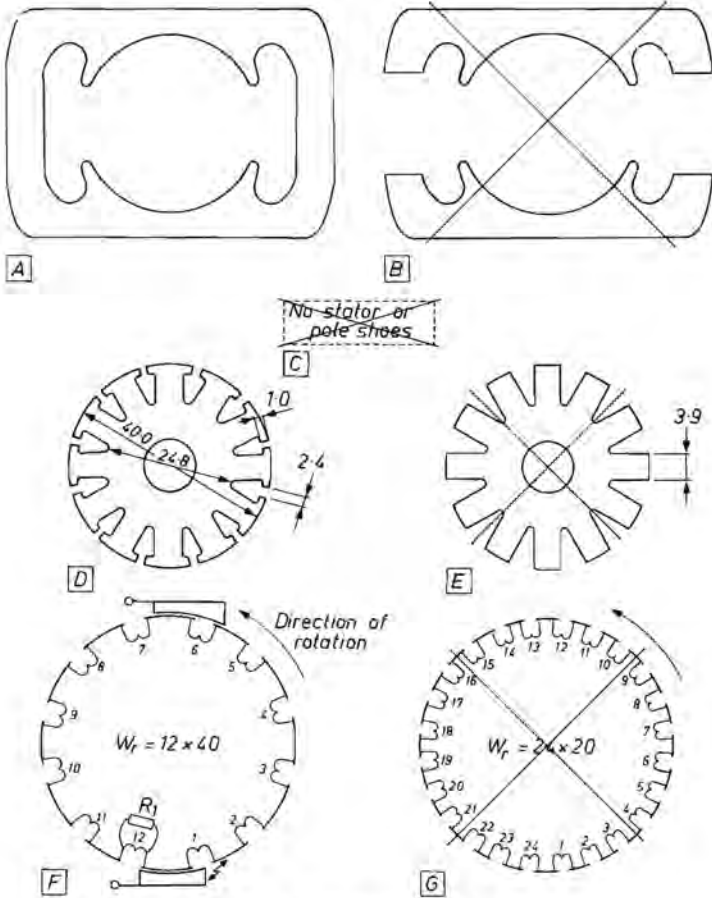


Fig. 5.17, see also table 5-VI.

TABLE 5-VI

measurement 6	the influence of the brush resistance														
case No.	rotor type	wind- ing of the rotor	sta- tor type	$w_s$	$\lambda$	$\delta$ (mm)	$t_z$ ( $\mu s$ )	$I_1$ (A)	$U_z$ (V)	$L_{comm}$ ( $\mu H$ )	commu- tating coils	short- cir- cued coils	see fig.	$R_1$ ( $\Omega$ )	remarks
1	D	F	A	—	0.5	0.4	14	0.5	12	336	1	6;12	5.10d	0	common case
2	D	F	A	—	0.5	0.4	14	0.5	12	336	1	6;12	5.10d	1	common case
3	D	F	A	—	0.5	0.4	14	0.5	12	336	1	6;12	5.10d	10	common case
4	D	F	A	—	0.5	0.4	15	0.5	12	360	1	6;12	5.10d	60	common case
5	D	F	A	—	0.5	0.4	16	0.5	12	384	1	6;12	5.10d	90	common case
6	D	F	A	—	0.5	0.4	17	0.5	12	408	1	6;12	5.10d	200	common case
7	D	F	A	—	0.5	0.4	18	0.5	12	432	1	6;12	5.10d	300	common case
8	D	F	A	—	0.5	0.4	18.5	0.5	12	444	1	6;12	5.10d	400	common case
9															
10															
11	D	F	A	—	0.5	0.4	42	0.5	12	1008	1	—	5.10a	—	
12															
13															
14															
15															
16															
17															
18															

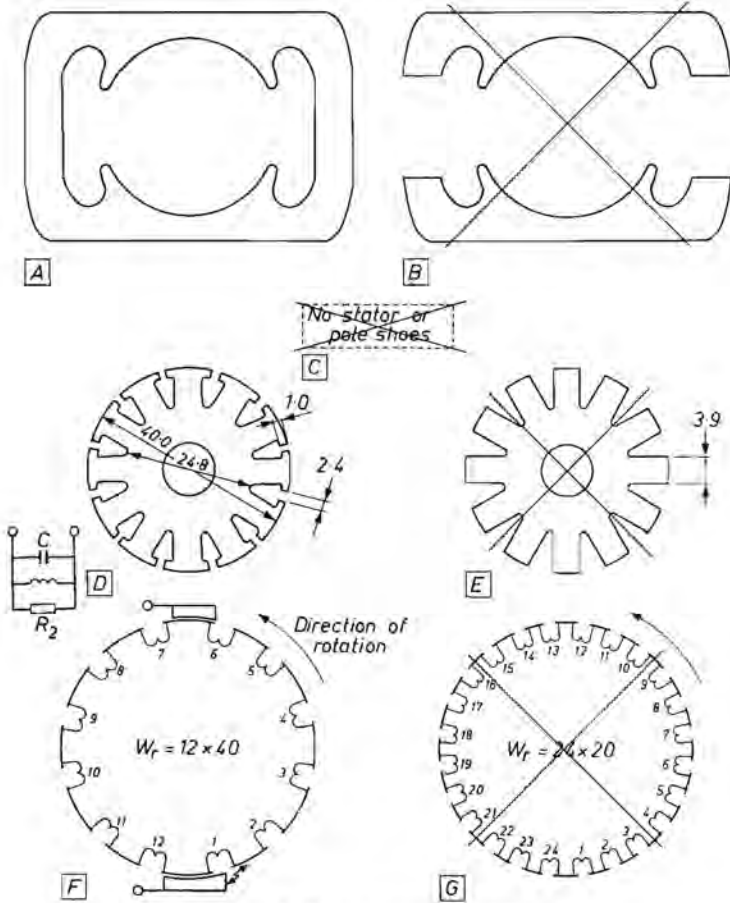


Fig. 5.18, see also table 5-VII.

TABLE 5-VII

measurement 7	short-circuited stator coils															
	case No.	rotor type	wind- ing of the rotor	sta- tor type	$w_s$	$\lambda$	$\delta$ (mm)	$t_z$ ( $\mu s$ )	$I_1$ (A)	$U_z$ (V)	$L_{comm}$ ( $\mu H$ )	com- mutat- ing coils	short- cir- cued coils	see fig.	$R_2$ ( $\Omega$ )	$C$ ( $\mu F$ )
1	D	F	A	400	0.5	0.4	42	0.5	12	1008	1	—	5.10a	$\infty$	—	
2	D	F	A	400	0.5	0.4	36	0.5	12	864	1	—	5.10a	10000	—	
3	D	F	A	400	0.5	0.4	34	0.5	12	816	1	—	5.10a	5000	—	
4	D	F	A	400	0.5	0.4	30	0.5	12	720	1	—	5.10a	3000	—	
5	D	F	A	400	0.5	0.4	26	0.5	12	624	1	—	5.10a	2000	—	
6	D	F	A	400	0.5	0.4	19	0.5	12	456	1	—	5.10a	1000	—	
7	D	F	A	400	0.5	0.4	16	0.5	12	384	1	—	5.10a	500	—	
8	D	F	A	400	0.5	0.4	14	0.5	12	336	1	—	5.10a	300	—	
9	D	F	A	400	0.5	0.4	13	0.5	12	312	1	—	5.10a	100	—	
10	D	F	A	400	0.5	0.4	13	0.5	12	312	1	—	5.10a	0	—	
11																
12	D	F	A	400	0.5	0.4	10	0.5	12	240	1	6;12	5.10d	0	—	common case
13																
14																
15	D	F	A	400	0.5	0.4	13	0.5	12	312	1	—	5.10a	—	0.02	
16	D	F	A	400	0.5	0.4	13	0.5	12	312	1	—	5.10a	—	>0.02	
17																
18	D	F	A	—	0.5	0.4	14	0.5	12	336	1	6;12	5.10d	—	—	common case



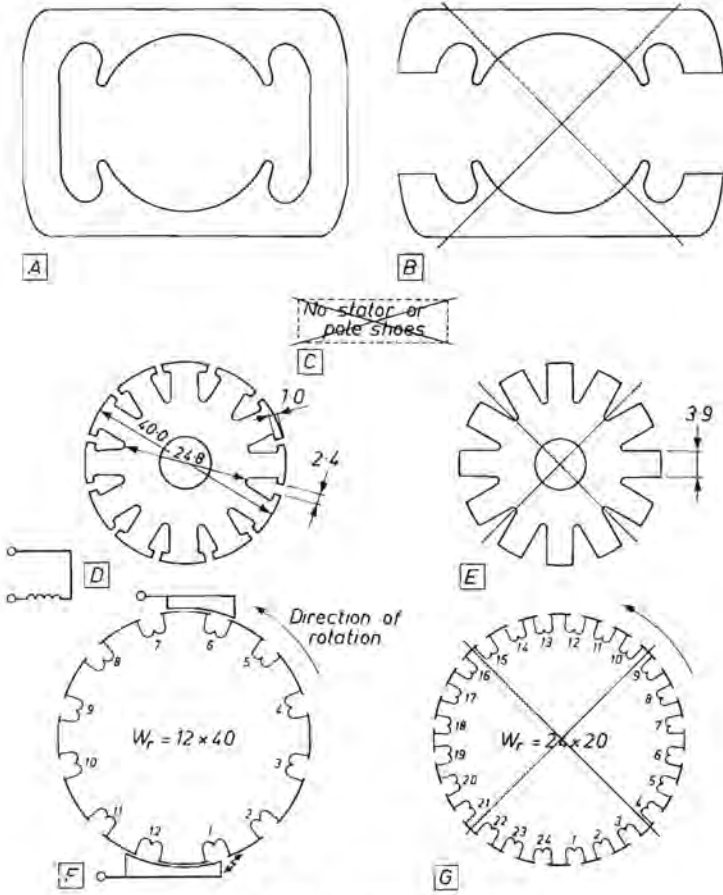


Fig. 5.19, see also table 5-VIII.

TABLE 5-VIII

measurement 8	saturation of the magnetic circuit															
	case No.	rotor type	wind- ing of the rotor	sta- tor type	$w_s$	$\lambda$	$\delta$ (mm)	$t_z$ ( $\mu s$ )	$I_1$ (A)	$U_z$ (V)	$L_{comm}$ ( $\mu H$ )	com- mutat- ing coils	short- cir- cued coils	see fig.	amp. turns of the stator	induc- tion in the rotor
1	D	F	A	400	0.5	0.4	14	0.5	12	336	1	6;12	5.10d	0	0	common case
2	D	F	A	400	0.5	0.4	11	0.5	12	264	1	6;12	5.10d	400	1.55	common case
3	D	F	A	400	0.5	0.4	9	0.5	12	216	1	6;12	5.10d	800	2.03	common case
4	D	F	A	400	0.5	0.4	8.5	0.5	12	204	1	6;12	5.10d	1200	2.27	common case
5	D	F	A	400	0.5	0.4	8	0.5	12	192	1	6;12	5.10d	1600	2.50	common case
6																
7																
8																
9	D	F	A	400	0.5	0.4	10	0.5	12	240	1	6;12	5.10d	—	—	common case
10				If the stator coils are short-circuited, see measurement 7, case 12												
11																
12																
13																
14																
15																
16																
17																
18																

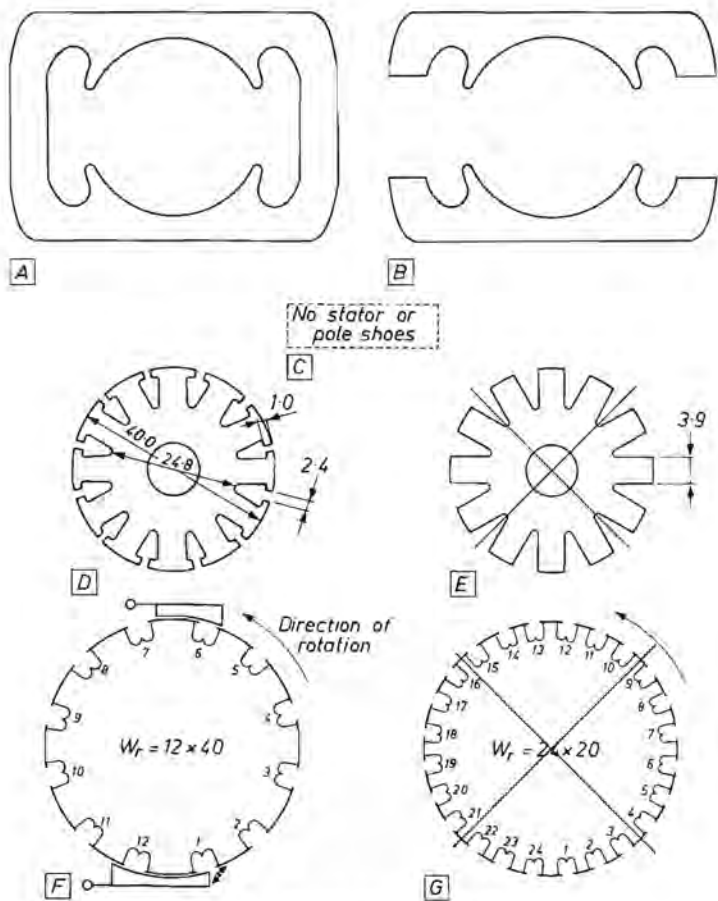


Fig. 5.20, see also table 5-IX.

TABLE 5-IX

measurement 9	the influence of the rotor length $l_r$													
	case No.	rotor type	winding of the rotor	sta- tor type	$w_s$	$\lambda$	$\delta$ (mm)	$t_z$ ( $\mu$ s)	$I_1$ (A)	$U_z$ (V)	$L_{comm}$ ( $\mu$ H)	commu- tating coils	short- cir- cued coils	see fig.
1	D	F	A	—	0	0.4	0.8	0.5	12	19	1	6;12	5.10d	common case
2	D	F	A	—	0.5	0.4	14	0.5	12	336	1	6;12	5.10d	common case
3	D	F	A	—	1	0.4	24	0.5	12	576	1	6;12	5.10d	common case
4														
5	D	F	B	—	0	0.4	0.8	0.5	12	19	1	6;12	5.10d	common case
6	D	F	B	—	0.5	0.4	10	0.5	12	240	1	6;12	5.10d	common case
7	D	F	B	—	1	0.4	19	0.5	12	456	1	6;12	5.10d	common case
8														
9	D	F	C	—	0	—	0.8	0.5	12	19	1	6;12	5.10d	common case
10	D	F	C	—	0.5	—	9	0.5	12	216	1	6;12	5.10d	common case
11	D	F	C	—	1	—	16	0.5	12	384	1	6;12	5.10d	common case
12														
13														
14														
15														
16														
17														
18														

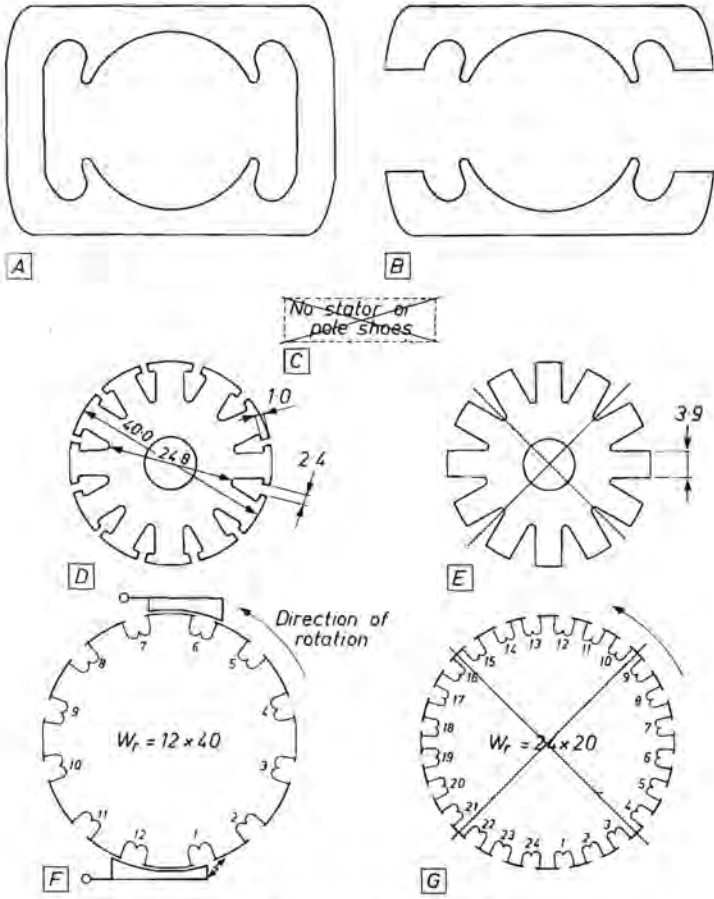


Fig. 5.21, see also table 5-X.

TABLE 5-X

measurement 10	the influence of the air-gap width $\delta$													
	case No.	rotor type	winding of the rotor	sta- tor type	$w_s$	$\lambda$	$\delta$ (mm)	$t_z$ ( $\mu s$ )	$I_1$ (A)	$U_z$ (V)	$L_{comm}$ ( $\mu H$ )	commu- tating coils	short- cir- cued coils	see fig.
1	D	F	A	—	0.5	0.4	14	0.5	12	336	1	6;12	5.10d	common case
2	D	F	A	—	0.5	0.8	13	0.5	12	312	1	6;12	5.10d	common case
3	D	F	A	—	0.5	1.2	12	0.5	12	288	1	6;12	5.10d	common case
4	D	F	C	—	0.5	—	9	0.5	12	216	1	6;12	5.10d	common case
5														
6														
7	D	F	B	—	0.5	0.4	12	0.5	12	288	1	6;12	5.10d	common case
8	D	F	B	—	0.5	0.8	11	0.5	12	264	1	6;12	5.10d	common case
9	D	F	B	—	0.5	1.2	10	0.5	12	240	1	6;12	5.10d	common case
10	D	F	C	—	0.5	—	9	0.5	12	216	1	6;12	5.10d	common case
11														
12														
13	D	F	A	—	0.5	0.4	42	0.5	12	1008	1	—	5.10a	
14	D	F	A	—	0.5	0.8	35	0.5	12	840	1	—	5.10a	
15	D	F	A	—	0.5	1.2	30	0.5	12	720	1	—	5.10a	
16	D	F	C	—	0.5	—	13	0.5	12	312	1	—	5.10a	
17														
18														

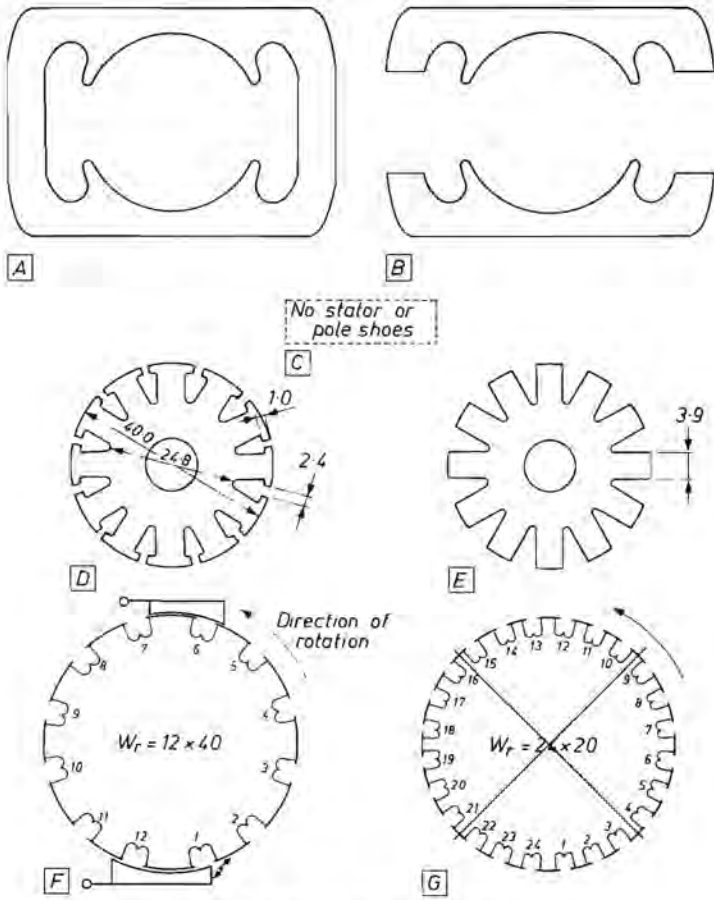


Fig. 5.22, see also table 5-XI.

TABLE 5-XI

measurement 11	influence of the shape of the rotor teeth													
case No.	rotor type	winding of the rotor	sta- tor type	$w_s$	$\lambda$	$\delta$ (mm)	$i_z$ ( $\mu$ s)	$I_1$ (A)	$U_z$ (V)	$L_{comm}$ ( $\mu$ H)	commu- tating coils	short- cir- cued coils	see fig.	remarks
1	D	F	C	—	0.5	—	9	0.5	12	216	1	6;12	5.10d	common case
2	E	F	C	—	0.5	—	8.5	0.5	12	204	1	6;12	5.10d	common case
3														
4														
5	D	F	B	—	0.5	0.4	12	0.5	12	288	1	6;12	5.10d	common case
6	E	F	B	—	0.5	0.4	11	0.5	12	264	1	6;12	5.10d	common case
7														
8														
9	D	F	A	—	0.5	0.4	14	0.5	12	336	1	6;12	5.10d	common case
10	E	F	A	—	0.5	0.4	12	0.5	12	288	1	6;12	5.10d	common case
11														
12														
13														
14														
15														
16														
17														
18														



few per cent. It may thus be concluded that the improvement in the commutation due to turning of the brushes is caused by the changed influence of the rotational e.m.f. and not by a change in  $L_{\text{comm}}$ .

*The influence of coils 7–12 on the value of  $L_{\text{comm}}$  for coil 1*

When commutation of coil 1 has ended, this coil is situated in the right-hand rotor circuit (see fig. 5.10a). Although the left-hand circuit with coils 7–12 is present in a real rotor, it can be removed from the set-up for the determination of  $L_{\text{comm}}$ . Removal of these coils might be expected to increase  $L_{\text{comm}}$ , as no energy can now be transported to or from them by magnetic coupling. This increase in  $L_{\text{comm}}$  is indeed found, but it amounts to no more than a few per cent.

**5.6. Evaluation of the results of the measurements**

In sec. 5.6.1, the value of  $L_{\text{comm}}$  is compared with the inductance of the same rotor coil, measured with an AC bridge. In sec. 5.6.2,  $l_z$  is related to the visible spark length in a real motor.

5.6.1. *The active inductance*

According to eqs (2.4) and (2.2), the permeance of the magnetic circuit of a small series motor is approximately equal to

$$A_{m\ o} = c_{41} A_{m\ 2\delta} = \frac{c_{41} \pi \mu_o l_r d_r}{4 \delta k_{\text{pole}} k_{\text{car}}} \quad (5.16)$$

If we neglect the influence of magnetic or electric coupling with other coils or eddy-current paths, the inductance of a rotor coil with  $w_{\text{coil } r}$  turns should be approximately equal to

$$L = A_{m\ o} (w_{\text{coil } r})^2 \quad (5.17)$$

For a motor like that used for the measurements of sec. 5.5, of relative rotor length  $\lambda = 0.5$ , the parameters involved in eqs (5.16) and (5.17) will have roughly the following values:

	$c_{41}$	= 0.9 (see eq. (2.4)),
rotor diameter	$d_r$	= 40 . 10 <sup>-3</sup> m,
rotor length	$l_r$	= 18 . 10 <sup>-3</sup> m,
number of turns of a rotor coil	$w_{\text{coil } r}$	= 40,
reciprocal relative pole arc	$k_{\text{pole}}$	= 1.3 (see eq. (1.2)),
carter factor	$k_{\text{car}}$	= 1.12,
air-gap width	$\delta$	= 0.4 . 10 <sup>-3</sup> m.

On the basis of these values we find  $L = 1750 \mu\text{H}$ . However, fig. 5.1 shows that the measured values of  $L$  determined with an AC bridge are much higher

at low frequencies. This is due to the influence on  $L$  of the leakage fluxes, which are not taken into account in eq. (5.17).

Comparison of fig. 5.1 with the values of  $L_{\text{comm}}$  indicated in fig. 5.10 shows that the active inductance  $L_{\text{comm}}$  is much lower than the inductance of a rotor coil measured at low frequencies with an AC bridge and is also lower than the inductance calculated in this section with the aid of eq. (5.17).

### 5.6.2. The spark decay time with respect to the length of the sparks

The circumferential length of a commutator is about 0.1 m. At a rotor speed of 18 000 r.p.m. (300 r.p.s.) the circumferential speed of the commutator is about  $30 \text{ m s}^{-1}$ . In the table of fig. 5.13 (with a complete stator as in a series motor),  $L_{\text{comm}} = 336 \text{ } \mu\text{H}$  and  $t_z = 14 \text{ } \mu\text{s}$  in the "common case", if the current jumps from 0 to  $I_1$ . In  $14 \text{ } \mu\text{s}$  the circumference of the rotor covers a distance  $30 \times 14 \cdot 10^{-6} \text{ m} \approx 0.4 \text{ mm}$ . This corresponds to a spark length of about 0.4 mm. In a real motor the current jump is generally less than from 0 to  $I_1$ . Voltages induced in the commutating coil during sparking may lengthen or shorten the spark time somewhat, but the above calculation indicates the basic reliability of the method of measurement used in this study.

## 5.7. Conclusions

The influence of the inductance of the commutating coil (including other magnetically and galvanically coupled coils or eddy-current paths) on commutation can be expressed in terms of the "active inductance"  $L_{\text{comm}}$ , defined by eq. (5.10).  $L_{\text{comm}}$  is not the inductance of the commutating coil measured at some well-defined frequency; it is a quantity that represents the influence of the commutating coil on the energy dissipated in the spark.

$L_{\text{comm}}$  can be measured by the method described in sec. 5.3. The main conclusions to be drawn from the results of the measurements are as follows.

- (1) The contribution of the end windings to  $L_{\text{comm}}$  can be neglected.
- (2) The width of the air gap, the saturation of the magnetic circuit and the position of the commutating coil have only little influence on the value of  $L_{\text{comm}}$ .
- (3) Complete or partial short-circuiting of the rotor or stator coils leads to a very marked drop in  $L_{\text{comm}}$ . It follows that the brushes used in a small commutator machine should always be wider than one segment.

The results of the measurements explain why the appearance of the segments in rotors with tapped coils is often alternately good and bad, and why the segments connected to the first coil wound (with both sides situated in the bottom of the slots) sometimes looks a little worse than the last one wound (with both sides situated in the top of the slots).

## 6. TEMPERATURE DISTRIBUTION AND HEAT TRANSPORT IN SMALL COMMUTATOR MACHINES

There are two cooling problems in electric machines:

- (1) how to transport the heat from the places where it is dissipated to the surface of the machine parts or to the surface of the cooling channels;
- (2) how to remove the heat from the above-mentioned surfaces.

The internal temperature distribution should also be known for the purposes of an optimization calculation, in order to know the relation between the permissible losses in the various parts of the machine. The heat transport and temperature distribution in small commutator machines are discussed in this chapter.

### 6.1. Losses in small commutator machines

The following losses occur in small commutator machines:

- (1) copper losses in the windings of the rotor,  $P_{Cu r}$ ;
- (2) copper losses in the windings of the stator of machines with a wound stator,  $P_{Cu s}$ ;
- (3)  $I^2 R$  losses in the brushes and in the brush contact resistance,  $P_{R brush}$ ;
- (4) commutation losses,  $P_{comm}$ , partly incorporated in (1), (2) and (3) above and partly directly removed from the spark by radiation, conduction or convection (see Held <sup>4</sup>);
- (5) mechanical losses due to brush friction,  $P_{mech brush}$ ;
- (6) mechanical losses due to bearing friction,  $P_{bearings}$ ;
- (7) mechanical losses due to air friction,  $P_{air}$ ;
- (8) iron loss in the rotor,  $P_{Fe r}$ ;
- (9) iron loss in the stator,  $P_{Fe s}$ ;
- (10) extra iron loss in the pole faces of the stator, caused by changes in magnetic induction when the rotor slots pass the pole faces; in this argument these losses are included in  $P_{Fe s}$  (point (9)).

The heat generated by the various effects mentioned above must be removed from the machine.

There are a number of reasons for limiting the permissible temperature rise in small commutator machines. If the temperature is too high, the insulating material in the slots of rotor and stator, the insulating layer around the winding wire, the oil or grease in the bearings, and mechanical parts made of thermoplastics, etc., will age too quickly. Moreover, brush wear may increase sharply, and the housing of the appliance may become too hot to hold.

C.E.E. specifications <sup>22</sup>) allow a temperature rise of 100 °C for commutator and brushes and of about 80 °C for the windings of rotor and stator, depending on the insulating material used. The temperature rise in the bearings is not limited by the C.E.E. specifications.

The temperature rise in the windings can be determined by measuring their resistance. Motors are tested under normal load and at the most unfavourable voltage between 0.9 and 1.1 times the rated voltage.

For vacuum cleaners, the normal load is defined in ref. 23, § 2 as the load obtained when the appliance is operated continuously with the air inlet adjusted to give a load  $P_m$ , calculated from the formula

$$P_m = 0.5(P_r + P_i),$$

where  $P_r$  is the input in watts when the appliance has been on circuit at the rated voltage, or at the upper limit of the rated voltage range, for 3 minutes, with the air inlet wide open.  $P_i$  is the input in watts when the appliance has been on circuit at the same voltage for 1 minute, with the air inlet sealed, immediately following the period with the air inlet open.

Other appliances have other definitions of the normal load. For drills, for example, the normal load is defined <sup>24)</sup> as the load in continuous operation with the drill in horizontal position and with a torque applied to the spindle such that the output load, in watts, is 15 times the diameter, in mm, of the largest drill borer which can be fitted in the chuck or 15 times the maximum diameter of the drill borer, in mm, marked on the drill, whichever is the higher.

## 6.2. A thermal network

When an electric machine is optimized, the optimum dimensions are found by mathematical variation of the dimensions of the rotor, the stator and the windings. Varying these dimensions has hardly any influence on the dimensions of the shaft, the bearings, the commutator and the brushes, and hence on the losses  $P_{R \text{ brush}}$ ,  $P_{\text{comm}}$ ,  $P_{\text{mech brush}}$  and  $P_{\text{bearings}}$ . It is therefore sufficient to consider the losses  $P_{\text{Cu r}}$ ,  $P_{\text{Cu s}}$ ,  $P_{\text{Fe r}}$  and  $P_{\text{Fe s}}$  in most cases.

These losses may be represented by the heat sources in the rotor coils, the stator coils, the rotor stack and the stator stack in the thermal network of fig. 6.1 respectively.

It can easily be shown that the temperature differences within each of these four heat capacities will never exceed a few degrees centigrade; it is therefore justified to draw each one as a separate block.

The thermal conductivities are shown joining these blocks.

The air cooling by convection and conduction and the radiation cooling are also represented by blocks, connected with the heat capacities by lines of the form — and - - - respectively. If the amount of air available for cooling is inadequate, the air temperature rises sharply. The temperatures of rotor and stator thus influence one another. The turbulence of the air in the air gap will also make a contribution here, but this will not be considered below, because the temperature difference between stator and rotor stack is generally limited.

The data of table 6-I refer to a small bi-polar series commutator motor of 300 W input power at 18 000 r.p.m. The rotor and stator of such a motor are shown in figs 6.2 and 6.3 respectively.

The rotor slots are insulated with paper 0.15 mm thick, and the stator slots with paper 0.2 mm thick. There are thermoplastic insulating discs 2 mm thick between the rotor stack and the end winding of the rotor.

The thermal conductivity of most insulating materials is roughly  $k_{ins} = 0.2 \text{ W m}^{-1} \text{ }^\circ\text{C}^{-1}$ . For copper and steel the corresponding values are about  $k_{Cu} = 390 \text{ W m}^{-1} \text{ }^\circ\text{C}^{-1}$  and  $k_{Fe} = 46 \text{ W m}^{-1} \text{ }^\circ\text{C}^{-1}$ .

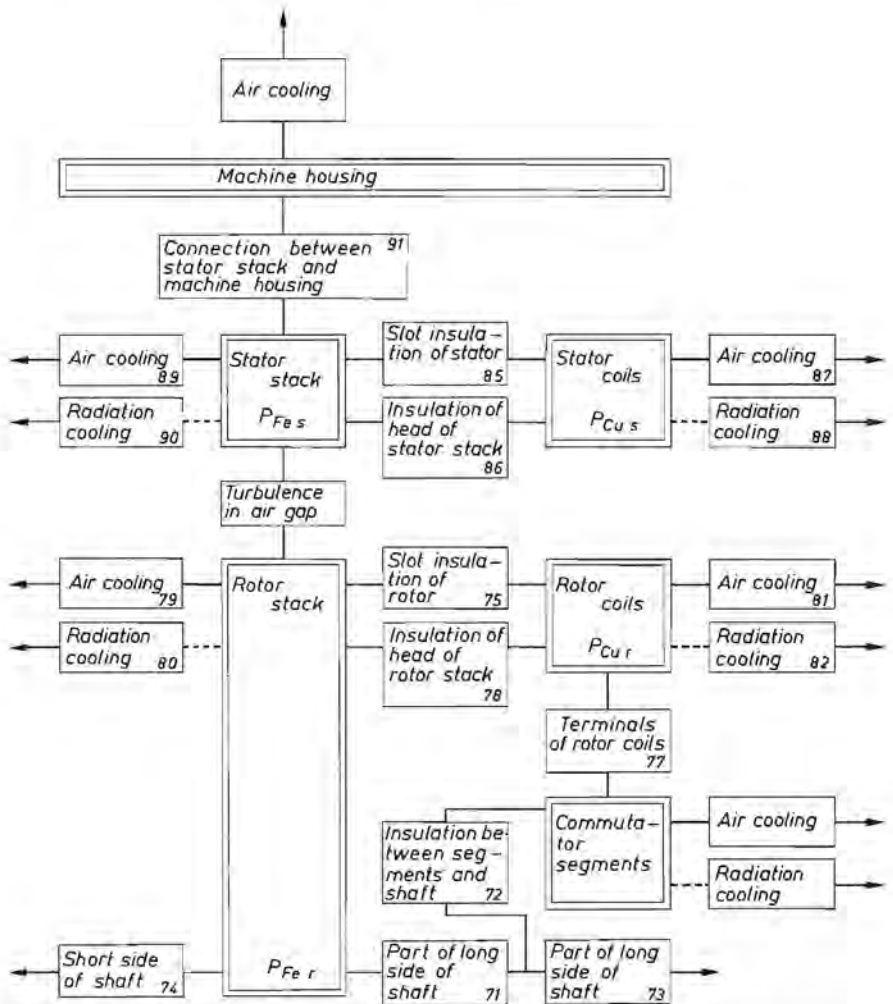


Fig. 6.1. Equivalent thermal network for a small commutator machine with wound stator.

TABLE 6-1

Survey of parameters for a small series motor of about 300 W input power at 18 000 r.p.m.; for explanation of symbols, see text and figs 1.8 and 6.4

$P_{Cu r}$	= 20	W	$l_{comm}$	= 20	mm
$P_{Cu s}$	= 30	W	$b_{ins comm}$	= 5	mm
$P_{Fe r}$	= 20	W	$h_{tooth}$	= 10	mm
$P_{Fe s}$	= 5	W	$b_{ins r}$	= 0.15	mm
$d$	= 40	mm	$d_{Cu r}$	= 0.3	mm
$d_r$	= 46	mm	$l_{ins r}$	= 2	mm
$l_r$	= 20	mm	$d_{coll s}$	= 10	mm
$l_s$	= 20	mm	$b_{ins s}$	= 0.2	mm
$d_{shaft}$	= 10	mm	$s_{w s}$	= 120	mm
$l_{71}$	= 20	mm	$\beta$	= 0.5	
$l_{73}$	= 20	mm	$k_{Cu r}$	= 0.3	
$l_{74}$	= 20	mm	$f_{(r)}$	= 0.25	
$l_{77}$	= 15	mm	$z$	= 12	
$d_{comm}$	= 30	mm			

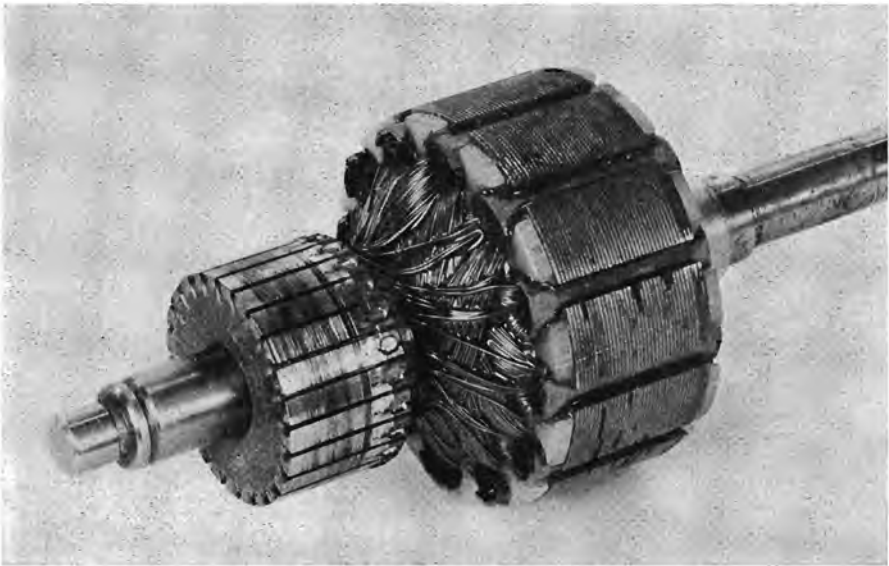


Fig. 6.2. Rotor of a small series motor.

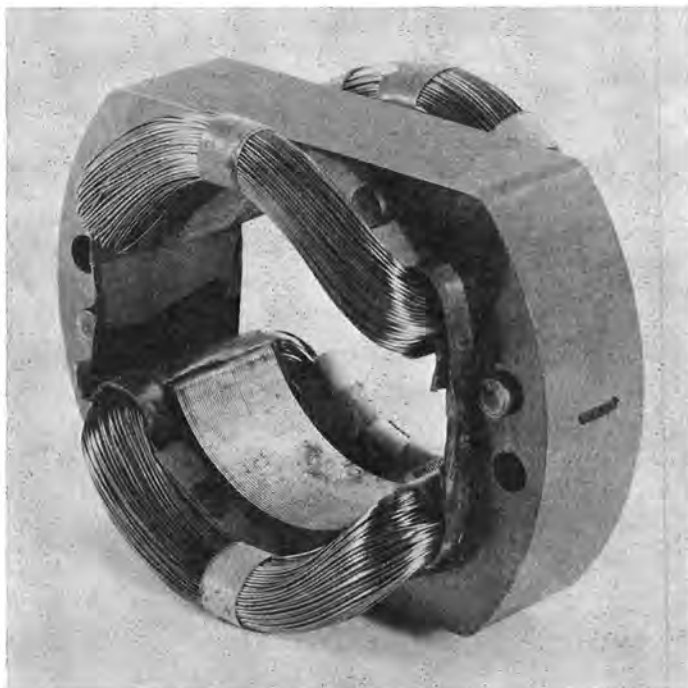


Fig. 6.3. Stator of a small series motor.

The thermal conductances for the motor of table 6-I may be written:

$$A_{\text{therm } 71} \approx \frac{k_{\text{Fe}} \pi (d_{\text{shaft}})^2}{4 l_{71}} = 0.18 \text{ W } ^\circ\text{C}^{-1}, \quad (6.1)$$

$$A_{\text{therm } 72} \approx \frac{k_{\text{ins}} d_{\text{comm}} l_{\text{comm}}}{2 b_{\text{ins comm}}} = 0.012 \text{ W } ^\circ\text{C}^{-1}, \quad (6.2)$$

$$A_{\text{therm } 73} \approx \frac{k_{\text{Fe}} \pi (d_{\text{shaft}})^2}{4 l_{73}} = 0.18 \text{ W } ^\circ\text{C}^{-1}, \quad (6.3)$$

$$A_{\text{therm } 74} \approx \frac{k_{\text{Fe}} \pi (d_{\text{shaft}})^2}{4 l_{74}} = 0.18 \text{ W } ^\circ\text{C}^{-1}, \quad (6.4)$$

$$A_{\text{therm } 75} \approx \frac{2 z k_{\text{ins}} h_{\text{tooth}} l_r}{b_{\text{ins r}}} = 6.4 \text{ W } ^\circ\text{C}^{-1}, \quad (6.5)$$

$$A_{\text{therm } 77} \approx \frac{4 z k_{\text{Cu}} \pi (d_{\text{Cu r}})^2}{4 l_{77}} = 0.088 \text{ W } ^\circ\text{C}^{-1}, \quad (6.6)$$

$$A_{\text{therm } 78} \approx \frac{2 k_{\text{ins}} \pi (1 - f_{(r)}) d^2}{4 l_{\text{ins r}}} = 0.188 \text{ W } ^\circ\text{C}^{-1}, \quad (6.7)$$

$$A_{\text{therm } 85} \approx \frac{4 k_{\text{ins}} \pi d_{\text{coil s}} l_s}{2 b_{\text{ins s}}} = 1.25 \text{ W } ^\circ\text{C}^{-1}; \quad (6.8)$$



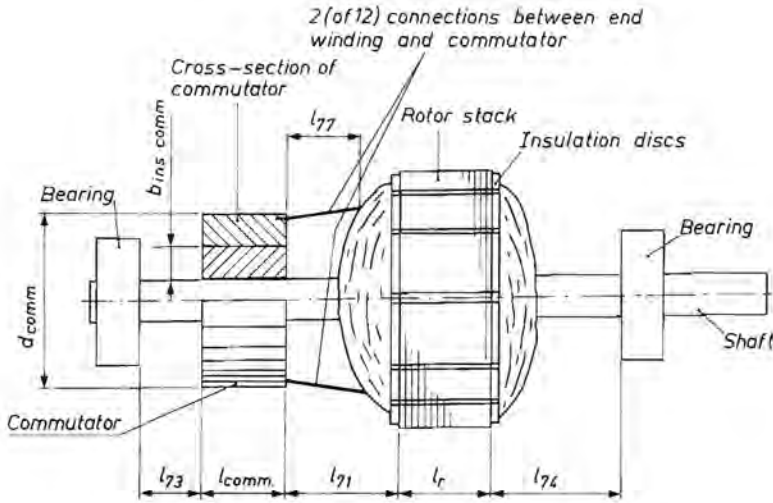


Fig. 6.4. Meaning of some parameters used in chapter 6.

$\Lambda_{\text{therm } 86}$  depends strongly on the construction of the motor. It is generally so low that it can be neglected.

Thermal radiation is expressed in watts at 400 K (127 °C), with  $k_{\text{rad}}$  taken as 0.5:

$$P_{\text{rad } 80} \approx 5.75 k_{\text{rad}} (\theta : 100)^4 \pi d_r l_r = 2.12 \text{ W}, \quad (6.9)$$

$$P_{\text{rad } 82} \approx \frac{2 \times 5.75 k_{\text{rad}} (\theta : 100^4) \pi d^2}{4} = 1.96 \text{ W}, \quad (6.10)$$

$$P_{\text{rad } 88} \approx 2 \times 5.75 k_{\text{rad}} (\theta : 100)^4 \pi s_{ws} d_{\text{coll } s} = 5.6 \text{ W}, \quad (6.11)$$

$$P_{\text{rad } 90} \approx 5.75 k_{\text{rad}} (\theta : 100)^4 \{6 d l_s + 2 \times 3 d^2\} = 10.6 \text{ W}. \quad (6.12)$$

In practice the thermal radiation will be less than that given by the above expressions, first because the temperature of the rotor and stator is generally much lower than 400 K and secondly because the heat radiated back from other hot parts of the motor has not been taken into consideration.

The heat generated in the rotor equals

$$P_{\text{Cu } r} + P_{\text{Fe } r} = 20 + 20 \text{ W} = 40 \text{ W}.$$

The heat radiated from the rotor is much less than

$$P_{\text{rad } 80} + P_{\text{rad } 82} = 2.12 + 1.96 \text{ W} = 4.08 \text{ W}.$$

The thermal radiation from the rotor can thus be completely neglected in a simplified network.



$\Lambda_{\text{therm } 75} = 6.4 \text{ W } ^\circ\text{C}^{-1}$ . This means that if there were a temperature difference of  $4^\circ\text{C}$  between winding and stack of the rotor,  $25.6 \text{ W}$  of heat would flow. That is more than either  $P_{\text{Cu } r}$  or  $P_{\text{Fe } r}$ . In practice, this means that the copper and iron of the rotor can be considered as having nearly the same temperature. Measurements show that this assumption is valid, so the winding and stack of the rotor can be combined to a single block in the thermal network.

$\Lambda_{\text{therm } 72}$  and  $\Lambda_{\text{therm } 77}$  are so small that we may assume that all the heat from the commutator is removed via the air and to a lesser extent by radiation. Only in low-voltage motors, where e.g.  $d_{\text{Cu } r}$  may be  $1 \text{ mm}$ , can  $\Lambda_{\text{therm } 77}$  not be neglected.

Figure 6.1 can now be simplified on the basis of the above arguments. The result is shown in fig. 6.5.

The losses and temperatures of rotor and stator are also shown in this diagram, together with the values of the thermal conductances.

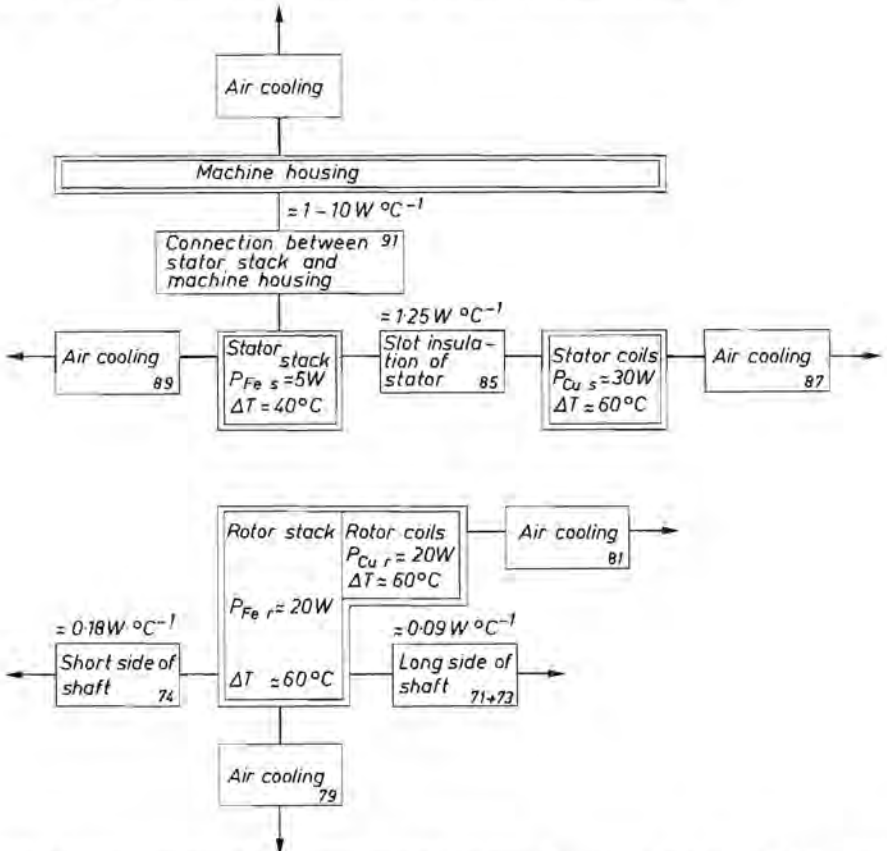


Fig. 6.5. Simplified equivalent thermal network for a small commutator machine with wound stator.

### 6.3. Conclusions

In small commutator machines, radiation cooling can be neglected in comparison with convection cooling. The thermal conduction between the commutator and the other parts of the rotor can also be neglected, except in low-voltage motors. The thermal conduction between the rotor stack and the rotor winding is so good that the rotor coils and stack can be considered as having the same temperature.

The copper losses and iron losses in the rotor,  $P_{Cu\ r} + P_{Fe\ r}$ , are removed by the shaft, by air cooling and to a slight extent by air turbulence via the air gap to the stator. The thermal conductance between the stator stack and the stator coils cannot be neglected, though it is in fact lower than in the rotor. The cooling of the stator stack is better than that of the coils.  $P_{Fe\ s}$ , the iron loss in the stator, is much smaller than  $P_{Cu\ s}$ , the copper loss in the stator, so  $P_{Cu\ s}$  is partly removed via the air and partly conducted away via the stator stack.

Figure 6.5 shows the simplified thermal network for a small series motor of about 300 W input power at 18 000 r.p.m.

## 7. DESCRIPTION, DIMENSIONING AND OPTIMIZATION

Esson's formula (eq. (7.1)) is generally used both for the description and for the dimensioning of commutator machines.

In this chapter we shall show that Esson's formula is in fact less suitable for the dimensioning of small commutator machines than our equation (1.26). To prove this assertion, eq. (1.26) is analyzed in sec. 7.10.

For optimization purposes, neither Esson's formula nor eq. (1.26) is really suitable. A satisfactory optimization method is described in sec. 7.2.

### 7.1. The concepts of description, design, dimensioning and optimization

It is useful to start with a clear definition of the concepts of description, design, dimensioning and optimization.

Description means: describing the properties and behaviour of an existing machine as functions of the frequency and amplitude of the input voltage, the speed, the load, etc.

Design (mechanical as well as electrical) means: choosing the mechanical and electrical construction of the machine. For instance, we may have to choose between bronze bearings or ball bearings, paper or plastic insulation, a commutator with slots or hooks, commutating poles or no commutating poles. The design of the machine is influenced by progress in technology and theoretical knowledge. Within one given design, there can be a great deal of variation in the values of the machine parameters.

Dimensioning means choosing the values of the parameters so that the design satisfies all the specifications, mechanically as well as electrically.

Optimization means determining optimum values of the parameters. An optimum machine is generally the cheapest solution that satisfies the specifications. In the present case, "cheap" refers to the manufacturing costs. If the energy costs cannot be neglected as in large electric machines, optimization generally means reducing the capitalized energy costs and manufacturing costs to a minimum.

### 7.2. A method of optimizing electric machines

It is difficult to optimize or even to dimension an electric machine for the following reasons.

- (1) Functionally as well as mechanically it is divided into two parts: rotor and stator. The dimensions of the rotor and the stator cannot be chosen separately. If for instance wide rotor teeth are chosen in the rotor of a series motor, the rotor slots will be narrow so that little copper is required in the rotor; but the wide rotor teeth can conduct a high magnetic flux. Since the air-gap induction will now be high, much copper is required in the stator.

- (2) The machine is divided into an electrical and a magnetic circuit. The magnetic circuit, consisting of the iron of rotor and stator, gives rise to iron loss. The electric circuit, consisting of the windings of rotor and stator, causes copper loss. The electric and magnetic circuits are interdependent.

It would be nice if there were one single formula that could be used to calculate all the optimum dimensions as a function of the required properties of the machine. However, such a formula does not exist and it is probably a waste of time looking for one all-purpose optimization formula.

A practicable optimization method is described below.

- (1) Describe the machine with the aid of formulas containing independent parameters. For a small series motor, these parameters are summed up in sec. 8.4. About 60 parameters are required.
- (2) Calculate the cost, behaviour and properties of the machine for all possible combinations of all parameters. This involves so much computation that a digital computer is required; but even a computer cannot calculate all possible combinations in an acceptable length of time. Only a limited number of parameters can therefore be varied, each one assuming a limited number of values.
- (3) The computer selects all machines that satisfy the specifications or that have better properties than required by the specifications.
- (4) Out of all the satisfactory machines, the cheapest one is selected. Of course, it is also possible to select a more expensive one if the higher costs are acceptable in the interests of better properties. This selection can be done by hand or by the computer.

### 7.3. Examples of descriptive formulas

Descriptive formulas describe the behaviour and properties of existing machines in terms of such quantities as voltage  $U$ , current  $I$ , resistance  $R$ , inductance  $L$ , magnetic flux  $\phi^{(1)}$ , speed  $n$ , numbers of turns  $w_r$ ,  $w_s$ , etc. Some examples of descriptive formulas are:

$$(1) \quad e = 2 k_E n w_r \phi^{(1)}. \quad (1.11)$$

This can be used to show e.g. what happens to the rotational e.m.f.  $e$  as the rotor speed  $n$  increases at constant flux  $\phi^{(1)}$ .

$$(2) \quad R_r = \frac{\rho_{Cu r} k_R w_r s_{w r}}{4 a_{Cu r}}. \quad (1.13)$$

This can show the variation of the rotor resistance with e.g. the number of turns  $w_r$ . It should be borne in mind that when  $w_r$  is varied, the cross-sectional area  $a_{Cu r}$  of the winding wire will generally have to vary too;  $w_r$  and  $a_{Cu r}$  are thus not independent parameters in eq. (1.13).

$$(3) \quad u - i(R_r + R_s) - L \frac{di}{dt} - e = 0. \quad (1.36)$$

This can show e.g. the influence of total rotor + stator resistance of a small AC series motor,  $R_r + R_s$ , on the relation between speed and current.

Descriptive formulas do not always describe the influence of the dimensions of the machine on its behaviour; we need dimensioning formulas for that.

#### 7.4. Examples of dimensioning formulas

Dimensioning formulas must contain the dimensions of the machine. An example of such a formula is:

$$d^5 = \frac{1}{\pi} \frac{\varrho_{Cu r}}{k_{Cu r} B_{max}^2} \frac{k_R}{k_E^2} \frac{k_{head r} + \lambda + 2 k_{ins head r}}{\lambda^2} \times \frac{1}{\beta^2 f_{(r)}} \frac{e^2}{R_r n^2}. \quad (1.26)$$

For  $f_{(r)}$  see eq. (1.24).

In this equation all the dimensions of the rotor are expressed in terms of the fictive rotor diameter  $d$  with the aid of the parameters  $\lambda$ ,  $\beta$ ,  $k_{shaft}$ ,  $k_{pole}$ ,  $k_{head r}$ ,  $k_{ins slots r}$  and  $k_{ins head r}$ . It can be used to study the influence of all the parameters on the dimensions of the rotor, as is done in sec. 7.10. It tells us e.g. that the rotor volume has an extreme minimum as a function of the relative flux-conducting rotor width  $\beta$ .

If we are to draw the right conclusions from a dimensioning formula, this formula must consist of independent or nearly independent parameters. This means that the value of one parameter is not influenced, or hardly influenced, by variations in other parameters, so that the influence of each parameter can be studied separately.

One example of an independent parameter is  $B_{max}$  in eq. (1.26).

Examples of non-independent parameters are the current density and the air-gap induction, as explained in secs 7.7 and 7.8.

#### 7.5. Examples of optimization formulas

An optimizing method was described in sec. 7.2. An example of an optimization formula is:

$$R_r = \frac{1}{8} \frac{\varrho_{Cu r}}{k_{Cu r} B_{max}^2} \frac{k_R}{k_E^2} \frac{s_{w r}}{A_{coils r} (b_{Fe r})^2 l_r^2 n^2}, \quad (1.25)$$

where

$$s_{w r} = 2(l_r + 2l_{ins r} + s_{head r}), \quad (1.16)$$

$$s_{\text{head } r} = k_{\text{head } r} d, \quad (1.18)$$

$$b_{Fe\ r} = \beta d \quad (1.6)$$

and  $A_{\text{colls } r}$  is given by eq. (1.24)

Equation (1.25) alone is not sufficient to optimize a motor, as the stator resistance  $R_s$ , rotor iron loss  $P_{Fe\ r}$ , etc. also have to be calculated; however, eq. (1.25) in combination with eqs (1.16), (1.18), (1.6) and (1.24) does give a suitable optimization formula.

It was mentioned in sec. 7.4 that a dimensioning formula must consist of nearly independent parameters. This is even more necessary for optimization formulas. If some parameters do depend on others, it must be possible to express them in terms of all the parameters concerned. For instance, the parameters  $k_{\text{ins slots } r}$  and  $k_{\text{ins head } r}$  occur in eq. (1.26). To calculate  $k_{\text{ins slots } r}$  and  $k_{\text{ins head } r}$ , we must thus know  $d$ ; but the object of eq. (1.26) is to calculate  $d$ . We thus have to start by substituting estimates of  $k_{\text{ins slots } r}$  and  $k_{\text{ins head } r}$  into eq. (1.26), and improving these estimates as necessary by an iterative method. This is a rather complicated procedure, but it has been chosen because it is in fact the simplest way of estimating the required value of  $d$ .

While eq. (1.26) gives an estimate of  $d$  as a function of  $R_r$  and other parameters, eqs (1.24), (1.6), (1.18), (1.16) and (1.25) give  $R_r$  as a function of  $d$  and other parameters. Now the rotor insulation occurs as  $l_{\text{ins } r}$  in (1.16) and as  $b_{\text{ins } r}$  in (1.24);  $b_{\text{ins } r}$  and  $l_{\text{ins } r}$  are thus independent parameters now. To calculate the required value of  $R_r$ ,  $R_r$  must be calculated an enormous number of times as a function of all the parameters and the best value of  $R_r$  selected. This procedure fits well into the optimization method described in sec. 7.2.

### 7.6. Rotor and stator resistances as parameters in dimensioning and optimization formulas

If an electric machine, e.g. a small series motor, is dimensioned, it must satisfy the specifications. The six most important items of the specification concern:

- (1) the required output power,
- (2) the required speed,
- (3) the input voltage,
- (4) the required efficiency,
- (5) the required shape of the speed-torque curve,
- (6) the permissible temperature rise of various parts of the machine.

The specifications may also cover other items, for instance one or more of the following:

- (7) the permissible stalling current,
- (8) the required or permissible stalling torque,
- (9) the permissible moment of inertia of the rotor,

- (10) the permissible volume,
- (11) the permissible weight,
- (12) the permissible level of radio interference,
- (13) the required life.

The specifications always contain items (1), (2) and (3), and at least one of the items (4), (5) and (6).

Items (4), (5) and (6) determine the quality of the machine. They must be expressed with the aid of such parameters that they can be introduced into the appropriate calculation.

For a given input voltage and a given output power, the current through the motor is nearly determined. This must be borne in mind in the following items.

- (a) The efficiency (item (4) above) is determined by the losses and the output power. The losses are: mechanical loss, iron loss and copper loss ( $i^2 R_r + i^2 R_s$ ). The value of  $R_r + R_s$  thus represents the contribution of the copper loss to the efficiency.
- (b) The shape of the speed-torque curve (item (5)) of a small commutator motor is influenced by the voltage drop  $i(R_r + R_s)$ ,  $i$  being almost constant; the influence of  $i(R_r + R_s)$  on the shape of the speed-torque curve is thus determined by the value of  $R_r + R_s$ .
- (c) The temperature rise in the stator (item (6)) is determined by  $i^2 R_s$  on the one hand and by the cooling efficiency on the other (as we saw in sec. 3.1, the iron losses are negligible here). The contribution of the copper loss in the stator to the temperature rise is represented by the value of  $R_s$ . In the rotor, the iron loss must be taken into consideration as well as the copper loss; the contribution of the copper loss in the rotor to the temperature rise in the rotor is represented by the value of  $R_r$ .

Summing up, we may state that  $R_r$  and  $R_s$  are nearly independent parameters which are very suitable for use in dimensioning and optimization formulas. If the iron loss in the rotor cannot be neglected and heating of the rotor is effected by the sum of copper and iron losses, the value chosen for  $R_r$  must be corrected so that the total loss in the rotor does not exceed the maximum permissible value. This correction procedure is described in the optimization method of chapter 8.

### 7.7. Use of air-gap induction, current density and specific load as parameters in the development of similarity relations

The internal power of a DC commutator motor can be described by Esson's formula:

$$P_\delta = \frac{\pi^2 n d_r^2 l_r S B_\delta}{k_{\text{pole}} k_{\text{car}}} = \frac{\pi^2 n \lambda d_r^3 S B_\delta}{k_{\text{pole}} k_{\text{car}}} \quad (7.1)$$



which can be changed into

$$P_{\delta} = \frac{c \pi^2 n d_r^3 l_r J B_{\delta}}{k_{\text{pole}} k_{\text{car}}} = \frac{c \pi^2 n \lambda d_r^4 J B_{\delta}}{k_{\text{pole}} k_{\text{car}}}, \quad (7.2)$$

where  $J$  is the current density in the rotor windings,  $S$  is the specific load in amperes per radian and  $B_{\delta}$  is the contribution of the stator field to the air-gap induction. The rotor field causes the real air-gap induction to be locally higher or lower than  $B_{\delta}$ .

However, eqs (7.1) and (7.2) are not completely correct, e.g. because (1) the air-gap flux is not fully surrounded by the rotor windings (see fig. 3.5b), (2) commutation losses occur.

In small machines with semi-enclosed slots and not many rotor coils, the above factors have more influence than in large machines.

According to our definition of sec. 7.1, eqs (7.1) and (7.2) are descriptive formulas.

Now similarity relations (relations between the various parameters of a machine when the scale of the machine is reduced or, more usually, increased) are also really descriptive formulas: the relations between the dimensions are not changed — the dimensions are simply all multiplied by the same number. The value of  $B_{\text{max}}/B_{\delta}$  does not change either.

Similarity relations based on eq. (7.2) have already been published in the literature (see e.g. Schuisky<sup>29</sup>). Independent of the dimensions,  $B_{\delta}$  and  $J$  are kept constant.  $B_{\text{max}}$  will thus also remain constant. In principle, therefore,  $B_{\text{max}}$  (in combination with other parameters) could be used instead of  $B_{\delta}$  in eq. (7.2) for the development of similarity relations. A constant current density means that the copper loss in the rotor is proportional to  $d_r^3$ . In practice, this presents no problem as regards cooling.

It may be concluded that eq. (7.2) (with  $P_{\delta} \propto d_r^4$ ) represents a suitable basis for the development of similarity relations. However, as will be shown in sec. 7.8, eq. (7.2) is not suitable for use as a dimensioning formula. Moreover, we shall now show that for small motors the internal power is not proportional to  $d_r^4$  but to  $d_r^5$ .

In small electric machines, the ratio  $i R_r/e$ , where  $i$  is the current through the machine,  $R_r$  is the rotor resistance and  $e$  is the rotational e.m.f., may be larger than in large electric machines. However,  $i R_r/e$  is limited with respect to specifications (4), (5) and (6) mentioned at the start of sec. 7.6.

Let us imagine  $e$  to be constant. If  $i R_r/e$  is also to be constant, we must have

$$i \propto \frac{1}{R_r}. \quad (7.3)$$



The internal power of the machine is then given by

$$P_{\delta} = e i \propto i \propto \frac{1}{R_r} \quad (7.4)$$

According to eq. (1.26)

$$R_r \propto d^{-5} \quad (7.5)$$

If  $R_r$  in eq. (7.4) is replaced by eq. (7.5) we find:

$$P_{\delta} \propto d^5 \quad (7.6)$$

Since  $d/d_r$  as well as  $f_{(r)}$  decrease if  $d$  decreases, eq. (7.6) becomes

$$P_{\delta} \propto d^{>5} \propto d_r^{>5} \quad (7.7)$$

### 7.8. Current density and specific load as parameters in dimensioning and optimization formulas

In sec. 7.7, Esson's formula was given in eq. (7.1). As we have seen, this formula is suitable for use as a descriptive formula. However, it has also been widely used for the dimensioning of commutator machines (see e.g. Postnikow <sup>16</sup>), Still and Siskind <sup>18</sup>) and Puchstein <sup>30</sup>)).

Now the specific load  $S$  occurring in eq. (7.1) has a number of disadvantages for use in a dimensioning formula:

- (1)  $S$  does not give any information about the copper loss in the rotor.
- (2) It does not give information about the voltage drop in the rotor resistance.
- (3) It gives no information about the optimum values of the relative flux-conducting width of the rotor  $\beta$ , the relative rotor length  $\lambda$  and the inductions  $B_{\max}$  and  $B_{\delta}$ .
- (4) If some parameters of the rotor are varied so as to change the value of the product  $d_r^2 l_r B_{\delta}$ ,  $S$  will vary too; in other words  $S$  is not an independent parameter.

The current density  $J$  in eq. (7.2) has comparable disadvantages:

- (1)  $J$  only gives information about the copper loss in the rotor if it is multiplied by the volume of copper in the rotor.
- (2) It gives no information about the voltage drop in the rotor resistance.
- (3) It does not give information about the optimum values of  $\beta$ ,  $\lambda$  and  $B_{\max}$  or  $B_{\delta}$ .
- (4) It is not an independent parameter, for a higher value of  $J$  is permissible in a small volume of copper than in a large volume.

It will now be clear that  $J$  and  $S$  are only of limited suitability as parameters in dimensioning formulas. As parameters in optimization formulas, they are quite unsuitable.

### 7.9. Magnetic induction in the iron and air-gap induction as parameters in dimensioning and optimization formulas

The relation between the air-gap induction  $B_\delta$  opposite the middle of a rotor tooth, and  $B_{\max}$ , the maximum induction in the iron of the rotor, may be written:

$$B_\delta = \frac{2 \beta k_{\text{pole}} k_{\text{car}} d B_{\max}}{\pi d_r} \quad (7.8)$$

The contribution of the stator ampere turns required for the air-gap width  $\delta$  is proportional to  $B_\delta$ .

The only advantage of  $B_\delta$  is that it gives direct information about the required number of ampere turns in the stator. However, that is not really very useful: correct choice of the rotor parameters has most influence on the cost and dimensions of the motor as a whole.  $B_\delta$  has the following disadvantages for use in dimensioning formulas:

- (1)  $B_\delta$  gives no information about the iron loss in the rotor.
- (2) It gives no information about the optimum values of the relative flux-conducting rotor width  $\beta$ , the relative rotor length  $\lambda$  and the induction  $B_{\max}$ .
- (3) It is not an independent parameter (see eq.(7.8)). If  $\beta$  is varied,  $B_\delta$  varies too.

It follows that, like  $J$  and  $S$ ,  $B_\delta$  is only of limited applicability as a parameter in dimensioning formulas. As parameter in optimization formulas, it is quite unsuitable.  $B_{\max}$  should be used instead, as is shown by the results of the optimization calculation in sec. 8.7.

### 7.10. Analysis of the rotor-dimensioning formula

In sec. 1.4 we derived the following rotor-dimensioning formula:

$$d^5 = \frac{1}{\pi} \frac{\rho_{\text{Cu } r} k_R k_{\text{head } r} + \lambda + 2 k_{\text{ins head } r}}{k_{\text{Cu } r} B_{\max}^2 k_\epsilon^2} \frac{1}{\lambda^2} \frac{1}{\beta^2 f_{(r)} R_r n^2} e^2 \quad (1.26)$$

where the rotor function  $f_{(r)}$  is given by

$$\begin{aligned} f_{(r)} = & (1 - \beta - k_{\text{shaft}}) \left( 1 + \beta + k_{\text{shaft}} - \frac{4}{\pi} \beta k_{\text{pole}} \right) + \\ & - 4 \left( \beta + k_{\text{shaft}} - \frac{2}{\pi} \beta k_{\text{pole}} \right) k_{\text{ins slots } r} + \\ & - \frac{4}{\pi} (1 - \beta - k_{\text{shaft}}) z k_{\text{ins slots } r}. \end{aligned} \quad (1.24)$$

In accordance with the conclusions of secs 7.8 and 7.9, this formula does not contain the parameters  $J$ ,  $S$  and  $B_\delta$ , but it does contain  $B_{\max}$  and  $R_r$ . The

suitability of the rotor resistance  $R_r$ , as a parameter in dimensioning formulas was indicated in sec. 7.6.

Of course, eq. (1.26) only concerns the rotor and not the complete motor; but it is found in practice that the machine as a whole is nearly as small and cheap as possible if the rotor is as small and cheap as possible. Consideration of eq. (1.26) will thus give a good impression of the optimum values of e.g.  $\beta$ ,  $\lambda$ ,  $B_{\max}$  and  $k_{\text{pole}}$ , without a complete optimization calculation for the whole machine — especially if no optimization method exists for the type of commutator machine in question.

Equation (1.26) is written as a product of six factors. No parameter appears in more than one factor. The parameters  $\rho_{\text{Cu } r}$ ,  $k_{\text{Cu } r}$ ,  $B_{\max}$ ,  $k_R$ ,  $k_E$ ,  $e$ ,  $R_r$  and  $n$  appear separately. In the fourth factor,  $\lambda$ ,  $k_{\text{head } r}$  and  $k_{\text{ins head } r}$  appear in a sum. Their influence must thus be studied together. In the fifth factor, the same is true of  $\beta$ ,  $k_{\text{shaft}}$ ,  $k_{\text{pole}}$  and  $k_{\text{ins slots } r}$  (which are involved in the expression for  $f_{(r)}$ ; see eq. (1.24)).

Below we shall consider the influence of  $B_{\max}$ ,  $n$ ,  $\lambda$ ,  $\beta$ ,  $k_{\text{shaft}}$ ,  $k_{\text{pole}}$  and  $k_{\text{head } r}$  on the iron loss  $P_{\text{Fe } r}$  and the volume  $V_r$  of the rotor. In fact  $V_r$ , which is given by

$$V_r = \frac{\pi}{4} d^2 l_r, \quad (7.9)$$

is only an approximation to the real rotor volume, as the fictive rotor diameter  $d$  is smaller than the real diameter  $d_r$ , while the contribution of the volume of copper and of insulation material is neglected in the definition of  $V_r$ .

The rotor resistance  $R_r$  is not varied in eq. (1.26). This means that the copper loss  $P_{\text{Cu } r}$  does not vary either, which is why only  $P_{\text{Fe } r}$  and  $V_r$  are studied below.

(1) *The influence of the maximum rotor induction  $B_{\max}$*

If only  $B_{\max}$  is varied,  $\beta$  and  $\lambda$  are constant. In that case  $V_r$  is proportional to  $d^3$ . According to eq. (1.26)

$$d^5 \propto B_{\max}^{-2},$$

so

$$V_r \propto d^3 \propto B_{\max}^{-6/5}. \quad (7.10)$$

If we assume that  $P_{\text{Fe } r}$  is proportional to  $B_{\max}^2$ , we find:

$$P_{\text{Fe } r} \propto B_{\max}^2 V_r = B_{\max}^2 B_{\max}^{-6/5} = B_{\max}^{4/5}. \quad (7.11)$$

The relations of eqs (7.10) and (7.11) are plotted in fig. 7.1.

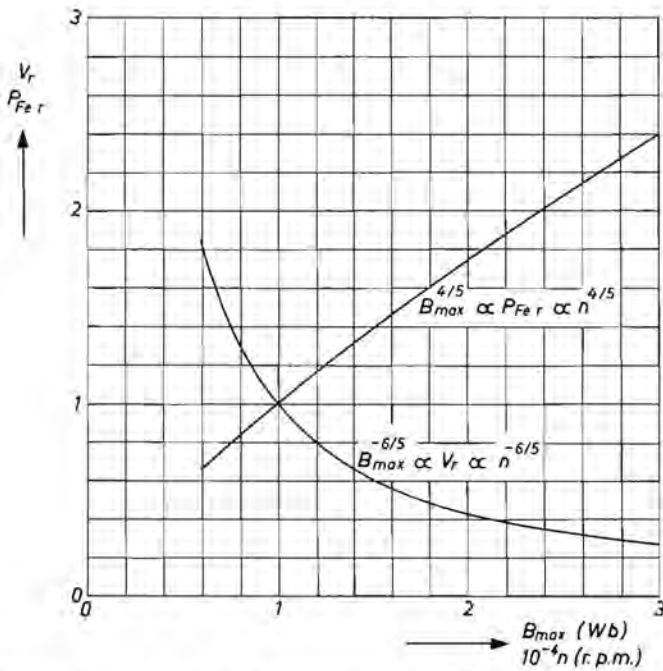


Fig. 7.1. Influence of rotor speed  $n$  and magnetic induction  $B_{max}$  on volume  $V_r$  (see eq. (7.9)) and iron loss  $P_{Fe\ r}$  of the rotor.

(2) *The influence of the rotor speed  $n$*

Both  $B_{max}$  and  $n$  occur squared in the denominator of eq. (1.26);  $n$  will thus have about the same influence on  $V_r$  and  $P_{Fe\ r}$  as  $B_{max}$  has, i.e.

$$V_r \propto n^{-6/5}, \tag{7.12}$$

$$P_{Fe\ r} \propto n^{4/5}. \tag{7.13}$$

These relations are also represented by the curves of fig. 7.9.

If  $B_{max}$  and  $n$  are increased,  $V_r$  will drop very sharply. If necessary, the increased iron loss can be compensated by choosing a lower value of  $R_r$ .

(3) *The influence of the relative rotor length  $\lambda$  and the relative length of an end winding  $k_{head\ r}$*

The influence of  $k_{ins\ head\ r}$  and  $k_{head\ r}$  is represented by the fourth factor of (1.26). The value of  $k_{ins\ head\ r}$  is so small that this parameter has been neglected; let us therefore simply consider  $(k_{head\ r} + \lambda)/\lambda^2$ .

If  $\beta$  and  $B_{max}$  and the other parameters are constant,  $V_r$  and  $P_{Fe\ r}$  are proportional to  $d^2 l_r = \lambda d^3$ .

Since  $d^3 \propto \left( \frac{k_{\text{head } r} + \lambda}{\lambda^2} \right)^{3/5}$ , we may write:

$$V_r \propto \lambda \left( \frac{k_{\text{head } r} + \lambda}{\lambda^2} \right)^{3/5} = \frac{(k_{\text{head } r} + \lambda)^{3/5}}{\lambda^{1/5}} \quad (7.14)$$

and

$$P_{\text{Fe } r} \propto \frac{(k_{\text{head } r} + \lambda)^{3/5}}{\lambda^{1/5}}. \quad (7.15)$$

Both eq. (7.14) and eq. (7.15) have minima at

$$\lambda = 0.5 k_{\text{head } r}. \quad (7.16)$$

In this case:

$$V_r \propto P_{\text{Fe } r} \propto 1.465 (k_{\text{head } r})^{2/5}. \quad (7.17)$$

Equations (7.14) and (7.15) are plotted in fig. 7.2. The minimum values of  $V_r$  and  $P_{\text{Fe } r}$  are strongly influenced by the value of  $k_{\text{head } r}$ . For the rotors of bipolar machines with former-wound coils or with coils directly wound in the slots and for rotors with only three rotor slots (also directly wound),  $k_{\text{head } r}$  is roughly 1.8, 1 and 0.6 respectively. For these three cases, the minimum values of  $V_r$  and  $P_{\text{Fe } r}$  will be roughly in the ratio 1.85 : 1.47 : 1.2. The corresponding values of  $\lambda$  are in the ratio 0.9 : 0.5 : 0.3.

It is thus very important that the rotor should have short end windings, first because this makes the machine smaller and cheaper, second because the smaller rotor means less iron loss.

As  $k_{\text{head } r}$  decreases, the importance of the correct value of  $\lambda$  increases.

(4) *The influence of the relative flux-conducting rotor width  $\beta$ , the relative fictive shaft diameter  $k_{\text{shaft}}$  and the relative reciprocal pole arc  $k_{\text{pole}}$*

The full expression for  $f_{(r)}$  is given in eq. (1.24). This is too complex for a general study. The influence of  $k_{\text{ins slots } r}$  has been neglected, since the thickness of the slot insulation is e.g. 0.15 mm in a slot 5 mm wide. Equation (1.24) then becomes:

$$f_{(r)} = (1 - \beta - k_{\text{shaft}}) \left( 1 + \beta + k_{\text{shaft}} - \frac{4}{\pi} \beta k_{\text{pole}} \right). \quad (7.18)$$

If only  $\beta$ ,  $k_{\text{pole}}$  and  $k_{\text{shaft}}$  are variable,  $V_r$  will be roughly proportional to  $d^3$ .

We now find from eqs (1.26) and (7.18) that

$$V_r \propto \left( \frac{1}{\beta^2 (1 - \beta - k_{\text{shaft}}) (1 + \beta + k_{\text{shaft}} - (4/\pi) \beta k_{\text{pole}})} \right)^{3/5} = \left( \frac{1}{\beta^2 f_{(r)}} \right)^{3/5}. \quad (7.19)$$

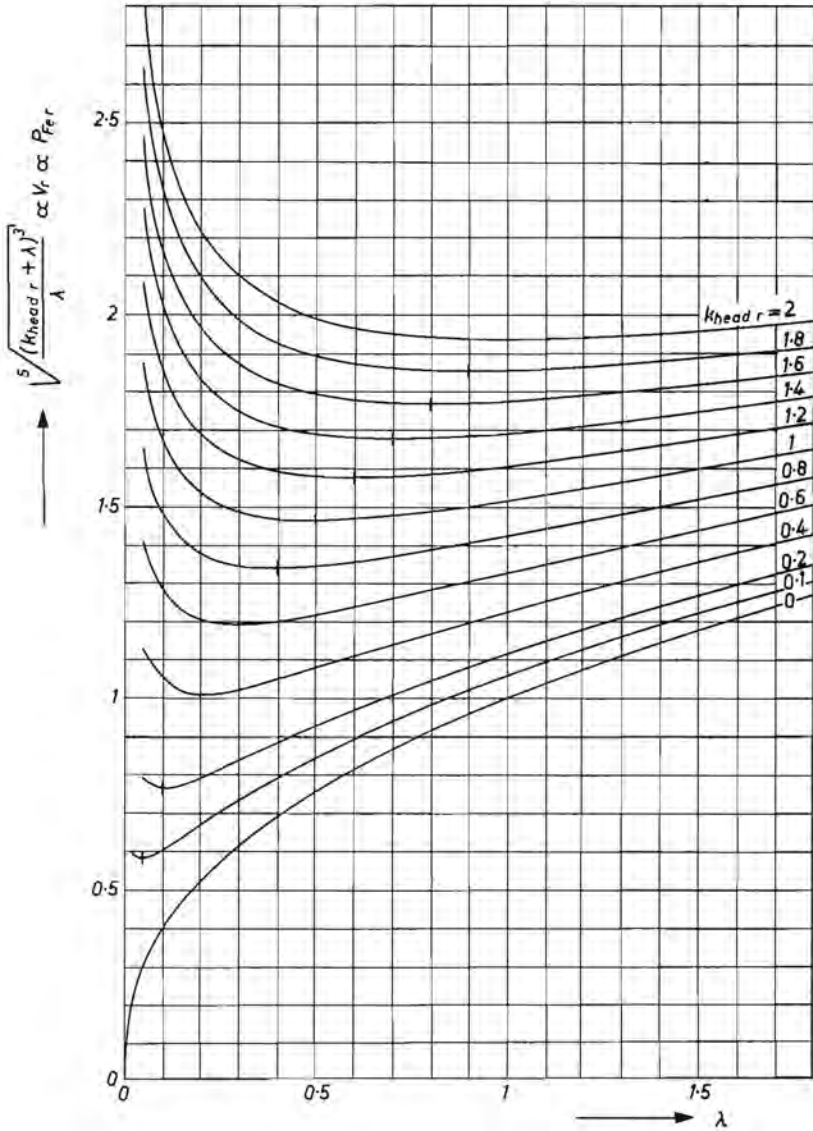


Fig. 7.2. The rotor volume  $V_r$  (see eq. (7.9)) and iron loss  $P_{Fe r}$ , as functions of the relative rotor length  $\lambda$  for various values of the relative length of the end windings  $k_{head} r$ . The vertical line on each curve indicates the position of the minimum.

The minimum of eq. (7.19) cannot easily be formulated, but this minimum appears clearly in the graphs of figs 7.3–7.6, which show  $(1/\beta^2 f_{(r)})^{3/5}$  as a function of  $\beta$  for values of  $k_{shaft}$  between 0 and 0.3.

$P_{Fe r}$  will be roughly proportional to  $\beta$  and to  $d^3$ , so we may write:

$$P_{Fe r} \propto \beta \left( \frac{1}{\beta^2 (1 - \beta - k_{shaft}) (1 + \beta + k_{shaft} - (4/\pi) \beta k_{pole})} \right)^{3/5} = \beta \left( \frac{1}{\beta^2 f(r)} \right)^{3/5} \quad (7.20)$$

This relation is plotted in figs 7.7 and 7.8, for various values of  $\beta$ ,  $k_{shaft}$  and  $k_{pole}$ .

7.10.1. *The optimum value of the relative rotor length*

Owing to the various imperfections of eq. (1.26), the real optimum relative rotor length  $\lambda$  will differ from the value determined from this equation. The following factors should be taken into account in this respect:

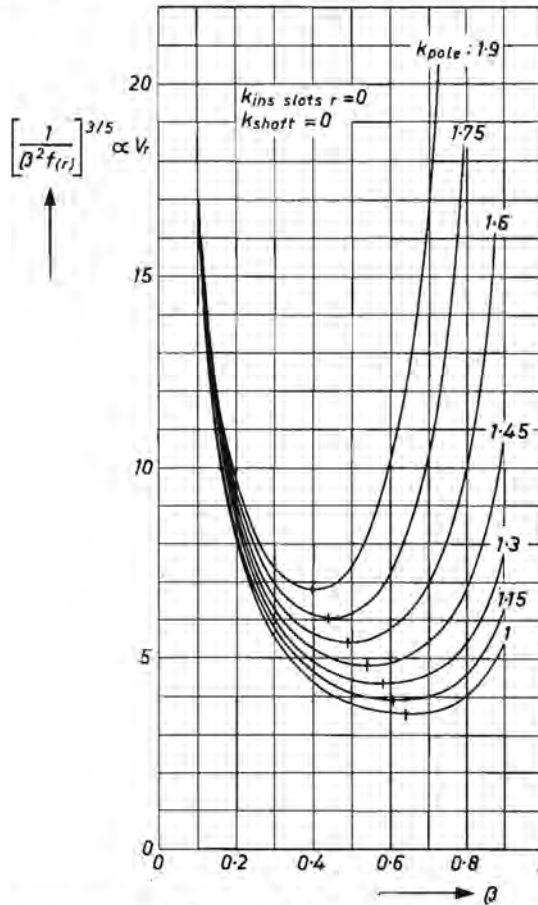


Fig. 7.3. The rotor volume  $V_r$  (see eq. (7.9)) as a function of the relative flux-conducting rotor width  $\beta$  for relative fictive shaft diameter  $k_{shaft} = 0$  and for various values of the reciprocal relative pole arc  $k_{pole}$ .

- (a) The required shaft diameter  $d_{\text{shaft}}$  depends on the mechanical requirements made on the system. If the fictive rotor diameter  $d$  is increased, it will be possible to decrease the rotor length  $l_r$  (at constant power), which means that the required value of  $d_{\text{shaft}}$  is more or less independent of  $d$ . If  $d$  is large,  $k_{\text{shaft}}$  is small, which is favourable as may be seen from figs 7.3–7.6.
- (b) The values of  $d_r - d$ ,  $l_{\text{ins } r}$  and  $b_{\text{ins } r}$  do not depend on the value of  $d$ . Their influence is thus relatively small when  $d$  is large.
- (c) The wires in the rotor slots are pulled down to the bottom of the slots by the wire spanner of the winding machine. This is done most effectively at the ends of the slots. A short slot length thus favours a high space factor  $k_{\text{Cu } r}$ .
- (d) Extra iron loss occurs in the edges of the laminations owing to stamping. This effect is relatively less in larger laminations than in small ones.
- (e) If  $l_r$  is small, the cost of stamping the laminations is low.

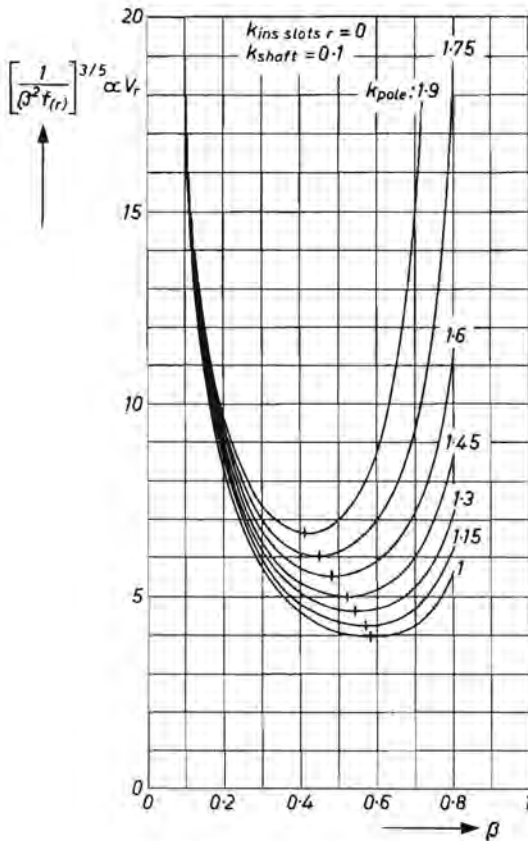


Fig. 7.4. As fig. 7.3, but with  $k_{\text{shaft}} = 0.1$ .



- (f) If  $d_r$  is large, the surface area of the end windings is large and the circumferential speed of the rotor is high; this improves the cooling of the rotor.
- (g) If  $d_r$  is large, the commutator diameter is relatively small. This makes it possible to wind the rotor after the commutator has been mounted. All the points mentioned above indicate that the most favourable value of  $\lambda$  is lower than fig. 7.2 suggests.

7.10.2. *The optimum value of the relative flux-conducting rotor width*

- (a) If  $\beta$  is large, the influence of  $b_{ins r}$  is large. This is unfavourable.
- (b) If  $\beta$  is large,  $d_{core}$  is large. This makes winding easier, which is especially valuable when the rotor is wound after the commutator has been mounted.
- (c) If  $\beta$  is large, the stator field is relatively high. Fewer ampere turns will thus be required in the rotor, making the rotor field and the inductance of a rotor coil relatively small. This is favourable for commutation.

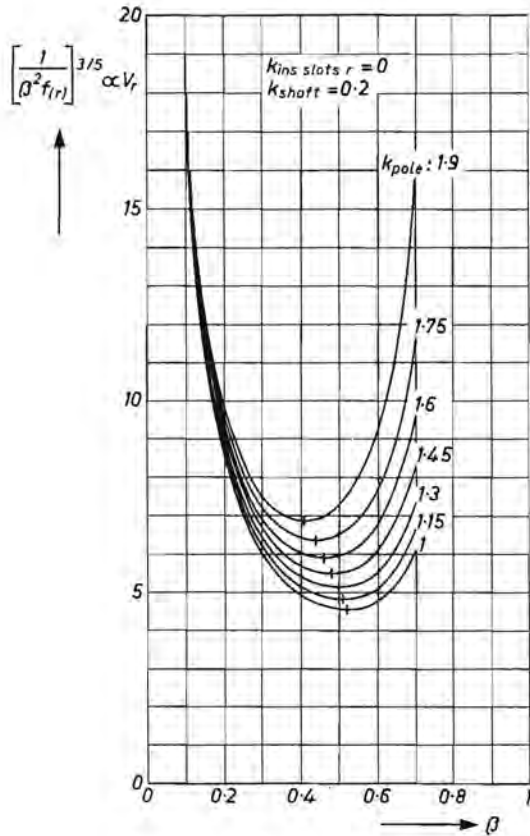


Fig. 7.5. As fig. 7.3, but with  $k_{shaft} = 0.2$ .

Points (b) and (c) indicate that the most favourable value of  $\beta$  will actually be larger than figs 7.3–7.8 suggest. However,  $\beta$  should not be chosen too high: the flux through the machine increases with  $\beta$  and so therefore do the amounts of copper and iron required in the stator.

**7.11. The optimum value of the relative flux-conducting rotor width at constant current density**

If the current density  $J$  is assumed to be constant, eq. (1.42) for the internal torque,

$$T_{\delta} = \frac{w_r \phi^{(1)} i}{\pi} \tag{1.42}$$

must be used as a dimensioning formula. This means that  $\phi^{(1)}$  and  $i w_r$  must be replaced by

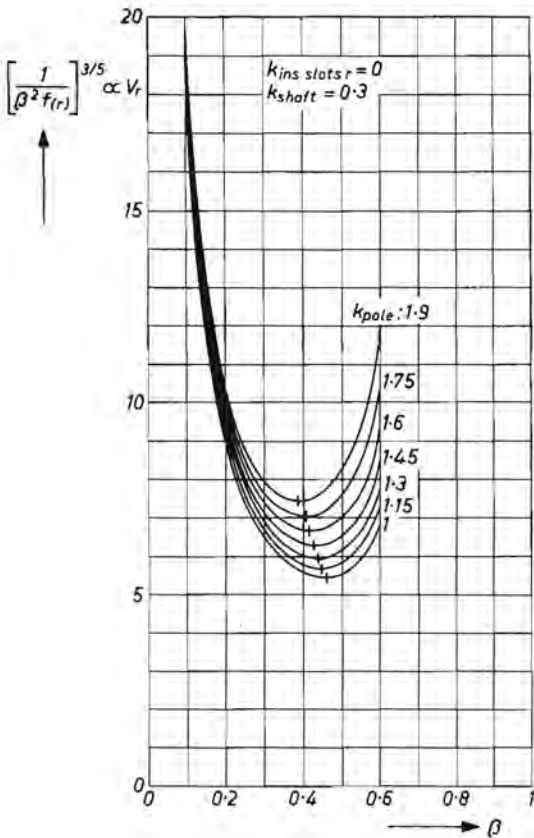


Fig. 7.6. As fig. 7.3, but with  $k_{shaft} = 0.3$ .

$$\phi^{(1)} = \beta \lambda d^2 B_{\max} \quad (1.9)$$

and

$$i w_r = \frac{\pi}{4} k_{Cu r} J f_{(r)} d^2, \quad (7.21)$$

which gives

$$T_\delta = \frac{k_{Cu r} \lambda \beta f_{(r)} d^4 J B_{\max}}{4}. \quad (7.22)$$

If we now write for the rotor volume

$$V_r = \frac{\pi}{4} d^2 l_r = \frac{\pi}{4} \lambda d^3, \quad (7.23)$$

we can replace  $(\pi/4) \lambda d^3$  in eq. (7.22) by  $V_r$ , giving

$$T_\delta = \frac{k_{Cu r} \beta f_{(r)} d V_r J B_{\max}}{\pi}. \quad (7.24)$$

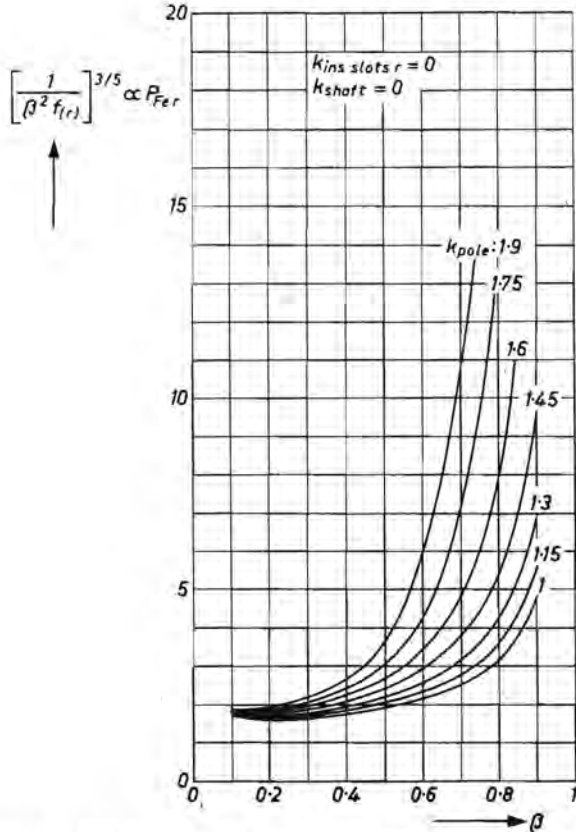


Fig. 7.7. The rotor iron loss  $P_{Fe r}$  as a function of the relative flux-conducting rotor width  $\beta$ , for relative fictive shaft diameter  $k_{shaft} = 0$  and for various values of the reciprocal relative pole arc  $k_{pole}$ .

This expression suggests that the fictive rotor diameter  $d$  should be chosen as large as possible in order to obtain a small rotor volume  $V_r$  at constant torque  $T_\delta$ . This means making the rotor diameter large and the rotor length short, i.e. making  $\lambda$  very small. This is in contradiction with the conclusions of sec. 7.10, which indicate an optimum value of  $\lambda$ . The reason is that eq. (7.24) neglects the effect of the end windings.

If  $k_{\text{ins slots}} = 0$ ,

$$f_{(r)} = (1 - \beta - k_{\text{shaft}}) \left( 1 + \beta + k_{\text{shaft}} - \frac{4}{\pi} \beta k_{\text{pole}} \right). \quad (7.18)$$

If the torque  $T_\delta$  and all parameters except  $d$ ,  $\beta$ ,  $k_{\text{shaft}}$  and  $k_{\text{pole}}$  are kept constant, we have:

$$d V_r \propto d^4 \propto \frac{1}{\beta f_{(r)}} \quad (7.25)$$

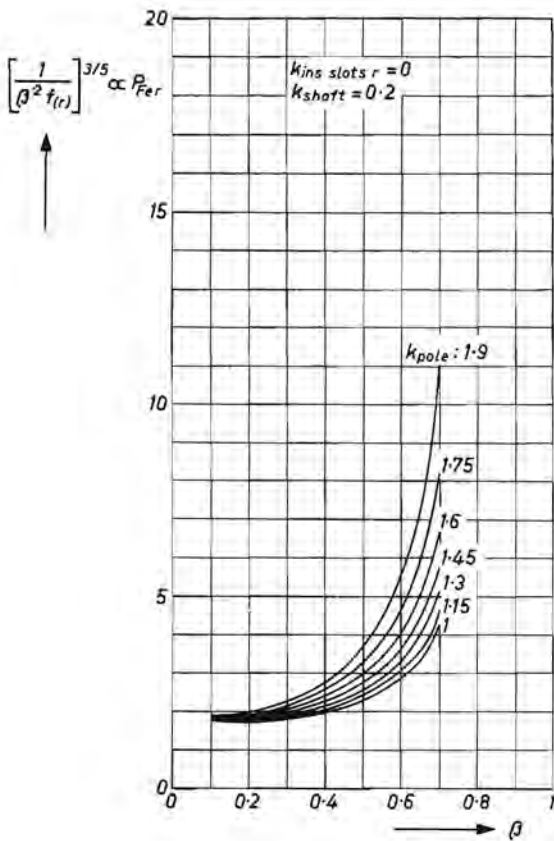


Fig. 7.8. As fig. 7.7, but with  $k_{\text{shaft}} = 0.2$ .

and

$$V_r \propto d^3 \propto \left( \frac{1}{\beta f(r)} \right)^{3/4} \quad (7.26)$$

The iron loss in the rotor is

$$P_{Fe r} \propto \beta V_r \propto \beta \left( \frac{1}{\beta f(r)} \right)^{3/4} \quad (7.27)$$

The relations (7.26) and (7.27) are plotted in figs 7.9 and 7.10. The minima of  $V_r$  in fig. 7.9 are found at much lower values of  $\beta$  than in fig. 7.5. Both figures are for the same values of  $k_{shaft}$  and  $k_{pole}$ . Apparently, taking a constant current density as the starting point of our argument leads to other conclusions than starting from a constant rotor resistance. To investigate the reason for this difference, we calculated the copper volume  $V_{Cu r}$  as a function of  $\beta$ ,

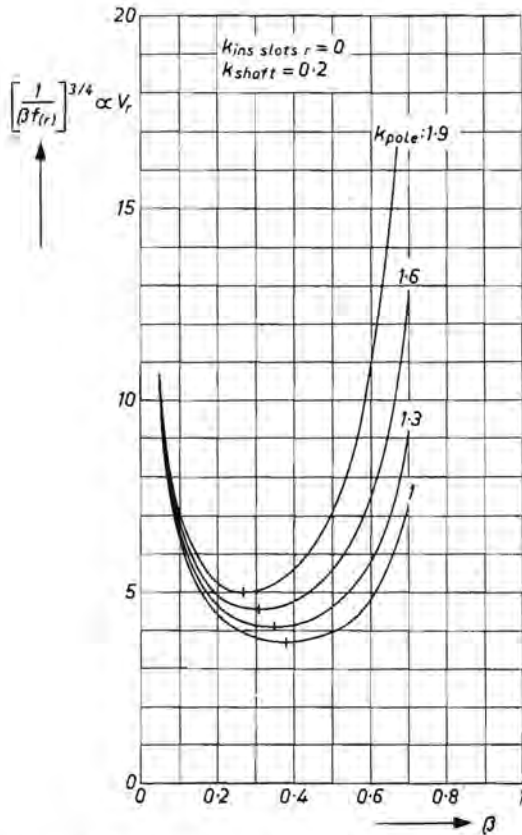


Fig. 7.9. The rotor volume  $V_r$  (see eq. (7.9)) as a function of the relative flux-conducting rotor width  $\beta$ , for relative fictive shaft diameter  $k_{shaft} = 0$  and for various values of the reciprocal relative pole arc  $k_{pole}$ , at constant current density  $J$  in the rotor.

at constant current density:

$$V_{Cu r} = 0.5 d (1 + \lambda) \frac{\pi}{4} d^2 f_{(r)} \propto d^3 (1 + \lambda) f_{(r)}. \quad (7.28)$$

If  $\lambda$  is constant, it follows from eqs (7.26) and (7.28) that

$$V_{Cu r} \propto d^3 f_{(r)} \propto \left( \frac{1}{\beta f_{(r)}} \right)^{3/4} f_{(r)} = \left( \frac{f_{(r)}}{\beta^3} \right)^{1/4}. \quad (7.29)$$

If the current density is constant, the copper loss  $P_{Cu r}$  in the rotor is proportional to  $V_{Cu r}$ :

$$P_{Cu r} \propto V_{Cu r} \propto \left( \frac{f_{(r)}}{\beta^3} \right)^{1/4}. \quad (7.30)$$

This relation is plotted in fig. 7.11.

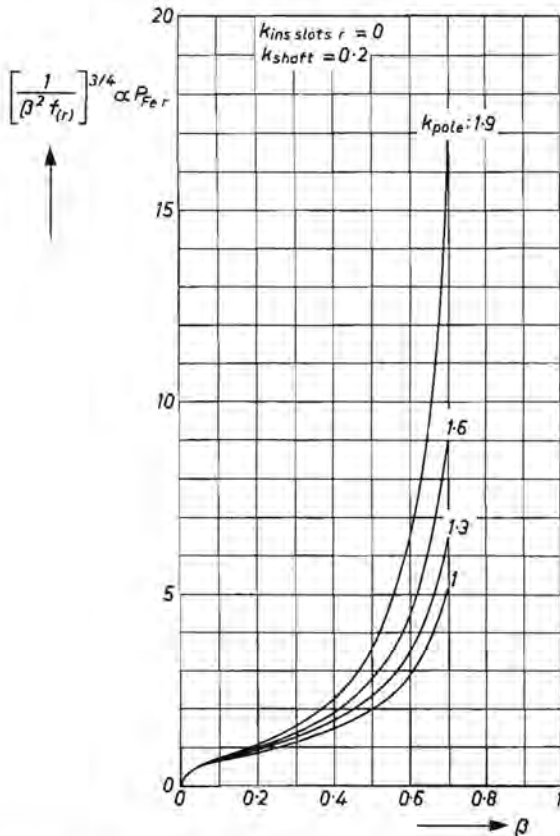


Fig. 7.10. Iron loss in the rotor  $P_{Fe r}$  as a function of the relative flux-conducting rotor width  $\beta$ , for relative fictive shaft diameter  $k_{shaft} = 0$  and for various values of the reciprocal relative pole arc  $k_{pole}$ , at constant current density  $J$  in the rotor.

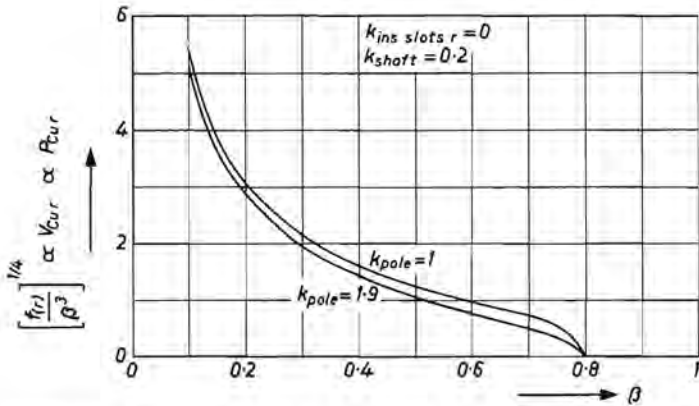


Fig. 7.11. Copper volume and copper loss in the rotor as functions of the relative flux-conducting rotor width  $\beta$  for relative fictive shaft diameter  $k_{shaft} = 0.2$  and for reciprocal relative pole arc  $k_{pole} = 1.0$  and  $1.9$ , at constant current density  $J$  in the rotor.

As  $\beta$  decreases,  $V_{Cu r}$  and  $P_{Cu r}$  increase steeply; the minimum of  $V_r$  is thus obtained at the expense of high copper losses and a large volume of copper in the rotor. A cheaper rotor of higher efficiency can thus be made if  $\beta$  is increased, which brings us back to the optimum values of  $\beta$  indicated in fig. 7.5. These results show that the assumption of a constant rotor resistance as basis of our considerations gives more reliable information about the optimum dimensions of the rotor than the assumption of constant current density. This is confirmed by the results of the optimization calculation in chapter 8.

### 7.12. Conclusions

The difference between description, design, dimensioning and optimization must be clearly realized in electric-machine design work. Bearing these differences in mind, we have considered in this chapter which parameters should be used in dimensioning formulas for the rotor of a small commutator machine. It appears that the rotor resistance  $R_r$  and the maximum magnetic induction in the iron  $B_{max}$  are to be preferred to the air-gap induction  $B_\delta$  and the current density  $J$  or the specific load  $S$ . Analysis of the rotor-dimensioning formula (1.26) indicates that correct choice of the relative rotor length  $\lambda$  and the relative flux-conducting rotor width  $\beta$  is very important.

## 8. THE OPTIMIZATION METHOD

In the previous chapters we have studied a number of points which can serve as basis for an optimization calculation, and derived the formulas required for this purpose. In this chapter, the optimization calculation is described in detail, and a specimen calculation is carried out.

The results of the specimen calculation are used for the optimization of a vacuum-cleaner motor, and the operation of this motor is compared with that of an existing motor under comparable conditions.

### 8.1. Formulas for the volume, weight and cost of the steel sheet required

The rotor laminations of a small series motor are generally stamped out of the middle of the stator laminations, which in their turn are stamped out of a strip of steel sheet (see fig. 8.1).

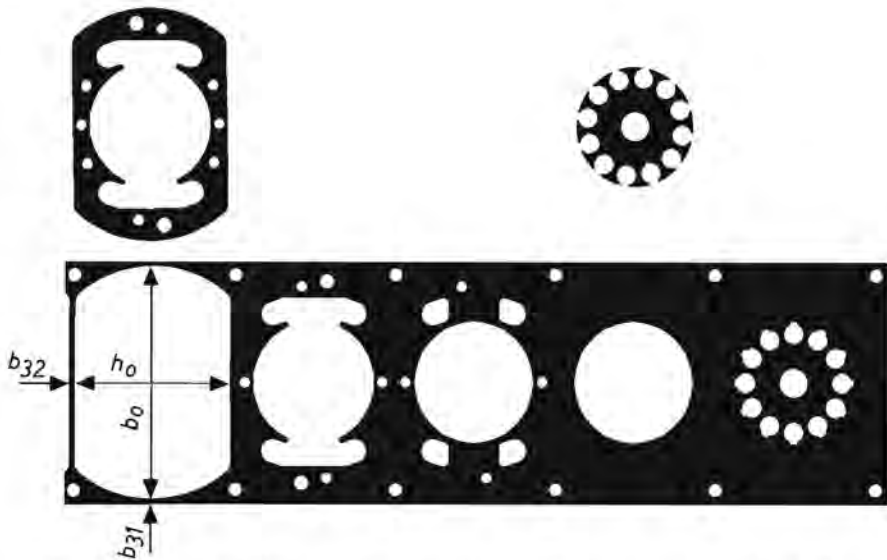


Fig. 8.1. Strip of steel sheet and the rotor and stator laminations as stamped out of it.

The total height  $h_0$  and the total width  $b_0$  of the laminations have already been illustrated in fig. 1.8. The width of the strip is  $b_0 + 2b_{31}$ , while a length  $h_0 + b_{32}$  is required for one stator + rotor lamination;  $b_{31}$  and  $b_{32}$  must be a few millimetres. If they are chosen too small, the stamped laminations will not be flat and the life of the dies will be reduced.

In a finished stack of laminations there is a thin layer of insulating paper, lacquer, oil, air or some other suitable substance between the laminations. The influence of this on the total volume of the assembly is expressed by the space



factor  $k_{Fe}$ , which is generally about 0.95. The volume of steel sheet required by the motor is then

$$V_{Fe} = k_{Fe} l_s (h_o + b_{32}) (b_o + 2 b_{31}). \quad (8.1)$$

If we denote the density of the steel sheet by  $g_{Fe}$ , the weight of the steel required will be

$$G_{Fe} = g_{Fe} k_{Fe} l_s (h_o + b_{32}) (b_o + 2 b_{31}) \quad (8.2)$$

and the cost of this steel sheet is

$$C_{Fe} = c_{Fe} g_{Fe} k_{Fe} l_s (h_o + b_{32}) (b_o + 2 b_{31}), \quad (8.3)$$

where  $c_{Fe}$  is the cost per kg.

The cost of stamping the laminations for one motor is proportional to the length of one stack. The cost of stamping one lamination is independent of the dimensions of the lamination over a wide range of values of  $h_o$  and  $b_o$ . If we denote the cost of stamping a stack with a length of one metre by  $c_{stamp}$ , the cost of the stamping for one motor will be

$$C_{stamp} = c_{stamp} l_s. \quad (8.4)$$

If  $l_s$  is smaller than  $l_r$ ,  $l_s$  must be replaced by  $l_r$  in eqs (8.1), (8.2), (8.3) and (8.4).

## 8.2. Formulas for the volume, weight and cost of the winding wire of rotor and stator

The total volume of copper in the rotor is

$$V_{Cu r} = a_{Cu r} w_r s_{w r}. \quad (8.5)$$

If we denote the density of copper by  $g_{Cu r}$ , we may write the weight of the copper required for one rotor:

$$G_{Cu r} = g_{Cu r} a_{Cu r} w_r s_{w r}. \quad (8.6)$$

Let  $c_{Cu r}$  be the specific copper cost, i.e. the cost of an amount of winding wire, the copper core of which weighs 1 kg;  $c_{Cu r}$  will thus be a few per cent higher than the cost per kg of complete winding wire. The cost of the winding wire required for one rotor is then

$$C_{Cu r} = c_{Cu r} g_{Cu r} a_{Cu r} w_r s_{w r}. \quad (8.7)$$

Similarly we find for the stator:

$$V_{Cu s} = a_{Cu s} w_s s_{w s}, \quad (8.8)$$

$$G_{Cu s} = g_{Cu s} a_{Cu s} w_s s_{w s}, \quad (8.9)$$

$$C_{Cu s} = c_{Cu s} g_{Cu s} a_{Cu s} w_s s_{w s}. \quad (8.10)$$

The rotor and stator have copper or sometimes aluminium cores of circular cross-section. The diameter of this core hardly differs from the nominal value. A layer of insulating lacquer is applied to the core; the thickness and density of this layer show much more variation than the diameter and density of the core itself. Figure 8.2 shows the nominal weight of enamelled winding wire, type D, according to the Dutch standard NLN-R923 as a percentage of the weight of the copper core, plotted against the nominal core diameter.

Even for very thin wire, the influence of the insulation layer on the weight is limited. The cost per kg of the complete winding wire is given by the dots in fig. 8.3.

To keep the formulas describing the motor as general and simple as possible, the space factors  $k_{Cu r}$  and  $k_{Cu s}$  refer to the copper core and not to the complete winding wire;  $V_{Cu r}$ ,  $V_{Cu s}$ ,  $G_{Cu r}$  and  $G_{Cu s}$  also refer to the copper core;  $g_{Cu r}$  and  $g_{Cu s}$  are the densities of copper in the rotor and in the stator. Because of this, the influence of the weight of the insulating layer must be taken into account in  $c_{Cu r}$  and  $c_{Cu s}$ . At a given core diameter of the winding wire,  $c_{Cu r}$  and  $c_{Cu s}$  can be found as the product of the corresponding percentage of fig. 8.2 and the cost of fig. 8.3. The resulting cost is plotted as the full curve in fig. 8.3.

In an optimization calculation, the cost of copper must be calculated for various values of the core diameters  $d_{Cu r}$  and  $d_{Cu s}$ . The corresponding values of the specific copper costs  $c_{Cu r}$  and  $c_{Cu s}$  must be stored in the memory of the computer. This can be done by expressing  $c_{Cu r}$  mathematically in terms

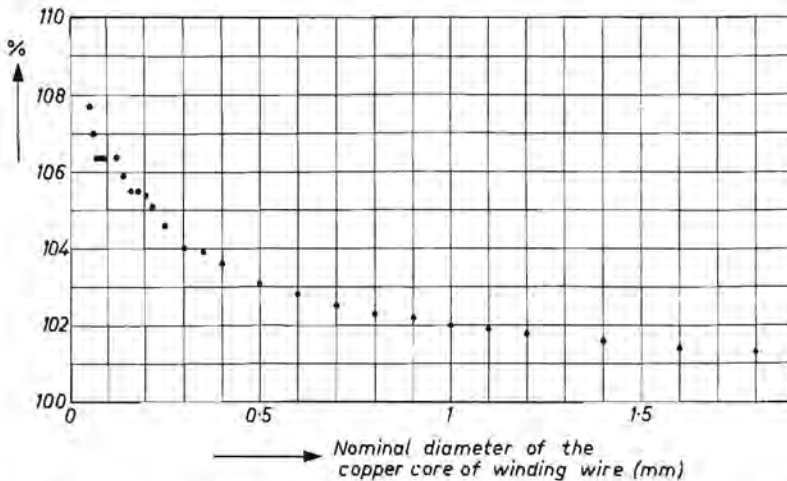


Fig. 8.2. The nominal weight of complete enamelled winding wire, type D, according to Dutch standard NLN-R923, as a percentage of the weight of its copper core, plotted against the nominal diameter of the copper core  $d_{Cu r}$  or  $d_{Cu s}$ .

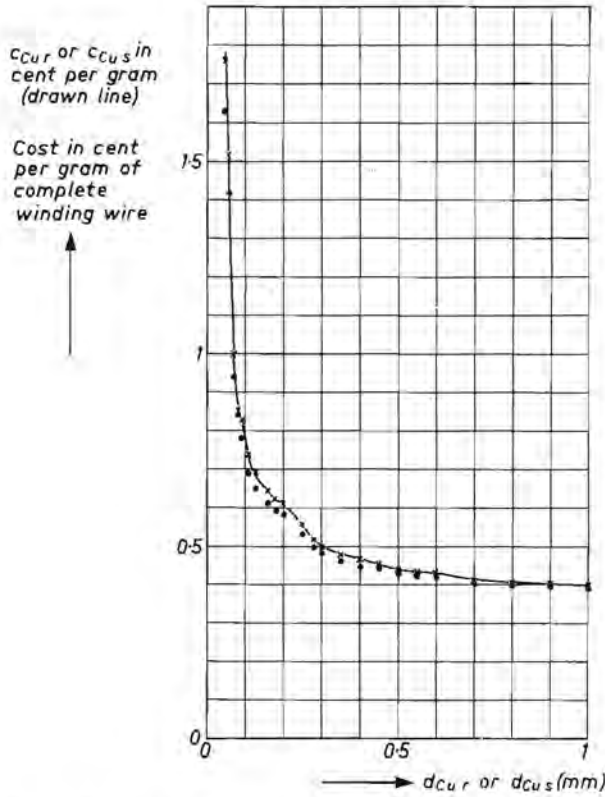


Fig. 8.3. Cost of enamelled winding wire as a function of the nominal core diameter  $d_{Cu r}$  or  $d_{Cu s}$ .

of  $d_{Cu r}$  and  $c_{Cu s}$  in terms of  $d_{Cu s}$ . In a limited range, we can use the approximations

$$c_{Cu r} = c_{24} - c_{25} d_{Cu r} + c_{26} d_{Cu r}^2 \quad (8.11)$$

and

$$c_{Cu s} = c_{34} - c_{35} d_{Cu s} + c_{36} d_{Cu s}^2. \quad (8.12)$$

Equation (8.11) has three unknown coefficients  $c_{24}$ ,  $c_{25}$  and  $c_{26}$ , which can be determined with three equations. Before the optimization calculation, we must estimate the values of  $d_{Cu r}$  that will occur in the calculations. The average estimated value of  $d_{Cu r}$  may be denoted by  $d_{22}$ . We now choose  $d_{21}$  and  $d_{23}$  in the neighbourhood of  $d_{22}$  so that

$$d_{23} - d_{22} = d_{22} - d_{21}. \quad (8.13)$$

The values of  $c_{Cu r}$  corresponding to  $d_{21}$ ,  $d_{22}$  and  $d_{23}$  can be read off from fig. 8.3. They are called  $c_{21}$ ,  $c_{22}$  and  $c_{23}$  respectively. Suitable values of  $d_{21}$  and  $d_{23}$  should be found by trial and error.

Now  $c_{24}$ ,  $c_{25}$  and  $c_{26}$  can be written

$$c_{24} = c_{21} - \frac{d_{21}(c_{22} - c_{21})}{d_{22} - d_{21}} + \frac{d_{21}d_{22}(c_{23} - 2c_{22} + c_{21})}{2(d_{22} - d_{21})^2}, \quad (8.14)$$

$$c_{25} = \frac{(d_{21} + d_{22})(c_{23} - 2c_{22} + c_{21})}{2(d_{22} - d_{21})^2} - \frac{c_{22} - c_{21}}{d_{22} - d_{21}}, \quad (8.15)$$

$$c_{26} = \frac{c_{23} - 2c_{22} + c_{21}}{2(d_{22} - d_{21})^2}. \quad (8.16)$$

Similarly, for the stator we choose  $d_{31}$ ,  $d_{32}$  and  $d_{33}$ ; the corresponding values of  $c_{c_{us}}$  are  $c_{31}$ ,  $c_{32}$  and  $c_{33}$  respectively. Again,

$$d_{33} - d_{32} = d_{32} - d_{31}, \quad (8.17)$$

$c_{34}$ ,  $c_{35}$  and  $c_{36}$  are now given by

$$c_{34} = c_{31} - \frac{d_{31}(c_{32} - c_{31})}{d_{32} - d_{31}} + \frac{d_{31}d_{32}(c_{33} - 2c_{32} + c_{31})}{2(d_{32} - d_{31})^2}, \quad (8.18)$$

$$c_{35} = \frac{(d_{31} + d_{32})(c_{33} - 2c_{32} + c_{31})}{2(d_{32} - d_{31})^2} - \frac{c_{32} - c_{31}}{d_{32} - d_{31}}, \quad (8.19)$$

$$c_{36} = \frac{c_{33} - 2c_{32} + c_{31}}{2(d_{32} - d_{31})^2}. \quad (8.20)$$

Finally, we must test whether eqs (8.11) and (8.12) approximate the cost per kg as a function of the core diameter with enough accuracy in the range of expected diameters. If not, other values of  $d_{21}$ ,  $d_{22}$ ,  $d_{23}$  and  $d_{31}$ ,  $d_{32}$ ,  $d_{33}$  must be tried.

### 8.3. The motor to be optimized and the starting points for the optimization calculation

A small series motor is generally used in vacuum cleaners, for the following reasons.

- (1) It is suitable for high speeds.
- (2) The form of the speed-torque curve is suitable for vacuum cleaners.
- (3) A brush life corresponding to an effective life of e.g. 10 to 15 years for the vacuum cleaner in an average household can easily be realized.
- (4) The radio interference caused by the motor can easily be suppressed.
- (5) The manufacturing costs are low compared with those of other motors which come into consideration.

Small series motors are also preferred in hand mixers, coffee grinders, hand tools, etc., for more or less the same reasons.

In future, semiconductors will be used more and more in small electric motors

to replace mechanical contacts in commutators, etc. However, it may be expected that small series motors will be used in small appliances for the next 10 to 20 years. At the present moment, it is thus still of economic importance to have a method of optimizing this type of motor.

#### 8.4. Survey of parameters used

All the parameters of the small series motor have been discussed in the previous chapters. They are listed below, together with a number of parameters required for the optimization calculation. The parameters are divided into nine groups. The values given for the various parameters concern what we shall refer to as the "average motor" from now on. The results of the optimization calculation given in table 8-I also refer to this "average motor".

##### A. Parameters concerning the specifications of the motor

mains voltage	$U$	220 V
mains frequency	$\nu$	$50 \text{ s}^{-1}$
required output power	$P_{\text{out req}}$	250 W
rotor speed	$n$	$320 \text{ s}^{-1}$
permissible losses in the rotor	$P_{\text{Cu Fe r req}}$	30 W
permissible copper loss in the stator	$P_{\text{Cu s req}}$	30 W

$U$  and  $\nu$  are input parameters;  $P_{\text{out req}}$  and  $n$  are output parameters. The temperature rise in the rotor and stator coils is represented by  $P_{\text{Cu Fe r req}}$  and  $P_{\text{Cu s req}}$  respectively.

##### B. Parameters concerning the properties of the materials used and the degree to which these materials are utilized

resistivity of copper in the rotor	$\rho_{\text{Cu r}}$	$23 \cdot 10^{-9} \Omega \text{ m}$
space factor of copper in the rotor	$k_{\text{Cu r}}$	0.35
resistivity of copper in the stator	$\rho_{\text{Cu s}}$	$23 \cdot 10^{-9} \Omega \text{ m}$
space factor of copper in the stator	$k_{\text{Cu s}}$	0.55
value of magnetic induction up to which it is proportional to the excitation	$B_{\text{prop}}$	$1.35 \text{ Wb m}^{-2}$
relative permeability of the steel sheet used	$\mu_r$	3000
specific iron loss in the rotor	$p_{\text{Fe}}$	$0.32 \text{ W Wb}^{-2} \text{ m}^{-1}$
space factor of steel sheet	$k_{\text{Fe}}$	0.95
see fig. 8.1	$b_{3.1}$	$2 \cdot 10^{-3} \text{ m}$
see fig. 8.1	$b_{3.2}$	$2.5 \cdot 10^{-3} \text{ m}$

The values of the resistivities  $\rho_{\text{Cu r}}$ ,  $\rho_{\text{Cu s}}$  and the specific iron loss are given for the operating temperature of the part of the motor in question.

*C. Parameters concerning the cost of the materials used*

The "cent" occurring in some parameters is the Dutch cent = 0.01 guilder.

density of copper	$g_{Cu r}$	$8950 \text{ kg m}^{-3}$
diameter of winding wire (see sec. 8.2)	$d_{21}$	$0.25 \cdot 10^{-3} \text{ m}$
diameter of winding wire (see sec. 8.2)	$d_{22}$	$0.4 \cdot 10^{-3} \text{ m}$
diameter of winding wire (see sec. 8.2)	$d_{23}$	$0.55 \cdot 10^{-3} \text{ m}$
specific cost of winding wire (see sec. 8.2)	$c_{21}$	$640 \text{ cent kg}^{-1}$
specific cost of winding wire (see sec. 8.2)	$c_{22}$	$550 \text{ cent kg}^{-1}$
specific cost of winding wire (see sec. 8.2)	$c_{23}$	$510 \text{ cent kg}^{-1}$
density of copper	$g_{Cu s}$	$8950 \text{ kg m}^{-3}$
diameter of winding wire (see sec. 8.2)	$d_{31}$	$0.25 \cdot 10^{-3} \text{ m}$
diameter of winding wire (see sec. 8.2)	$d_{32}$	$0.4 \cdot 10^{-3} \text{ m}$
diameter of winding wire (see sec. 8.2)	$d_{33}$	$0.55 \cdot 10^{-3} \text{ m}$
specific cost of winding wire (see sec. 8.2)	$c_{31}$	$640 \text{ cent kg}^{-1}$
specific cost of winding wire (see sec. 8.2)	$c_{32}$	$550 \text{ cent kg}^{-1}$
specific cost of winding wire (see sec. 8.2)	$c_{33}$	$510 \text{ cent kg}^{-1}$
density of steel	$g_{Fe}$	$7800 \text{ kg m}^{-3}$
specific cost of steel sheet	$c_{Fe}$	$88 \text{ cent kg}^{-1}$
specific cost of stamping the laminations	$c_{stamp}$	$1550 \text{ cent m}^{-1}$

*D. Parameters concerning the thickness of the insulating layers in rotor and stator*

thickness of rotor slot insulation	$b_{ins r}$	$0.15 \cdot 10^{-3} \text{ m}$
thickness of rotor head insulation	$l_{ins r}$	$2 \cdot 10^{-3} \text{ m}$
thickness of stator slot insulation	$b_{ins s}$	$0.2 \cdot 10^{-3} \text{ m}$
thickness of stator head insulation	$l_{ins s}$	$4 \cdot 10^{-3} \text{ m}$

*E. Mechanical parameters*

fictive shaft diameter	$d_{shaft \text{ fict}}$	$8 \cdot 10^{-3} \text{ m}$
air-gap width	$\delta$	$0.4 \cdot 10^{-3} \text{ m}$
number of rotor teeth	$z$	12
relative length of rotor end windings	$k_{head r}$	1
reciprocal relative pole arc	$k_{pole}$	1.3
carter factor	$k_{car}$	1.1
see eq. (1.1) and fig. 1.8	$b_{23}$	$2 \cdot 10^{-3} \text{ m}$
see fig. 1.8	$b_{33}$	$5 \cdot 10^{-3} \text{ m}$
see eq. (1.27) and fig. 1.8	$b_{39}$	$2 \cdot 10^{-3} \text{ m}$

*F. Parameters concerning commutation and the dimensions of brushes and commutator*

angle through which the brushes are turned against the direction of rotation of the rotor	$\alpha_{brush}$	$15^\circ$
relative active rotational e.m.f.	$k_E$	0.85
relative active rotor resistance	$k_R$	0.9

G. *Parameters, concerning the magnetic circuit*

tangent of the angle which the right-hand linear portion of the normalized magnetization curve makes with the horizontal axis	$m$	0.12
see eq. (1.28)	$k_{35}$	1.1
see eq. (1.29)	$k_{36}$	1.1
see eq. (2.19)	$c_{37}$	1.1

H. *Design parameters, the optimum value of which must be calculated*

rotor length (relative rotor length)	$l_r (\lambda)$
fictive rotor diameter	$d$
relative flux-conducting rotor width	$\beta$
peak value of magnetic induction in the magnetic circuit	$B_{\text{peak}}$

I. *Parameters required for the optimization calculation*

number of rotor turns	$w_{r \text{ temp}}$	500
torque distortion factor	$c_{\text{mech temp}}$	0.5
stator-coil diameter	$d_{\text{coil s temp}}$	$4 \cdot 10^{-3} \text{ m}$
see step 48 of the computer programme in sec. 8.5	$c_l$	1.2
rotor length	$l_r \text{ temp}$	$2 \cdot 10^{-3} \text{ m}$
fictive rotor diameter	$d_{\text{temp}}$	$28 \cdot 10^{-3} \text{ m}$
relative flux-conducting rotor width	$\beta_{\text{temp}}$	0.34
peak value of magnetic induction in the magnetic circuit	$B_{\text{peak temp}}$	$1.4 \text{ Wb m}^{-2}$

The parameters of group I are only needed for the computer programme. They are defined in sec. 8.5. There is in general little latitude in the choice of the parameters of groups A to G. In many cases, the cheapest motor is obtained when these parameters have their minimum value. Examples of such parameters are:  $P_{\text{out req}}$ ,  $c_{\text{stamp}}$ ,  $k_{\text{pole}}$ ,  $\alpha_{\text{brush}}$ , etc. In other cases, the cheapest motor is obtained when the parameters are maximum. Examples of such parameters are:  $k_{\text{Cu r}}$ ,  $P_{\text{Cu s req}}$ ,  $k_E$ , etc. Although these parameters should generally be maximized or minimized, it is interesting to study what happens to the cost of the motor when they are varied. This has been done in the optimization calculation of sec. 8.7 for  $k_{\text{Cu r}}$ ,  $k_{\text{Cu s}}$ ,  $c_{\text{Fe}}$ ,  $c_{\text{stamp}}$ ,  $k_{\text{pole}}$ ,  $\alpha_{\text{brush}}$  and  $p_{\text{Fe}}$ . The optimum value of the design parameters  $l_r$ ,  $d$ ,  $\beta$  and  $B_{\text{peak}}$  of group H is neither the maximum nor the minimum, but somewhere in between. These optimum values are determined by the optimization calculation.

In principle all the parameters mentioned above are independent. For instance,



$k_{Cu r}$  is defined in such a way that it does not depend on the values of  $\beta$  and  $b_{ins r}$ . But of course there are always secondary effects in practice which mean that all the parameters are not perfectly independent.

### 8.5. The computer programme

The computer programme is shown at the end of this section. Before describing the programme, however, we shall specify the manner of presentation of the results.

The computer prints out the results in tabular form; a typical table is shown in table 8-1. The figures in one such table refer to one motor with a fixed value of each of the parameters of groups A to G of sec. 8.4. In each table, the values of  $d$ ,  $\beta$  and  $B_{peak}$  are varied over a wide range, so that their optimum values can be selected by visual inspection. In principle, this could also be done by the computer. For each combination of parameters, the following quantities are presented.

- (1) The ratio between the ampere turns of the rotor  $w_r$  and the stator  $w_s$ .
- (2) The ratio of the rotor copper loss  $P_{Cu r}$  to the total rotor losses  $P_{Cu Fe r}$ . This shows the division of the losses between the copper and the iron in the rotor.
- (3) The value of the torque distortion factor  $c_{mech}$  (see eq. (2.41)); as shown in sec. 2.3, the current distortion factor  $c_e$  can now be calculated as  $c_e = c_{mech} / \sqrt{2}$  (eq. (2.45)).
- (4) The value of the relative rotor length  $\lambda$ .
- (5) resp. (6) The ratio of the cost of the winding wire in the rotor  $C_{Cu r}$  resp. stator  $C_{Cu s}$  to the total variable costs  $C_0$ .
- (7) The total variable costs  $C_0$ .

One problem in realizing the calculation programme is how to start the sequence of calculations, as the following examples will show.

- (a) The required value of  $R_s$  can be calculated if the values of  $P_{Cu s}$ ,  $I_{peak}$  and  $c_e$  are known, for  $P_{Cu s} = c_e^2 I_{peak}^2 R_s$ . The value of  $c_e$  can only be calculated from the normalized differential equation (2.34). But to solve eq. (2.34), we must know  $R_s$ .
- (b)  $d_{coil s}$  can be calculated with the aid of eq. (1.35), if  $R_s$ ,  $s_{w s}$ ,  $w_s$ ,  $q_{Cu s}$  and  $k_{Cu s}$  are known. But the value of e.g.  $s_{w s}$  depends on the value of  $d_{coil s}$ . To avoid such problems, the following calculation sequence was chosen.

#### *Sequence of calculation in the computer programme*

- A. The values of  $d_{coil s}$  and  $c_{mech}$  are estimated as  $d_{coil s temp}$  and  $c_{mech temp}$ . They will later be corrected, at steps 35 and 44 of the programme.
- B.  $\beta$ ,  $d$ ,  $B_{peak}$  and  $l_r$  are each given a certain value. We now calculate the value of  $P_{out}$  when  $P_{Cu s}$  and  $P_{Cu Fe r}$  have their required values  $P_{Cu s req}$



and  $P_{Cu\ Fe\ r\ req}$  respectively. Initially,  $l_r$  is intentionally chosen much too small, so that  $P_{out}$  will be much smaller than  $P_{out\ req}$ . At step 48 of the programme,  $P_{out}$  is compared with  $P_{out\ req}$ . As long as  $P_{out}$  is too small,  $l_r$  is multiplied by a factor  $c_l$  of about 1.2 and the programme is repeated from step 16 to step 47.

- C. After the programme has been repeated a number of times between steps 16 and 48,  $l_r$  will become so large that  $P_{out} > P_{out\ req}$ . Now  $l_r$  is interpolated linearly between the last (too large) value and the one before that, leading to a value corresponding very closely to  $P_{out\ req}$ . This is done in step 49 of the programme. Now the programme is repeated once more from step 16 to step 42 and then to step 50, from where it is continued until the end.
- D.  $c_{mech}$  occurs at step 24. The first time that the programme is passed through, the value of  $c_{mech}$  equals  $c_{mech\ temp}$ , as introduced into the programme at step 6. Every time the programme is passed through after that, the value of  $c_{mech}$  is that calculated at step 44 during the previous computation cycle: in this way  $c_{mech}$  converges step by step on its final, correct value.
- E. The first time that the programme is passed through,  $d_{coil\ s}$  occurs in steps 16 and 17 as  $d_{coil\ s\ temp}$ . At step 35,  $d_{coil\ s}$  is corrected and the corrected value is used in steps 36 and 37. During each successive computation cycle,  $d_{coil\ s}$  is corrected anew in step 35; it thus tends to its final, correct value by an iterative process, just like  $c_{mech}$  in item D above.
- F. The only function of step 46 is to ensure that the value of  $P_{out}$  calculated during the last computation cycle is available at step 49. This value of  $P_{out}$  is denoted by  $P_{out\ temp}$ .
- G. It is not possible to calculate  $w_r$  and  $w_s$  with the terminal voltage as a starting point; we therefore do things the other way round. An arbitrary number of rotor turns,  $w_{r\ temp}$ , is chosen initially, and at step 53 the corresponding terminal voltage  $U_{peak\ temp}$  is calculated. At steps 55 and 56,  $w_r$  and  $w_s$  are corrected so as to make the motor suitable for the specified terminal voltage; the values of  $w_{rt}$ ,  $R_r$ ,  $I_{peak}$ ,  $R_s$ ,  $w_s$  and  $a_{Cu\ s}$  used before step 55 are thus not the final values of the variables.

A place is reserved in the memory of the computer for each quantity occurring in the programme. As soon as a quantity has been calculated, the value obtained is stored at the appropriate memory address. If a given quantity is recalculated, the old value in the memory is replaced by the new one; for example, at step 7 the value of  $d_{coil\ s\ temp}$  is initially stored in the memory at the address reserved for  $d_{coil\ s}$ . This value is used at steps 16 and 17 of the programme. At step 35, the value of  $d_{coil\ s}$  is corrected, and the corrected value replaces  $d_{coil\ s\ temp}$  in the memory. The corrected value is used at steps 36 and 37. When the programme is repeated after step 48 this corrected

value is used at steps 16 and 17, corrected anew at step 35, and so on.

We now give the operations of the computer programme in their correct sequence. Finally, a block diagram of the computer programme is given in fig. 8.4.

*The computer programme for the optimization of small series motors*

Step No.	Operation	Equation No.																		
1.	$d = d_{temp}$																			
2.	$\beta = \beta_{temp}$																			
3.	$B_{peak} = B_{peak temp}$																			
4.	$l_r = l_{r temp}$																			
5.	$w_r = w_{r temp}$																			
6.	$c_{mech} = c_{mech temp}$																			
7.	$d_{coils} = d_{coils temp}$																			
8.	$d_r = d + 2 b_{23}$	(1.1)																		
9.	$s_{head r} = k_{head r} d$	(1.18)																		
10.	$b_{Fe r} = \beta d$	(1.6)																		
11.	$A_{coils r} = \frac{\pi}{4} d^2 - \frac{\pi}{4} (b_{Fe r} + d_{shaft fict})^2 +$ $- b_{Fe r} k_{pole} (d - b_{Fe r} - d_{shaft fict}) +$ $- (\pi b_{Fe r} + \pi d_{shaft fict} - 2 b_{Fe r} k_{pole}) b_{ins r} +$ $- (d - b_{Fe r} - d_{shaft fict}) z b_{ins r}$	(variant of 1.24)																		
12.	$f_{(j;m)peak} = \frac{B_{peak}}{1.5 B_{prop}}$																			
13.	$j_{peak}$ from: <table style="display: inline-table; vertical-align: top; margin-left: 20px;"> <tr> <td><math>j_{peak} &lt; -1.85</math></td> <td><math>f_{(j;m)peak} = -1 + m(j_{peak} + 1)</math></td> </tr> <tr> <td><math>-1.85 \leq j_{peak} &lt; -1.35</math></td> <td><math>f_{(j;m)peak} = -1 + 1.7 m(j_{peak} + 1.35)</math></td> </tr> <tr> <td><math>-1.35 \leq j_{peak} &lt; -1</math></td> <td><math>f_{(j;m)peak} = -0.86 + 0.4(j_{peak} + 1)</math></td> </tr> <tr> <td><math>-1 \leq j_{peak} &lt; -0.65</math></td> <td><math>f_{(j;m)peak} = -0.65 + 0.6(j_{peak} + 0.65)</math></td> </tr> <tr> <td><math>-0.65 \leq j_{peak} &lt; 0.65</math></td> <td><math>f_{(j;m)peak} = j_{peak}</math></td> </tr> <tr> <td><math>0.65 \leq j_{peak} &lt; 1</math></td> <td><math>f_{(j;m)peak} = 0.65 + 0.6(j_{peak} - 0.65)</math></td> </tr> <tr> <td><math>1 \leq j_{peak} &lt; 1.35</math></td> <td><math>f_{(j;m)peak} = 0.68 + 0.4(j_{peak} - 1)</math></td> </tr> <tr> <td><math>1.35 \leq j_{peak} &lt; 1.85</math></td> <td><math>f_{(j;m)peak} = 1 + 1.7 m(j_{peak} - 1.35)</math></td> </tr> <tr> <td><math>1.85 \leq j_{peak}</math></td> <td><math>f_{(j;m)peak} = 1 + m(j_{peak} - 1)</math></td> </tr> </table>	$j_{peak} < -1.85$	$f_{(j;m)peak} = -1 + m(j_{peak} + 1)$	$-1.85 \leq j_{peak} < -1.35$	$f_{(j;m)peak} = -1 + 1.7 m(j_{peak} + 1.35)$	$-1.35 \leq j_{peak} < -1$	$f_{(j;m)peak} = -0.86 + 0.4(j_{peak} + 1)$	$-1 \leq j_{peak} < -0.65$	$f_{(j;m)peak} = -0.65 + 0.6(j_{peak} + 0.65)$	$-0.65 \leq j_{peak} < 0.65$	$f_{(j;m)peak} = j_{peak}$	$0.65 \leq j_{peak} < 1$	$f_{(j;m)peak} = 0.65 + 0.6(j_{peak} - 0.65)$	$1 \leq j_{peak} < 1.35$	$f_{(j;m)peak} = 0.68 + 0.4(j_{peak} - 1)$	$1.35 \leq j_{peak} < 1.85$	$f_{(j;m)peak} = 1 + 1.7 m(j_{peak} - 1.35)$	$1.85 \leq j_{peak}$	$f_{(j;m)peak} = 1 + m(j_{peak} - 1)$	(2.1)
$j_{peak} < -1.85$	$f_{(j;m)peak} = -1 + m(j_{peak} + 1)$																			
$-1.85 \leq j_{peak} < -1.35$	$f_{(j;m)peak} = -1 + 1.7 m(j_{peak} + 1.35)$																			
$-1.35 \leq j_{peak} < -1$	$f_{(j;m)peak} = -0.86 + 0.4(j_{peak} + 1)$																			
$-1 \leq j_{peak} < -0.65$	$f_{(j;m)peak} = -0.65 + 0.6(j_{peak} + 0.65)$																			
$-0.65 \leq j_{peak} < 0.65$	$f_{(j;m)peak} = j_{peak}$																			
$0.65 \leq j_{peak} < 1$	$f_{(j;m)peak} = 0.65 + 0.6(j_{peak} - 0.65)$																			
$1 \leq j_{peak} < 1.35$	$f_{(j;m)peak} = 0.68 + 0.4(j_{peak} - 1)$																			
$1.35 \leq j_{peak} < 1.85$	$f_{(j;m)peak} = 1 + 1.7 m(j_{peak} - 1.35)$																			
$1.85 \leq j_{peak}$	$f_{(j;m)peak} = 1 + m(j_{peak} - 1)$																			

Step No.	Operation	Equation No.
14.	$h_o = d + 2 b_{33}$	derived from fig. 1.8
15.	$b_{35} = 0.5 k_{35} \beta d$	(1.28)
16.	$h_{38} = 0.5 d + b_{33} - b_{ins s} - 0.5 d_{coll s} - b_{35}$	(1.30)
17.	$r_{38} = 0.5 d + b_{23} + \delta + b_{39} + b_{ins s} + 0.5 d_{coll s}$	(1.31)
18.	$\alpha_{coll s} = \cos^{-1} \frac{h_{38}}{r_{38}}$	(1.32)
19.	$l_s = l_r$	
20.	$\phi^{(1)}_{peak} = \beta d l_r B_{peak}$	variant of (1.9)
21.	$e_{peak} = 2 k_E n w_r \phi^{(1)}_{peak}$	(1.11)
22.	$s_{w r} = 2 (l_r + 2 l_{ins r} + s_{head r})$	(1.16)
23.	$R_r = \frac{1}{8} \frac{\rho_{Cu r}}{k_{Cu r} B_{peak}^2} \frac{k_R}{k_E^2 A_{coll s r} b_{Fe r}^2 l_r^2} \frac{s_{w r}}{n^2} \frac{e_{peak}^2}{n^2}$	(1.15)
24.	$c_e = c_{mech} / 2$	(2.45)
25.	$P_{Fe r} = p_{Fe} \beta d^2 l_r B_{peak}^2$	(3.5)
26.	$P_{Cu r} = P_{Cu Fe r req} - P_{Fe r}$	
27.	$I_{peak} = \left( \frac{P_{Cu r}}{c_e^2 R_r} \right)^{1/2}$	variant of (2.42)
28.	$R_s = \left( \frac{P_{Cu s req}}{c_e^2 I_{peak}^2} \right)^{1/2}$	variant of (2.43)
29.	$A_{m 2\delta} = \frac{\pi \mu_o l_r d_r}{4 \delta k_{pole} k_{car}}$	(2.29)
30.	$c_{41} = \frac{4 \delta k_{pole} k_{car} \beta \mu_r}{4 \delta k_{pole} k_{car} \beta \mu_r + 3 \pi d_r}$	(2.5)
31.	$A_{m o} = c_{41} A_{m 2\delta}$	(2.4)
32.	$w_s = \frac{w_r \alpha_{brush}}{\pi} + \frac{1.5 \beta d l_r B_{prop} j_{peak}}{I_{peak} A_{m o}}$	derived from (2.6) and (2.11)
33.	$s_{w s} = 2 l_s + 4 l_{ins s} + 4 r_{38} \alpha_{coll s}$	(1.33)
34.	$a_{Cu s} = \frac{\rho_{Cu s} s_{w s} w_s}{R_s}$	variant of (1.35)

Step No.	Operation	Equation No.
35.	$d_{\text{coll } s} = \left( \frac{2 w_s a_{\text{Cu } s}}{\pi k_{\text{Cu } s}} \right)^{1/2}$	variant of (1.34)
36.	$h_{38} = 0.5 h_0 - b_{33} - b_{\text{ins } s} - 0.5 d_{\text{coll } s} - b_{35}$	(1.30)
37.	$r_{38} = 0.5 d + b_{23} + \delta + b_{39} + b_{\text{ins } s} + 0.5 d_{\text{coll } s}$	(1.31)
38.	$\alpha_{\text{coll } s} = \cos^{-1} \frac{h_{38}}{r_{38}}$	(1.32)
39.	$s_{w s} = 2 l_s + 4 l_{\text{ins } s} + 4 r_{38} \alpha_{\text{coll } s}$	(1.33)
40.	$R_s = \frac{\rho_{\text{Cu } s} s_{w s} w_s}{a_{\text{Cu } s}}$	(1.35)
41.	$R_{\text{norm}} = \frac{R_r + R_s}{2 k_E w_r n A_{m o} (w_s - w_r \alpha_{\text{brush}}/\pi)}$	(2.36)
42.	$L_{\text{norm}} = \frac{1}{2 k_E n w_r (w_s - \alpha_{\text{brush}} w_r/\pi)} \times$ $\times \left[ \frac{w_r^2}{12 c_{41} k_{\text{pole}}^2} + c_{37} w_s^2 - \frac{2 \alpha_{\text{brush}}}{\pi} w_r w_s + \frac{(\alpha_{\text{brush}})^2 w_r^2}{\pi^2} \right]$	(2.37)
43.	$\omega = 2 \pi \nu$	
44.	$c_{\text{mech}}$ from: $j_{\text{peak}} \leq 0.65: c_{\text{mech}} = 0.5$ $0.65 < j_{\text{peak}} \leq 1.35: c_{\text{mech}} = 0.5 - (0.086 - 0.143 R_{\text{norm}}) (j_{\text{peak}} - 0.65)$ $1.35 < j_{\text{peak}}: c_{\text{mech}} = 0.44 + 0.1 R_{\text{norm}} +$ $- \left( 0.1 + 0.1 R_{\text{norm}} - 0.375 m - 0.1 (1 - 2.5 m) \frac{R_{\text{norm}}}{\omega L_{\text{norm}}} \right) (j_{\text{peak}} - 1.35)$	(2.46)
45.	$P_\delta = 2 k_E c_{\text{mech}} n w_r \phi_{\text{peak}}^{(1)} I_{\text{peak}}$	(2.44)
46.	$P_{\text{out temp}} = P_{\text{out}}$	
47.	$P_{\text{out}} = P_\delta - P_{\text{Fe } t}$	(8.21)
48.	If $P_{\text{out}} < P_{\text{out req}}$ : $l_r = c_l l_r$ and go to 16	
49.	If $P_{\text{out}} \geq P_{\text{out req}}$ $l_r = (P_{\text{out req}} - P_{\text{out temp}}) \frac{l_r - l_r/c_l}{P_{\text{out}} - P_{\text{out temp}}} + \frac{l_r}{c_l}$ go to 16 and from 42 go to 50	

Step No.	Operation	Equation No.
50.	$U_{\text{norm prop}} = 0.65 [(1 + R_{\text{norm}})^2 + (\omega L_{\text{norm}})^2]^{1/2}$	(2.38)
51.	$c_u$ from: $j_{\text{peak}} \leq 0.65: c_u = \frac{j_{\text{peak}}}{0.65}$ $0.65 < j_{\text{peak}} \leq 1.35: c_u = 1 + (0.743 + 0.43 R_{\text{norm}})(j_{\text{peak}} - 0.65)$ $1.35 < j_{\text{peak}}: c_u = 1.52 + 0.3 R_{\text{norm}} +$ $\quad + \left( 0.18 + 2(m - 0.08) + \frac{0.29 R_{\text{norm}}}{\omega L_{\text{norm}}} \right) (j_{\text{peak}} - 1.35)$	(2.47)
52.	$U_{\text{norm}} = c_u U_{\text{norm prop}}$	(2.39)
53.	$U_{\text{peak temp}} = 3 k_E w_r n \beta d l_r B_{\text{prop}} U_{\text{norm}}$	variant of (2.32)
54.	$U_{\text{peak}} = U \sqrt{2}$	
55.	$w_r = w_r \frac{U_{\text{peak}}}{U_{\text{peak temp}}}$	
56.	$w_s = w_s \frac{U_{\text{peak}}}{U_{\text{peak temp}}}$	
57.	$a_{\text{Cu r}} = \frac{k_{\text{Cu r}} A_{\text{colls r}}}{2 w_r}$	(1.14)
58.	$d_{\text{Cu r}} = \left( \frac{4 a_{\text{Cu r}}}{\pi} \right)^{1/2}$	
59.	$a_{\text{Cu s}} = \frac{\pi k_{\text{Cu s}} (d_{\text{colls}})^2}{2 w_s}$	(1.34)
60.	$d_{\text{Cu s}} = \left( \frac{4 a_{\text{Cu s}}}{\pi} \right)^{1/2}$	
61.	$G_{\text{Cu r}} = g_{\text{Cu r}} a_{\text{Cu r}} w_r s_w r$	(8.6)
62.	$G_{\text{Cu s}} = g_{\text{Cu s}} a_{\text{Cu s}} w_s s_w s$	(8.9)
63.	$b_{36} = 0.5 k_{36} \beta d$	(1.29)
64.	$b_o = 2(r_{38}^2 - h_{38}^2)^{1/2} + d_{\text{colls}} + 2 b_{\text{ins}} + 2 b_{36}$ derived from fig. 1.8	
65.	$G_{\text{Fe}} = g_{\text{Fe}} k_{\text{Fe}} l_s (h_o + b_{32}) (b_o + 2 b_{31})$	(8.2)

Step No.	Operation	Equation No.
66.	$c_{24} = c_{21} - \frac{d_{21}(c_{22} - c_{21})}{d_{22} - d_{21}} + \frac{d_{21}d_{22}(c_{23} - 2c_{22} + c_{21})}{2(d_{22} - d_{21})^2}$	(8.14)
67.	$c_{25} = \frac{(d_{21} + d_{22})(c_{23} - 2c_{22} + c_{21})}{2(d_{22} - d_{21})^2} - \frac{c_{22} - c_{21}}{d_{22} - d_{21}}$	(8.15)
68.	$c_{26} = \frac{c_{23} - 2c_{22} + c_{21}}{2(d_{22} - d_{21})^2}$	(8.16)
69.	$c_{34} = c_{31} - \frac{d_{31}(c_{32} - c_{31})}{d_{32} - d_{31}} + \frac{d_{31}d_{32}(c_{33} - 2c_{32} + c_{31})}{2(d_{32} - d_{31})^2}$	(8.18)
70.	$c_{35} = \frac{(d_{31} + d_{32})(c_{33} - 2c_{32} + c_{31})}{2(d_{32} - d_{31})^2} - \frac{c_{32} - c_{31}}{d_{32} - d_{31}}$	(8.19)
71.	$c_{36} = \frac{c_{33} - 2c_{32} + c_{31}}{2(d_{32} - d_{31})^2}$	(8.20)
72.	$c_{Cu r} = c_{24} - c_{25}d_{Cu r} + c_{26}d_{Cu r}^2$	(8.11)
73.	$c_{Cu s} = c_{34} - c_{35}d_{Cu s} + c_{36}d_{Cu s}^2$	(8.12)
74.	$C_{Cu r} = c_{Cu r} G_{Cu r}$	(8.7)
75.	$C_{Cu s} = c_{Cu s} G_{Cu s}$	(8.10)
76.	$C_{Fe} = c_{Fe} G_{Fe}$	(8.3)
77.	$C_{stamp} = c_{stamp} l_s$	(8.4)
78.	$C_o = C_{Cu r} + C_{Cu s} + C_{Fe} + C_{stamp}$	(1.43)

### 8.6. Specimen calculation

As mentioned in sec. 8.3, this specimen calculation refers to the motor of a vacuum cleaner. The required output power  $P_{out req}$  includes the mechanical losses in the motor:

$$P_{out} = P_\delta - P_{Fe r}. \quad (8.21)$$

$P_{out req} = 250$  W. The speed is about 19 000 r.p.m., so  $n = 320$  s<sup>-1</sup>. The cooling of the motor is good. Study of comparable motors shows that  $P_{Cu s req}$ , the permissible copper loss in the stator and  $P_{Cu Fe r req}$ , the permissible sum of copper and iron losses in the rotor, can each be about 30 W without making the temperature of the copper in the rotor and stator too high.

Most motor parameters, e.g.  $k_{Fe}$ ,  $\rho_{Cu r}$ ,  $d_{shaft}$ , etc. were given only one

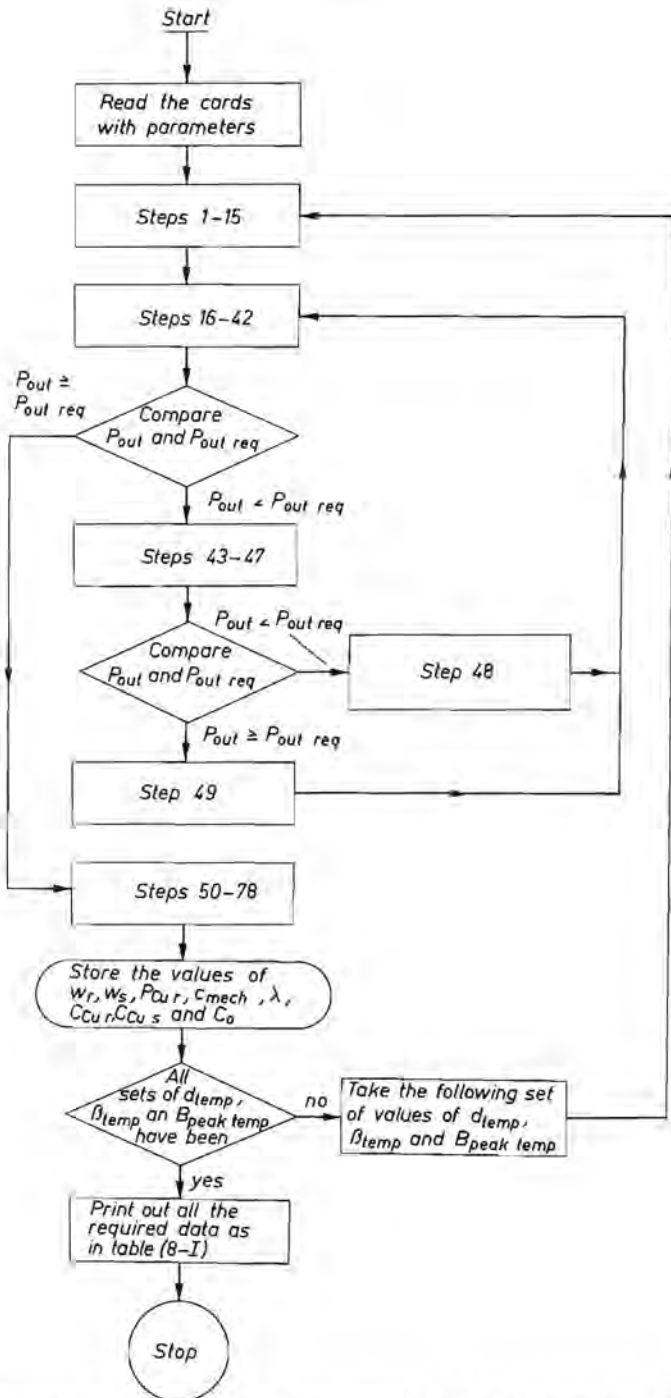


Fig. 8.4. Block diagram of the computer programme for the optimization calculation.

TABLE 8-I

Computed results for the "average motor", with  $P_{out req} = 250 W$ ,  $P_{Cu Fe req} = 30 W$  and  $P_{Cu s req} = 30 W$ . The values of the parameters of the "average motor" were summed up in sec. 8.4. The zeros in this table mean that no motor satisfying the specifications can be made for the combination of parameters in question

		$\frac{50 w_r}{w_s}$	$\frac{100 P_{Cu r}}{P_{Cu Fe r}}$	$100 c_{mech}$	$100 \lambda$	$\frac{100 C_{Cu r}}{C_o}$	$\frac{100 C_{Cu s}}{C_o}$	$C_o$
$\frac{10 B_{peak}}{\beta} \rightarrow$		14 16 18 20 22	14 16 18 20 22	14 16 18 20 22	14 16 18 20 22	14 16 18 20 22	14 16 18 20 22	14 16 18 20 22
$d = 28$	0-34	13 15 16 19 23	79 77 74 72 69	49 48 47 46 44	167 142 124 111 102	18 19 19 19 18	6 8 10 13 18	183 163 150 142 143
	0-42	17 20 22 26 32	75 72 69 66 61	49 48 47 46 44	159 137 121 109 103	14 14 14 14 13	8 10 13 17 24	177 160 150 145 153
	0-50	25 29 35 0 0	67 62 55 0 0	49 48 47 0 0	182 160 150 0 0	9 9 8 0 0	9 12 16 0 0	202 188 185 0 0
	0-58	0 0 0 0 0	0 0 0 0 0	0 0 0 0 0	0 0 0 0 0	0 0 0 0 0	0 0 0 0 0	0 0 0 0 0
	0-66	0 0 0 0 0	0 0 0 0 0	0 0 0 0 0	0 0 0 0 0	0 0 0 0 0	0 0 0 0 0	0 0 0 0 0
$d = 34$	0-34	11 12 13 15 18	82 80 78 76 73	49 48 47 46 44	78 68 60 54 50	30 31 32 31 30	7 10 12 16 22	147 136 128 125 130
	0-42	13 15 17 20 24	80 77 74 71 68	49 48 47 46 44	73 63 57 51 48	24 25 25 24 22	10 13 17 22 30	136 128 123 123 133
	0-50	17 20 23 28 34	75 71 67 63 58	49 48 47 46 44	75 66 60 56 53	18 18 17 16 14	12 16 21 27 37	138 132 130 134 151
	0-58	26 31 39 0 0	65 58 47 0 0	49 48 47 0 0	92 84 85 0 0	11 10 9 0 0	14 18 22 0 0	163 161 173 0 0
	0-66	0 0 0 0 0	0 0 0 0 0	0 0 0 0 0	0 0 0 0 0	0 0 0 0 0	0 0 0 0 0	0 0 0 0 0
0-74	0 0 0 0 0	0 0 0 0 0	0 0 0 0 0	0 0 0 0 0	0 0 0 0 0	0 0 0 0 0	0 0 0 0 0	
$d = 40$	0-34	9 11 12 13 16	83 81 78 76 73	49 48 47 46 44	45 40 35 32 30	42 43 43 42 39	8 11 14 18 24	146 139 134 133 142
	0-42	12 13 15 17 21	81 78 75 72 69	49 48 47 46 44	42 37 33 30 28	35 36 35 34 30	12 15 19 25 33	134 129 127 129 143
	0-50	15 17 20 23 29	77 74 70 66 61	49 48 47 46 44	42 37 34 31 30	27 27 26 24 21	15 20 25 32 42	130 127 128 134 156
	0-58	20 24 28 35 0	70 65 59 50 0	49 48 47 46 0	47 43 40 39 0	18 18 17 15 0	17 23 29 36 0	137 137 142 158 0
	0-66	35 0 0 0 0	49 0 0 0 0	49 0 0 0 0	73 0 0 0 0	9 0 0 0 0	17 0 0 0 0	190 0 0 0 0
0-74	0 0 0 0 0	0 0 0 0 0	0 0 0 0 0	0 0 0 0 0	0 0 0 0 0	0 0 0 0 0	0 0 0 0 0	
$d = 46$	0-34	9 10 11 13 15	83 81 79 76 74	49 48 47 46 45	29 26 23 21 20	52 52 52 51 47	9 12 15 19 25	162 157 154 155 167
	0-42	11 12 14 16 19	81 78 75 72 69	49 48 47 46 44	27 24 21 20 18	45 45 44 42 37	13 17 21 26 35	146 144 144 149 166
	0-50	13 15 18 21 26	78 74 70 66 61	49 48 47 46 44	27 24 22 20 19	36 36 34 31 27	17 22 27 34 45	138 138 141 150 177
	0-58	17 21 24 30 42	72 67 61 54 39	49 48 47 46 43	29 26 25 24 26	26 25 23 21 16	21 27 33 41 50	138 141 148 165 209
	0-66	26 34 0 0 0	59 47 0 0 0	49 48 0 0 0	38 37 0 0 0	15 14 0 0 0	22 28 0 0 0	157 171 0 0 0
0-74	0 0 0 0 0	0 0 0 0 0	0 0 0 0 0	0 0 0 0 0	0 0 0 0 0	0 0 0 0 0	0 0 0 0 0	



value during the calculation because for some reason or other only that one value is possible.

The values of other parameters, e.g.  $k_{pole}$ , are varied. It is clear that  $k_{pole}$  should be as small as possible. However, it is difficult to make  $k_{pole}$  smaller than 1.3 in practice. The values of  $k_{pole}$  used in the calculations were chosen to show whether it is worth while trying to make  $k_{pole}$  smaller than 1.3.

If all the variable parameters have their most common value, we speak of the "average motor". The values of the parameters in this "average motor" have already been given in sec. 8.4. In the presentation of the results in sec. 8.7 the variable parameters have the values for the "average motor", unless stated otherwise. The tabulated results of table 8-I are also for the "average motor".

### 8.7. Results of the specimen calculation

The results of the calculation for the "average motor" mentioned in secs 8.4 and 8.6 are tabulated in table 8-I. The right-hand group of columns in this table shows  $C_o$  as a function of  $d$ ,  $\beta$  and  $B_{peak}$ . The fourth group of columns shows the corresponding values of  $\lambda$ . The lowest value of  $C_o$  can be estimated by interpolation as a function of  $d$ ,  $\beta$  and  $B_{peak}$ . It is found to be  $C_o = 122$  cents, for  $d = 36$  mm,  $\beta = 0.42$  and  $B_{peak} = 1.85$  Wb m<sup>-2</sup>. The corresponding value of  $\lambda$  is 0.46.

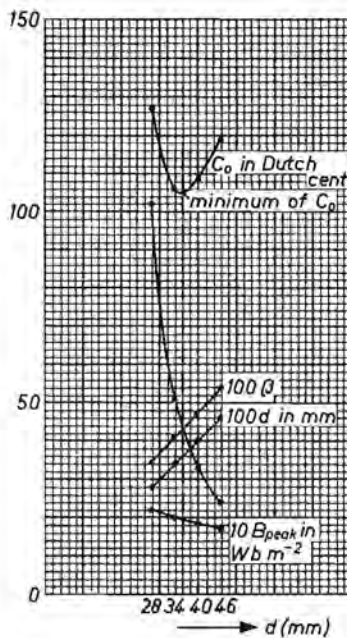


Fig. 8.5. Minimum values of overall variable costs  $C_o$  and corresponding values of some other parameters as a function of the fictive rotor diameter  $d$  for the "average motor".

All the tables printed out by the computer can be treated in the same way. Results obtained in this way are plotted in the graphs of figs 8.6–8.11.

Figure 8.5 was derived from table 8-I by finding the optimum values of  $\beta$  and  $B_{\text{peak}}$  for  $d = 28, 34, 40$  and  $46$  mm. Figures 8.5–8.11 show clearly the influence of  $d, \delta, k_{\text{Cu r}}, k_{\text{Cu s}}, c_{\text{Fe}}, c_{\text{stamp}}, k_{\text{pole}}, \alpha_{\text{brush}}, p_{\text{Fe}}, P_{\text{Cu s req}}$  and  $P_{\text{Cu Fe r req}}$  on the total variable costs  $C_o$ , but some explanatory remarks are in place here.

(1) *Estimated and real value of  $m$*

$m$ , the tangent of the angle which the right-hand linear portion of the normalized magnetization curve makes with the horizontal axis, was estimated as  $m = 0.12$  in sec. 8.4. This value of  $m$  was taken for the “average motor”. If  $m$  is varied from 0.10 to 0.14,  $C_o$  is found not to change, because the optimum value of  $B_{\text{peak}}$  is small and the form of the start of the magnetization curve does not depend on  $m$ . If a motor should be made with a larger value of  $B_{\text{peak}}$ , e.g. to improve commutation, we must check afterwards whether the value of  $m$  for the motor really is 0.12.

(2) *Correctness of the expression for the iron loss in the rotor*

The iron loss in the rotor was assumed to be given by

$$P_{\text{Fe r}} = p_{\text{Fe}} \beta B_{\text{peak}}^2 d^2 l_r. \quad (3.5)$$

If this assumption were completely wrong, wrong conclusions would be expected. Figure 8.9 shows that  $p_{\text{Fe}}$  does influence  $C_o$ , but has hardly any influence on the optimum values of  $\beta, d, \lambda, B_{\text{peak}}$  and  $w_s/w_r$ .

(3) *Influence of  $B_{\text{prop}}$  on the optimum value of  $B_{\text{peak}}$*

In all the calculated cases, the optimum value of the magnetic induction  $B_{\text{peak}}$  was found to be about  $1.85 \text{ Wb m}^{-2}$ , for  $B_{\text{prop}} = 1.35 \text{ Wb m}^{-2}$ . This value of  $B_{\text{peak}}$  may be assumed to be generally applicable, as  $B_{\text{prop}}$  is about  $1.35 \text{ Wb m}^{-2}$  for all the types of steel sheet used in practice.

(4) *Influence of  $c_{\text{Fe}}, c_{\text{Cu r}}$  and  $c_{\text{Cu s}}$  on the optimum values of  $\beta, \lambda$  and  $B_{\text{peak}}$*

Figure 8.7b shows the influence on  $C_o$  of  $c_{\text{Fe}}$ , the cost per kg of the steel sheet used. Of course,  $C_o$  increases with  $c_{\text{Fe}}$ , but the optimum values of  $\beta, \lambda, B_{\text{peak}}$  and  $w_s/w_r$  hardly change.  $C_o$  depends linearly on  $c_{\text{Fe}}, c_{\text{Cu r}}, c_{\text{Cu s}}$  and  $c_{\text{stamp}}$  as follows:

$$C_o = c_{\text{Cu r}} G_{\text{Cu r}} + c_{\text{Cu s}} G_{\text{Cu s}} + c_{\text{Fe}} G_{\text{Fe}} + c_{\text{stamp}} I_s. \quad (8.22)$$

If the optimum values of  $\beta, \lambda, B_{\text{peak}}$  and  $w_s/w_r$  hardly change with  $c_{\text{Fe}}$ , they will hardly change if  $c_{\text{Cu r}}$  and  $c_{\text{Cu s}}$  are both varied, because of the linear relation of eq. (8.22). A motor, once optimized, thus remains optimal if the relation between the costs per kg of copper and iron varies.

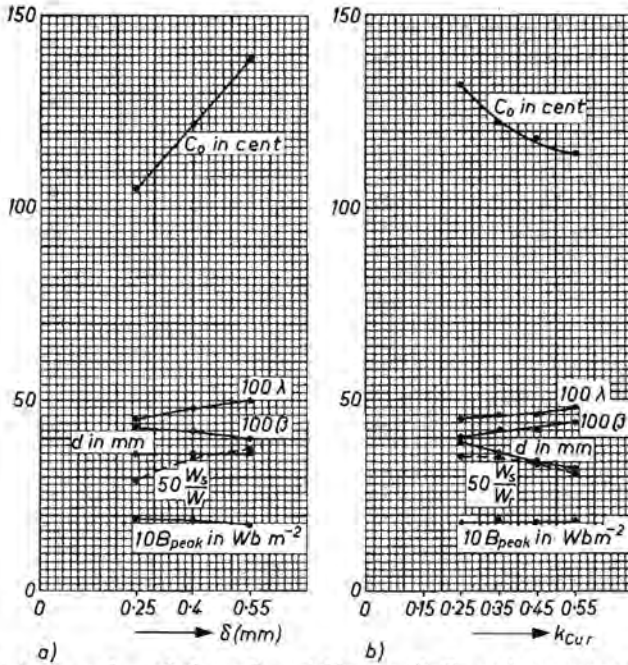


Fig. 8.6. Minimum value of "overall variable costs"  $C_0$  and corresponding value of  $\beta$ ,  $\lambda$ ,  $d$ ,  $w_s/w_r$  and  $B_{peak}$  as a function of (a) the air-gap width  $\delta$ ; (b) the space factor of copper in the rotor  $k_{Cu r}$ .

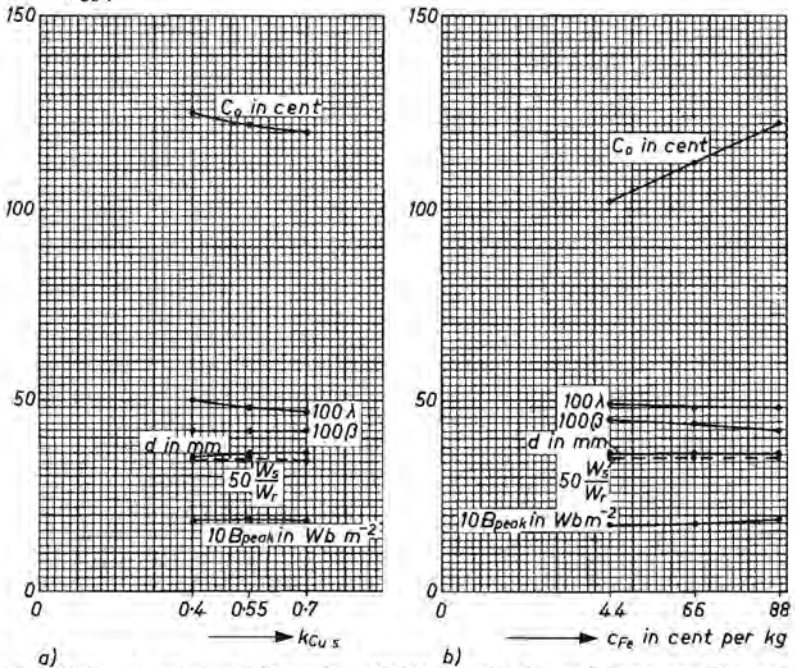


Fig. 8.7. Minimum value of "overall variable costs"  $C_0$  and corresponding value of  $\beta$ ,  $\lambda$ ,  $d$ ,  $w_s/w_r$  and  $B_{peak}$  as a function of (a) the space factor of copper in the stator  $k_{Cu s}$ ; (b) the cost per kilogramme of steel sheet  $c_{Fe}$ .

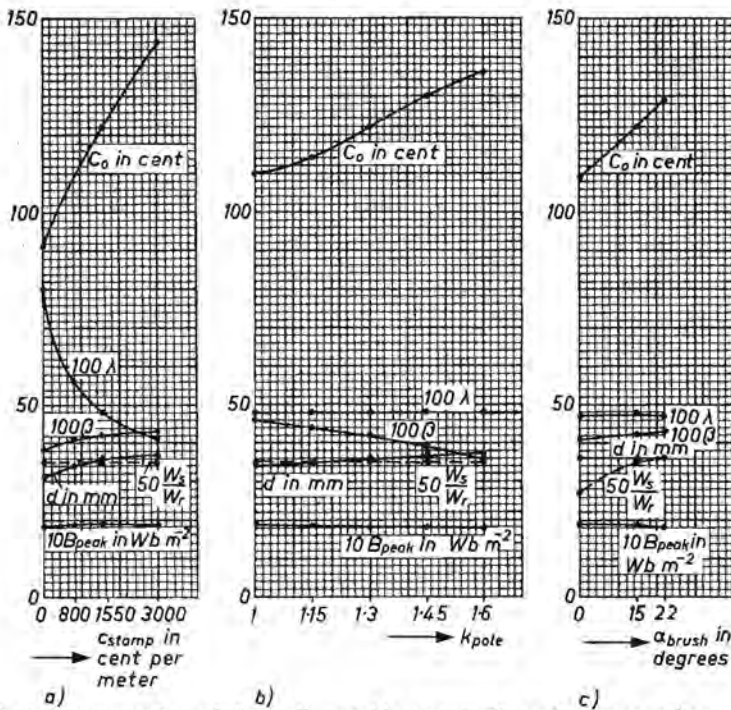


Fig. 8.8. Minimum value of "overall variable costs"  $C_0$  and corresponding value of  $\beta$ ,  $\lambda$ ,  $d$ ,  $w_s/w_r$  and  $B_{peak}$  as a function of (a) the cost of stamping the laminations for a stack with a length of 1 metre  $c_{stamp}$ ; (b) the reciprocal relative pole arc  $k_{pole}$ ; (c) the angle through which the brushes are turned against the direction of rotation of the small series motor,  $\alpha_{brush}$ .

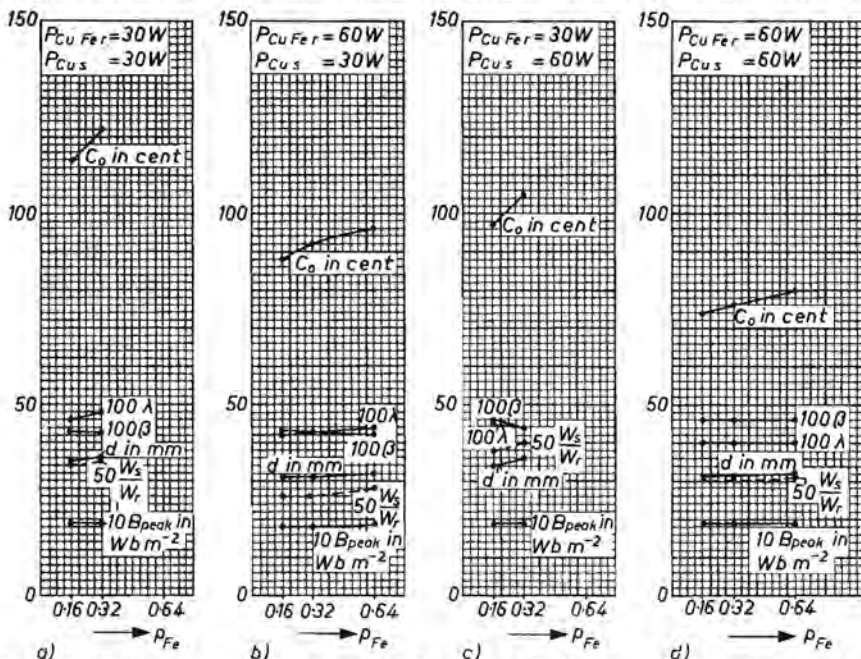


Fig. 8.9. Minimum value of "overall variable costs"  $C_0$  and corresponding value of  $\beta$ ,  $\lambda$ ,  $d$ ,  $w_s/w_r$  and  $B_{peak}$  as a function of the specific iron loss in the rotor  $P_{Fe}$ .

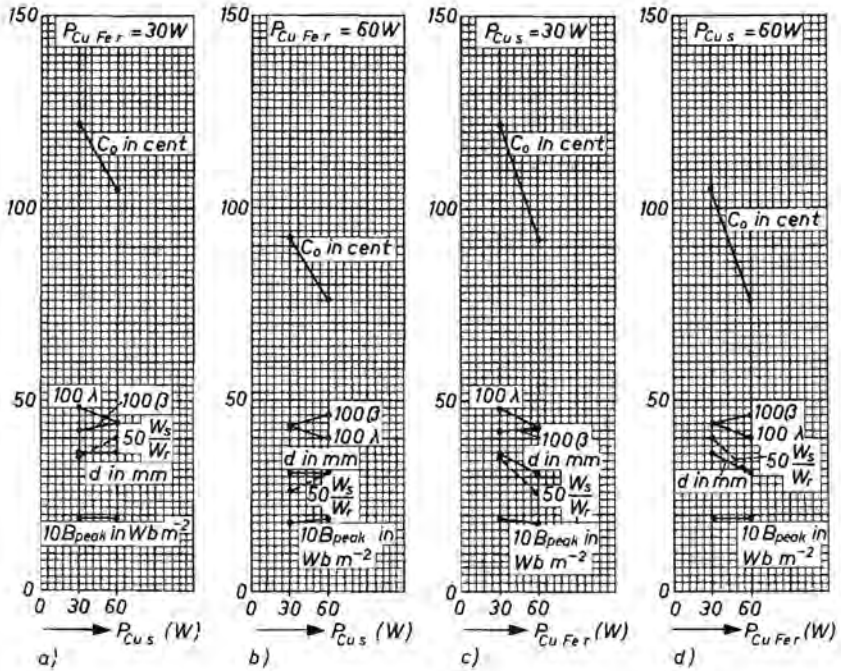


Fig. 8.10. Minimum value of "overall variable costs"  $C_0$  and corresponding value of  $\beta$ ,  $\lambda$ ,  $d$ ,  $w_s/w_r$  and  $B_{peak}$  as a function of (a) and (b) the losses in the stator coils  $P_{Cu_s}$  and (c) and (d) the losses in the rotor  $P_{Cu_{Fe_r}}$ .

(5) The influence of  $c_{stamp}$  on the optimum values of  $\beta$ ,  $\lambda$ ,  $B_{peak}$  and  $w_s/w_r$

The influence of  $c_{stamp}$ , the cost of stamping the laminations of a stack with a length of one metre, on  $B_{peak}$  and  $w_s/w_r$  can be neglected (see fig. 8.8a). The optimum value of  $\beta$  decreases slightly if  $c_{stamp}$  decreases almost to zero. In that case the optimum value of  $\lambda$  increases, as might be expected.

(6) The influence of  $k_{Cu_r}$  and  $k_{Cu_s}$  on  $C_0$

If the space factors  $k_{Cu_r}$  and  $k_{Cu_s}$  of the copper in rotor and stator increase,  $C_0$  decreases, as figs 8.6b and 8.7a show. This is to be expected. However,  $C_0$  does not change much. The values of  $k_{Cu_r}$  and  $k_{Cu_s}$  may be expected to be about 0.3 and 0.55 respectively in practice. If they are chosen much higher, the winding of rotor and stator becomes difficult and expensive.

(7) The influence of  $k_{pole}$  and  $\delta$  on the rotor field

Lower values of  $k_{pole}$  and the air-gap width  $\delta$  give a lower value of  $C_0$  (see figs 8.8b and 8.6a). However, low values of  $k_{pole}$  and  $\delta$  also give a high rotor field, which has an adverse influence on commutation.

(8) The influence of  $P_{Cu s req}$  and  $P_{Cu Fe r req}$  on  $C_0$

If more power loss is allowed in rotor and stator,  $C_0$  decreases (see figs 8.10 and 8.11). However, if  $P_{Cu Fe r req}$  is doubled,  $C_0$  decreases twice as much as if  $P_{Cu s req}$  is doubled. It is thus important to choose  $P_{Cu Fe r req}$  as large as possible with a view to minimizing  $C_0$ .

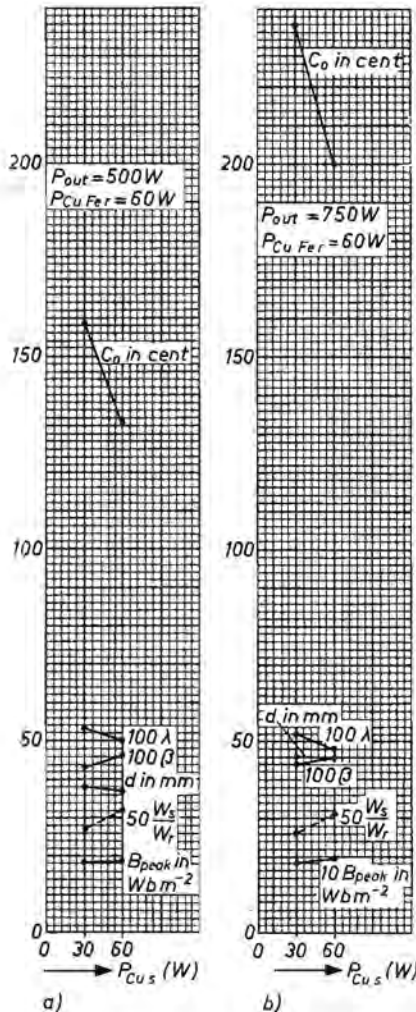


Fig. 8.11. Minimum value of "overall variable costs"  $C_0$  and corresponding value of  $\beta$ ,  $\lambda$ ,  $d$ ,  $w_s/w_r$  and  $B_{peak}$  as a function of the losses in the stator coils  $P_{Cu s}$ .



(9) *The optimum values of  $d$  and  $\lambda$*

Choosing a value for  $d$  comes down in fact to choosing a value for  $\lambda$ . Figure 8.5 shows the influence of  $d$  on  $C_o$ . Choosing  $d$  some millimetres to the left of the optimum makes  $C_o$  increase more than if  $C_o$  is chosen an equal distance to the right of the optimum, so  $d$  should not be chosen too small, and  $\lambda$  should not be chosen too large. The imperfections of eq. (1.26) mentioned at the end of sec. 7.10 lead to the same conclusion.

(10) *The combined influence of the parameters on  $C_o$*

Apart from  $d$  (or  $\lambda$ ) and  $\beta$ , none of the parameters has an extreme influence on  $C_o$ . However, if a wrong value of several parameters is chosen at the same time, the combined influence can be very important. For the "average motor", for example,  $C_o = 122$  cents, with  $\beta = 0.42$ ,  $\lambda = 0.42$ ,  $B_{\text{peak}} = 1.85 \text{ Wb m}^{-2}$  and  $k_{\text{pole}} = 1.3$ . If only these parameters are changed to  $\beta = 0.34$ ,  $\lambda = 1$ ,  $B_{\text{peak}} = 2.2 \text{ Wb m}^{-2}$  and  $k_{\text{pole}} = 1.6$ , we find  $C_o = 195$  cents.

(11) *The optimum values of  $\beta$ ,  $\lambda$  and  $B_{\text{peak}}$*

It appears that the optimum values of  $\beta$ ,  $\lambda$  and  $B_{\text{peak}}$  are hardly influenced by the values of the other parameters, except that the optimum value of  $\lambda$  increases considerably if  $c_{\text{stamp}}$  decreases to zero. The optimum values are about

$$\begin{aligned}\lambda &= 0.42-0.50, \\ \beta &= 0.4-0.45, \\ B_{\text{peak}} &= 1.8-1.9 \text{ Wb m}^{-2}.\end{aligned}$$

These optimum values certainly hold for motors with an output power of about 250 to 750 W, a loss of about 30–60 W in the stator coils and the same value in the rotor, at 19 000 r.p.m. However, other calculations have shown that if the speed, power losses and output power are varied in a wider range, roughly the same optimum values are found.

It was shown in sec. 7.9 that  $B_{\text{max}}$  (or  $B_{\text{peak}}$  in the AC case) is to be preferred to  $B_\delta$  as a parameter. The optimum value of  $B_{\text{peak}}$  varies very little.  $B_\delta$  can be calculated from eq. (7.8). If the optimum value of  $B_\delta$  is calculated for all the cases of figs 8.5–8.11, it is found not to vary much, but it does vary considerably more than  $B_{\text{peak}}$ .

### 8.8. Evaluation of the results

This chapter describes an optimization calculation for a small series motor, based on formulas involving more than fifty parameters.

The computer calculates all the results to sixteen places of decimals. Any

doubts which we may have as to the results do not thus concern the calculations, but the accuracy with which the phenomena have been described for the purposes of these calculations.

These doubts concern two different groups of phenomena:

(1) *Phenomena that have not been described at all*

These phenomena are not very important, but they do have some influence on the motor. For instance:

- (a) The input voltage of the motor will never be fully sinusoidal.
- (b) The relation between the voltage drop and the current in brushes and commutator may differ from the form assumed, especially if the commutator is unrounded so that the brushes jump.

(2) *Phenomena that are described, but not quite correctly*

For instance:

- (a) The shape of the magnetization curve, described by  $f_{(j;m)}$ .
- (b) The iron loss in the rotor.

It will be obvious that we make no claims to perfection for this optimization calculation. However, it is not possible to indicate exactly the error in the calculated results; they have to be interpreted on the basis of practical insight and experience.

We may conclude in general that the errors in the description of the motor will lead to errors in the calculated sizes, weights and costs.

However, every calculation involves roughly the same errors, so that calculated differences will be quite accurate. It may therefore be concluded that the calculated optimum values of the design parameters  $\beta$ ,  $\lambda$  and  $B_{\text{peak}}$  are accurate enough to be used in practice without further correction.

### 8.9. Comparison with the results of measurement

To test the reliability of the optimization method, we compared the operation of the motor of an existing vacuum cleaner ("old motor") with that of a "new motor", the design parameters of which were nearly optimum, viz.  $\beta = 0.5$ ,  $\lambda = 0.34$  and  $B_{\text{peak}} = 2 \text{ Wb m}^{-2}$ .

The shape of the rotor and stator laminations of the old and new motors is shown in fig. 8.12. The rotor of the old motor has an unfavourable shape: the sides of the teeth are neither straight nor parallel, and  $b_{\text{Fe core}}$  is much larger than  $b_{\text{Fe teeth}}$ .

Further details about the two motors are tabulated in table 8-II. Both motors were tested under normal load conditions, according to the C.E.E. specifications mentioned in sec. 6.1. During the test, each motor was fixed in the same vacuum cleaner with the same compressor. In both cases, therefore, the vacuum



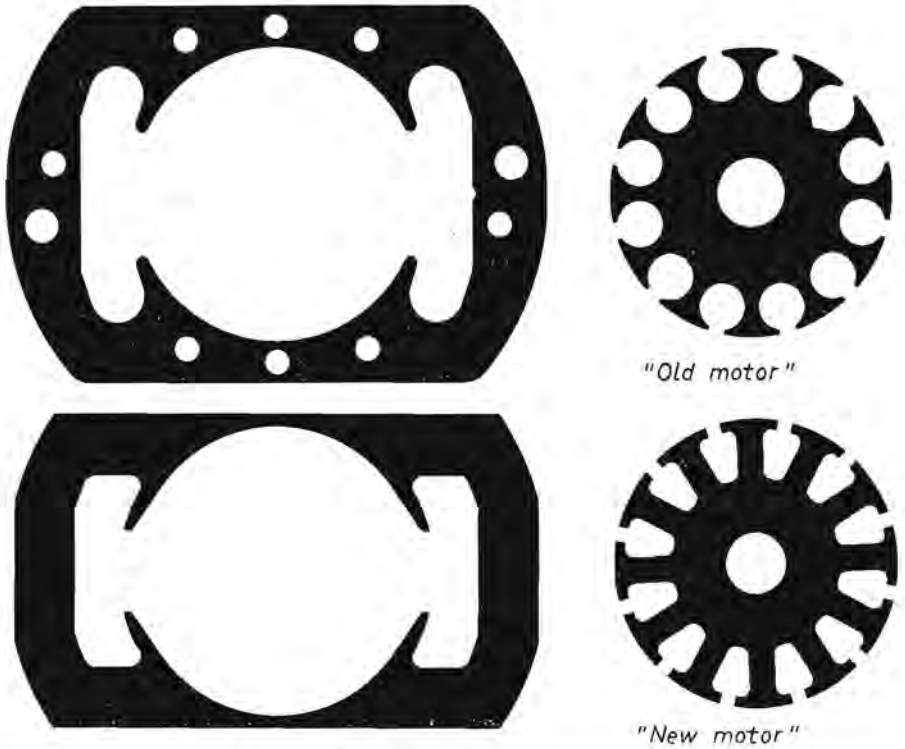


Fig. 8.12. Shape and dimensions of the rotor and stator laminations of an existing vacuum-cleaner motor (the old motor) and one calculated on the principles developed in this thesis (the new motor).

cleaner delivered the same amount of air at the same pressure, and the cooling conditions were the same.

The main points which arise from inspection of this table are as follows.

- (1) The "new motor" is much cheaper than the old one, mainly owing to the difference in  $\beta$ . Because  $\beta$  is small in the old motor, it has a longer stack and a higher value of  $B_{\text{peak}}$ .
- (2) The copper loss in the stator coils of the new motor is lower than in the old one, so the temperature rise in the stator coils of the new motor is also lower.
- (3)  $B_{\text{peak}}$  for the new motor is much lower than for the old one. The iron loss in the rotor of the new motor is therefore also lower. The copper loss in the rotor coils of the new motor is higher than in the old one, but the sum of the copper and iron losses in the rotor of the new motor is lower. In chapter 6 we showed that the temperature rise in the rotor was determined by the sum of the copper and iron losses in the rotor and by the quantity of the cooling. As expected, the temperature rise in the rotor coils of the new motor was smaller.

TABLE 8-II

Operating parameters of an existing small series motor for a vacuum cleaner (the "old motor") and of a motor designed with the aid of the optimization calculation described in this thesis (the "new motor"); cent = 0.01 Dutch guilder

quantity		old motor	new motor	units
fictive rotor diameter	$d$	42	41	mm
rotor diameter	$d_r$	47	46	mm
rotor length	$l_r$	19	13.5	mm
relative rotor length	$\lambda$	0.45	0.34	—
width of a rotor tooth	$b_{\text{tooth}}$	2.4	4.3	mm
number of rotor teeth	$z$	12	12	—
relative flux-conducting rotor width	$\beta$	0.28	0.52	—
shaft diameter	$d_{\text{shaft}}$	11	10	mm
rotor-core diameter	$d_{\text{core}}$	30.5	28	mm
see fig. 1.1	$b_{35}$	10	10	mm
see fig. 1.1	$b_{36}$	10	10	mm
overall height of the motor	$h_o$	61	51	mm
overall width of the motor	$b_o$	90	87	mm
see fig. 8.1	$b_{31}$	2	2	mm
see fig. 8.1	$b_{32}$	2.5	2.5	mm
number of rotor turns	$w_r$	24 × 35	24 × 37	—
number of stator turns	$w_s$	2 × 240	2 × 190	—
active inductance of a rotor coil	$L_{\text{comm}} \propto d_r l_r (w_{\text{coil } r})^2$	1.09	0.85	m <sup>2</sup>
rotor winding-wire diameter	$d_{\text{Cu } r}$	0.25	0.25	mm
stator winding-wire diameter	$d_{\text{Cu } s}$	0.45	0.45	mm
weight of rotor copper	$G_{\text{Cu } r}$	44	45	g
weight of stator copper	$G_{\text{Cu } s}$	136	96	g
weight of required steel sheet	$G_{\text{Fe}}$	885	515	g
cost of rotor winding wire	$C_{\text{Cu } r}$	25	25	cent
cost of stator winding wire	$C_{\text{Cu } s}$	62	44	cent
cost of required steel sheet	$C_{\text{Fe}}$	78	45	cent
cost of stamping	$C_{\text{stamp}}$	29	21	cent
overall variable costs	$C_o$	194	135	cent
rotor speed	$n$	320	320	s <sup>-1</sup>
peak value of magnetic induction	$B_{\text{peak}}$	2.5	2.0	Wb m <sup>-2</sup>
copper loss in the rotor	$P_{\text{Cu } r}$	17	19	W
copper loss in the stator	$P_{\text{Cu } s}$	20	16	W
input power	$P_{\text{in}}$	308	296	W
temperature rise in rotor coils		43	36	°C
temperature rise in stator coils		39	31	°C

- (4) As shown in chapter 5, the active inductance of a rotor coil at the end of commutation is assumed to be roughly proportional to  $d_r l_r (w_{\text{coil } r})^2$ . As far as the active inductance  $L_{\text{comm}}$  is concerned we would therefore expect the brush life of the new motor to be longer than that of the old one. However, we have no experimental data on this point.

### 8.10. Conclusions

The most important design parameters of a small series motor are the relative rotor length  $\lambda$ , the relative flux-conducting rotor width  $\beta$  and the maximum value of the magnetic induction in the magnetic circuit in the AC case,  $B_{\text{peak}}$ . It is striking that for a very wide range of speeds, output powers and permissible power losses in the stator and rotor, and for all possible values of all the other parameters, roughly the same optimum values were always found for  $\beta$ ,  $\lambda$  and  $B_{\text{peak}}$ . They lay in the ranges:

$$\begin{aligned}\beta &= 0.4 - 0.45, \\ \lambda &= 0.42 - 0.50, \\ B_{\text{peak}} &= 1.8 - 1.9 \text{ Wb m}^{-2}.\end{aligned}$$

These optimal values do not change if the cost per kg of the steel sheet or winding wire used changes.

$L_{\text{comm}}$ , the active inductance of the commutating rotor coil, is lower for an optimized motor than for one of arbitrary design. A lower value of  $L_{\text{comm}}$  means less brush wear and a longer life.

The savings in manufacturing costs for an optimized motor compared with one of arbitrary design can be considerable. Various other conclusions are found in sec. 8.7.

LIST OF SYMBOLS

symbol	dimensions	definition/sections in which symbol occurs
The "cent" mentioned in this list is the Dutch cent, or 0.01 guilder (Hfl. 0.01)		
$A_{\text{coils } r}$	$\text{m}^2$	cross-sectional area of all the rotor coils together/1.4, 7.5, 8.5
$A_{\text{coil } s}$	$\text{m}^2$	cross-sectional area of one stator coil/1.5
$a_{\text{Cu } r}$	$\text{m}^2$	cross-sectional area of the copper core of one rotor wire/1.4, 7.3, 8.2, 8.5
$a_{\text{Cu } s}$	$\text{m}^2$	cross-sectional area of the copper core of one stator wire/1.5, 8.2, 8.5
$A_{\text{slots } r}$	$\text{m}^2$	cross-sectional area of all the rotor slots together/1.4
$b_{\text{aperture}}$	m	width of a rotor slot aperture, see fig. 4.5/4.3, 4.4
$b_{\text{Fe core}}$	m	flux-conducting width of the rotor core/1.3, 8.9
$b_{\text{Fe } r}$	m	flux-conducting rotor width/1.3, 1.4, 2.1, 7.5, 8.5
$b_{\text{Fe teeth}}$	m	flux-conducting width of the rotor teeth/1.3, 8.9
$b_{\text{ins comm}}$	m	thickness of the insulation between the shaft and the segments of the commutator see fig. 6.4/6.2
$b_{\text{ins } r}$	m	thickness of the insulation in the rotor slots, see fig. 1.8/1.4, 6.2, 7.5, 7.10, 8.4, 8.5
$b_{\text{ins } s}$	m	thickness of the insulation in the stator slots, see fig. 1.8/1.5, 6.2, 8.4, 8.5
$B_{\text{max}}$	$\text{Wb m}^{-2}$	maximum magnetic induction in the rotor as function of position/1.3, 1.4, 1.5, 2.1, 3.4, 3.5, 7.4, 7.5, 7.7, 7.8, 7.9, 7.10, 7.11, 7.12, 8.7, summ.
$B_{\text{max core}}$	$\text{Wb m}^{-2}$	$B_{\text{max}}$ in the rotor core/1.3, 1.9
$B_{\text{max tooth}}$	$\text{Wb m}^{-2}$	$B_{\text{max}}$ in the rotor teeth/1.3, 1.9
$b_0$	m	overall width of the stator of the small series motor, see fig. 1.8/8.1, 8.5, 8.9
$B_{\text{peak}}$	$\text{Wb m}^{-2}$	maximum value of alternating $B_{\text{max}}$ /2.1, 3.5, 8.4, 8.5, 8.7, 8.8, 8.9, 8.10, summ.
$B_{\text{peak core}}$	$\text{Wb m}^{-2}$	$B_{\text{peak}}$ in the rotor core/1.3

symbol	dimensions	definition/sections in which symbol occurs
$B_{\text{peak temp}}$	$\text{Wb m}^{-2}$	value of $B_{\text{peak}}$ chosen temporarily for the optimization calculation/8.4, 8.5, 8.6
$B_{\text{peak tooth}}$	$\text{Wb m}^{-2}$	maximum value of alternating $B_{\text{max}}$ in a rotor tooth/1.3
$b_{\text{pitch}}$	m	tooth pitch of the rotor, see fig. 4.1/4.0, 4.2, 4.4
$B_{\text{prop}}$	$\text{Wb m}^{-2}$	value of $B_{\text{max}}$ up to which no saturation occurs/2.1, 2.2, 8.4, 8.5, 8.7
$b_{\text{slot}}$	m	width of a rotor slot, see fig. 4.1/4.0
$b_{\text{tip}}$	m	width of the tip of a rotor tooth in a rotor with semi-enclosed slots, see fig. 4.5/4.3, 4.4
$b_{\text{tooth}}$	m	width of one rotor tooth, see fig. 1.8/1.3, 1.4, 8.9
$B_{\alpha}$	$\text{Wb m}^{-2}$	air-gap induction at angle $\alpha$ , see fig. 2.6/2.2
$B_{\delta}$	$\text{Wb m}^{-2}$	air-gap induction/1.7, 2.2, 7.7, 7.8, 7.9, 7.10, 7.11, 8.7, summ.
$b_{2\frac{3}{4}}$	m	distance from the periphery of the rotor to which the rotor slots are filled with windings, see fig. 1.8 and eq. (1.1)/1.3, 1.5, 8.4, 8.5
$b_{31,32}$	m	see fig. 8.1/8.1, 8.4, 8.5, 8.9
$b_{33}$	m	see fig. 1.8/1.5, 8.4, 8.5
$b_{35}$	m	local width of stator yoke, see fig. 1.8/1.5, 8.5, 8.9
$b_{36}$	m	local width of stator yoke, see fig. 1.8/1.5, 3.1, 8.5, 8.9
$b_{39}$	m	thickness of tip of stator pole, see fig. 1.8/1.5, 8.4, 8.5
$b_{39 \text{ min}}$	m	minimum required value of $b_{39}$ with respect to stamping/1.5
$C_{\text{Cu r}}$	cent	cost of winding wire of the rotor/1.8, 1.9, 8.2, 8.5, 8.6, 8.7, 8.9
$c_{\text{Cu r}}$	cent $\text{kg}^{-1}$	cost of an amount of winding wire for the rotor, the copper core of which weighs 1 kg/8.2, 8.5, 8.7
$C_{\text{Cu s}}$	cent	cost of winding wire of the stator/1.8, 1.9, 8.2, 8.5, 8.6, 8.7, 8.9

symbol	dimensions	definition/sections in which symbol occurs
$c_{Cu s}$	cent $kg^{-1}$	cost of an amount of winding wire for the stator, the copper core of which weighs 1 kg/8.2, 8.5, 8.7
$c_e$	—	current distortion factor, see eq. (2.40)/1.7, 2.3, 2.4, 8.5
$C_{Fe}$	cent	cost of steel sheet required for rotor and stator/1.8, 1.9, 8.1, 8.5, 8.9
$c_{Fe}$	cent $kg^{-1}$	cost of steel sheet per kilogramme/8.1, 8.4, 8.5, 8.7
$c_l$	—	factor by which the rotor length is multiplied in the optimization calculation/8.4, 8.5
$c_{mech}$	—	torque distortion factor, see eq. (2.41)/1.7, 2.3, 2.4, 8.5, 8.6, 8.7
$c_{mech temp}$	—	value of $c_{mech}$ temporarily chosen in the optimization calculation/8.4, 8.5
$C_o$	cent	"overall variable costs" of the small series motor, see eq. (1.43)/1.8, 1.9, 8.5, 8.6, 8.7, 8.9, summ.
$C_{stamp}$	cent	cost of stamping the laminations of rotor and stator/1.8, 1.9, 8.1, 8.5, 8.9
$c_{stamp}$	cent $m^{-1}$	cost of stamping the laminations for a stack (of rotor and stator) with a length of 1 metre/8.1, 8.4, 8.5, 8.7
$c_u$	—	relative mains voltage, see eq. (2.39)/2.3, 8.5
$c_{21, 22, 23}$	cent $kg^{-1}$	values of $c_{Cu r}$ for rotor wire of diameters $d_{21, 22, 23}$ /8.2, 8.4, 8.5
$c_{24}$	cent $kg^{-1}$	coefficients of eq. (8.11), calculated with the aid of eqs (8.14), (8.15) and (8.16)/8.2, 8.5
$c_{25}$	cent $kg^{-1} m^{-1}$	
$c_{26}$	cent $kg^{-1} m^{-2}$	
$c_{31, 32, 33}$	cent $kg^{-1}$	values of $c_{Cu s}$ for stator wire of diameters $d_{31, 32, 33}$ /8.2, 8.4, 8.5
$c_{34}$	cent $kg^{-1}$	coefficients of eq. (8.12), calculated with the aid of eqs (8.18), (8.19) and (8.20)/8.2, 8.5
$c_{35}$	cent $kg^{-1} m^{-1}$	
$c_{36}$	cent $kg^{-1} m^{-2}$	
$c_{37}$	—	ratio of the magnetic fluxes $\phi^{(1)}_{37}$ and $\phi^{(1)}_{s r}$ /2.2, 8.4, 8.5
$c_{41}$	—	ratio of $A_{m o}$ and $A_{m 2\delta}$ , see eq. (2.4)/2.1, 2.2, 5.6, 8.5

symbol	dimensions	definition/sections in which symbol occurs
$d$	m	fictive rotor diameter, see fig. 1.8/1.3, 1.4, 1.5, 1.9, 2.1, 2.2, 3.5, 6.2, 7.4, 7.5, 7.7, 7.9, 7.10, 7.11, 8.4, 8.5, 8.7, 8.9, summ.
$d_{\text{coils}}$	m	diameter of the circular cross-section of a stator coil, see fig. 1.8/1.5, 6.2, 8.5
$d_{\text{coils temp}}$	m	value of $d_{\text{coils}}$ temporarily chosen in the optimization calculation/8.4, 8.5
$d_{\text{comm}}$	m	commutator diameter, see fig. 6.4/6.2
$d_{\text{core}}$	m	rotor-core diameter, see fig. 1.8/1.3, 1.4, 7.10, 8.9
$d_{\text{Cu r}}$	m	diameter of the copper core of the winding wire of the rotor/6.2, 8.2, 8.5, 8.9
$d_{\text{Cu s}}$	m	diameter of the copper core of the winding wire of the stator/8.2, 8.5, 8.9
$d_r$	m	rotor diameter, see fig. 1.8/1.1, 1.3, 1.7, 2.1, 2.2, 3.1, 4.4, 5.5, 5.6, 6.2, 7.7, 7.8, 7.9, 7.10, 8.5, 8.9
$d_{\text{shaft}}$	m	shaft diameter, see fig. 1.8/1.3, 6.2, 7.10, 8.6, 8.9
$d_{\text{shaft fict}}$	m	fictive shaft diameter, see fig. 1.8/1.3, 1.4, 8.4, 8.5
$d_{\text{temp}}$	m	value of $d$ temporarily chosen in the optimization calculation/8.4, 8.5, 8.6
$d_{2.1, 2.2, 2.3}$	m	diameters of the copper core of winding wire of the rotor/8.2, 8.4, 8.5
$d_{3.1, 3.2, 3.3}$	m	diameters of the copper core of winding wire of the stator/8.2, 8.4, 8.5
$e$	V	instantaneous value of the rotational e.m.f. of a commutator machine, see eq. (1.11)/1.4, 1.6, 2.2, 7.3, 7.4, 7.5, 7.7, 7.10
$e_{\text{peak}}$	V	peak value of an alternating rotational e.m.f./8.5
$f_{(j;m)}$	—	normalized stator magnetic flux as function of $j$ and $m$ , described by eq. (2.1)/2.1, 2.2, 2.3, 2.4, 8.8
$f_{(j;m)\text{peak}}$	—	peak value of alternating $f_{(j;m)}$ /2.3, 8.5
$f_{(r)}$	—	rotor function, defined in eq. (1.20)/1.4, 6.2, 7.4, 7.10, 7.11

symbol	dimensions	definition/sections in which symbol occurs
$G_{Cu r}$	kg	weight of the copper core of rotor winding wire/8.2, 8.5, 8.7, 8.9
$g_{Cu r}$	$kg\ m^{-3}$	density of copper (or aluminium) used for rotor winding wire/8.2, 8.4, 8.5
$G_{Cu s}$	kg	weight of the copper core of stator winding wire/8.2, 8.5, 8.7, 8.9
$g_{Cu s}$	$kg\ m^{-3}$	density of copper (or aluminium) used for stator winding wire/8.2, 8.4, 8.5
$G_{Fe}$	kg	weight of steel sheet, required for rotor and stator/8.1, 8.5, 8.7, 8.9
$g_{Fe}$	$kg\ m^{-3}$	density of steel/3.1, 8.1, 8.4, 8.5
$G_{yoke}$	kg	approximate weight of the yoke of the stator of a small series motor/3.1
$h_o$	m	overall height of the stator of the small series motor, see fig. 1.8/8.1, 8.5, 8.9
$h_{tooth}$	m	height (length) of a rotor tooth, see fig. 1.8/1.4, 6.2
$h_{3\beta}$	m	see fig. 1.8/1.5, 8.5
$I$	A	current through part of the resistance network/4.1
$i$	A	current through measuring device of fig. 5.2/5.1
$i$	A	instantaneous value of the current in a small series motor/1.6, 2.0, 2.1, 2.2, 2.3, 7.3, 7.6, 7.7, 7.11
$I_{eff}$	A	effective value of alternating current $i$ in the small series motor/2.3
$I_{peak}$	A	peak value of alternating current $i$ in the small series motor/2.3, 8.5
$i_{spark}$	A	spark current between a brush and commutator at the end of commutation see fig. 5.5b/5.3
$I_1, I_2$	A	currents through part of the resistance network/4.1
$I_1$	A	current through the right-hand rotor circuit, see e.g. fig. 5.6/5.2, 5.3, 5.5, 5.6
$I_2$	A	current through the left-hand rotor circuit, see e.g. fig. 5.6/5.2, 5.3



symbol	dimensions	definition/sections in which symbol occurs
$i_1$	A	current in the short-circuited rotor coil, see e.g. fig. 5.5/5.3
$i_1 \dots i_{12}$	A	currents through the 12 rotor coils/5.3
$i_s$	A	current through the stator coil/5.3
$i_z$	A	current through Zener diode/5.3.
$J$	$A\ m^{-2}$	current density/7.7, 7.8, 7.9, 7.10, 7.11, summ.
$J$	$N\ m\ s^{-2}$	moment of inertia of the rotor and coupled masses/1.6
$j$	—	normalized ampere turns/2.1, 2.2, 2.3
$j_{eff}$	—	effective value of alternating normalized ampere turns/2.3
$j_{peak}$	—	peak value of alternating $j$ /2.3, 8.5
$k_{car}$	—	carter factor/1.5, 1.7, 2.1, 2.2, 4.0, 4.1, 4.2, 4.3, 4.4, 4.5, 5.6, 7.7, 7.9, 8.4, 8.5
$k_{Cu}$	$W\ m^{-1}\ ^\circ C^{-1}$	thermal conductivity of copper/6.2
$k_{Cu\ r}$	—	space factor of copper in the rotor, defined in eq. (1.14)/1.3, 1.4, 1.5, 1.9, 6.2, 7.4, 7.5, 7.10, 7.11, 8.2, 8.4, 8.5, 8.7
$k_{Cu\ s}$	—	space factor of copper in the stator, see eq. (1.34) and text above this equation/1.5, 8.2, 8.4, 8.5, 8.7
$k_E$	—	relative active rotational e.m.f., see eq. (1.11) and text above this equation/1.4, 1.7, 2.2, 2.3, 7.3, 7.4, 7.5, 7.10, 8.4, 8.5
$k_{Fe}$	—	space factor of steel sheet in the rotor and stator stack/8.1, 8.4, 8.5, 8.6
$k_{Fe}$	$W\ m^{-1}\ ^\circ C^{-1}$	thermal conductivity of steel/6.2
$k_{head\ r}$	—	relative length of rotor end windings, see eq. (1.18)/1.4, 7.4, 7.5, 7.10, 8.4, 8.5
$k_{ins}$	$W\ m^{-1}\ ^\circ C^{-1}$	thermal conductivity of insulation materials/6.2
$k_{ins\ head\ r}$	—	relative thickness of rotor-head insulation, see eq. (1.17)/1.4, 7.4, 7.5, 7.10
$k_{ins\ slots\ r}$	—	relative thickness of rotor-slot insulation, see eq. (1.23)/1.4, 7.4, 7.5, 7.10, 7.11
$k_{pole}$	—	reciprocal relative pole arc, see eq. (1.2)/1.3, 1.4, 1.5, 2.1, 2.2, 5.6, 7.4, 7.7, 7.9, 7.10, 7.11, 8.4, 8.5, 8.6, 8.7

symbol	dimensions	definition/sections in which symbol occurs
$k_R$	—	relative active rotor resistance, see eq. (1.13) and text above this equation/1.4, 1.7, 7.3, 7.4, 7.5, 7.10, 8.4, 8.5
$k_{rad}$	$W m^{-2} K^{-4}$	absorption factor/6.2
$k_{shaft}$	—	relative shaft diameter, see eq. (1.22)/1.4, 7.4, 7.10, 7.11
$k_{35}; k_{36}$	—	see eqs (1.28) and (1.29) respectively/1.5, 8.4, 8.5
$L$	$V s A^{-1}$	inductance of a rotor coil/5.6
$L$	$V s A^{-1}$	over-all inductance of a small series motor/1.6, 1.7, 2.2, 7.3
$L_{comm}$	$V s A^{-1}$	active inductance of a rotor coil at the end of commutation, see eq. (5.10) and text above this equation/5.0, 5.3, 5.4, 5.5, 5.6, 5.7, 8.9, 8.10
$l_{comm}$	m	length of the commutator, see fig. 6.4/6.2
$l_{ins r}$	m	thickness of rotor-head insulation, see fig. 1.8/1.4, 6.2, 7.5, 7.10, 8.4, 8.5
$l_{ins s}$	m	thickness of stator-head insulation, see fig. 1.8/1.5, 8.4, 8.5
$l_{lam}$	m	thickness of a rotor lamination/3.3, 3.4
$L_{norm}$	—	normalized over-all inductance of a small series motor, see eq. (2.34)/2.2, 2.3, 8.5
$L_{perp}$	$V s A^{-1}$	inductance of the rotor with respect to normal component of the rotor field, see eq. (2.22) and text above this equation/2.2
$l_r$	m	length of the rotor stack, see fig. 1.8/1.3, 1.4, 1.7, 2.1, 2.2, 3.5, 5.4, 5.5, 5.6, 6.2, 7.5, 7.7, 7.8, 7.11, 8.1, 8.4, 8.5, 8.7, 8.9, summ.
$l_{r temp}$	m	value of $l_r$ temporarily chosen in the optimization calculation/8.4, 8.5
$l_s$	m	length of the stator stack, see fig. 1.8/1.5, 3.1, 6.2, 8.1, 8.5, 8.7
$l_{71}; l_{73}; l_{74}$	m	length of three parts of the shaft, see fig. 6.4/6.2
$l_{77}$	m	length of the rotor winding wire between the commutator and the end windings, see fig. 6.4/6.2

symbol	dimensions	definition/sections in which symbol occurs
$m$	—	tangent of the angle which the right-hand linear portion of the normalized magnetization curve makes with the horizontal axis/2.1, 2.2, 2.3, 2.4, 8.4, 8.5, 8.7
$n$	$s^{-1}$	rotor speed in revolutions per second/1.4, 1.6, 1.7, 2.2, 2.3, 3.4, 3.5, 7.3, 7.4, 7.5, 7.7, 7.10, 8.4, 8.5, 8.6, 8.9
$P_{air}$	W	air friction losses/6.1
$P_{bearings}$	W	power losses in the bearings/6.1, 6.2
$P_{comm}$	W	commutation losses/6.1, 6.2
$P_{Cu Fe r}$	W	sum of copper and iron losses in the rotor/8.5, 8.7
$P_{Cu Fe r req}$	W	permissible value of $P_{Cu Fe r}$ /8.4, 8.5, 8.6, 8.7
$P_{Cu r}$	W	copper losses in the rotor/2.3, 6.1, 6.2, 6.3, 7.10, 7.11, 8.5, 8.6, 8.7, 8.9
$P_{Cu s}$	W	copper losses in the stator/2.3, 6.1, 6.2, 6.3, 8.5, 8.9
$P_{Cu s req}$	W	permissible value of $P_{Cu s}$ /8.4, 8.5, 8.6, 8.7
$P_{eddy}$	W	iron losses in the rotor due to eddy currents/3.4
$P_{\Gamma}$	W	input power at maximum air intake/6.1
$P_{Fe}$	W $Wb^{-2} m^{-1}$	specific iron losses in the rotor, see eq. (3.5)/3.5, 8.4, 8.5, 8.7
$p_{Fe}$	W	instantaneous value of the iron losses in the rotor/1.6
$P_{Fe r}$	W	iron losses in the rotor/3.4, 3.5, 6.1, 6.2, 6.3, 7.5, 7.10, 7.11, 8.5, 8.6, 8.7
$P_{Fe s}$	W	iron losses in the stator/6.1, 6.2, 6.3
$P_{hyst}$	W	iron losses in the rotor due to hysteresis/3.4
$P_i$	W	input power at minimum air inlet/6.1
$P_{in}$	W	input power/8.9
$P_m$	W	input power at average air inlet/6.1
$P_{mech}$	W	mechanical power losses/1.6
$P_{mech brush}$	W	mechanical power losses in brushes and commutator/6.1, 6.2
$P_{out}$	W	output power/8.5, 8.6
$p_{out}$	W	instantaneous output power/1.6

symbol	dimensions	definition/sections in which symbol occurs
$P_{out\ req}$	W	required value of $P_{out}$ /8.4, 8.5, 8.6, 8.7
$P_{out\ temp}$	W	value of $P_{out}$ temporarily chosen in the optimization calculation/8.5
$P_{rad\ 80:82:88:90}$	W	heat radiated from various parts of the small series motor/6.2
$P_{R\ brush}$	W	brush resistance losses/6.1, 6.2
$P_{\delta}$	W	internal power/2.3, 7.7, 8.5, 8.6
$p_{\delta}$	W	instantaneous value of $P_{\delta}$ /1.6
$R$	$\Omega$	resistance in fig. 5.2/5.1
$R$	$\Omega$	resistance of part of the resistance network/4.1, 4.4
$R_{brush}$	$\Omega$	resistance of two brushes in series/1.7
$R_{coll}$	$\Omega$	resistance of a short-circuited rotor coil/5.3
$R_{m\ Fe}$	A $V^{-1} s^{-1}$	reluctance of the iron of the magnetic circuit of a small series motor/2.1
$R_{m\ pitch\ i}$	A $V^{-1} s^{-1}$	reluctance of parts of the air gap, see eq. (4.1) and text above this equation/4.0, 4.2
$R_{m\ pitch\ flect}$		
$R_{pitch\ i}; R_{pitch\ flect}$	$\Omega$	resistance of parts of the resistance network/4.2
$R_{norm}$	—	normalized resistance of a small series motor, see eq. (2.34)/ 2.2, 2.3, 8.5
$R_{m\ 2\delta}$	A $V^{-1} s^{-1}$	reluctance of both air gaps in series/2.1
$R_r$	$\Omega$	rotor resistance/1.4, 1.6, 1.9, 2.0, 2.2, 2.3, 2.4, 7.3, 7.4, 7.5, 7.6, 7.7, 7.10, 8.5, summ.
$R_s$	$\Omega$	stator resistance/1.5, 1.6, 1.9, 2.0, 2.2, 2.3, 2.4, 7.3, 7.5, 7.6, 8.5, summ.
$r_{3B}$	m	radius, see fig. 1.8/1.5, 8.5
$S$	A $m^{-1}$	specific load/7.7, 7.8, 7.9, 7.10, 7.12, summ.
$S_{head\ r}$	m	length of an end winding/1.4, 7.5, 8.5
$S_{w\ r}$	m	length of a rotor turn/1.4, 7.3, 7.5, 8.2, 8.5
$S_{w\ s}$	m	length of a stator turn/1.5, 6.2, 8.2, 8.5.
$t$	s	time/2.2, 2.3
$T_{air}$	N m	air-friction loss torque/3.2, 3.4
$T_{eddy}$	N m	eddy-current loss torque/3.4
$T_{eddy\ shaft}$	N m	eddy-current loss torque of the shaft/3.4
$T_{Fe}$	N m	iron-loss torque/1.6, 3.2, 3.4
$T_{Fe=}$	N m	iron-loss torque measured with DC excitation/3.4

symbol	dimensions	definition/sections in which symbol occurs
$T_{Fe\sim}$	N m	iron-loss torque measured with AC excitation/3.4
$T_{Fe\sim calc}$	N m	calculated value of iron-loss torque with AC excitation/3.4
$T_{hyst}$	N m	hysteresis-loss torque/3.4
$T_{mech}$	N m	mechanical loss torque/1.6
$T_{out}$	N m	output torque/1.6
$T_{pole}$	N m	loss torque due to extra eddy-current losses in the stator poles/3.4
$t_z$	s	simulated spark decay time/5.3, 5.5, 5.6
$T_\delta$	N m	internal torque/1.6, 7.11
$U$	V	voltage in the resistance network/4.1
$U$	V	voltage in fig. 5.2./5.1
$U$	V	effective value of sinusoidal alternating mains voltage/8.4, 8.5
$u$	V	instantaneous value of sinusoidal alternating mains voltage/1.6, 2.2, 7.3
$U_{brush\ 1,2}$	V	voltages between brush and segments/5.3
$u_{m\ o}$	A	net number of ampere turns generating the stator flux $\phi^{(1)}$ , see eq. (2.6)/2.1
$u_{m\ prop}$	A	value of $u_{m\ o}$ up to which no saturation occurs/2.1
$U_{m\ r}$	A	number of rotor ampere turns/1.1
$U_{m\ s}$	A	number of stator ampere turns/1.1, 1.5, 3.4
$u_{m\ r\ perp}$	A	component of $u_{m\ r}$ perpendicular to the polar axis/2.2
$u_{m\ r\ par}$	A	component of $u_{m\ r}$ parallel to the polar axis/2.2
$u_{m\ s}$	A	number of stator ampere turns/2.2
$U_{norm}$	—	normalized mains voltage, see eq. (2.34)/2.2, 2.3, 8.5
$U_{norm\ prop}$	—	value of $U_{norm}$ up to which no saturation occurs, see eq. (2.38) and text above this equation/2.3, 8.5
$U_{peak}$	V	peak value of alternating mains voltage/2.2, 8.5
$U_{peak\ temp}$	V	value of $U_{peak}$ temporarily chosen in the optimization calculation/8.5

symbol	dimensions	definition/sections in which symbol occurs
$U_{\text{segment}}$	V	voltage between two commutator segments/5.3
$U_{\text{spark}}$	V	spark voltage between brush and segment/5.3
$U_Z$	V	Zener voltage/5.3, 5.5
$V_{\text{Cu r}}$	$\text{m}^3$	volume of copper in the rotor/7.11, 8.2
$V_{\text{Cu s}}$	$\text{m}^3$	volume of copper in the stator/8.2
$V_{\text{Fe}}$	$\text{m}^3$	volume of steel sheet required for the small series motor/8.1
$V_r$	$\text{m}^3$	fictive rotor volume, see eq. (7.3)/7.10, 7.11
$V_{10; 15}$	$\text{W kg}^{-1}$	loss figures of steel sheet/3.0, 3.2
$w_{\text{coil r}}$	—	number of turns of a rotor coil/5.5, 5.6, 8.9
$W_{\text{perp}}$	J	magnetic energy of the component of the rotor field perpendicular to the polar axis/2.2
$w_r$	—	number of rotor turns/1.4, 1.6, 2.1, 2.2, 2.3, 7.3, 7.11, 8.2, 8.5, 8.6, 8.7, 8.9.
$w_{r \text{ par}} (w_{r \text{ perp}})$	—	number of rotor turns corresponding to the component of the rotor field parallel (perpendicular) to the polar axis/2.2
$w_{r \text{ temp}}$	—	number of rotor turns temporarily chosen in the optimization calculation/8.4, 8.5
$w_s$	—	number of stator turns/1.5, 2.1, 2.2, 5.3, 8.2, 8.4, 8.5, 8.6, 8.7, 8.9
$W_Z$	J	energy dissipated in the Zener diode during one simulated spark/5.3.
$W_\delta$	J	portion of $W_{\text{perp}}$ occurring in the air gap/2.2
$z$	—	number of rotor slots or rotor teeth/1.3, 1.4, 1.7, 4.0, 6.2, 7.9, 8.4, 8.9
$\alpha$	rad	rotor angular position/5.3
$\alpha$	rad	angle in fig. 2.6/2.2
$\alpha_{\text{brush}}$	rad	angle through which the brushes of the small series motor are turned against the direction of rotation of the rotor/2.1, 2.2, 8.4, 8.5, 8.7
$\alpha_{\text{coil s}}$	rad	see fig. 1.8/1.5, 8.5
$\alpha_{\text{max}}$	rad	maximum value of $\alpha$ , see fig. 2.6/2.2

symbol	dimensions	definition/sections in which symbol occurs
$\beta$	—	relative flux-conducting rotor width/1.3, 1.4, 1.5, 1.9, 2.1, 2.2, 3.5, 6.2, 7.4, 7.5, 7.8, 7.9, 7.10, 7.11, 7.12, 8.4, 8.5, 8.7, 8.8, 8.9, 8.10, summ.
$\beta_{temp}$	—	value of $\beta$ temporarily chosen in the optimization calculation/8.4, 8.5, 8.6
$\gamma$	—	factor used in calculation of the carter factor, see eq. (4.2)/4.0, 4.2, 4.3, 4.4, 4.5
$\delta$	m	air-gap width/1.5, 2.1, 2.2, 4.0, 4.2, 4.3, 4.4, 4.5, 5.5, 5.6, 8.4, 8.5, 8.7
$\Theta$	K	temperature in degrees Kelvin/6.2
$\lambda$	—	relative rotor stack length, see eq. (1.7)/1.3, 1.4, 1.9, 5.0, 5.4, 5.6, 7.4, 7.7, 7.8, 7.9, 7.10, 7.11, 7.12, 8.4, 8.5, 8.6, 8.7, 8.8, 8.9, 8.10, summ.
$A_{m\ o}$	V s A <sup>-1</sup>	permeance of the stator circuit/2.1, 5.6, 8.5
$A_{m\ pitch}$	V s A <sup>-1</sup>	permeance per tooth pitch, see eq. (4.1) and text above this equation/4.0
$A_{m\ pitch\ fict}$	V s A <sup>-1</sup>	fictive value of $A_m$ pitch, see eq. (4.1) and text above this equation/4.0
$A_{m\ 2\delta}$	V s A <sup>-1</sup>	permeance of both air gaps in series/2.1, 2.2, 5.6, 8.5
$A_{i\ therm\ 71-86}$	W °C <sup>-1</sup>	thermal conductances, see fig. 6.1/6.2
$A$	V s A <sup>-1</sup>	permeance, see eq. (5.14)/5.5
$\mu_r$	—	relative permeability/2.1, 8.4, 8.5
$\nu$	s <sup>-1</sup>	frequency/3.0, 3.4, 5.0, 8.4, 8.5
$\rho_{Cu\ r}$	Ω m	resistivity of copper in the rotor/1.4, 7.3, 7.4, 7.5, 7.10, 8.4, 8.5, 8.6
$\rho_{Cu\ s}$	Ω m	resistivity of copper in the stator/1.5, 8.4, 8.5
$\rho_{Fe}$	Ω m	resistivity of steel sheet/3.3, 3.4
$\phi$	Wb	total magnetic flux in small series motor, see eq. (2.13) and text above this equation/2.2
$\phi$	Wb	total magnetic flux through commutating rotor coil, see eq. (5.4) and text above this equation/5.3

symbol	dimensions	definition/sections in which symbol occurs
$\phi^{(1)}$	Wb	part of the stator flux surrounded by one rotor turn, see fig. 3.6/1.3, 1.4, 1.5, 1.6, 2.0, 2.1, 2.2, 2.3, 3.4, 7.3, 7.11
$\phi_{\text{par}}$	Wb	component of the total rotor flux parallel to the polar axis/2.2
$\phi^{(1)}_{\text{peak}}$	Wb	peak value of alternating flux $\phi^{(1)}$ /2.3, 3.4, 8.5
$\phi^{(1)}_{\text{prop}}$	Wb	value of $\phi^{(1)}$ up to which no saturation occurs/2.1
$\phi_{\text{perp}}$	Wb	component of total rotor flux normal to polar axis/2.2
$\phi^{(1)}_{r s}$	Wb	component of rotor flux surrounded by the stator coils/2.2
$\phi^{(1)}_{r \text{ leak}}$	Wb	rotor leak flux/2.2
$\phi^{(1)}_{s r}$	Wb	component of stator flux surrounded by the rotor coils in geometrically neutral position/2.2
$\phi_1^{(1)}$	Wb	magnetic flux through the rotor, see fig. 3.6/3.4
$\phi_{1-12;s}$	Wb	total magnetic flux through commutating rotor coil generated by the rotor coils 1-12 and the stator coil respectively/5.3
$\phi^{(1)}_{35}; \phi^{(1)}_{36}$	Wb	magnetic fluxes through parts of the stator circuit, see fig. 1.8/1.5
$\phi^{(1)}_{37}$	Wb	magnetic flux generated by the stator coils/1.5, 2.2
$\omega$	$s^{-1}$	circular frequency/2.2, 2.3, 8.5



REFERENCES

- 1) Walter Kiefer, Beitrag zur Kühlung elektrischer Maschinen kleiner Leistung mit Durchzugsbelüftung, Diss. T.H. Stuttgart, 1961.
- 2) Elmar R. Hauschild, Statisches und dynamisches Verhalten von Druckfedern in Köcherbürstenhaltern elektrischer Kleinmotoren, Diss. T.H. Stuttgart, 1964.
- 3) Lothar Woerner, Form und Verhalten von Preßstoff-Kleinkommutatoren bei Drehung, Diss. T.H. Stuttgart, 1961.
- 4) Martin Held, Rückwirkung und Verluste durch Kommutierungsströme bei Universalmotoren, Diss. T.H. Stuttgart, 1961, pp. 21-26.
- 5) Fritz Schröter, Die Kommutierungsfähigkeit der Kohlebürste, ETZ-B, Heft 3, 49-55, Febr. 1962.
- 6) Erich Gruber, Problemen des Bürstenverschleisses bei Universalmotoren, Diss. T.H. Stuttgart, 1957.
- 7) K. Padmanabhan and A. Srinivasan, Some important aspects in the phenomenon of commutator sparking, IEEE Trans. on Power Apparatus Systems **84**, 396-401, 1965.
- 8) Jerzy Pustola, Eisenverluste in Universalmotoren, ETZ-A **89**, H 10, 233-239, 1968.
- 9) Paul D. Agarwal, Eddy-current losses in solid and laminated iron, Trans. AIEE Communications and electronics **78**, 169-181, 1959.
- 10) C. Feldmann, Electrotechnische Constructie, Waltmann, Delft, 1934, Vol. 1, 2nd ed.
- 11) Hermann Kuhnle, Die Ständerjochentlastung bei zweipoligen Universalmotoren, Diss. T.H. Stuttgart, 1969.
- 12) Edward Grant and Leon M. Roszyk, Design considerations for permanent magnet motors, Appliance engineer, 1968, vol. II, nr. 4, pp. 27-32.
- 13) A. Gladun, Der optimale Entwurf von Universalmotoren, Mitteilung XI. Internationales Wissenschaftliches Kolloquium der T.H. Ilmenau, 1966.
- 14) A. Gladun, Die optimale Dimensionierung der Wicklungen für Universalmotoren mit gegebenem Blechpaket, Elektrie **4**, 148-150, 1968.
- 15) L. I. Stolov, On the optimum geometry of d.c. fractional horse-power motors, Elektrichestvo **5**, 50-52, 101-108, 1968.
- 16) I. M. Postnikow, Die Wahl optimaler geometrischer Abmessungen elektrischer Maschinen, V.E.B. Verlag Technik, Berlin, 1955.
- 17) Adolf Wilhelm Mohr, Beitrag zur Kommutierung bei Universalmotoren, Diss. T.H. Stuttgart, 1957.
- 18) Alfred Still and Charles S. Siskind, Elements of electrical machine design, McGraw-Hill Book Company, Inc., New York, 3rd ed., 1954, pp. 9-19.
- 19) G. W. Carter, The electromagnetic field in its engineering aspects, Longmans, Green and Co., London, 1954, sec. 6.4.
- 20) Kurt Binder, Grenzbedingungen der Lichtbogenbildung bei der Kommutierung, ETZ-A **81**, H 16, 558-562, 1960.
- 21) G. W. Carter, Distribution of mechanical forces in magnetised material, Proc. IEE **112**, 1771-1777, 1965.
- 22) CEE specification for electric motor-operated appliances for domestic and similar purposes, publication 10, part I, 2nd ed., Oct. 1964.
- 23) CEE particular specification for vacuum cleaners and water suction cleaning appliances, publication 10, part II, section A, 2nd ed., May 1965.
- 24) CEE specification for portable motor-operated tools, publication 20, May 1960.
- 25) Karl Mühleisen, Beitrag zur Geräuschuntersuchung an elektrischen Maschinen kleiner Leistung, Diss. T.H. Stuttgart, 1958.
- 26) R. Lawrenz, Beitrag zur Approximation von Magnetisierungskennlinien, Elektrie **7**, 262-265, 1967.
- 27) Otto Erich Pöllot, Nutfrequente Schwankungen des magnetischen Flusses bei Universalmotoren und ihre Unterdrückung, ETZ-A **77**, H 4, 108-112, Febr. 1966.
- 28) Willi Schröter, Die Berechnung des magnetischen Kreises von Universalmotoren, Diss. T.H. Stuttgart, 1956.
- 29) W. Schuisky, Elektromotoren, ihre Eigenschaften und ihre Verwendung für Antriebe, Springer Verlag, Vienna, 1951, p. 30 etc.
- 30) A. F. Puchstein, The design of small d.c. motors, John Wiley and Sons, New York - London, 1961, Art. 138.
- 31) Rudolf Richter, Elektrische Maschinen I, Verlag Birkhäuser, Basel, 1951, pp. 177-180.

## Summary

Many types of small appliances are powered by small bi-polar AC series commutator motors, without compensation coils or commutating poles; such motors are called "small series motors" in this thesis. The small series motor is cheaper and smaller than other types of small electric motors and can provide high speeds.

Because of the economic importance of the small series motor, an optimization method for this type of motor has been needed for a long time. In this case, optimization means ensuring that the motor satisfies all the specifications with the minimum manufacturing costs. Such an optimization method is developed in this thesis.

First of all, the characteristic properties of small commutator machines are described. Five separate studies required for the optimization calculation are then carried out. The properties, weight, cost, etc. of the small series motor are now described with the aid of formulas containing a total of nearly sixty parameters. The formulas have such a form and contain such parameters that they are suitable for optimization calculations. For example, the air-gap induction  $B_g$ , the current density  $J$  and the specific load  $S$  do not occur in these optimization formulas. They are replaced by the magnetic induction in the magnetic circuit,  $B_{max}$  (in the AC case by  $B_{peak}$ ) and by  $R_r$  and  $R_s$ , the resistances of rotor and stator respectively.

The results of the optimization calculation show that there are three very important parameters, the values of which should be chosen correctly. These are the relative rotor stack length  $\lambda$  (the ratio of rotor stack length  $l_r$  to fictive rotor diameter  $d$ ); the relative flux-conducting rotor width  $\beta$  (the ratio of the width of the flux path in the rotor to the fictive rotor diameter) and the peak value (in the AC case) of the magnetic induction in the iron  $B_{peak}$ . Over a very wide range of values of output powers, speeds and permissible losses in a motor with a stator of the type shown in fig. 1.4, these parameters are found to be about within the narrow ranges

$$\begin{aligned}\beta &= 0.40-0.45, \\ \lambda &= 0.42-0.50, \\ B_{peak} &= 1.8-1.9 \text{ Wb m}^{-2}.\end{aligned}$$

In small series motors designed without the aid of an optimization method, the value of  $\beta$  is generally chosen much too small, and the values of  $\lambda$  and  $B_{peak}$  much too large. In such cases, the sum  $C_0$  of the costs of the winding wire and steel sheet required and the cost of stamping the laminations can be considerably lowered with the aid of the results of the optimization calculation. The commutation of the optimized motor is generally also improved, thanks to the lower value of the active inductance of the rotor coils.

### **Curriculum vitae**

De schrijver werd op 24 oktober 1931 geboren in Nieuwolda.

Na de Openbare Lagere School in Woldendorp doorliep hij de Openbare School voor Uitgebreid Lager Onderwijs in Winschoten en behaalde in 1948 het diploma MULO-B.

Daarna ging hij naar de toenmalige Middelbare Technische School in Groningen en behaalde in 1952 het diploma van de studierichting Elektrotechniek.

Hij bracht toen twee jaar in militaire dienst door en ging daarna studeren aan de Technische Hogeschool in Delft alwaar hij in 1960 afstudeerde op een onderwerp uit de microgolfttechniek: berekeningen aan een "field displacement isolator".

Vanaf die tijd werkt de schrijver in de laboratoria van de Hoofd Industrie Groep Huishoudelijke Apparaten der N.V. Philips' Gloeilampenfabrieken in Drachten aan de ontwikkeling van motoren voor huishoudelijke apparaten, zoals bijvoorbeeld:

éénfaze-synchroonmotoren met permanent magnetische rotor, gelijkstroom-collectormotoren met permanent magnetische stator voor toepassing in elektrische scheerapparaten, wasautomaten en dergelijke, en collector-seriemotoren voor toepassing in bijvoorbeeld elektrische scheerapparaten, handmixers en stofzuigers.

STELLINGEN

gevoegd bij het proefschrift getiteld

**OPTIMIZATION OF SMALL  
AC SERIES COMMUTATOR MOTORS**

te verdedigen op 19 oktober 1971

door

R. H. DIJKEN

## I

De uitspraak, gedaan in hoofdstuk 8 van dit proefschrift, dat de gunstigste waarde van de relatieve fluxgeleidende rotordoorsnede  $\beta$  van de kleine serie-collectormotor groter en de gunstigste waarde van de relatieve rotorlengte  $\lambda$  kleiner is dan algemeen toegepast, is ook geldig voor andere typen kleine collectormotoren. Een optimaliseringsberekening voor een kleine collectormotor, waarin de statorflux, die via stalen poolschoenen wordt toegevoerd aan de rotor, afkomstig is van naast de rotor opgestelde permanente magneten, geeft gunstigste waarden voor  $\beta$  en  $\lambda$  van respectievelijk ongeveer 0,5 en 0,35. Deze waarden blijken nauwelijks afhankelijk te zijn van de eigenschappen en de prijs per kilogram van het gebruikte magneetmateriaal.

## II

Rotoren van motoren voor aandrijving van gereedschapsmachines, die frequent worden in- en uitgeschakeld, moeten bij voorkeur een zo klein mogelijk massa-traagheidsmoment hebben, vooral als de kinetische energie van de draaiende rotor relatief groot is ten opzichte van de kinetische energie van de overige bewegende delen van de machine. In het algemeen wordt verondersteld, dat zo'n rotor erg slank moet zijn. Wanneer het een kleine collectormotor betreft kan worden aangetoond, dat uitgaande van gegeven waarden van het nominale toerental, het aanlooppoppel en het bij geblokkeerde rotor opgenomen elektrische vermogen de rotor inderdaad vrij slank moet zijn, maar dat de gunstigste waarde van de relatieve rotorlengte  $\lambda$  niet groter is dan 2.

## III

Als de prijs van aluminium wikkeldraad per kilogram niet hoger is dan die van koperen wikkeldraad, is het in kleine elektrische machines economisch aantrekkelijk, koper te vervangen door aluminium. Als we dezelfde eigenschappen in nominaal bedrijf eisen, zullen de uitwendige afmetingen toenemen met niet meer dan ongeveer 10%. Ook zullen het massa-traagheidsmoment van de rotor en het gewicht van de machine groter worden. De kostprijs van de machine kan in het gunstigste geval met ongeveer 20% dalen, terwijl de machine thermisch beter bestand is tegen overbelasting, aanloop en geblokkeerde toestand. Iets dergelijks kan men aantonen voor kleine transformatoren.

## IV

Mits goed gedimensioneerd kan een inwendig gekoelde collectormachine met bewikkelde stator goedkoper worden geproduceerd dan een qua eigenschappen vergelijkbare collectormachine waarin de statorflux wordt ontleend aan permanente magneten.

## V

Wanneer een gelijkstroom-seriemotor en een gelijkstroom-shuntmotor dezelfde afmetingen hebben en zo bewikkeld zijn, dat beide in aanlooptoestand dezelfde magnetische bronspanningen en koperverliezen hebben in de rotorspoelen en ook in de statorspoelen, dan is het aanloopkoppel van beide motoren even groot. De uitspraak, dat de seriemotor een groter aanloopkoppel heeft dan de shuntmotor is dus in zijn algemeenheid niet juist.

## VI

De temperatuur van de rotorspoelen van kleine collectormotoren kan tijdens continu zowel als tijdens veranderlijk bedrijf tot op enkele graden nauwkeurig worden bepaald door een thermokoppel aan te brengen in het uiteinde van een tot het midden van het blikpakket in de as geboord centrisc gat dat ter plaatse van het thermokoppel gevuld is met een vet- of oliesoort of een andere stof, die een goede thermische verbinding waarborgt tussen het stilstaande thermokoppel en de draaiende as, zonder dat het thermokoppel merkbaar extra wordt verwarmd door inwendige wrijving in genoemde stof.

## VII

Kortsluiting van een rotorspoel onder één van de beide borstels van een kleine tweepolige collectormachine met een even aantal collectorlamellen verkleint de werkzame zelfinductie van een commuterende rotorspoel onder de andere borstel. Daardoor zullen de borstels zodanig gaan slijten, dat de commutatie onder beide borstels vrijwel gelijktijdig eindigt, ook als de borstels niet symmetrisch staan opgesteld.

## VIII

Het begrijpen van en het rekenen aan magnetische en electromagnetische verschijnselen wordt eenvoudiger door onder andere de volgende maatregelen:

1. Magnetische velden niet beschrijven met behulp van magnetische veldsterkte  $H$  en magnetische inductie  $B$ , maar met magnetisatie  $M$  en magnetische inductie  $B$ .
2. Het begrip magnetische veldsterkte  $H$  laten vervallen.
3. De naam van de magnetische inductie  $B$  wijzigen in magnetische veldsterkte  $B$ .
4.  $\mu_0$  vervangen door  $1/\epsilon_0 c^2$ .
5. Het begrip magnetische poolsterkte  $M$  laten vervallen; het niet kwantitatieve begrip magneetpool kan worden gehandhaafd.
6. Het begrip magnetisch dipooltje laten vervallen ten gunste van het begrip kringstroompje.

## IX

De krachten die magneten op elkaar uitoefenen, worden meestal beschreven door aan een magneet twee magnetische polen toe te kennen met ieder een poolsterkte  $M$ . Twee magneetpolen  $M_1$  en  $M_2$  worden daarbij verondersteld een kracht op elkaar uit te oefenen die evenredig is met het produkt van  $M_1$  en  $M_2$  en die omgekeerd evenredig is met het kwadraat van hun onderlinge afstand  $r$ . Deze beschrijvingswijze is niet algemeen bruikbaar. Als twee magneetpolen zich in elkaars invloedssfeer bevinden, is in sommige situaties de kracht die ze op elkaar uitoefenen zelfs nul.

Een  $B$ - $M$  kromme en een  $M$ - $H$  kromme geven een betere visuele indruk van het magnetische gedrag van een materiaal dan de algemeen gebruikte  $B$ - $H$  kromme.

## XI

Een kringstroompje, geplaatst in een elektrisch veld  $\mathbf{E}$ , waarvan rot  $\mathbf{E}$  van nul verschilt, ondervindt onder andere een koppel om zijn as, dat volgens de klassieke theorie het magnetisch moment van het kringstroompje doet toe- of afnemen. Het magnetisch moment van een electron of proton wordt verondersteld in een als boven bedoeld elektrisch veld niet te veranderen. Voor wat betreft hun magnetisch gedrag zijn een electron of proton en een kringstroompje daarom niet equivalent.

## XII

Een kringstroompje met magnetisch moment  $\mathbf{m}$ , geplaatst in een evenwijdig magnetisch veld  $\mathbf{B}_x$ , dat zich verdicht in een richting  $y$  loodrecht op  $\mathbf{B}_x$ , ondervindt onder andere een kracht die gelijk is aan  $(\mathbf{m} \cdot \nabla \mathbf{B}_x / \partial y) \mathbf{n}$ , waarbij  $\mathbf{n}$  een eenheidsvector in  $y$ -richting is. Een magnetisch dipooltje ondervindt deze kracht niet. Naast het verschil in energieopname of afgifte bij een verplaatsing, dat door Carter wordt opgemerkt in<sup>21)</sup>, is ook het bovenstaande een reden, dat de veelal veronderstelde equivalentie tussen het magnetische dipooltje en het kringstroompje niet zonder meer bestaat.

## XIII

Het is zinvol, internationaal genormaliseerde symbolen in te voeren voor de grootheid kostprijs, alsmede voor afgeleide grootheden zoals bijvoorbeeld kostprijs per volumeenheid en per gewichtseenheid.

## XIV

Voor het wetenschappelijk en technisch rekenen zal het gebruik van programmeerbare elektronische tafelrekenmachines in de toekomst een steeds belangrijker rol gaan spelen in vergelijking tot analoge en digitale computers en aansluitingen op time-sharing computers.

Als het afgegeven vermogen van lasers of van vergelijkbare toestellen zodanig kan worden opgevoerd, dat zij in staat zijn op voldoende afstand mensen en wapens buiten gevecht te stellen, is voor het eerst in de geschiedenis een verdediging zoveel sterker dan een aanval, dat een veroveringsoorlog niet meer mogelijk is.